SYNTHESIS AND EVALUATION OF LABELED PHOSPHATIDYLGLYCEROL PROBES TO ELUCIDATE MECHANISMS BEHIND CHOLESTEROL TRAFFICKING IN NIEMANN-PICK TYPE C DISEASE

by

Zachary J. Struzik

A Dissertation

Submitted to the Faculty of Purdue University

In Partial Fulfillment of the Requirements for the degree of

Doctor of Philosophy

Department of Chemistry

West Lafayette, Indiana

May 2022

THE PURDUE UNIVERSITY GRADUATE SCHOOL

STATEMENT OF COMMITTEE APPROVAL

Dr. David H. Thompson, Chair

Department of Chemistry

Dr. Jean Chmielewski

Department of Chemistry

Dr. Shelley A. Claridge

Department of Chemistry

Dr. Mingji Dai

Department of Chemistry

Approved by:

Dr. Christine Hrycyna

This dissertation is dedicated to my family.

For their endless love, support, and encouragement

ACKNOWLEDGMENTS

I could not have achieved what I have without the wonderful mentors I had throughout my undergraduate and graduate studies. First and foremost, I would like to thank my graduate school advisor Dr. David Thompson. His efforts to put the interests of his students' education and goals over his own is something I will be forever grateful for. I appreciate every opportunity he has given me to become a better, and I am thankful for his support and guidance that has molded me into the scientist I am today. Additionally, I would also like to acknowledge my undergraduate research advisor Dr. John Parker for teaching me the basics of research and experimental design. I would like to acknowledge Dr. Jason Keleher for facilitating my passion for organic chemistry. Without the many chemistry courses I had with him, I would have never pursued organic synthesis.

I would also like to acknowledge my past and current lab members for their support and friendship as well. My predecessors Brad Loren, Shayak Samaddar, Craig Sweet, Sam Ewan, and Zinia Jaman were always there to answer any questions I had. Specifically, I would like to thank Brad for being my mentor my first year and providing me guidance on my first project. Shayak and Craig pushed me to think deeper about the applications of my project beyond the synthesis and provided endless guidance while I was preparing for my candidacy examination. Shruti Biyani and Aayush have also supported me through my numerous periods of struggles with my projects. My undergraduate students have also been essential for my success. I am grateful to have worked with such intelligent junior scientists that were able to think critically about problems and make research work as efficiently as possible. I would like to give a special thanks to Tim Grotzer and Ashley Weerts, whom I was able to mentor and publish with.

TABLE OF CONTENTS

LIST OF TABLES

LIST OF FIGURES

ABSTRACT

Niemann-Pick Type C (NPC) disease is a rare lysosomal storage disorder that occurs in about 1/89,000 to 1/120,000 live births and is characterized by an aberrant accumulation of cholesterol within the late endosome/lysosome of cells. Symptoms of this disease include splenomegaly, neurological deterioration, and often death before adulthood. Mutations in the membrane bound NPC1 or luminal NPC2 proteins lead to a decrease in cholesterol efflux within the lysosomes by which excess cholesterol crystallizes within membranes resulting in cell death. It has been demonstrated that increasing the amount of the lysosomal specific phospholipid Bis(monoacylglycero)phosphate (BMP), also known as Lysobisphosphatidic acid (LBPA), in cells increases the rate of cholesterol transport in *npc1*-/- cells, but not in *npc*2-/- cells, indicating a strong synergistic relationship between the NPC2 protein and the lysosomal membranes. Increasing the amount of phosphatidyl glycerol (PG), a hypothesized precursor to BMP, has also shown an increase in cholesterol egress. While it is hypothesized that the increase in cholesterol clearance in the latter is due to the biosynthesis of LBPA from PG, there is no study to directly confirm this phenomenon. Therefore, we set out to synthesize diastereochemically pure PG containing isotopically labeled oleyl acyl chains to examine LBPA levels using lipidomic analysis of *npc1*-/- cells post treatment with PG.

Initially, efforts centered around the use of phosphoramidite methodology commonly encountered in DNA oligonucleotide synthesis. While this route proved to be successful in making PG in modest yield (52%), reproducibility of this route with consistent yields was hindered due to the use of tetrabutylammonium fluoride (TBAF) in the final global deprotection step. Thus, we set out to discover a phosphorylated intermediate that did not require TBAF in the final step or contain easily hydrolysable protecting groups. It was discovered that H-phosphonate methodology using

diphenyl phosphite for phosphorylation of the glycerol headgroup and backbone proved to be robust enough for PG synthesis. In this strategy, PG can be isolated in two steps from the final protected intermediate by first oxidizing the H-phosphonate from P^{III} to P^{V} followed by deprotection of the glycerol head group under acidic conditions. Additionally, the H-phosphonate strategy also allowed us to omit headgroup modification prior to phosphorylation which reduced the number of synthetic steps from 11 steps to 7 steps. As a result, we were able to synthesize diastereochemically pure PG more consistently than the previous route in 75% yield. The route was further modified further to incorporate asymmetric acyl chains allowing the selective installation of a labeled acyl chain on the *sn*-1 or *sn*-2 positions of the phosphoglycerol backbone. The results from the lipidomic experiments indicate that increased LBPA concentrations in cells rise upon incubation with labeled PG. Additionally, increases in lyso-PG and acyl-PG are also observed leading to several hypotheses on how LBPA might be synthesized from PG. Future directions on this effort include identification of phospholipid species made from PG containing asymmetrically labeled acyl chains. Synthesis of photoaffinity labeled PG is also underway to determine the protein partners involved in PG metabolism.

CHAPTER 1. BACKGROUND AND LITERATURE REVIEW

Niemann-Pick Type C disease (NPC) is a rare autosomal recessive lysosomal storage disorder found predominately in children that often results in death before the age of 20. NPC is caused by an aberrant accumulation of cholesterol within the late endosome/lysosome compartment of cells. This dissertation is focused on the synthesis of labeled phosphatidylglycerol probes containing ^{13}C acyl chains to elucidate mechanisms behind cholesterol trafficking in NPC. The purpose of these probes was to monitor the movement of acyl chains from one phospholipid species to another using hydrophilic interaction liquid chromatography coupled to tandem mass spectrometry, in an effort to identify metabolic intermediates and enzymes involved in the production of a lysosomal specific phospholipid known as bis(monoacylglycero)phosphate (BMP), a molecule of growing interest in NPC. Chapter 1 provides literature review of lysosomal functions and NPC overview with a concentration on BMP. Chapters 2 and 3 focus on the novel syntheses of diastereochemically pure PG containing unsymmetric acyl chains to provide a robust route for installation of labeled oleyl chains onto the phosphoglycerol backbone. Finally, Chapter 4 is focused on monitoring the metabolic products of PG and progress towards the synthesis of photoaffinity probes in an effort to establish involved protein partners.

1.1 Lysosomes

Lysosomes are digestive organelles that are made up of an acidic lumen and a single phospholipid bilayer membrane typically ranging between 0.1 – 1.2 µm in diameter with a heterogenous morphology.[1] First discovered in rat liver by de Duve *et al.*[2-3], they were originally described as saclike structures containing a variety of acid hydrolases surrounded by a membrane. Lysosomes contain more than 50 different types of hydrolytic enzymes called acid hydrolases

including phosphatases, nucleases, proteases, lipases, sulfatases and others that are responsible for the degradation of cellular waste, nutrient sensing, recycling, as well as autophagy.[4-5] These enzymes break down proteins, polysaccharides, and lipids into their fundamental building blocks.[6-7] Acid hydrolases are specifically targeted to the lysosomes by mannose-6-phosphate residues (M6P) that are recognized by M6P receptors in the *trans*-Golgi network (TGN).[8] From there, the enzymes are repackaged into clathrin coated vesicles that, upon removal of clathrin, fuse with late endosomes to form the late endosome/lysosome complex (LE/LY). Binding of M6P to its corresponding oligosaccharide occurs at pH 6.5 – 7, and releases it in the interior of the lysosome when the pH drops below 6.[9] Upon release of the hydrolase enzymes, the M6P receptors are then recycled and sent back to the TGN for further use.

The acidic pH required for activity of the acid hydrolases present in the lumen of the lysosome is maintained by active transportation of protons via vacuolar ATPase (VATPase).[10] Since the concentration of H^+ of the lysosome (pH 4.5 -5.5) is approximately 100 – 1000 fold higher than the cytosol, expenditure of energy in the form of ATP hydrolysis is necessary to maintain this acidity. At higher pH levels, the enzymes become inactive making the acidic pH for lysosomal function essential. To highlight the importance of this statement, efforts to kill tumor cells by rendering lysosomal enzymes inactive simply raising the lysosomal pH have been employed with small molecules. Two diprotic weak-based drugs, chloroquine (CQ) (pKa_1 = 8.1, pKa_2 = 10.2) and hydroxychloroquine (HCQ) (pKa_1 = 8.3, pKa_2 = 9.7), have been used to exploit the large pH gradient between the extracellular pH (6.5) in the tumor microenvironment and the alkaline cytosol of the tumor cell (7.12 – 7.65).[11-12] The driving force for HCQ and CQ to partition into the lysosome is proportional to the square of the hydrogen ion gradient compared to a monoprotic base like ammonia chloride that is only proportional to the hydrogen ion gradient.[13]

Once inside the lysosome, CQ and HCQ become protonated, thus raising the pH. The inhibition of hydrolase enzymes prevents the fusion of autophagosomes with lysosomes, and therefore prevents degradation of engulfed material.[14] As a result, tumor cell growth is inhibited, and apoptosis is enhanced through autophagic flux.

The formation of lysosomes represents an intersection between the secretory pathways and endocytic pathways (Figure 1.1). Lysosomes originate from budding of the TGN. In the former, lysosomal proteins are packaged and shipped from the TGN while the latter involves the formation of vesicles at the cell surface. In the endocytic pathway, material can be taken into the cell through endocytosis at the plasma membrane. In this process, budding occurs in a clathrin dependent or independent manner from the plasma membrane and forms what is known as an early endosome (EE). In the EE, material is either sent to the lysosomes for degradation, recycled and rapidly transported back to the plasma membrane via Rab mediated transport, or sent to the TGN for further trafficking.[15] Intraluminal vesicles (ILVs) can form in the EE by inward budding of the endosomal membrane mediated by endosomal sorting complex required for transport (ESCRT).[16] This step in the maturation process from early to late endosomes is what is responsible for the formation of multivesicular bodies where cargo proteins are transported for degradation.

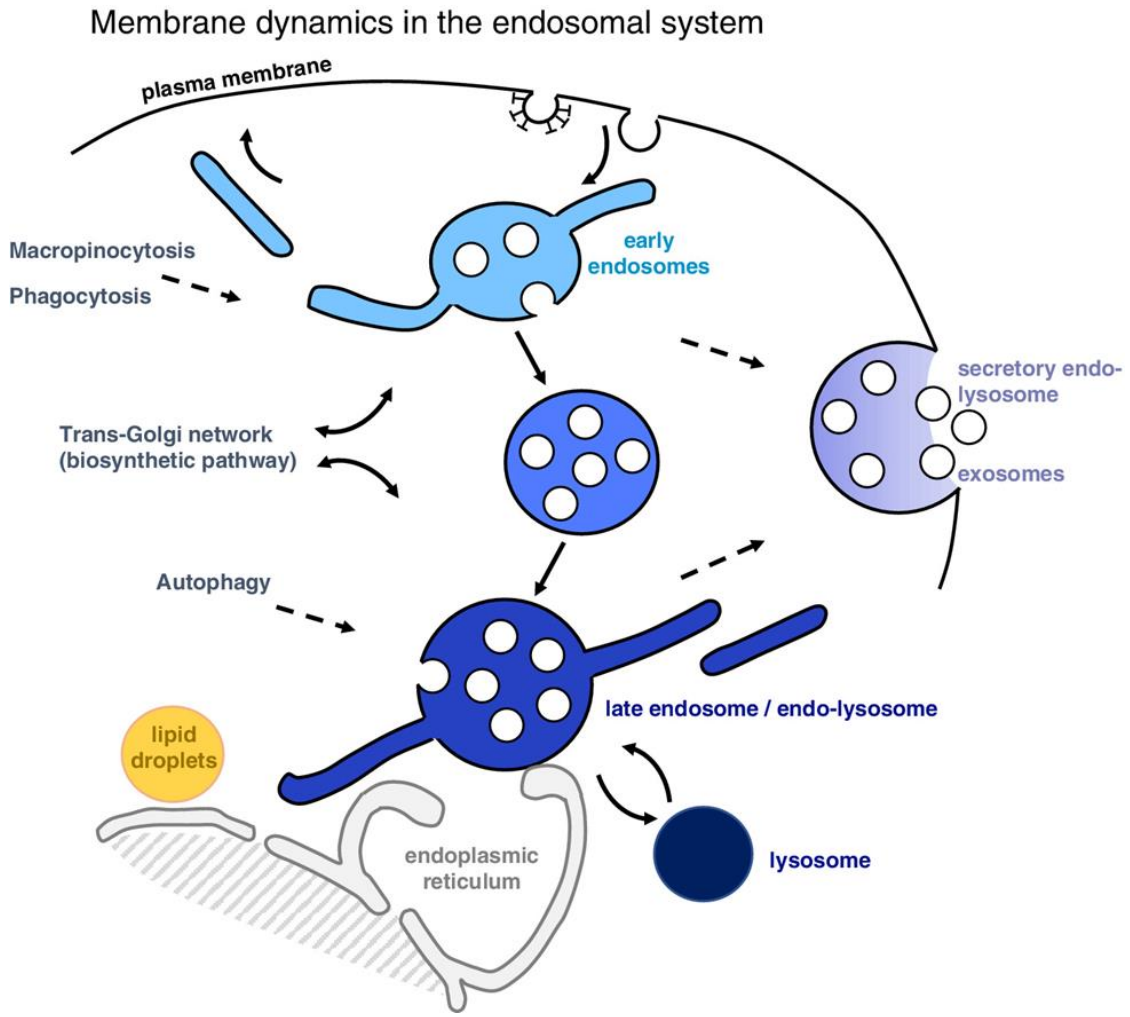

Figure 1.1. Outline of the endocytic pathway in animal cells. EEs are formed by endocytosis via phagocytosis, pinocytosis, or receptor-mediated endocytosis. Certain proteins and lipids not destined for the LE/LY may be recycled back to the plasma membrane, or routed by retrograde transport to the TGN. Sorting of components destined for the LE/LY is achieved by the formation of ILVs that are formed from the limiting membrane as the EE matures into an LE. Eventually, some ILVs are delivered to lysosomes where they are degraded together with their protein cargo. Late endosomes and lysosomes exchange membrane components and solutes, forming a transient hybrid endo-lysosome, which is then re-converted into secondary lysosomes, where hydrolases are stored. As this maturation process occurs, VATPase pumps protons into the lumen to lower the pH of the vesicles. Material may exit the cell by LE/LY as well by fusing with the plasma membrane and forming secretory vesicles or exosomes. The endocytic pathway also intersects with other vesicular pathways such as autophagy, and engages in other membrane contact sites with organelles such as the endoplasmic reticulum or Golgi apparatus. Figure reproduced from Gruenberg *et al.*[17].

The definitions of the lysosome, EE, late endosome (LE), and LE/LY may seem unclear as there are many similarities between each of these vesicles. This is in part due to the constantly changing environment of the same vesicles as they proceed down the chain of transportation and metabolism of engulfed material. The EE was originally thought to be a transportation mechanism of endocytosed material for cells whereas today it is understood to have many other functions that relate to sorting and recycling. In general, the EE is located near the cell surface while the late endosome is usually perinuclear and characterized by the formation of ILVs. It is still under debate whether or not the LE should be defined by vesicular transport or the maturation of EE (e.g., change in pH, formation of ILVs, etc.). However, evidence suggests that one clear difference is that the late endosome is more likely to receive traffic from the TGN.[18] Morphologically, LE tend to be more spherical than EE and are juxtanuclear. The lysosome is born from the TGN and contains a single lipid bilayer while the LE/LY may have both a limiting membrane as well as ILVs due to fusion of a lysosome with a late endosome.

1.2 Lysosomal Storage Disorders

1.2.1 Uncontrolled Substrate Accumulation and Impairment of Autophagic Processes

It is important to note that the M6P tag distinguishes secretory proteins from lysosomal proteins. If tagging of lysosomal proteins with M6P does not occur, subsequent breakdown of the hydrolase's substrate in the lysosome will not occur. This may cause the substrate to accumulate within the lysosome. Aberrant accumulation of a given substrate within the lysosome can be deleterious not only for the lysosome, but it can also disrupt cellular homeostasis and can ultimately lead to cell death. The buildup of undigested material can result in a rare class of diseases known as lysosomal storage disorders (LSDs). LSDs were originally described as

lysosomal enzyme deficiency states in 1965 by H.G. Hers when he discovered what later became known as Pompe disease.[19-20] Examples of accumulated intermediate metabolic products include lipofuscins, gangliosides, sterols, sphingolipids, sulfatides, triglycerides and sphingomyelin.[21-23] There are nearly 50 LSDs known; all of which are single gene disorders.[24] These diseases can arise due to deficiencies in acid hydrolases, but they can also arise due to other proteins within the lysosome that are responsible for digesting endocytosed material. Since Hers' discovery, the definition of these storage disorders expanded to include dysfunction in non-lysosomal enzymes as well as soluble and transmembrane proteins of the lysosome. Additionally, all LSDs are autosomal recessive disorders except for Hunter's disease, Fabry's disease, and Danon disease.[25-27] The autosomal recessive nature makes LSDs most common in children. Collectively, LSDs affect about 1/5,000 – 1/7,000 live births and represent heterogeneity with respect to different populations and regions.[28] For instance, Gaucher disease (GD) is an LSD that arises due to a mutation in the GBA gene that results in a deficiency in β-glucocerebroside. In the general population, GD affects 0.39 to 5.80 per 100,000 live births, but in Ashkenazi Jews, GD can be as high as 1/850 live births.[29-31]

While cells can tolerate some loss of enzyme activity and still moderate substrate accumulation, there exists a 'critical threshold' by which cells can operate with this loss in activity.[32] Below this threshold, cells can no longer tolerate the excess substrate and accumulation occurs. The manifestation of LSDs can be attributed to structural changes in cells, such as enlargement, that ultimately result in physical and cognitive abnormalities. The uncontrolled accumulation of substrate can also result in complete organ failure. For example, Pompe disease is a type of LSD in which intralysomal accumulation of glycogen results in cardiomyopathy due to deficiencies in acid α-glucosidase: a carbohydrate hydrolase that releases α-glucose.[33-34] Large

amounts of glycogen in vacuoles were observed in all tissues examined, which lead to an enlarged heart. In another example, Stargardt disease is caused by a mutation in either the ABCA4 or ELOVL4 genes.[35-37] Both of these genes are responsible for making proteins that are located in photoreceptor cells in the retina. The ABCA4 protein is responsible for removing toxic substances from the eye such as lipofuscin which accumulate upon its absence, thus resulting in cell death. Mutations in the ELOVL4 protein results in protein aggregates and interfere with retinal cell functions; this effect also results in cell death. In both cases, vision can be impaired, and patients of this disease may go blind.

In addition to cellular and organ dysfunction, LSDs seem to also cause brain failure in roughly two-thirds of all lysosomal diseases.[22] Symptoms of LSDs that cause brain failure typically involve manifestation into dementia, motor system dysfunction, seizures, blindness, etc. The reason as to why this happens has eluded experts in the field despite the advances in genomics and modern biochemical assays. One possible explanation for the connection between LSDs and cellular degradation is the impairment of autophagy.[38-40] Autophagy is the process in which cells maintain homeostasis by selectively removing damaged organelles or macromolecules that, if accumulated, may become toxic. On the other hand, cells can also non-selectively recycle cytosolic materials upon starvation to generate energy. The process of autophagy begins with the formation of isolated membrane vesicles known as phagophores that resides in the cytosol. Phagophores are predominately formed in the endoplasmic reticulum, but have also been cited to form from the mitochondria, Golgi apparatus, and plasma membrane.[41-44] As they mature, phagophores elongate and form double-membrane vesicles called autophagosomes and engulf autophagic cargo. Autophagosomes can then either fuse directly with lysosomes, or first fuse with endosomes and

then with lysosomes to form autolysosomes where cargo is then consumed. The maturation of autophagic vesicles and metabolism of cargo is known as the autophagic flux (Figure 1.2).[45]

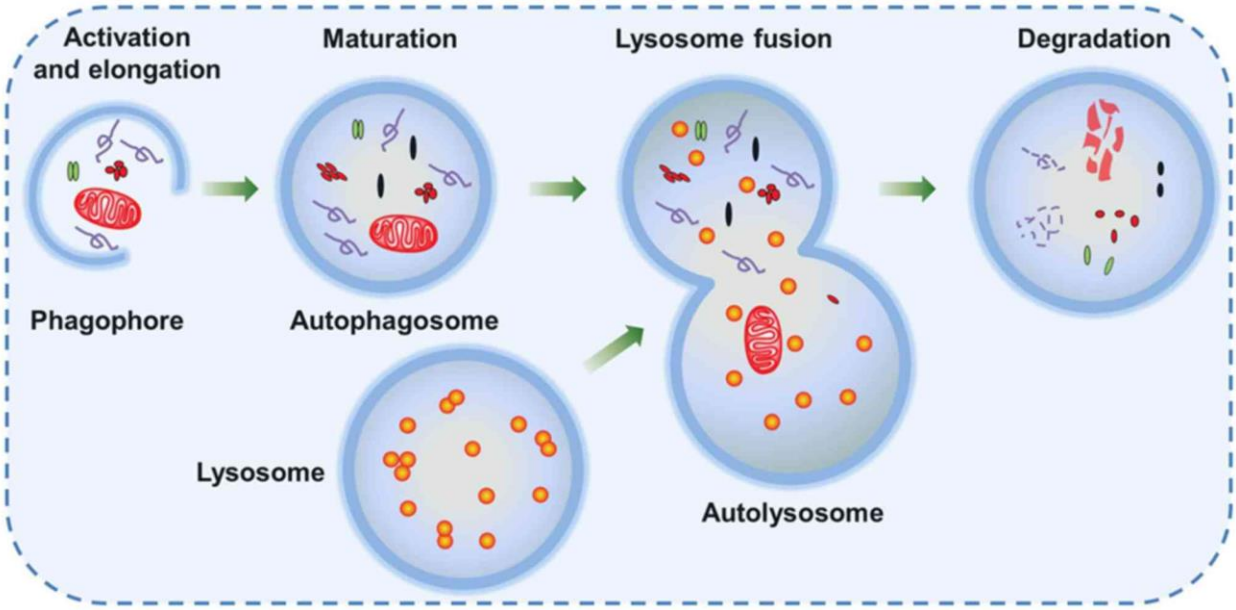

Figure 1.2. Steps of the autophagic flux. Autophagy is activated upon cellular stress conditions. The process begins with the formation of a double-membrane vesicle known as a phagophore that elongates into an autophagosome. These vesicles engulf intracellular degradation components, including mitochondria, damaged organelles and lipid droplets. The mature autophagosome with intracellular degradation components then fuses with the lysosome and forms an autolysosome, which provides an acidic environment for hydrolytic enzymes to hydrolyze the engulfed components. Figure reproduced from Li *et al*.[45]

There are several mechanisms by which autophagy is regulated. The primary function of autophagy is to serve as a survival mechanism rather than a cell death mechanism. Under nutrient-rich conditions, the rapamycin complex 1 ($mTORC_1$) pathway is a commonly targeted mechanism by which cells grow and proliferate by manufacturing proteins.[46] Secondary targets for autophagy modulation include the Unc-51 like kinase-1 (ULK_1) complex and AMP-activated protein kinase (AMPK).[47] Upon inhibition of mTORC1, the cell becomes starved, and autophagy is stimulated. Independent of $mTORC_1$, autophagy can also be influenced by increasing the levels of inositol triphosphate (IP_3), Ca^{2+}, cyclic adenosine monophosphate (cAMP), and nitric oxide.[48-51]

Impairment of autophagic flux has been cited in a number of neurodegenerative diseases including Niemann-Pick Type C disease (NPC) that will be described in greater detail later.[52-55] Von Gierk's diseases, a deficiency in glucose-6-phosphatase-α, decreases the ability of glycogen to be broken down into glucose primarily in the liver and kidney. *G6pc-/-* mice exhibited decreased autophagy in the liver via downregulation of sirtuin-1.[56-59] However, Glycogen Storage Diesease Type 1a (GSDIa) dogs that were treated with rapamycin, an agent used to induce autophagy, experienced decreased levels of hepatic triglyceride and glycogen content, translating to a decreased liver size.[60] In a second example, Lafora disease (LD) is a glycogen storage disorder that arises due to mutations in EPM_2A and EPM_2B.[61] LD is characterized by neurodegeneration and intracellular accumulation of poorly branched glycogen deposits. Knockout of EPM_2A and EPM_2B in mice resulted in decreased autophagosome production suggesting an impairment of autophagy.[58, 62] Although not an LSD by definition, Alzheimer's disease is a macromolecular storage disorder that results from the impaired metabolism of amyloid precursor protein (APP), thus resulting in accumulation of extracellular senile plaques made from amyloid-β (AB) leading to brain failure.[63] Presenilin-1 (PS-1) is an enzyme that cleaves APP into AB where it is degraded via autophagy. However, mutations in PS-1 impair lysosomal acidification which results in impaired autophagic flux and prevented autophagosome maturation.[58, 64]

1.2.2 Diagnostic Techniques and Treatments for Lysosomal Storage Disorders

It should be appreciated by now that the vesicular transport vesicles in cells play a much larger role in cellular homeostasis than transporting cargo from one point to another or serving primarily as a "garbage disposal" for cargo. Impairments in the lysosome via LSDs have major implications in the entire trafficking network and overall health of the cell. While the cause of LSDs may seem straightforward, the diagnosis of LSDs can be more complex. Diagnosis typically

occurs well after the patient symptoms are first presented, usually after patients show developmental decline after a period of normal development.[65] There are a broad spectrum and overlap of phenotypes that can make recognition of these diseases difficult, and therefore clinical suspicion based solely on presentation of symptoms is not very effective. NPC, a cholesterol and sphingolipid storage disorder, is a disease in which patients are commonly misdiagnosed with psychotic syndromes, Alzheimer's disease, Parkinson's disease, Wilson's disease, Creutzfeldt-Jakob disease, multiple sclerosis, Wernicke encephalopy, and others.[66]

Due to the rare nature and large number of these LSDs, it is understandable why a physician may misdiagnose based on the clinical presentation of LSDs that they are less familiar with. The lack of familiarity of LSDs within the general population further amplifies this problem as the disease becomes more difficult to diagnose due to late onset of symptoms that may not occur right at birth.[67] Furthermore, these diseases usually require biochemical assays on blood, urine, or skin fibroblasts in infants and children that are only available through specialized laboratories.[68] These assays typically screen for increased levels of accumulated substrates. Dyes that stain specific substrates may be used to identify increased levels of the analyte of interest. In cases where UV/Vis experiments cannot be performed, other techniques may be employed to identify the analyte of interest such as thin-layer chromatography and high-pressure liquid chromatography.[69-70] Enzyme analysis is another method used to rapidly diagnose LSDs. This technique is commonly employed in diseases such as Niemann-Pick Type A and B, acid lipase deficiency, Krabbe disease, and more.[71] In these examples, leukocytes and plasma are analyzed for enzymes involved in the digestion of glycosphingolipids and oligosaccharides. Targeted enzymes may be analyzed with specific fluorescent tags such as 4-methylumbelliferone. While this enables the analysis to be rapid, it may decrease the sensitivity of the enzyme potentially due to the susceptibility to mutant forms

of the enzyme.[72] This will require more material from the patient. One possible alternative to the fluorescence tag method is by using tandem mass spectrometry (MS-MS), especially when using dried blood spots.

Molecular screening assays may also be performed to determine mutations in selected genes and proteins to identify point mutations. Mutation scanning is a type of molecular screening assay that is used to identify gene mutations without knowing the location of the genes. Mutation scanning such as high resolution melting, a post PCR technique, was employed to identify genetic variants in a German NPC population.[73] Another mutation scanning technique such as denaturation high performance liquid chromatography (dHPLC), also a post PCR technique used to screen DNA samples by analysis using reversed phase columns to identify denatured DNA strands upon temperature changes. In a Gaucher patient, dHPLC was employed to identify three novel mutations in a Colombian population.[74] DNA sequencing is a third type of molecular screening that identifies precise location of nucleotides within genes. This method is ideal for patients who have disorders with no existing biochemical markers. Next generation sequencing (also known as massively parallel sequencing) is used to investigate DNA sequencing in large regions.[75] This approach overcomes the scalability limitations of traditional Sanger sequencing by attaching DNA molecules to beads that allows millions of DNA sequencing reactions to happen in parallel. This technique was recently implemented to identify one-point mutation and a deletion of acid alpha-glucosidase (GAA) in Pompe disease.[76]

Treatments for LSDs have also proven to be a challenge. To date, there are no cures for patients with LSDs. While certain strategies such as enzyme replacement therapy (ERT) may enhance the quality of life, this merely decreases the rate of the disease pathogenesis.[65, 77] The difficulty in creating more effective therapies for LSDs is due to the necessity to transverse the

blood brain barrier (BBB) after intravenous injection of agent. As explained earlier, the patients of many LSDs will eventually develop brain failure.[22] Therefore, targeting therapies to the brain is essential for limiting the neurodegenerative effects. The BBB is a highly selective semipermeable network made up of continuous endothelium with tight junctions between endothelial cells.[78] The role of the BBB is designed to protect the brain from circulating pathogens. The BBB prevents molecules larger than 400 – 600 Da and small polar molecules to pass through, but allows lipophilic molecules that meet the criteria for passive transport through.[78] Regulation of passive transport is carried out via efflux pumps that reject undesired small molecules back to the circulatory system. Transportation of small polar molecules (e.g. glucose, amino acids, organic ions, nucleosides, etc.) may cross the BBB through carrier mediated transport.[79] Larger macromolecules such as peptides and proteins are transported by receptor-mediated or adsorption mediated endocytotic transport, and may be used in targeting strategies to deliver small molecule cargo.[78]

ERT has been the mainstream approach to treating LSDs, but it is limited to non-neuronal manifestations of disease. Furthermore, the ERT approach requires repeated injection of therapeutic agent as patients remain unable to produce the mutated or deficient enzyme. The goal of ERT is to deliver purified functional enzymes to lysosomes that enhance the activity of digested substrates. The earliest FDA approval of an ERT was for Gaucher's disease in 1991.[80] Intravaneous injection of enzymes into the blood stream typically do not cross the blood brain barrier. Direct injection of ERT to the central nervous system have also been explored to bypass the BBB.[81] However, this is not ideal for patients as these approaches require repeated injections into the brain or spine.

The use of an ERT strategy is primarily implemented for LSDs that display little to no neurological symptoms; although there have been attempts to create delivery systems for ERT that transverse the BBB via nanoparticles (NPs).[82] NPs based approaches have also been used to transport small molecules that don't meet the criteria to cross BBB.[83] NPs incorporating small molecules act similarly to a "Trojan Horse" in which NPs can disguise the payload as material that cells can take in. They can protect the incorporated cargo from degradation as well enhance the bioavailability of the drug attributed to longer circulation times within the blood stream compared to the free drug. Additionally, because the cargo is shielded from the surrounding environment until the NP breaks down at its target site, it can reduce the toxicity of the therapeutic agent. Some examples of biodegradable and bioavailable NP delivery systems that have been used to transverse the BBB include polymers, lipids, metal NPs, and exosomes.[84-87] The use of NPs can be used to ameliorate some of the pitfalls of ERT, specifically the lack of targeting and high dosing of the selected enzyme. Recently, a (poly lactic-co-glycolic acid) (PLGA) based NP was targeted to the brain using cross-linked enzyme aggregates to treat Krabbe disease, an LSDs caused by a deficiency in galactocerebrosidase, which is responsible for the metabolism of the sphingolipids galactosylceramide and psychosine.[88-89] These NPs promoted recovery in the brain of mice to levels similar to the control. Both targeted and non-targeted versions of the NPs accumulated in the liver, but only the targeted NPs ended up in the brain.

As LSDs are single gene disorders, they are ideal candidates for gene therapy strategies. The critical threshold for most lysosomal enzymes is 10-15% of residual enzyme activity. Below this threshold, disease does not occur.[90] Therefore, only a fraction of the total lysosomal activity needs to be restored for the cell to maintain homeostasis. Gene therapy can be divided into ex vivo and in vivo strategies. In the ex vivo approach, cells are extracted from donors and transduced by

a viral vector to over express the therapeutic enzyme before transplantation back into the patients. One successful example of ex vivo gene therapy was the use of hematopoietic stem cells that were used for infantile metachromic leukodystrophy, an LSD that characterized by the accumulation of sulfatides in the cells of the central nervous system.[91] After 18 to 24 months of treatment in infants, disease progression halted when normally disease progression would be rapidly increasing. Most *in vivo* gene approaches take advantage of direct administration of recombinant adeno-associated vectors (rAAV) usually intravenously or locally to the central nervous system. AAVs are small viruses that infect humans but lacks pathogenicity.[92] This gives rAAV the transduction efficiency of a virus but is also considered safe. An additional advantage is that specific rAAV therapies such as AAV9 can cross the blood brain barrier allowing transduction of the CNS after administration.[93] Recent advances in large scale AAV vector production has allowed for the translation of preclinical studies to clinical trials including intravaneous high-dose AAV9 therapy in type I and type II GM1 gangliosidosis patients[94], AAV6 therapy for adult Fabry disease[95], AAV8 therapy to adults with late onset Pompe disease[96], and others.

1.3 Niemann-Pick Type C Disease

1.3.1 History of Niemann-Pick Diseases

Niemann-Pick Disease (NPD) is a group of heterogenous LSDs associated with the accumulation of cholesterol and sphingomyelin in the lysosome.[97] NPD was first described in 1927 by two German pediatricians: Albert Niemann and Ludwig Pick. NPD can be classified into four subtypes: A, B, C, and D. An autopsy in 1914 performed by Niemann in Irene D., a child who had died at 18 months old and had been ill her entire life, revealed an enlarged liver, spleen, and lymph nodes that were yellow and fatty.[98] Tissue cells were replaced by large vacuolated cells that

Niemann believed to be similar to, but not identical with Gaucher disease. In 1927, Pick identified Type B and confirmed that Type A is different from Gaucher disease.[99-100] Type A is the most severe form of NPD that occurs early in infancy and results in significant damage to the brain. Type B typically starts in childhood and has mild symptoms compared to type A without brain damage. Types A and B are similar in that they are caused by mutations in the SMPD1 gene that results in deficient activity of the enzyme responsible for the breakdown of sphingomyelin.[101] Type C and D are cause by mutations in the NPC1 or NPC2 genes that result in the impairment of cholesterol trafficking within the LE/LY, leading to an uncontrolled accumulation of lipids.[97] The NPC1 mutation occurs in chromosome 18q11 and is present in about 95% of patients.[97, 102] The other 5% of NPC patients experience mutations in the chromosome 14q42.3.[103] This chromosome was originally thought to encode for the human epididymal protein 1 (HE1), but observation of reduced cholesterol accumulation with *npc2-/-* patient fibroblasts upon supplementation with HE1 inspired the name change to NPC2 as it was evident this protein was required for cholesterol trafficking. Type C differs from Type D in that the latter is associated with their Nova Scotia Acadian origin.[97] Type C and Type D are interchangeable, and are both categorized into Type C. It was discovered in 1966 by Brady and co-workers that there was a severe deficiency in sphingomyelin in type A, which was extended to type B.[104-105] However, types C and D did not demonstrate this problem. In turn, types C and D evolved into a cholesterol storage disorder while Types A and B were designated as a sphingomyelin disorder.

Niemann-Pick Type C disease (NPC) occurs in about 1/89,000 to 1/120,000 live births, although the incidence rates can vary among ethnicity groups can vary.[106] The age of onset of NPC can occur anywhere from the neonatal period to well into adulthood. NPC was first identified when fibroblasts cultured from NPC patients revealed high concentrations of unesterified cholesterol,

distinguishing it from other LSDs.[107-108] However, the disease predominately presents itself from the early childhood to early adulthood periods, often resulting in death between the ages of 10 and 25. While systemic involvement precedes the onset of neurological involvement, the systemic involvement may only be present in approximately 15% of patients at the point of diagnosis.[97] Neurological disorders consist mainly of ataxia, dysphagia, dementia, and vertical supranuclear gaze palsy.[66]

1.3.2 Symptomatic Progression of Niemann-Pick Type C Disease

The early infantile stage (2 months – 2 years) of NPC can be characterized by the presence of hepatosplenomegaly.[97] While NPC is not specific to any given region of the body, as cholesterol in necessary in all cells, certain regions may appear abnormally large compared to others due to large amounts of cholesterol accumulation in the respective regions. Hepatosplenomegaly, or the enlargement of the spleen or liver, is a hallmark of NPC disease as most cholesterol production occurs in the liver. Neonatal cholestatis, an impaired flow of bile from the liver cells to the intestine of a newborn, typically resolves itself in within 2 - 4 months of being born leaving only hepatosplenomegaly behind. However, infants that do not observe improvement develop acute neonatal cholestasis which results in liver failure and ultimately death within 6 months. Neurologically, a loss of motor skills may be observed leading to children with NPC lacking the ability to walk. Patients demonstrated onset of NPC at this stage typically leads to death before the age of 5.

The majority of NPC patients experience the onset of symptoms between the ages of 6 and 15 years of age, also known as the juvenile period.[97] Hepatosplenomegaly may begin at this stage. However, patients where organomegaly was observed in the early stages of infancy may see this reduced by the onset of neurological symptoms. Difficulty paying attention and retaining

information in school is not uncommon. Similarly to the early infantile stage, motor skills become impaired as the child, at a variable rate, starts to become clumsier while walking (gait problems) and has difficulty running. Most patients who show symptoms in the juvenile period usually do not survive past the age 30, although some patients can.

Patients that experience NPC during the adolescent and adult stage (15 years and older) usually suffer from severe neurological deterioration.[97] It's often the late onset of symptoms that misdiagnosis occurs as absence of hepatosplenomegaly leaves only neurological symptoms to be commonly observed. Neurological onset in the adult stage, however, may not arise until possibly 50 years of age or older. Onset of symptoms at this stage might also present psychiatric impairment before motor skill impairment. Psychiatric impairments usually consist of psychosis and patients may develop disorders such bipolar disorders, obsessive-compulsive disorders, and transient visual hallucinations.

1.3.3 Diagnosis and Treatment of Niemann-Pick Type C Disease

As mentioned previously, the diagnosis of NPC can be quite challenging. In most cases, only after the disease presents itself does laboratory testing begin (Figure 1.3). The first line of laboratory testing typically involves screening for elevated plasma metabolites such as cholestane-3β, 5α, 6β-triol, 7-ketocholesterol, 25-hydroxycholesterol, lyso-sphingomyelin isoforms and bile acid.[109-111] Interestingly, the reported levels of 24(S)-hydroxycholesterol were lower than controls.[111-112] The limitations associated with these tests are mainly that these biomarkers are not necessarily specific to NPC, and often requires specialized laboratories with expertise in handling and analyzing these molecules. As a second line of diagnostic testing, genetic screening may be carried out. Currently, there exists about 700 known variants of NPC1 leading to impaired function, and about 420 of them are thought to be pathogenic.[109] Genetic screening is the only reliable

method to diagnose carriers of the mutated NPC1 and/or NPC2 proteins. Additionally, it may assist in correlating the phenotype to the genotype. The disadvantages associated with this method of diagnosis include the inability to identify certain genetic mutations associated with routine screening methods as well as variation between ethnicities. After genetic testing, filipin staining of skin fibroblast cholesterol content may be carried out. Filipin is a poly-ene dye that specifically binds to cholesterol aggregates to emit an intense blue fluorescence when illuminated. While still useful, it is no longer considered the gold standard of NPC diagnosis as it requires invasive skin biopsies and analysis is long, expensive, challenging, and labor intensive.[113] With that said, it's very useful in assessing the pathology of the disease, and when used in corroboration with data acquired from the previously described diagnostic methods can be a very power analytical technique.

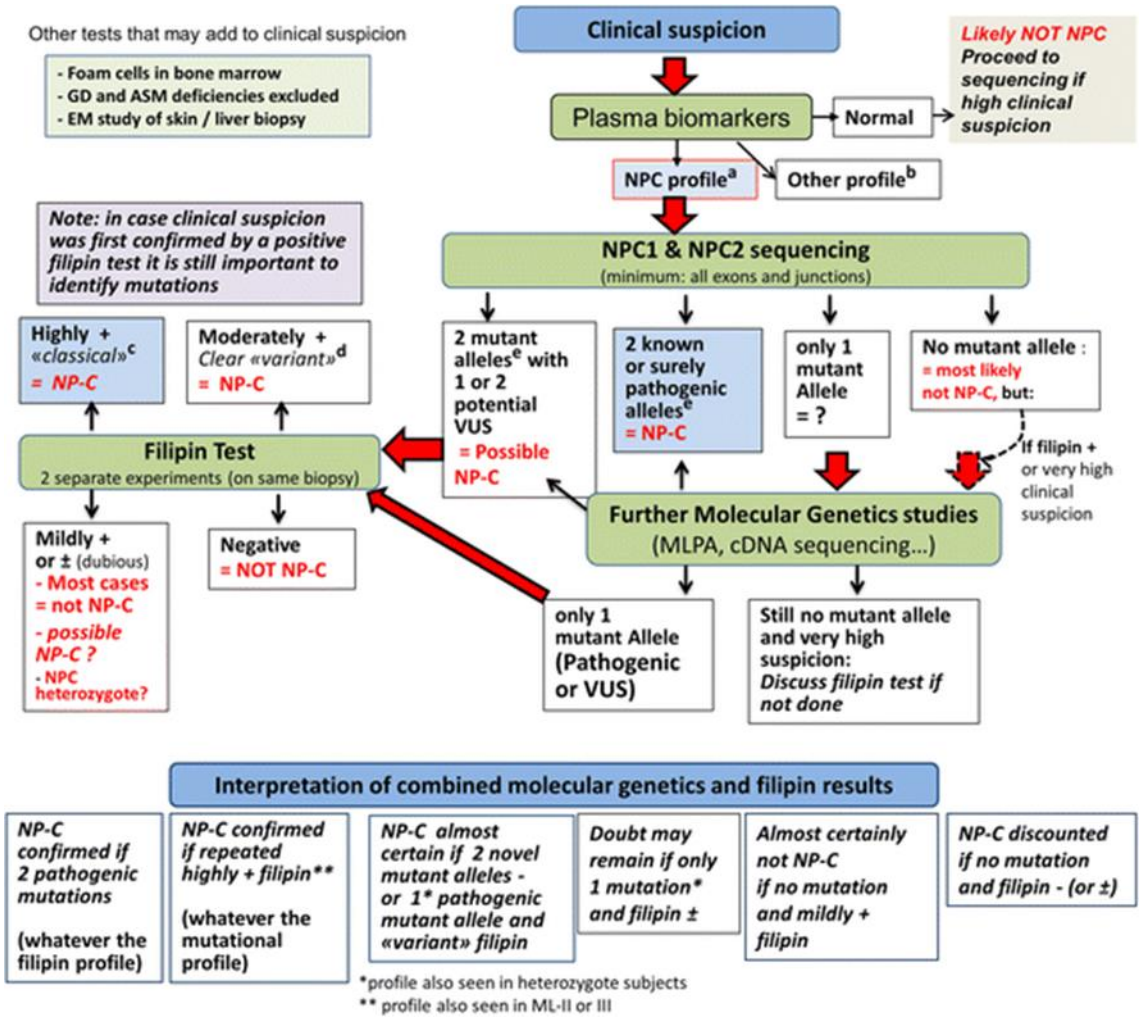

Figure 1.3. "Niemann-Pick disease type C laboratory diagnosis algorithm. Abbreviations: GD: Gaucher disease; ASMD: acid sphingomyelinase deficiency; EM: electron microscopy; VUS: variant of unknown significance; MLPA: Multiplex Ligation-dependent Probe Amplification (evaluates copy number changes, allows detection of large deletions or false homozygous status with a deletion on the other allele); lysoSM: lysosphingomyelin." Figure reproduced from Geberhiwot *et al*.[109]

Several therapeutic strategies, while not FDA approved, have been attempted to treat NPC. Cholesterol-lowering agents were successful in reducing hepatic cholesterol levels, but proved unsuccessful in extrahepatic tissues, specifically in the brain.[114-116] Sphingolipid-lowering drugs such as miglustat, a drug approved for Gaucher disease, showed delayed onset of neurological symptoms by blocking glycosphingolipid production in the brain.[117] This therapy is approved for use in Australia, Canada, New Zealand, and other countries in Europe, Asia, and South America.

Biological therapies have been explored as well such as ERT strategies, gene therapy, and stem cell therapy, although no improvement in neurological function was observed.[118] Non-steroidal anti-inflammatory drugs such as ibuprofen have shown reduced markers of inflammation, but much like the previously described approaches, no neurological improvement was observed.[119]

Cyclodextrin (CD) based therapies have shown the most promise thus far as they form inclusion complexes that allows for removal of accumulated membrane cholesterol content. CDs are a class of cyclic oligosaccharides that are composed of 6 (α-CD), 7 (β-CD), or 8 (γ-CD) glucose molecules. CDs are water soluble molecules that have hydrophilic exteriors as the hydroxyl groups of glucose are presented on the outside of the molecule while the inside of the cavity is hydrophobic. This gives CDs the ability to potentially solubilize hydrophobic molecules in aqueous conditions as the inside of the CD cavity can shield hydrophobic species from the aqueous environment by forming inclusion complexes where the complexed molecule resides within the CD cavity during transportation. Of the many variants of CDs examined, 2-hydroxypropyl-β-cyclodextrin (HP-β-CD) has shown the most success both in animal models and clinical trials. One study involving molecular dynamic simulations suggests that CD takes up cholesterol from the lysosomal membrane in a 2:1 ratio, respectively.[120] How cholesterol is trafficked once complexed with CD is still under debate. One hypothesis suggests that CD promotes lysosomal exocytosis.[121-123] However, this idea is disputed as the total cellular cholesterol contents remain unchanged and SREBP2 gene remains suppressed. To address this pitfall in the literature, a recent study that utilized radiolabeled cholesterol and cholesterol esters suggested that cholesterol rescued by CD is redistributed by the cell primarily to the plasma membrane and endoplasmic reticulum rather than being expelled entirely via exocytosis.[124]

Unfortunately, monomeric CD that is administered intravenously suffers from drawbacks such as rapid renal clearance[125-126] as well as the inability to cross the blood brain barrier[127], thereby preventing any therapeutic effect regarding cognitive impairment. This requires NPC patients to receive high and frequent doses of monomeric CD (2000-4000 mg/kg every 1 – 2 weeks) as intrathecal injections into the spine to expose the central nervous system to CD.[128-129] Attempts to address these issues have been carried out using CD based polymers.[130] As an example, CD based polyrotaxanes have been designed to create long circulating nanoparticles which may contain dozens copies of CDs onboard the polymer core. The increased bioavailability and blood circulation is due to their high molecular weight and rod-like shape preventing rapid excretion through the kidneys as well as association of these structures with serum proteins.[131-132] These polyrotaxanes were designed with pH cleavable or targeting endcaps such as cholesterol with the goal of targeting the lysosomes via receptor mediated endocytosis or the blood brain barrier via transcytosis.[133-134] It was determined that, depending on the tissue, these polyrotaxanes could be dosed >10 fold lower concentrations than free CD.[135] In another strategy, HP-β-CD was polymerized via acetal linkages that, upon entering the lysosome, degrade into monomeric CD.[136] This agent has shown promise in penetrating the BBB as well as extending the lifespan of mice at a 5-fold lower dosage than free CD administration.

1.3.4 Cholesterol: Structure, Function, and Trafficking

Cholesterol is a type of lipid (sterol) that is present in about 20 – 40 mol% of all eukaryotic membranes where most of cholesterol present is concentrated within the plasma membrane (65% - 90%).[137-139] Its structure is based around four fused rings in a trans configuration providing a planar and rigid conformation (Figure 1.4). Two methyl groups protrude from the plane of the four-ring core. On one end of the molecule is a flexible isooctyl side chain that buries itself within

the lipid layer of the bilayer while the hydroxyl group on the other end is exposed to the aqueous environment and participates in hydrogen bonding with water and the phosphate head groups of the lipids (Figure 1.5).[140]

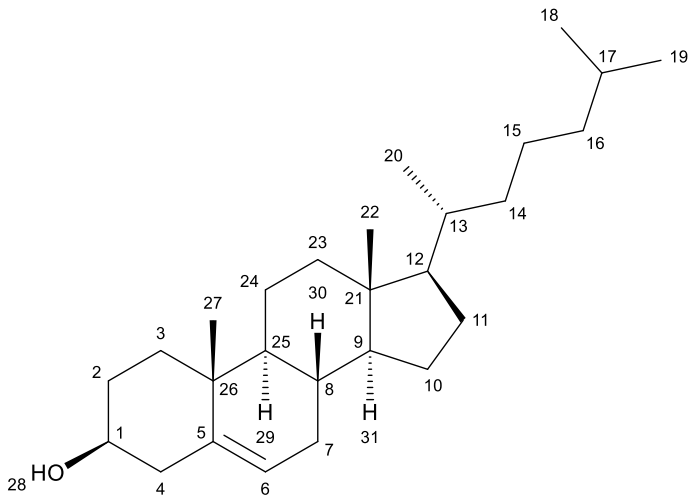

Figure 1.4. Molecular Structure of cholesterol.

Cholesterol embedded in membranes with unsaturated lipid acyl chains generally experience higher free energies (less negative) than saturated lipid acyl chains.[140-141] Interestingly, computational studies by Ermilova et al. revealed an unusually high amount of cholesterol molecules in a “flipped” conformation in which the hydroxyl group is oriented within the hydrophobic layer of lipid bilayers made up of PC containing 22:6 acyl chains, thus potentially giving rise to many possible orientations of cholesterol within a bilayer.[141] One of the main roles of cholesterol in membranes is to provide stability either by decreasing the membrane fluidity and permeability in its presence or increasing the membrane fluidity and permeability in its absence.[142] In the latter, this is accomplished by forming a membrane in the liquid disordered phase.[142-144] Importantly, cholesterol is involved in the formation of lipid rafts: complex domains containing high concentrations of saturated lipids and cholesterol that are believed to have implications in

cellular signaling. In neurons, cholesterol can operate in tandem with other phospholipids to act as insulators to facilitate the speed of electrical impulses among nerve tissue. Cholesterol is synthesized in the endoplasmic reticulum and cytoplasm by all animal cells and is a precursor for the synthesis of steroid hormones, bile acid, and vitamin D. The production of cholesterol begins with acetate where it is then synthesized into squalene by 3-hydroxy-3-methylglutaryl-coenzyme A reductase (HMG-CoA) and gets synthesized into cholesterol via a lanosertol intermediate (Figure 1.6).[145] During endocytosis, cholesterol plays an important role in the formation of intracellular vesicles in caveolae and clathrin dependent pathways. Up to 80% of daily cholesterol production takes place in the liver and intestines, although this number can vary.[32] The brain is also a site of high cholesterol production that is responsible for up to 25% of the of the total unesterified cholesterol content.[146]

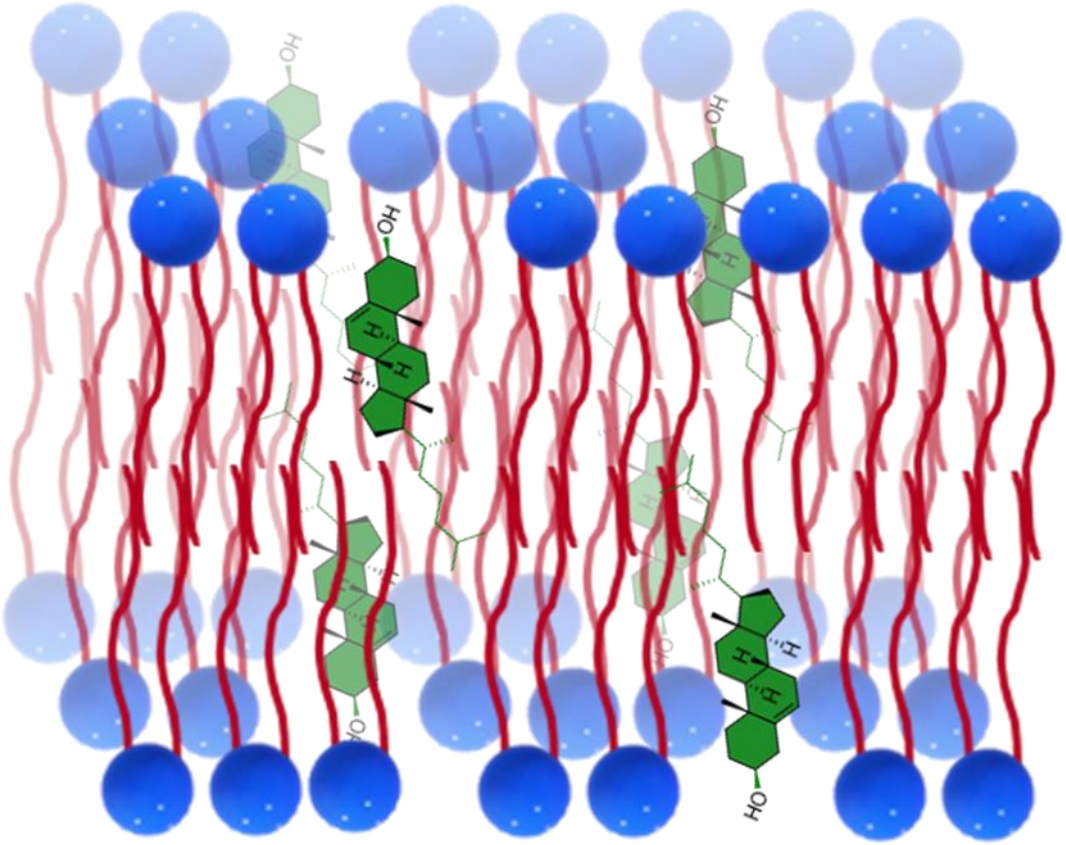

Figure 1.5. Typical orientation of cholesterol within membranes. The hydroxyl group is oriented towards the aqueous environment where it can hydrogen bond with the phosphate head groups of neighboring lipids and water. The isooctyl chain is positioned towards the interior of the bilayer near other hydrophobic regions of neighboring phospholipids and membrane proteins.

Cholesterol homeostasis in cells is regulated in a complex manner either by the sterol regulatory element binding proteins (SREBPs)[144] or the liver X receptors (LXRs).[147] In the former, increases in cellular cholesterol levels occur by way of transcription of gene products (i.e. HMG-CoA), whereas LXR activation decreases cellular cholesterol levels from peripheral cells. While the LXR pathway is known to be activated by oxysterols, the mechanisms that connect the membrane to LXR activation is not very well understood. On the other hand, the SREBP is activated in sterol-poor conditions where it transported to the Golgi for proteolytic release of the transcription factor which is then transported to the nucleus to activate sterol regulated genes such

as HMG-CoA and low-density lipoprotein receptors (LDLR). The ER-Golgi transport of SREBP is inhibited in a cholesterol rich environment where sterols induce conformational changes in the Golgi escort protein and ER anchor protein, SCAP, and INSIG, respectively. Additionally, proteasomal degradation of HMG-CoA is enhanced in the presence of lanosterol.

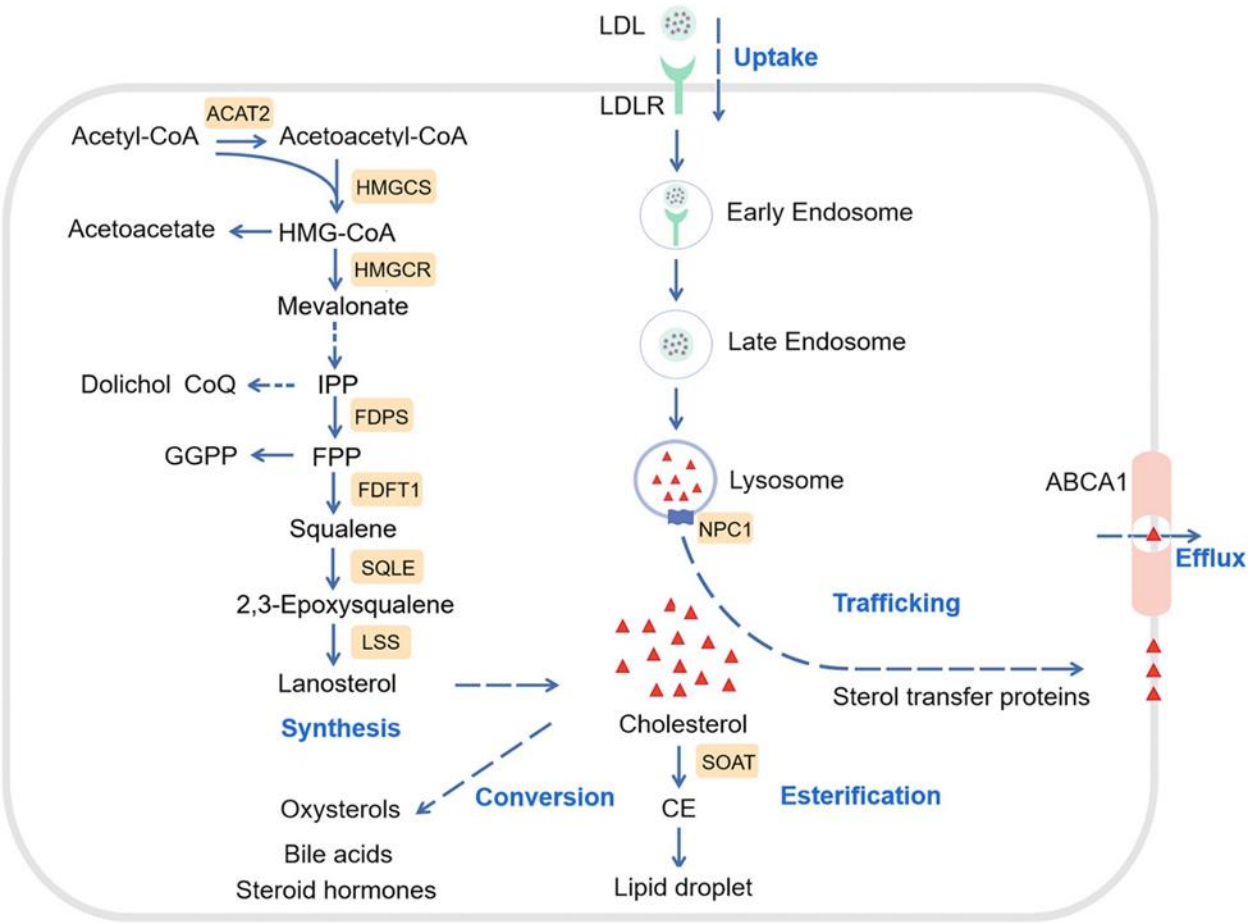

Figure 1.6. Intracellular cholesterol homeostasis and metabolism is maintained by biosynthesis, uptake, efflux, conversion, and esterification. (a) The biosynthesis pathway converts acetyl-CoA into cholesterol through nearly 30 enzymatic reactions, among which HMG-CoA and squalene epoxidase (SQLE) are the two key speed-limiting enzymes. ACAT2: Acetyl Coenzyme A Acetyltransferase 2, FDFT1: Farnesyl-diphosphate farnesyltransferase 1. (b) Most cellular cholesterol is taken in as low-density lipoproteins (LDL) via LDLR-mediated endocytosis. (c) After trafficking of cholesterol derived from LDL through the lysosome by NPC1 and NPC2, it is redistributed to the endoplasmic reticulum or plasma membrane. (d) Elevated cholesterol can be converted to cholesteryl ester (CE) by sterol O-acyltransferase (SOAT) and stored in lipid droplets or catalyzed to produce oxysterols, bile acids and steroid hormones. (e) Excess cholesterol in cells is excreted to extracellular via ABCA1/ABCG1. Figure reproduced from Xu *et al*.[145]

Humans obtain cholesterol via de novo synthesis or dietary consumption in a ratio of about 70:30, respectively.[32] This distribution can vary, however, based on genetic makeup and diets. Cells that acquire cholesterol externally do so via receptor mediated endocytosis of LDL. The LDL receptors responsible for engulfing cholesterol are present on the plasma membrane of most cells and bind Apolipoproteins B and E, both of which are responsible for transportation of cholesteryl ester nanoparticles.[148] The endocytosed cholesterol esters are then trafficked to the acidic lysosomes via MVBs where acid lipase hydrolyzes the esters to fatty acids and cholesterol. Lysosomal membranes are normally cholesterol poor while the early and recycling endosomal compartments are high in cholesterol content, which implies that cholesterol from the endosomal membrane leaves upon merging with the lysosome.[149-150] This is evidenced by the fact that cholesterol is enriched within the inner membranes of the lysosome which develop during endosome maturation.

While not impossible, it is highly unlikely that cholesterol exits the membranes of the LE/LY via spontaneous diffusion into the cytosol. Schoer *et al.* monitored the rate transfer of dehydroergosterol (DHE), a fluorescent analog of cholesterol, between various cellular donor-acceptor membranes.[151] Spontaneous diffusion from the lysosomal membrane was incredibly slow with a $t_{1/2}$ of > 4 days equating to 100-fold greater transfer rate than those found in functioning cells, 65-fold greater than plasma membranes, 42-fold greater than microsomal membranes, and 62-fold greater than the mitochondrial domains. These results make sense as cholesterol, although technically amphiphilic, is an extremely hydrophobic molecule, thus requiring the use of specialized machinery for mobilization. The LE/LY contain two proteins responsible for cholesterol trafficking: NPC1 and NPC2. Both of them are essential for normal cholesterol trafficking as aberrant accumulation of cholesterol is observed in the absence of one of the proteins.

The NPC1 protein is a large integral membrane protein consisting of 1278 amino acids and is located in the limiting membrane of the LE/LY.[152-153] It is comprised of 3 luminal domains: the N-terminal domain, domain C (middle luminal domain) and domain I. NPC1 also contains 13 transmembrane spanning domains (TM) with TMs 3 -7 make up a sterol sensing domain (SSD). Interestingly, all five SSD-forming TMs are exposed to the lipid bilayer. This might allow the SSD to be available for interactions with other membrane bound sterols as well as other integral membrane proteins.[154] A full length NPC1 cryoelectron microscopy (cryo-EM) image revealed that the NTD resides atop the other luminal domains through a proline rich linker. One can think of the NTD as being the "head" of the protein structure while the shoulder and the arms are made up by domains I and C. The N-terminal domain participates in a hydrophobic hand-off mechanism where the NPC2 protein delivers cholesterol by binding to NPC1 in a pH dependent manner (Figure 1.7).[156-158] Evidence has suggested that NPC2 binds to domain C to deliver cholesterol to NPC1 at low pH levels.[157] This further highlights the significance of the increased acidity during the maturation of the EE to the LE/LY. While the SSD's full function is not entirely understood, it is believed that this is the last stop for cholesterol in the LE/LY before being repackaged into cholesterol ester nanodroplets and transported to the plasma membrane, endoplasmic reticulum, or golgi via trafficking enzymes. NPC1 also contains a region which has been hypothesized to provide a mechanism of endosomal escape for viruses such as the Ebola virus (EBOV)[154], HIV-1[159], and SARS-CoV-2.[160] The surface glycoprotein of the endocytosed virus undergoes proteolytic cleavage of the glycoproteins present on the virus by cathepsin. Upon binding of the cleaved glycoprotein to domain C of NPC1, the viral contents are released from the endosome allowing viral infection of the host. It has also been demonstrated that NPC1 deficient cells do not result in EBOV infection while infection can still occur in NPC2 deficient cells.[161] Ironically, this

means NPC1 patients may be immune to such viruses as the mutated NPC1 protein might limit the ability of the viral contents to escape the LE/LY.

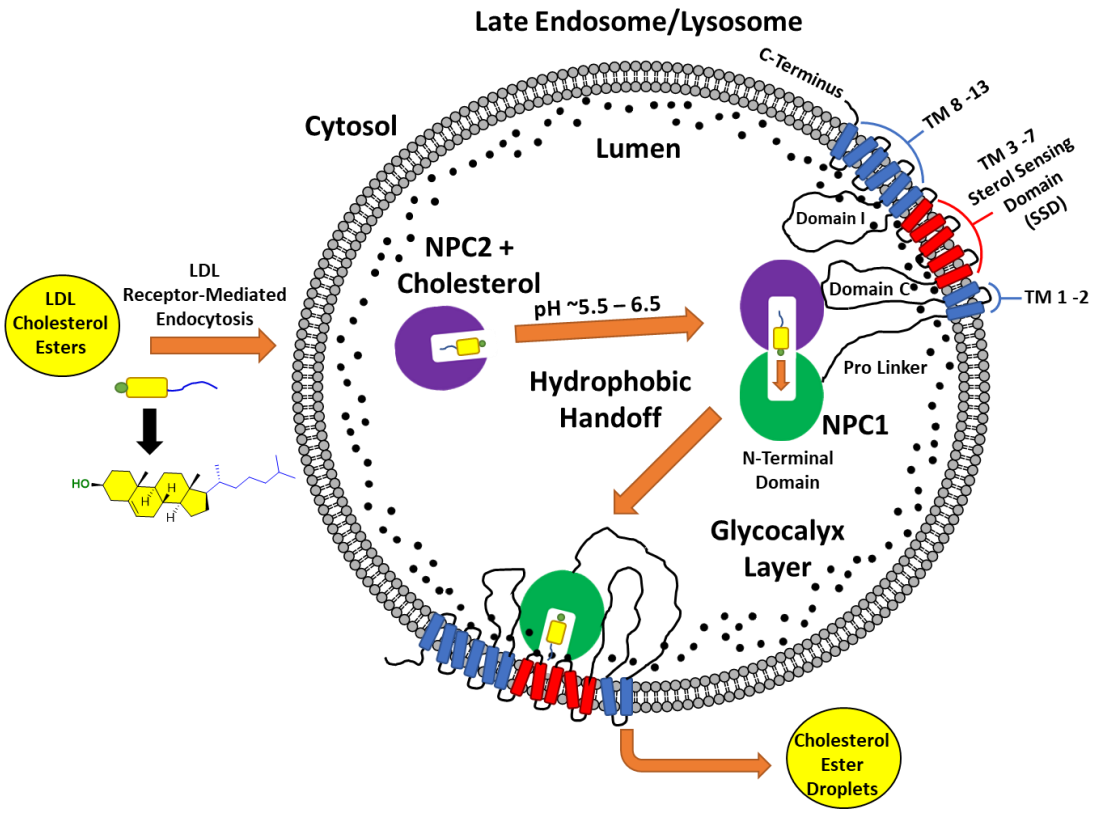

Figure 1.7. Trafficking of cholesterol by the NPC proteins. Cholesterol esters are delivered lysosome by apolipoproteins B and E via receptor-mediated endocytosis of low-density lipoproteins (LDL). Each LDL particle contains about 500 molecules of free cholesterol and about 1500 molecules of esterified cholesterol.[162] Cholesterol and cholesterol esters are situated within the binding site of the lumen-soluble NPC2 via its isooctyl chain where it works in tandem with acid lipase to hydrolyze the ester to a fatty acid that the cell can use (not shown). Hydrolysis of the fatty acid exposes the alcohol of cholesterol to the aqueous lumen of the lysosome, thus solubilizing the substrate. Under acidic conditions, NPC1 adopts a flexible conformation to accept cholesterol by a hydrophobic handoff mechanism after NPC2 binds to Domain C of NPC1. Cholesterol is then delivered to the sterol sensing domain where it is repackaged as cholesterol esters and sent to the endoplasmic reticulum, Golgi, or other organelles for further processing.

The NPC2 protein is a small single luminal domain protein consisting of 132 amino acids (14.5 kDa) (Figure 1.8).[163-164] While abundant in the human epididymis, the NPC2 protein is present in several tissues indicating a global function. NPC2 binds cholesterol in a 1:1

stoichiometry with submicromolar affinity (K_d = 30-50 nM) at both neutral and acidic pH.[165] The bovine apoNPC2 high resolution crystal structure revealed a structure composed almost exclusively of β-sheets and a loosely packed region within the protein that is believed to be a cholesterol binding site. This binding site is thought to expand as the volume of the cavity is not large enough to accommodate a cholesterol molecule as the three identified cavities collectively are only 180 $Å^3$ in volume in the fully closed form of apoNPC2 while the intermediate conformation contains an increased cavity volume of 310 $Å^3$.[164] This idea was further supported by mutagenesis studies that revealed three conserved residues essential for cholesterol binding within the binding pocket. It was later discovered that subtle repositioning of the β-sheets creates a tunnel that molds around the cholesterol molecule for binding. In sterol bound NPC2, the cavity increases to 720 A^3 which is large enough to accommodate for the hydrophobic portion of cholesterol which occupies a total volume of 740 A^3. The tunnel that forms is almost exclusively generated by hydrophobic residues being comprised of Tyr, Val, Leu, Pro, Ile, Trp, and Phe. This hydrophobic cavity accommodates for the entrance of cholesterol via its iosoctyl side chain. In this conformation, the hydroxyl group of cholesterol interacts with the aqueous lumen of the lysosome. Two aromatic amino acid residues located at the rim of the NPC2 entrance, Tyr-100 and Phe-66, π-stack to form a "gated" complex in the apoNPC2 form and separate via reposition of the β-sheets to allow the entrance of cholesterol. Residues Trp-109 and Trp-122 located inside the binding pocket are fluorescent in the absence of cholesterol, but are quenched when cholesterol is present. This fluorescence effect is particularly useful for bioanalytical assays to monitor sterol binding with NPC2.

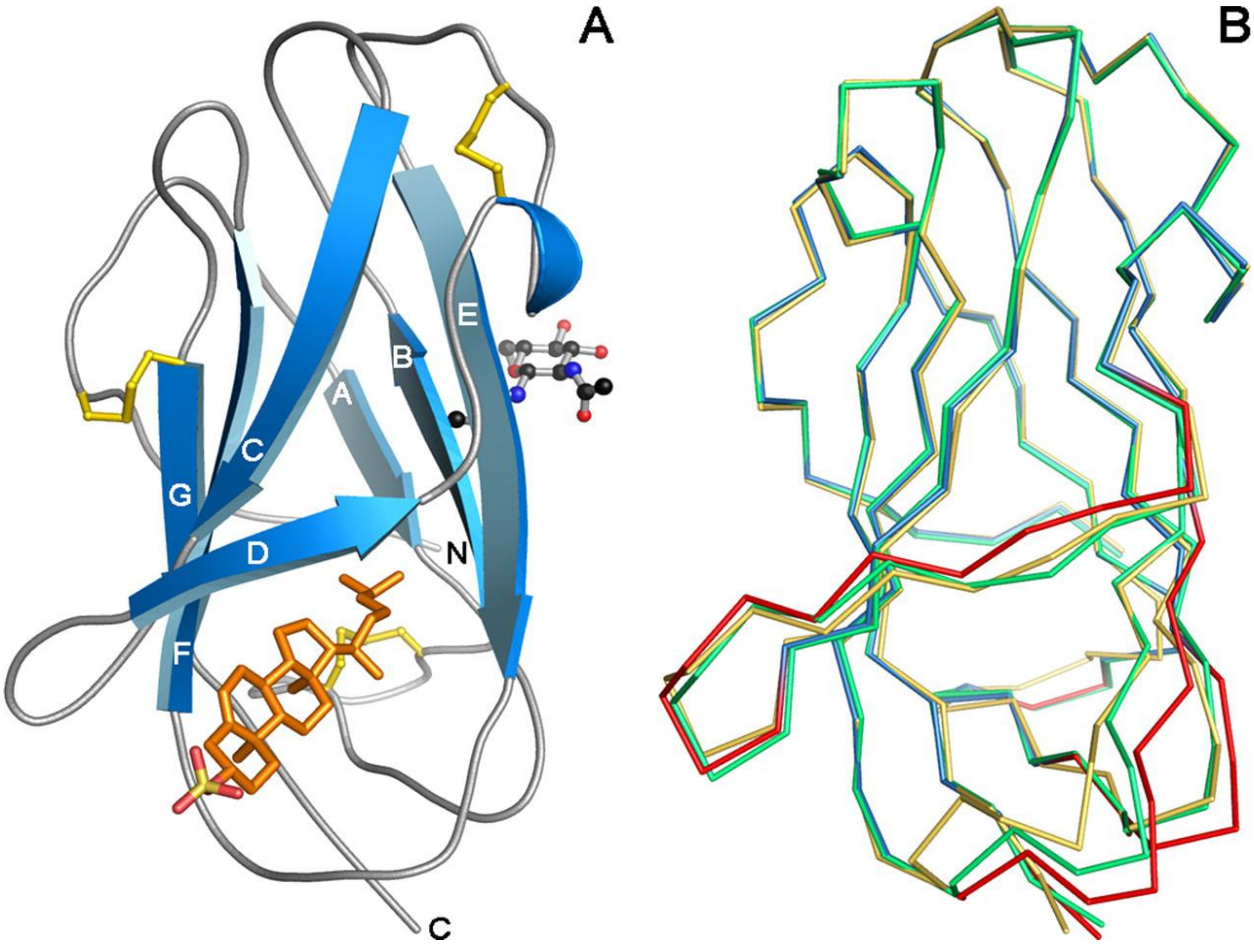

Figure 1.8. "Backbone displacements in apo- and sterol-bound NPC2. A, NPC2 is shown in ribbon representation (blue) with cholesterol sulfate (carbon in gold, oxygen in red, sulfur in yellow) bound in the protein interior between strands βD and βE. The three disulfide bonds in NPC2 (yellow) and the N-acetylglucosamine remnant of glycosylation at Asn-39 (carbon in black, oxygen in red, nitrogen in blue) are shown in stick and ball-and-stick representation, respectively. B, Cα traces of superimposed models of sterol-bound NPC2 (MolB, blue) and two apoNPC2 structures (MolA, green, and Protein Data Bank 1NEP, gold) are shown with regions of the largest displacements (r.m.s.d. >0.4 Å) highlighted in red in the model of sterol-bound NPC2." Figure reproduced from Xu *et al*.[164]

It requires approximately 4.5 x 10^5 NPC2 molecules/cell to rescue *npc2* fibroblasts.[166] Full rescue of these cells requires 2-3 days. There are ~2.5 x 10^9 cholesterol molecules per cell equating to approximately 1.5 x 10^8 cholesterol molecules present in the lysosome (~6% of total cellular cholesterol content), and in the absence of NPC1 or NPC2 this number can be up to 10-fold higher. This amounts to an excess of roughly 1.5 x 10^9 cholesterol molecules that are present in cells with

deficient NPC1 or NPC2 requiring the redistribution of about 3000 cholesterol molecules. Therefore, an estimated cholesterol mobilization rate would be 1 cholesterol molecule/NPC2 protein/minute.[166]

1.3.5 Bis(monoacylglycero)phosphate: An Important Lysosomal-Specific Phospholipid

First isolated from pig and rabbit lung in 1967 by Body and Gray[23], bis(monoacylglycero)phosphate (BMP), formerly known as lysobisphosphatidic acid (LBPA), is a negatively charged glycerophospholipid located in the ILMs of the LE/LY. BMP comprises ~15% of the lysosomal lipid population and less that 1% of the global cellular lipid population making it an important lipid for the LE/LY.[150] In alveolar macrophages BMP represents about 18% of the total cellular phospholipids, and in bacteria the distribution can be as high as 4%. BMP is primarily located on the inner membranes of the LE/LY.[168] Kobayashi *et al.* used the first anit-BMP monoclonal antibody (C64) isolated from baby hamster kidney cells to explore the structure and function of the intraluminal membranes of the lysosome. They discovered that the C64 antibody caused disorganization of the membranes and resulted in increased cholesterol accumulation that resembled an NPC phenotype. Aside from NPC2, BMP has also been shown to have interactions with other lysosomal enzymes such as heat shock protein 70, acid sphingomyelinase, phospholipase A2, and another luminal lysosomal hydrolases.[169] The composition of the acyl chains also vary as most human cells contain dioleyl (18:1-18:1) BMP[168], although arachidonic acid (20:4), linoelic acid (18:2), and docosahexanoic acid (22:6) has also been observed in significant concentrations.[170] However, these BMP levels and disrete species can vary depending on disease phenotype. In NPC1 patients, di-22:6-BMP levels have been observed to be up to 50-fold higher than normal.[171] This observation is not unique to NPC, however, as elevated BMP levels are also observed in other LSDs such as Stargardt[172], GM1 gangliosidosis[173], and Gaucher

disease[174] to name a few. Furthermore, acyl chain composition of the elevated BMP species also varies. For example, Stargardt disease results in enrichment of di-22:6 species while Gaucher disease results in increased di-18:1 species. In the case of NPC, increases in di-18:1 was the most prevalent BMP species observed.[175]

The reported structure of BMP also contains an unusual stereochemistry in that it contains an *sn*-1 phosphoglycerol backbone while most glycerophospholipids contain an *sn*-3 phosphoglycerol backbone.[176-179] The *sn*-3:*sn*-1' BMP has been isolated in baby hamster kidney cells and rat uterine stromal cells.[177, 180] However, this is believed to be an intermediate for *sn*-1:*sn*-1' BMP formation.[181] One hypothesis for this unique stereochemical arrangement might be that BMP is designed to remain inert to other lysosomal enzymes that might react with it. For example, phospholipase A2, the enzyme responsible for hydrolyzing esters on the *sn*-2 position of phospholipids, requires an *sn*-3 phosphoglycerol backbone.[182-183] BMP contains one acyl chain on both the headgroup and backbone which are believed to be located on the *sn*-2 and *sn*-2' positions of the glycerol moieties. However, it was first isolated with acyl chains being located on the *sn*-3 and *sn*-1' positions.[167] This is expected to be an intermediate in the biogenesis of BMP as the inversion of stereochemistry has not occurred. The latter configuration is more thermodynamically stable than the former[184], thus it has eluded scientists as to how BMP is synthesized biochemically and why cells have favored such a unique stereochemical configuration. It is thought that because most isolation procedures operate under mildly acidic conditions, this could catalyze an acyl chain migration from the secondary to primary alcohols and thus be the reason why it was originally isolated with both acyl chains being located on the primary positions of the glycerol moieties (Figure 1.9).

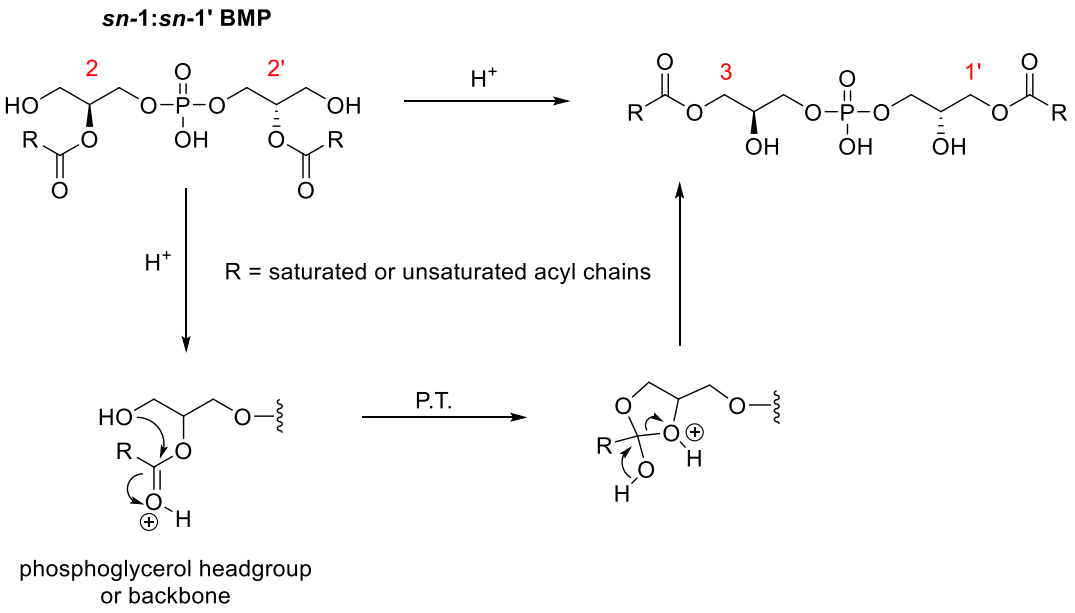

Figure 1.9. Proposed mechanism of acid-catalyzed acyl chain migration from the *sn*-2 and *sn*-2' positions of BMP to the *sn*-3 and *sn*-1' positions. P.T. = proton transfer step.

The structure of the BMP species relates to its function. Mono-, di-, or poly-unsaturated acyl chains on PL creates increasingly more separation between molecules than saturated ones due to the cis double bonds in these acyl chains, resulting in higher membrane fluidity.[185] It would, therefore, make sense that most cells favor unsaturated acyl chain BMP species in the LE/LY to enable increased vesicle fusion. With regard to positioning of the esters and unusual stereochemistry of the phosphoglycerol backbone, the same rational follows. To probe this hypothesis, various structural isomers of BMP were synthesized to examine their biophysical properties (Figure 1.10).[186] These isomers consisted of 1,3'-dimyristoyl-*sn*3:*sn*1' BMP (3,1'-DMBMP), 3,3'-dimyristoyl- *sn*1:*sn*1' BMP (1,1'-DMBMP), and 1,2-dimyristoyl-*sn*3:*sn*1' phosphatidyl glycerol (DMPG). Differential scanning calorimetry was performed on lipid films of samples to examine their thermotropic phase behavior. It was discovered that a higher phase transition temperature was associated with the 3,1'-DMBMP species than the 1,1'-DMBMP and DMPG. Small and wide-angle X-ray scattering experiments provided further insight and revealed

more tilt associated with the 1,1'-DMBMP, resulting in a smaller lamellar distance than 3,1'-DMBMP. To explain the differences between the DMBMP species, molecular dynamic simulations were conducted for membranes consisting of 128 molecules. The average tilt angles simulated for 1,1'-DMBMP and 3,1'-DMBMP were 11.6 and 20.2°, respectively, giving rise to membrane areas of approximately 0.56 nm^2 and 0.50 nm^2. Intermolecular hydrogen bonding of glycerol motifs was the explanation for these differences. These data collectively support the hypothesis that the unusual configuration associated with BMP is possibly associated with increased membrane fluidity for vesicle formation and fusion as the naturally occurring *sn*1:*sn*1' isomer packs more loosely than the synthetic *sn*3:*sn*1' isomer. Due to synthetic limitations involving acyl chain migration during the final deprotection step, the *sn*2:*sn*2' isomers were unfortunately unable to be isolated and evaluated.

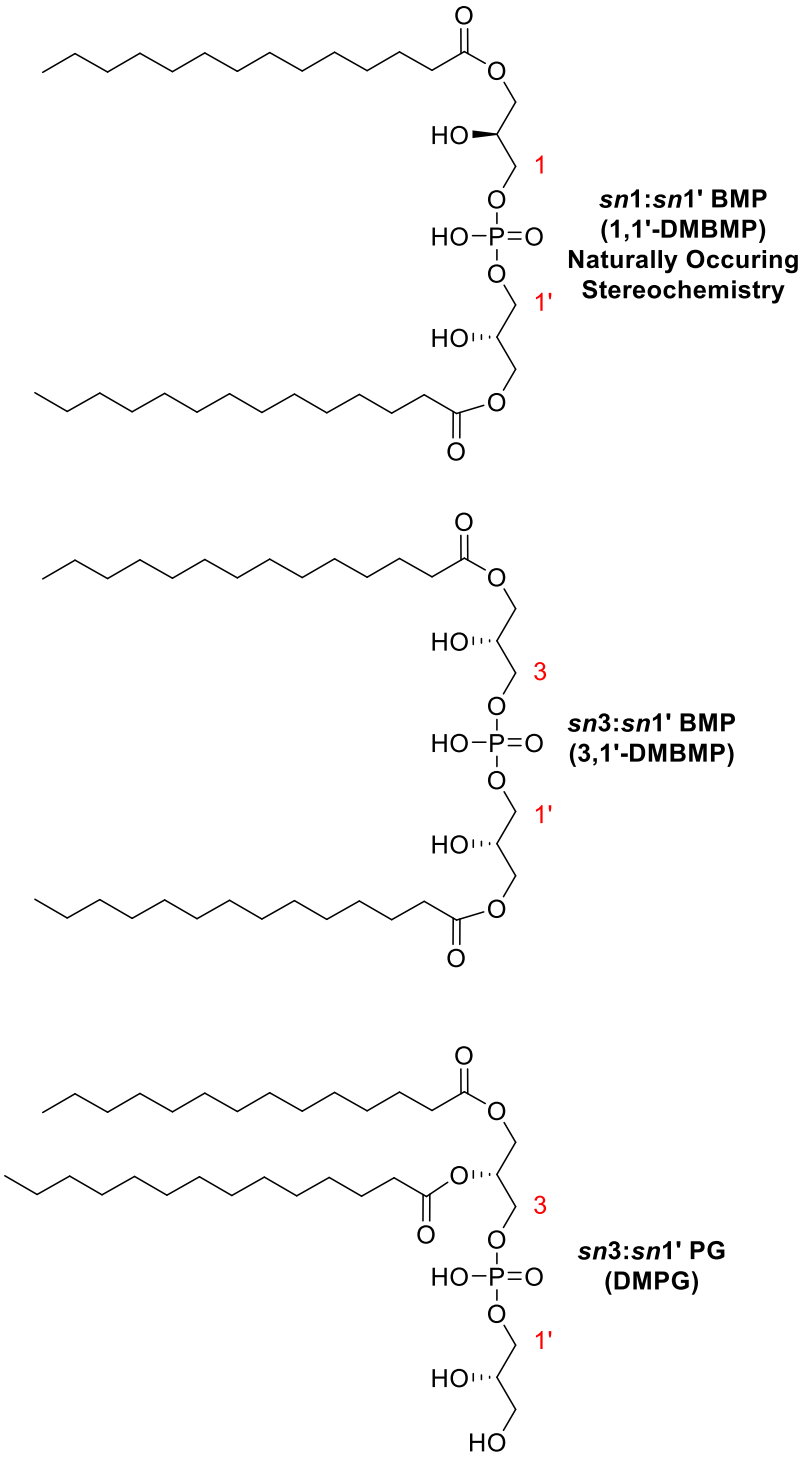

Figure 1.10. Structural isomers of BMP examined by Hayakawa *et al*.[186]

The biosynthetic pathway of BMP is still largely under debate, especially regarding the enzymes involved. It is largely believed that BMP is synthesized from a phosphatidylglycerol (PG) precursor. PG is a structural isomer of BMP. This idea was first proposed by Poorthius and Hostetler who postulated that lysosomes convert PG to BMP via a series of intermediates.[187] PG is a glycerol phospholipid with phosphodiester linkages at the *sn*-3 and *sn*-1 positions. PG not only acts as a membrane constituent, but has also been shown to be involved in the biosynthesis of other lipids including cardiolipin.[188-189] As mentioned previously, a large amount of BMP is present in lung macrophages. PG is also most abundant in the lungs comprising about 11% of the lipids present whereas it makes up only about 1-2% everywhere else in the body. Evidence has suggested that PG is a precursor to BMP, as BMP content in cells increases with increasing PG concentration.[181, 190-191] Additional evidence was presented by Hullin-Matsuda *et al.* when they demonstrated that cells lacking functional phosphatidylglycerophosphate (PGP) synthase, a key enzyme in the metabolic pathway of PG, resulted in decreased BMP synthesis by 2-fold compared to wildtype cells.[185] On the other hand, overexpression of PGP synthase resulted in a 2-5 fold increase in BMP production. Direct evidence for the metabolism of PG to BMP, however, is still lacking.

Waite and co-workers have proposed a biosynthetic pathway of PG to BMP (Figure 1.11).[181, 190-191] In the first step, a lysophosphatidylglycerol intermediate would be synthesized via hydrolysis by phospholipase A2 of the *sn*-2 ester of PG. In the second step, reacylation of lyso-PG on the *sn*-2' position would be carried out by a transacylase identified in a macrophage-like cell line. In this transformation, lyso-PG would act as both an acyl donor as well as an acyl acceptor evidenced by the formation of a glycerophosphoglycerol (GPG) species.[190] At this stage, the *sn*-1 ester would still be present on the phosphoglycerol backbone. The rearrangement of the backbone

from an *sn*-3 to an *sn*-1 configuration would most likely occur at this stage. It is still unclear whether or not this would be enzyme mediated. If it is enzyme mediated, the *sn*-1 ester could possibly be removed by phospholipase A1 or another enzyme followed by removal and reconfiguration of the naked phosphoglycerol backbone unit from an *sn*-3 phosphate to an *sn*-1 phosphate. After the stereochemical conversion, the final step would likely constitute a re-esterification of the *sn*-2 position, possibly via transacylation with another acyl donor.[190] While the beginning steps are supported with some experimental evidence, the route does not provide substantial evidence for how the required inversion of stereochemistry would be carried out. Additionally, this route does not consider other possible intermediates involved in the pathway such as the production of acyl-PG, also known as hemi-BMP, which might result.

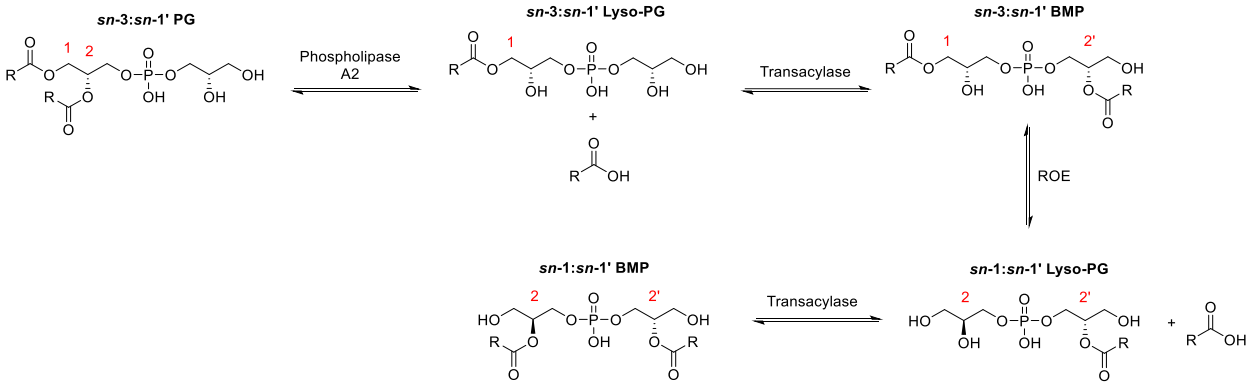

Figure 1.11. Proposed biological mechanism of PG to BMP by Waite and co-workers.[181,190-191] In the second step, a second lyso-PG intermediate is postulated to donate an acyl chain to lyso-PG yielding a GPG molecule. ROE = Reorientation enzyme.

1.3.6 The Relationship Between NPC2 and BMP

Mutations inside the binding pocket of NPC2 result in impaired rescue of cholesterol deposits from *npc2-/-* cells as expected.[163, 166] This can be attributed to the overall lower cholesterol binding observed. Interestingly, it was also determined in the same study that surface mutations present on the outside of NPC2 resulted in a normal cholesterol binding compared to the wildtype,

yet was unable to rescue *npc2-/-* cells. This surprising result led to the hypothesis that the NPC2 protein was responsible for more than just cholesterol binding, and that potentially surface interactions with membranes were involved to facilitate cholesterol trafficking within the lysosomes. To test this hypothesis, Cheruku *et al.* explored the mechanism by which NPC2 interacted with membranes by incubating the protein in small unilamellar vesicles (SUVs) comprised of different phospholipids (PL): egg phosphatidyl choline (EPC), phosphatidyl serine (PS), phosphatidyl inositol (PI), and BMP.[192] It was observed that SUVs comprised of zwitterionic PL such as EPC did not result in any noticeable cholesterol transfer to membranes while SUVs containing negatively charged anionic PL such as PS, PI, and BMP all resulted in noticeable cholesterol transfer with BMP showing the largest cholesterol transfer rate.[192-193] Furthermore, the cholesterol transfer rate increased with an increased negatively-charged PL concentration in SUVs. This experiment provided evidence that there was not only a collisional transfer mechanism of cholesterol to membranes rather than a passive diffusion of cholesterol between NPC2 and the membranes of the SUVs, but it also demonstrated that the transfer rate depended on both the charge and structure of the PL. In a follow-up study, it was determined that SUVs containing BMP had a 200-fold larger increase in cholesterol transfer than the zwitterionic SUVs containing PC when incubated with NPC2.[193] In addition, the acyl chain composition of BMP played a role, confirming the significance of a structural relationship with NPC2 rather than just electrostatic interactions. The stereochemistry of the phosphoglycerol headgroup and backbone of BMP did not seem to play a significant role, however, as small variations in cholesterol transfer were observed in three diastereomers of BMP evaluated.

While increasing the BMP concentration in *npc1-/-* cells results in increased cholesterol egress, improved cholesterol mobilization was not observed in *npc2-/-* cells.[194] Moreau *et al.* have

recently demonstrated that drug induced increases in BMP levels lead to decreased cholesterol accumulation in NPC cells.[195] By treating cells with thioperamide, an HRH_3 specific antagonist, they were able to increase the BMP concentrations in cells and decrease the cholesterol overload by about 25% compared to the control. It was noted that behavioral improvement was not observed in *npc1-/-* mice unless it was used in combination with miglustat, suggesting that raising BMP levels alone might not lead to cognitive improvement. Furthermore, treatment of cells with PG not only rescued NPC1 cells and aided in cholesterol egress, but also stimulated autophagy in Purkinje cells most likely due to the 50% increased production of BMP from PG.[196] This increase in autophagic flux was attributed to an increase in sphingomyelinase activity. Acid sphingomyelinase (ASM), an enzyme responsible for the breakdown of sphingomyelin and ceramide to phosphorylcholine, is known to be impaired in NPC1.[197-199] While its connection to autophagy is not fully understood, knock-down of ASM leads to decreased autophagosome formation while amino acid deprivation activated ASM activity in HL-60 cells.[200] Upon increased PG concentrations, it was also observed that increased autolysosome formation and intracellular redistribution of cholesterol to the plasma membrane and endoplasmic reticulum occurred, providing a potential NPC1 independent pathway for cholesterol egress from the lysosome.[196]

It should be appreciated by now that there is an apparent strong synergistic relationship between NPC2 and BMP specifically over other lysosomal membrane phospholipids leading to increased cholesterol efflux. Furthermore, this highlights the significance of the intraluminal vesicles of the LE/LY since BMP is largely enriched in these areas. The rate of cholesterol transfer as a function of BMP concentration in SUVs also increases in an exponential fashion. The protein-lipid interactions can largely be attributed to the hydrophobic knob of NPC2.[201] In bovine NPC2, a loop domain consisting largely of hydrophobic amino acids is predicted to be highly membrane

interactive with a ΔG of -4.6 kcal/mol. Interestingly, this region is located right near the opening of the protein. McCauliff *et al.* showed that point mutations on various regions of NPC2 including the hydrophobic knob portion led to lower cholesterol transfer rates in zwitterionic PC unilamellar vesicles. However, interactions between BMP-rich unilamellar vesicles and mutant NPC2 proteins yielded a different result. While mutations outside of the hydrophobic knob resulted in negligible differences in cholesterol transfer rates compared to the wild type, point mutations on the hydrophobic knob resulted in decreased cholesterol transfer rates up to 15% of the wild type. Acyl chain composition is also a factor as mentioned previously. BMP stereoisomers containing oleyl chains resulted in ~6 fold higher relative binding compared to BMP containing myristoyl chains of the same stereochemical configuration.[193] Additionally, the naturally occurring dioleyl BMP (*sn*-1:*sn*-1') displayed higher relative binding of NPC2 compared to the synthetic stereoisomers (*sn*-3:*sn*-3' and *sn*-1:*sn*-3') which showed similar binding.[193] Electrostatic interactions between NPC2 and BMP are also postulated to play a minor role in interactions. Adjacent to the hydrophobic knob is a positively charged region believed to interact with the negative charge of BMP.[201]

In addition to protein lipid interactions, NPC2 is also believed to facilitate membrane-membrane interactions via BMP as well.[202-203] It was determined from turbidity assays that when NPC2 containing mutations that affect cholesterol binding, no aggregation of membranes of zwitterionic PC SUVs were observed as fluorescence intensity did not vary compared to the control whereas the wildtype NPC2 did. In large unilamellar vesicles (LUVs) containing 25% BMP, a 16-fold increase in membrane aggregation was observed compared to 100% PC LUVS.[201] In another study by Berzina *et al.*, it was demonstrated through FRAP experiments that cholesterol transfer between the plasma membrane and LE/LY depends strongly on a functional NPC2

protein.[204] It was observed that in *npc2-/-* cells enriched with dehydroergosterol (DHE) contained a fractional intracellular DHE of ~0.5 not treated with NPC2 while treated cells contained ~0.3 intracellular DHE. Additionally, the decrease in LE/LY DHE observed was accompanied by an increase in the plasma membrane DHE levels in diseased cells treated with NPC2, possibly indicating an induction of membrane-membrane interactions by NPC2.

1.4 Specific Aims

While progress has been made in establishing relationships and functions of NPC2 and BMP within the LE/LY, many questions pertaining to the underlying mechanisms of cholesterol transport via NPC2 remain unanswered. For example, the biosynthetic pathway responsible for the production of BMP from PG, or whether PG makes BMP, lacks conclusive evidence. Both BMP and PG treatment in *npc2-/-* cells, but not *npc1-/-* cells, results in increased cholesterol egress. Is this due to the transformation of PG to BMP, thus increasing interactions with NPC2 and increasing the rate of cholesterol efflux from cells? Or does PG act in an independent manner, and the production of BMP from PG is not the primary mechanism of increased cholesterol efflux. Additionally, the acyl chain composition of PG and BMP as well as the stereochemistry of BMP have noticeable contributions in cholesterol efflux? How do NPC cells respond to PG species with different structural properties? An in-depth understanding of PG metabolism may have large implications in not only understanding the NPC disease pathology but quite possibly establishing markers for diagnostic strategies as well as revealing therapeutic opportunities.

In order to investigate the biochemical relevance of PG in NPC, synthetic probes of PG are needed to monitor its metabolism. Unfortunately, the synthetic probes required to answer these questions are not commercially available. Additionally, naturally occurring PG (*sn*-3:*sn*-1') is also not available as most PG is sold with a racemic headgroup. Therefore, a robust synthesis of PG is

required as the desired labeled fatty acids are expensive (~$4,000/g). We wanted to create PG containing ^{13}C-labeled acyl chains on the phosphoglycerol backbone. These probes allowed us to monitor the metabolic products of PG. The labeled acyl chains provided a means of lipid monitoring as acyl chain rearrangement is essential for phospholipid biosynthesis (Figure 1.12). First, labeled PG constructs were made into liposomes. From there, they were incubated with HeLa cells where they were extracted for lipidomic analysis and used in filipin staining assays of skin fibroblasts to measure cholesterol efflux. By utilizing hydrophilic interaction liquid chromatography coupled to tandem mass spectrometry (HILIC-MS/MS), the products made from PG were determined. The expected outcomes of these experiments were that a positive correlation between the concentration of ^{13}C PG administered to cells and ^{13}C BMP levels would be observed. We also anticipated an increased rate in cholesterol efflux from diseased cells arising from the expected increase in BMP concentrations. In order to obtain the most insight from these proposed experiments, PG constructs with unsymmetrical labels were required. Specifically, two probes were synthesized: an *sn*-2 labeled probe and a probe containing simultaneous labeling of both the *sn*-1 and *sn*-2 chains. This will allow us to not only be able to identify products synthesized but it will also aid in establishing potential enzyme partners involved in metabolism, an area of the literature in which empirical evidence is lacking. To further provide mechanistic insights regarding enzyme partners, synthesis of photoaffinity labeled PG probes as well that contain diazirines as the reactive functional group are currently underway. Upon irradiation with UV light, lipids may cross link inside the binding pocket of relevant enzymes, thus allowing proteomic analysis to identify protein partners. These objectives a robust and novel route towards diastereochemically pure PG to carry out the syntheses of all the proposed constructs.

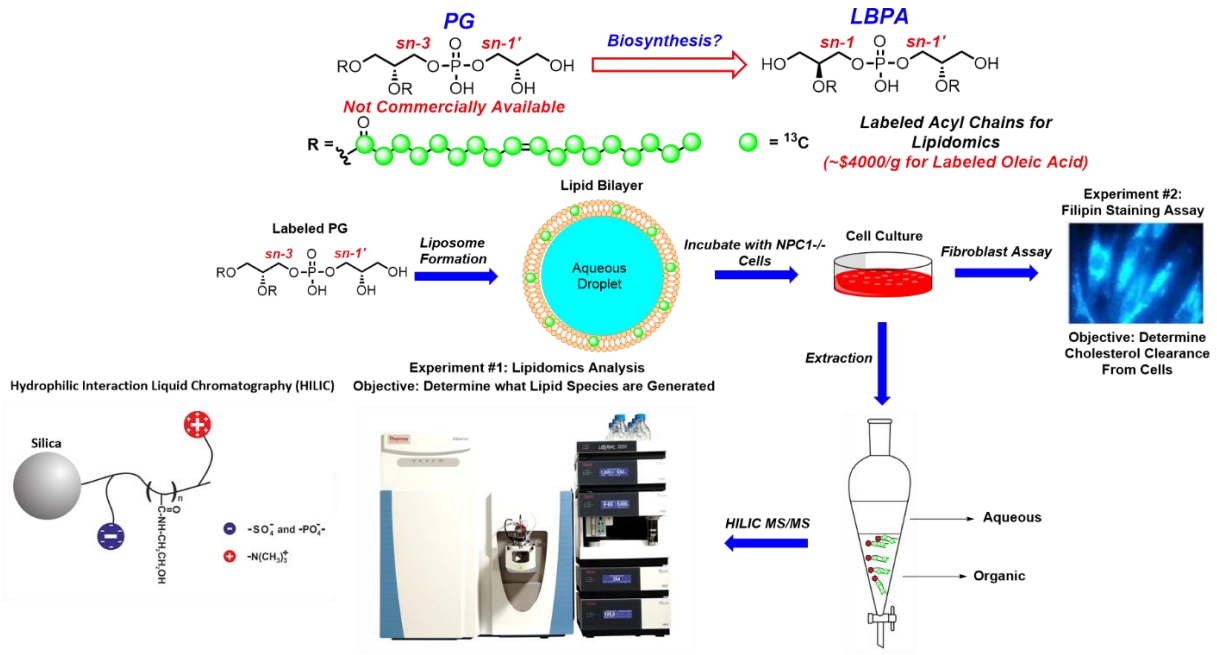

Figure 1.12. Experimental workflow of synthesized ^{13}C labeled PG probes. After synthesis of isotopically labeled PG, they were formulated into liposomes and incubated with HeLa cells or NPC1-/- cells. In one experiment, lipids were extracted and analyzed via HILIC-MS/MS where lipid products made from PG may were determined. In a separate experiment, cellular cholesterol content from skin fibroblasts of NPC patients upon treatment with PG can be evaluated.

1.5 References

1. Xu, H.; Ren, D., Lysosomal physiology. *Annual review of physiology* **2015,** *77*, 57-80.

2. de Duve, C.; Pressman, B. C.; Gianetto, R.; Wattiaux, R.; Appelmans, F., Tissue fractionation studies. 6. Intracellular distribution patterns of enzymes in rat-liver tissue*. *Biochemical Journal* **1955,** *60* (4), 604-617.

3. de Duve, C.; Wattiaux, R., Functions of Lysosomes. *Annual Review of Physiology* **1966,** *28* (1), 435-492.

4. Feher, J., 2.1 - Cell Structure. In *Quantitative Human Physiology (Second Edition)*, Feher, J., Ed. Academic Press: Boston, 2017; pp 101-119.

5. Lawrence, R. E.; Zoncu, R., The lysosome as a cellular centre for signalling, metabolism and quality control. *Nature Cell Biology* **2019,** *21* (2), 133-142.

6. Perera, R. M.; Zoncu, R., The Lysosome as a Regulatory Hub. *Annual Review of Cell and Developmental Biology* **2016,** *32* (1), 223-253.

7. Feng, X.; Yang, J., Lysosomal Calcium in Neurodegeneration. *Messenger (Los Angel)* **2016,** *5* (1-2), 56-66.

8. Coutinho, M. F.; Prata, M. J.; Alves, S., Mannose-6-phosphate pathway: A review on its role in lysosomal function and dysfunction. *Molecular Genetics and Metabolism* **2012,** *105* (4), 542-550.

9. Uzman, A., Molecular biology of the cell (4th ed.): Alberts, B., Johnson, A., Lewis, J., Raff, M., Roberts, K., and Walter, P. *Biochemistry and Molecular Biology Education* **2003,** *31* (4), 212-214.

10. Cooper, G. M., *The Cell: A Molecular Approach. 2nd edition*. Sinauer Associates 2000: 2000.

11. Solomon, V. R.; Lee, H., Chloroquine and its analogs: a new promise of an old drug for effective and safe cancer therapies. *European journal of pharmacology* **2009,** *625* (1-3), 220-33.

12. Martin, R. E.; Marchetti, R. V.; Cowan, A. I.; Howitt, S. M.; Bröer, S.; Kirk, K., Chloroquine transport via the malaria parasite's chloroquine resistance transporter. *Science (New York, N.Y.)* **2009,** *325* (5948), 1680-2.

13. Halcrow, P. W.; Geiger, J. D.; Chen, X., Overcoming Chemoresistance: Altering pH of Cellular Compartments by Chloroquine and Hydroxychloroquine. *Frontiers in Cell and Developmental Biology* **2021,** *9*.

14. Zamani, M.; Taher, J.; Adeli, K., Complex role of autophagy in regulation of hepatic lipid and lipoprotein metabolism. *J Biomed Res* **2017,** *31* (5), 377-385.

15. Jovic, M.; Sharma, M.; Rahajeng, J.; Caplan, S., The early endosome: a busy sorting station for proteins at the crossroads. *Histol Histopathol* **2010,** *25* (1), 99-112.

16. Wenzel, E. M.; Schultz, S. W.; Schink, K. O.; Pedersen, N. M.; Nähse, V.; Carlson, A.; Brech, A.; Stenmark, H.; Raiborg, C., Concerted ESCRT and clathrin recruitment waves define the timing and morphology of intraluminal vesicle formation. *Nature Communications* **2018,** *9* (1), 2932.

17. Gruenberg, J., Life in the lumen: The multivesicular endosome. *Traffic* **2020,** *21* (1), 76-93.

18. Tu, Y.; Zhao, L.; Billadeau, D. D.; Jia, D., Endosome-to-TGN Trafficking: Organelle-Vesicle and Organelle-Organelle Interactions. *Frontiers in Cell and Developmental Biology* **2020,** *8*.

19. Hers, H. G., Inborn Lysosomal Diseases. *Gastroenterology* **1965,** *48*, 625-33.

20. HERS, H., α-Glucosidase deficiency in generalized glycogen-storage disease (Pompe's disease). *Biochemical Journal* **1963,** *86* (1), 11-16.

21. Platt, F. M., Sphingolipid lysosomal storage disorders. *Nature* **2014,** *510* (7503), 68-75.

22. Cox, T. M.; Cachón-González, M. B., The cellular pathology of lysosomal diseases. *The Journal of pathology* **2012,** *226* (2), 241-54.

23. Ballabio, A.; Gieselmann, V., Lysosomal disorders: from storage to cellular damage. *Biochimica et biophysica acta* **2009,** *1793* (4), 684-96.

24. Vellodi, A., Lysosomal storage disorders. *British Journal of Haematology* **2005,** *128* (4), 413-431.

25. Hopkin, R. J.; Grabowski, G. A., Lysosomal Storage Diseases. In *Harrison's Principles of Internal Medicine, 19e*, Kasper, D.; Fauci, A.; Hauser, S.; Longo, D.; Jameson, J. L.; Loscalzo, J., Eds. McGraw-Hill Education: New York, NY, 2014.

26. Wraith, J. E.; Scarpa, M.; Beck, M.; Bodamer, O. A.; De Meirleir, L.; Guffon, N.; Meldgaard Lund, A.; Malm, G.; Van der Ploeg, A. T.; Zeman, J., Mucopolysaccharidosis type II (Hunter syndrome): a clinical review and recommendations for treatment in the era of enzyme replacement therapy. *Eur J Pediatr* **2008,** *167* (3), 267-277.

27. Cenacchi, G.; Papa, V.; Pegoraro, V.; Marozzo, R.; Fanin, M.; Angelini, C., Review: Danon disease: Review of natural history and recent advances. *Neuropathology and Applied Neurobiology* **2020,** *46* (4), 303-322.

28. Fuller, M.; Meikle, P. J.; Hopwood, J. J., Epidemiology of lysosomal storage diseases: an overview. In *Fabry Disease: Perspectives from 5 Years of FOS*, Mehta, A.; Beck, M.; Sunder-Plassmann, G., Eds. Oxford PharmaGenesis, Oxford, 2006.

29. Revel-Vilk, S.; Szer, J.; Zimran, A., Gaucher Disease and Related Lysosomal Storage Diseases. In *Williams Hematology, 10e*, Kaushansky, K.; Prchal, J. T.; Burns, L. J.; Lichtman, M. A.; Levi, M.; Linch, D. C., Eds. McGraw-Hill Education: New York, NY, 2021.

30. Zimran, A.; Gelbart, T.; Westwood, B.; Grabowski, G. A.; Beutler, E., High frequency of the Gaucher disease mutation at nucleotide 1226 among Ashkenazi Jews. *Am J Hum Genet* **1991,** *49* (4), 855-859.

31. Nalysnyk, L.; Rotella, P.; Simeone, J. C.; Hamed, A.; Weinreb, N., Gaucher disease epidemiology and natural history: a comprehensive review of the literature. *Hematology* **2017,** *22* (2), 65-73.

32. Grundy, S. M., Absorption and Metabolism of Dietary Cholesterol. *Annual Review of Nutrition* **1983,** *3* (1), 71-96.

33. Nair, V.; Belanger, E. C.; Veinot, J. P., Lysosomal storage disorders affecting the heart: a review. *Cardiovascular Pathology* **2019,** *39*, 12-24.

34. Lim, J.-A.; Li, L.; Raben, N., Pompe disease: from pathophysiology to therapy and back again. *Front Aging Neurosci* **2014,** *6*, 177-177.

35. Agbaga, M.-P.; Mandal, M. N. A.; Anderson, R. E., Retinal very long-chain PUFAs: new insights from studies on ELOVL4 protein. *Journal of lipid research* **2010,** *51* (7), 1624-1642.

36. Zernant, J.; Schubert, C.; Im, K. M.; Burke, T.; Brown, C. M.; Fishman, G. A.; Tsang, S. H.; Gouras, P.; Dean, M.; Allikmets, R., Analysis of the ABCA4 Gene by Next-Generation Sequencing. *Investigative Ophthalmology & Visual Science* **2011,** *52* (11), 8479-8487.

37. Tanna, P.; Strauss, R. W.; Fujinami, K.; Michaelides, M., Stargardt disease: clinical features, molecular genetics, animal models and therapeutic options. *British Journal of Ophthalmology* **2017,** *101* (1), 25.

38. Lieberman, A. P.; Puertollano, R.; Raben, N.; Slaugenhaupt, S.; Walkley, S. U.; Ballabio, A., Autophagy in lysosomal storage disorders. *Autophagy* **2012,** *8* (5), 719-730.

39. Myerowitz, R.; Puertollano, R.; Raben, N., Impaired autophagy: The collateral damage of lysosomal storage disorders. *EBioMedicine* **2021,** *63*, 103166.

40. Monaco, A.; Fraldi, A., Protein Aggregation and Dysfunction of Autophagy-Lysosomal Pathway: A Vicious Cycle in Lysosomal Storage Diseases. *Frontiers in Molecular Neuroscience* **2020,** *13*.

41. Vaart, A. v. d.; Griffith, J.; Reggiori, F., Exit from the Golgi Is Required for the Expansion of the Autophagosomal Phagophore in Yeast Saccharomyces cerevisiae. *Molecular Biology of the Cell* **2010,** *21* (13), 2270-2284.

42. Yamashita, S.-I.; Kanki, T., How autophagy eats large mitochondria: Autophagosome formation coupled with mitochondrial fragmentation. *Autophagy* **2017,** *13* (5), 980-981.

43. Moreau, K.; Rubinsztein, D. C., The plasma membrane as a control center for autophagy. *Autophagy* **2012,** *8* (5), 861-863.

44. Morel, E., Endoplasmic Reticulum Membrane and Contact Site Dynamics in Autophagy Regulation and Stress Response. *Frontiers in Cell and Developmental Biology* **2020,** *8*.

45. Li, F.; Guo, H.; Yang, Y.; Feng, M.; Liu, B.; Ren, X.; Zhou, H., Autophagy modulation in bladder cancer development and treatment (Review). *Oncol Rep* **2019,** *42* (5), 1647-1655.

46. Meijer, A. J.; Lorin, S.; Blommaart, E. F.; Codogno, P., Regulation of autophagy by amino acids and MTOR-dependent signal transduction. *Amino Acids* **2015,** *47* (10), 2037-2063.

47. Alers, S.; Löffler, A. S.; Wesselborg, S.; Stork, B., Role of AMPK-mTOR-Ulk1/2 in the regulation of autophagy: cross talk, shortcuts, and feedbacks. *Mol Cell Biol* **2012,** *32* (1), 2-11.

48. Sarkar, S.; Korolchuk, V. I.; Renna, M.; Imarisio, S.; Fleming, A.; Williams, A.; Garcia-Arencibia, M.; Rose, C.; Luo, S.; Underwood, B. R.; Kroemer, G.; O'Kane, C. J.; Rubinsztein, D. C., Complex inhibitory effects of nitric oxide on autophagy. *Mol Cell* **2011,** *43* (1), 19-32.

49. Ugland, H.; Naderi, S.; Brech, A.; Collas, P.; Blomhoff, H. K., cAMP induces autophagy via a novel pathway involving ERK, cyclin E and Beclin 1. *Autophagy* **2011,** *7* (10), 1199-211.

50. Criollo, A.; Maiuri, M. C.; Tasdemir, E.; Vitale, I.; Fiebig, A. A.; Andrews, D.; Molgó, J.; Díaz, J.; Lavandero, S.; Harper, F.; Pierron, G.; di Stefano, D.; Rizzuto, R.; Szabadkai, G.; Kroemer, G., Regulation of autophagy by the inositol trisphosphate receptor. *Cell Death & Differentiation* **2007,** *14* (5), 1029-1039.

51. Bootman, M. D.; Chehab, T.; Bultynck, G.; Parys, J. B.; Rietdorf, K., The regulation of autophagy by calcium signals: Do we have a consensus? *Cell calcium* **2018,** *70*, 32-46.

52. Sarkar, S.; Carroll, B.; Buganim, Y.; Maetzel, D.; Ng, Alex H. M.; Cassady, J. P.; Cohen, M. A.; Chakraborty, S.; Wang, H.; Spooner, E.; Ploegh, H.; Gsponer, J.; Korolchuk, Viktor I.; Jaenisch, R., Impaired Autophagy in the Lipid-Storage Disorder Niemann-Pick Type C1 Disease. *Cell Reports* **2013,** *5* (5), 1302-1315.

53. Guo, H.; Zhao, M.; Qiu, X.; Deis, J. A.; Huang, H.; Tang, Q.-Q.; Chen, X., Niemann-Pick type C2 deficiency impairs autophagy-lysosomal activity, mitochondrial function, and TLR signaling in adipocytes. *Journal of lipid research* **2016,** *57* (9), 1644-1658.

54. Lee, H.; Lee, J. K.; Park, M. H.; Hong, Y. R.; Marti, H. H.; Kim, H.; Okada, Y.; Otsu, M.; Seo, E.-J.; Park, J.-H.; Bae, J.-H.; Okino, N.; He, X.; Schuchman, E. H.; Bae, J.-s.; Jin, H. K., Pathological roles of the VEGF/SphK pathway in Niemann–Pick type C neurons. *Nature Communications* **2014,** *5* (1), 5514.

55. Sarkar, S.; Carroll, B.; Buganim, Y.; Maetzel, D.; Ng, A. H.; Cassady, J. P.; Cohen, M. A.; Chakraborty, S.; Wang, H.; Spooner, E.; Ploegh, H.; Gsponer, J.; Korolchuk, V. I.; Jaenisch, R., Impaired autophagy in the lipid-storage disorder Niemann-Pick type C1 disease. *Cell Rep* **2013,** *5* (5), 1302-15.

56. Chou, J. Y.; Jun, H. S.; Mansfield, B. C., Glycogen storage disease type I and G6Pase-β deficiency: etiology and therapy. *Nature reviews. Endocrinology* **2010,** *6* (12), 676-88.

57. Farah, B. L.; Landau, D. J.; Wu, Y.; Sinha, R. A.; Loh, A.; Bay, B.-H.; Koeberl, D. D.; Yen, P. M., Renal endoplasmic reticulum stress is coupled to impaired autophagy in a mouse model of GSD Ia. *Molecular Genetics and Metabolism* **2017,** *122* (3), 95-98.

58. Palhegyi, A. M.; Seranova, E.; Dimova, S.; Hoque, S.; Sarkar, S., Biomedical Implications of Autophagy in Macromolecule Storage Disorders. *Frontiers in Cell and Developmental Biology* **2019,** *7*.

59. SOKAL, J. E.; LOWE, C. U.; SARCIONE, E. J., Liver Glycogen Disease (Von Gierke's Disease). *Archives of Internal Medicine* **1962,** *109* (5), 612-624.

60. Farah, B. L.; Landau, D. J.; Sinha, R. A.; Brooks, E. D.; Wu, Y.; Fung, S. Y. S.; Tanaka, T.; Hirayama, M.; Bay, B.-H.; Koeberl, D. D.; Yen, P. M., Induction of autophagy improves hepatic lipid metabolism in glucose-6-phosphatase deficiency. *Journal of Hepatology* **2016,** *64* (2), 370-379.

61. Nitschke, F.; Ahonen, S. J.; Nitschke, S.; Mitra, S.; Minassian, B. A., Lafora disease — from pathogenesis to treatment strategies. *Nature Reviews Neurology* **2018,** *14* (10), 606-617.

62. Criado, O.; Aguado, C.; Gayarre, J.; Duran-Trio, L.; Garcia-Cabrero, A. M.; Vernia, S.; San Millán, B.; Heredia, M.; Romá-Mateo, C.; Mouron, S.; Juana-López, L.; Domínguez, M.; Navarro, C.; Serratosa, J. M.; Sanchez, M.; Sanz, P.; Bovolenta, P.; Knecht, E.; Rodriguez de Cordoba, S., Lafora bodies and neurological defects in malin-deficient mice correlate with impaired autophagy. *Human molecular genetics* **2012,** *21* (7), 1521-33.

63. Knopman, D. S.; Amieva, H.; Petersen, R. C.; Chételat, G.; Holtzman, D. M.; Hyman, B. T.; Nixon, R. A.; Jones, D. T., Alzheimer disease. *Nature Reviews Disease Primers* **2021,** *7* (1), 33.

64. Lee, J. H.; Yu, W. H.; Kumar, A.; Lee, S.; Mohan, P. S.; Peterhoff, C. M.; Wolfe, D. M.; Martinez-Vicente, M.; Massey, A. C.; Sovak, G.; Uchiyama, Y.; Westaway, D.; Cuervo, A. M.; Nixon, R. A., Lysosomal proteolysis and autophagy require presenilin 1 and are disrupted by Alzheimer-related PS1 mutations. *Cell* **2010,** *141* (7), 1146-58.

65. Kelly, J. M.; Bradbury, A.; Martin, D. R.; Byrne, M. E., Emerging therapies for neuropathic lysosomal storage disorders. *Progress in Neurobiology* **2017,** *152*, 166-180.

66. Evans, W. R. H.; Hendriksz, C. J., Niemann-Pick type C disease - the tip of the iceberg? A review of neuropsychiatric presentation, diagnosis and treatment. *BJPsych Bull* **2017,** *41* (2), 109-114.

67. Wilcox, W. R., Lysosomal storage disorders: the need for better pediatric recognition and comprehensive care. *The Journal of pediatrics* **2004,** *144* (5 Suppl), S3-14.

68. Marsden, D.; Levy, H., Newborn screening of lysosomal storage disorders. *Clinical chemistry* **2010,** *56* (7), 1071-9.

69. Peelen, G. O.; de Jong, J. G.; Wevers, R. A., HPLC analysis of oligosaccharides in urine from oligosaccharidosis patients. *Clinical chemistry* **1994,** *40* (6), 914-21.

70. McLaren, J.; Ng, W. G., Radial and linear thin-layer chromatographic prodedures compared for screening urines to detect oligosaccharidoses. *Clinical chemistry* **1979,** *25* (7), 1289-92.

71. Meikle, P. J.; Fietz, M. J.; Hopwood, J. J., Diagnosis of lysosomal storage disorders: current techniques and future directions. *Expert Review of Molecular Diagnostics* **2004,** *4* (5), 677-691.

72. Harzer, K.; Rolfs, A.; Bauer, P.; Zschiesche, M.; Mengel, E.; Backes, J.; Kustermann-Kuhn, B.; Bruchelt, G.; van Diggelen, O. P.; Mayrhofer, H.; Krägeloh-Mann, I., Niemann-Pick disease type A and B are clinically but also enzymatically heterogeneous: pitfall in the laboratory diagnosis of sphingomyelinase deficiency associated with the mutation Q292 K. *Neuropediatrics* **2003,** *34* (6), 301-6.

73. Zech, M.; Nübling, G.; Castrop, F.; Jochim, A.; Schulte, E. C.; Mollenhauer, B.; Lichtner, P.; Peters, A.; Gieger, C.; Marquardt, T.; Vanier, M. T.; Latour, P.; Klünemann, H.; Trenkwalder, C.; Diehl-Schmid, J.; Perneczky, R.; Meitinger, T.; Oexle, K.; Haslinger, B.; Lorenzl, S.; Winkelmann, J., Niemann-Pick C disease gene mutations and age-related neurodegenerative disorders. *PloS one* **2013,** *8* (12), e82879.

74. Pomponio, R. J.; Cabrera-Salazar, M. A.; Echeverri, O. Y.; Miller, G.; Barrera, L. A., Gaucher disease in Colombia: mutation identification and comparison to other Hispanic populations. *Mol Genet Metab* **2005,** *86* (4), 466-72.

75. Slatko, B. E.; Gardner, A. F.; Ausubel, F. M., Overview of Next-Generation Sequencing Technologies. *Curr Protoc Mol Biol* **2018,** *122* (1), e59-e59.

76. Tsai, A. C.; Hung, Y. W.; Harding, C.; Koeller, D. M.; Wang, J.; Wong, L. C., Next generation deep sequencing corrects diagnostic pitfalls of traditional molecular approach in a patient with prenatal onset of Pompe disease. *American journal of medical genetics. Part A* **2017,** *173* (9), 2500-2504.

77. Desnick, R. J.; Thorpe, S. R.; Fiddler, M. B., Toward enzyme therapy for lysosomal storage diseases. *Physiological Reviews* **1976,** *56* (1), 57-99.

78. Bellettato, C. M.; Scarpa, M., Possible strategies to cross the blood–brain barrier. *Italian Journal of Pediatrics* **2018,** *44* (2), 131.

79. Barar, J.; Rafi, M. A.; Pourseif, M. M.; Omidi, Y., Blood-brain barrier transport machineries and targeted therapy of brain diseases. *Bioimpacts* **2016,** *6* (4), 225-248.

80. Li, M., Enzyme Replacement Therapy: A Review and Its Role in Treating Lysosomal Storage Diseases. *Pediatric Annals* **2018,** *47* (5), e191-e197.

81. King, B.; Setford, M. L.; Hassiotis, S.; Trim, P. J.; Duplock, S.; Tucker, J. N.; Hattersley, K.; Snel, M. F.; Hopwood, J. J.; Hemsley, K. M., Low-dose, continual enzyme delivery ameliorates some aspects of established brain disease in a mouse model of a childhood-onset neurodegenerative disorder. *Experimental neurology* **2016,** *278*, 11-21.

82. Salvalaio, M.; Rigon, L.; Belletti, D.; D'Avanzo, F.; Pederzoli, F.; Ruozi, B.; Marin, O.; Vandelli, M. A.; Forni, F.; Scarpa, M.; Tomanin, R.; Tosi, G., Targeted Polymeric Nanoparticles for Brain Delivery of High Molecular Weight Molecules in Lysosomal Storage Disorders. *PloS one* **2016,** *11* (5), e0156452-e0156452.

83. Zhang, T.-T.; Li, W.; Meng, G.; Wang, P.; Liao, W., Strategies for transporting nanoparticles across the blood–brain barrier. *Biomaterials Science* **2016,** *4* (2), 219-229.

84. Chowdhury, A.; Kunjiappan, S.; Panneerselvam, T.; Somasundaram, B.; Bhattacharjee, C., Nanotechnology and nanocarrier-based approaches on treatment of degenerative diseases. *International Nano Letters* **2017,** *7* (2), 91-122.

85. Rojo, J.; Sousa-Herves, A.; Mascaraque, A., 1.24 - Perspectives of Carbohydrates in Drug Discovery. In *Comprehensive Medicinal Chemistry III*, Chackalamannil, S.; Rotella, D.; Ward, S. E., Eds. Elsevier: Oxford, 2017; pp 577-610.

86. Bhattacharjee, S., DLS and zeta potential - What they are and what they are not? *Journal of controlled release : official journal of the Controlled Release Society* **2016,** *235*, 337-351.

87. Patra, J. K.; Das, G.; Fraceto, L. F.; Campos, E. V. R.; Rodriguez-Torres, M. d. P.; Acosta-Torres, L. S.; Diaz-Torres, L. A.; Grillo, R.; Swamy, M. K.; Sharma, S.; Habtemariam, S.; Shin, H.-S., Nano based drug delivery systems: recent developments and future prospects. *Journal of Nanobiotechnology* **2018,** *16* (1), 71.

88. Grosso, A. D.; Galliani, M.; Angella, L.; Santi, M.; Tonazzini, I.; Parlanti, G.; Signore, G.; Cecchini, M., Brain-targeted enzyme-loaded nanoparticles: A breach through the blood-brain barrier for enzyme replacement therapy in Krabbe disease. *Science Advances* **2019,** *5* (11), eaax7462.

89. Svennerholm, L.; Vanier, M. T.; Månsson, J. E., Krabbe disease: a galactosylsphingosine (psychosine) lipidosis. *Journal of lipid research* **1980,** *21* (1), 53-64.

90. Edelmann, M. J.; Maegawa, G. H. B., CNS-Targeting Therapies for Lysosomal Storage Diseases: Current Advances and Challenges. *Frontiers in Molecular Biosciences* **2020,** *7*.

91. Boucher, A. A.; Miller, W.; Shanley, R.; Ziegler, R.; Lund, T.; Raymond, G.; Orchard, P. J., Long-term outcomes after allogeneic hematopoietic stem cell transplantation for metachromatic leukodystrophy: the largest single-institution cohort report. *Orphanet journal of rare diseases* **2015,** *10*, 94-94.

92. Daya, S.; Berns, K. I., Gene therapy using adeno-associated virus vectors. *Clin Microbiol Rev* **2008,** *21* (4), 583-593.

93. Liu, D.; Zhu, M.; Zhang, Y.; Diao, Y., Crossing the blood-brain barrier with AAV vectors. *Metabolic Brain Disease* **2021,** *36* (1), 45-52.

94. Weismann, C. M.; Ferreira, J.; Keeler, A. M.; Su, Q.; Qui, L.; Shaffer, S. A.; Xu, Z.; Gao, G.; Sena-Esteves, M., Systemic AAV9 gene transfer in adult GM1 gangliosidosis mice reduces lysosomal storage in CNS and extends lifespan. *Human molecular genetics* **2015,** *24* (15), 4353-4364.

95. Yasuda, M.; Huston, M. W.; Pagant, S.; Gan, L.; St Martin, S.; Sproul, S.; Richards, D.; Ballaron, S.; Hettini, K.; Ledeboer, A.; Falese, L.; Cao, L.; Lu, Y.; Holmes, M. C.; Meyer, K.; Desnick, R. J.; Wechsler, T., AAV2/6 Gene Therapy in a Murine Model of Fabry Disease Results in Supraphysiological Enzyme Activity and Effective Substrate Reduction. *Mol Ther Methods Clin Dev* **2020,** *18*, 607-619.

96. Salabarria, S. M.; Nair, J.; Clement, N.; Smith, B. K.; Raben, N.; Fuller, D. D.; Byrne, B. J.; Corti, M., Advancements in AAV-mediated Gene Therapy for Pompe Disease. *J Neuromuscul Dis* **2020,** *7* (1), 15-31.

97. Vanier, M. T., Niemann-Pick disease type C. *Orphanet Journal of Rare Diseases* **2010,** *5* (1), 16.

98. Bloom, W., Splenomegaly (Type Gaucher) and Lipoid-Histiocytosis (Type Niemann). *Am J Pathol* **1925,** *1* (6), 595-626.9.

99. Pick, L., Über die lipoidzellige splenohepatomegalie typus Niemann-Pick als stoffwechselerkrankung. *Med. Klin* **1927,** *23*, 1483-1486.

100. Schuchmann, E. H.; McGovern, M.; Simonaro, C. M.; Wasserstein, M. P.; Desnick, R. J., Acid Sphingomyelinase-Deficient Niemann–Pick Disease. In *Lysosomal Storage Disorders*, Barranger, J. A.; Cabrera-Salazar, M. A., Eds. Springer US: Boston, MA, 2007; pp 257-268.

101. Schuchman, E. H.; Desnick, R. J., Types A and B Niemann-Pick disease. *Molecular Genetics and Metabolism* **2017,** *120* (1), 27-33.

102. Morris, J. A.; Zhang, D.; Coleman, K. G.; Nagle, J.; Pentchev, P. G.; Carstea, E. D., The genomic organization and polymorphism analysis of the human Niemann-Pick C1 gene. *Biochemical and biophysical research communications* **1999,** *261* (2), 493-8.

103. Naureckiene, S.; Sleat, D. E.; Lackland, H.; Fensom, A.; Vanier, M. T.; Wattiaux, R.; Jadot, M.; Lobel, P., Identification of HE1 as the Second Gene of Niemann-Pick C Disease. *Science (New York, N.Y.)* **2000,** *290* (5500), 2298-2301.

104. Kanfer, J. N.; Young, O. M.; Shapiro, D.; Brady, R. O., The metabolism of sphingomyelin. I. Purification and properties of a sphingomyelin-cleaving enzyme from rat liver tissue. *The Journal of biological chemistry* **1966,** *241* (5), 1081-4.

105. Brady, R. O.; Kanfer, J. N.; Mock, M. B.; Fredrickson, D. S., The metabolism of sphingomyelin. II. Evidence of an enzymatic deficiency in Niemann-Pick diseae. *Proceedings of the National Academy of Sciences of the United States of America* **1966,** *55* (2), 366-9.

106. Burton, B. K.; Ellis, A. G.; Orr, B.; Chatlani, S.; Yoon, K.; Shoaff, J. R.; Gallo, D., Estimating the prevalence of Niemann-Pick disease type C (NPC) in the United States. *Molecular Genetics and Metabolism* **2021,** *134* (1), 182-187.

107. Kruth, H. S.; Comly, M. E.; Butler, J. D.; Vanier, M. T.; Fink, J. K.; Wenger, D. A.; Patel, S.; Pentchev, P. G., Type C Niemann-Pick disease. Abnormal metabolism of low density lipoprotein in homozygous and heterozygous fibroblasts. *Journal of Biological Chemistry* **1986,** *261* (35), 16769-16774.

108. Pentchev, P. G.; Kruth, H. S.; Comly, M. E.; Butler, J. D.; Vanier, M. T.; Wenger, D. A.; Patel, S., Type C Niemann-Pick disease. A parallel loss of regulatory responses in both the uptake and esterification of low density lipoprotein-derived cholesterol in cultured fibroblasts. *Journal of Biological Chemistry* **1986,** *261* (35), 16775-16780.

109. Geberhiwot, T.; Moro, A.; Dardis, A.; Ramaswami, U.; Sirrs, S.; Marfa, M. P.; Vanier, M. T.; Walterfang, M.; Bolton, S.; Dawson, C.; Héron, B.; Stampfer, M.; Imrie, J.; Hendriksz, C.; Gissen, P.; Crushell, E.; Coll, M. J.; Nadjar, Y.; Klünemann, H.; Mengel, E.; Hrebicek, M.; Jones, S. A.; Ory, D.; Bembi, B.; Patterson, M.; on behalf of the International Niemann-Pick Disease, R., Consensus clinical management guidelines for Niemann-Pick disease type C. *Orphanet Journal of Rare Diseases* **2018,** *13* (1), 50.

110. Sitarska, D.; Ługowska, A., Laboratory diagnosis of the Niemann-Pick type C disease: an inherited neurodegenerative disorder of cholesterol metabolism. *Metabolic brain disease* **2019,** *34* (5), 1253-1260.

111. Ribas, G. S.; Souza, H. M.; de Mari, J.; Deon, M.; Mescka, C.; Saraiva-Pereira, M. L.; Kessler, R.; Trapp, F.; Michelin, K.; Burin, M.; Vargas, C. R.; Giugliani, R., Selective screening of Niemann-Pick type C Brazilian patients by cholestane-3β,5α,6β-triol and chitotriosidase measurements followed by filipin staining and NPC1/NPC2 gene analysis. *Clinica chimica acta; international journal of clinical chemistry* **2016,** *459*, 57-62.

112. Porter, F. D.; Scherrer, D. E.; Lanier, M. H.; Langmade, S. J.; Molugu, V.; Gale, S. E.; Olzeski, D.; Sidhu, R.; Dietzen, D. J.; Fu, R.; Wassif, C. A.; Yanjanin, N. M.; Marso, S. P.; House, J.; Vite, C.; Schaffer, J. E.; Ory, D. S., Cholesterol oxidation products are sensitive and specific blood-based biomarkers for Niemann-Pick C1 disease. *Science translational medicine* **2010,** *2* (56), 56ra81.

113. Wassif, C. A.; Cross, J. L.; Iben, J.; Sanchez-Pulido, L.; Cougnoux, A.; Platt, F. M.; Ory, D. S.; Ponting, C. P.; Bailey-Wilson, J. E.; Biesecker, L. G.; Porter, F. D., High incidence of unrecognized visceral/neurological late-onset Niemann-Pick disease, type C1, predicted by analysis of massively parallel sequencing data sets. *Genetics in Medicine* **2016,** *18* (1), 41-48.

114. Reid, P. C.; Lin, S.; Vanier, M. T.; Ohno-Iwashita, Y.; Harwood, H. J., Jr.; Hickey, W. F.; Chang, C. C.; Chang, T. Y., Partial blockage of sterol biosynthesis with a squalene synthase inhibitor in early postnatal Niemann-Pick type C npcnih null mice brains reduces neuronal cholesterol accumulation, abrogates astrogliosis, but may inhibit myelin maturation. *Journal of neuroscience methods* **2008,** *168* (1), 15-25.

115. Erickson, R. P.; Garver, W. S.; Camargo, F.; Hossain, G. S.; Heidenreich, R. A., Pharmacological and genetic modifications of somatic cholesterol do not substantially alter the course of CNS disease in Niemann-Pick C mice. *Journal of inherited metabolic disease* **2000,** *23* (1), 54-62.

116. Patterson, M., Niemann-Pick Disease Type C. In *GeneReviews(®)*, Adam, M. P.; Ardinger, H. H.; Pagon, R. A.; Wallace, S. E.; Bean, L. J. H.; Gripp, K. W.; Mirzaa, G. M.; Amemiya, A., Eds. University of Washington, Seattle, **1993**.

117. Pineda, M.; Walterfang, M.; Patterson, M. C., Miglustat in Niemann-Pick disease type C patients: a review. *Orphanet journal of rare diseases* **2018,** *13* (1), 140-140.

118. Madra, M.; Sturley, S. L., Niemann-Pick type C pathogenesis and treatment: from statins to sugars. *Clin Lipidol* **2010,** *5* (3), 387-395.

119. Smith, D.; Wallom, K. L.; Williams, I. M.; Jeyakumar, M.; Platt, F. M., Beneficial effects of anti-inflammatory therapy in a mouse model of Niemann-Pick disease type C1. *Neurobiology of disease* **2009,** *36* (2), 242-51.

120. López, C. A.; de Vries, A. H.; Marrink, S. J., Computational microscopy of cyclodextrin mediated cholesterol extraction from lipid model membranes. *Scientific Reports* **2013,** *3* (1), 2071.

121. Chen, F. W.; Li, C.; Ioannou, Y. A., Cyclodextrin Induces Calcium-Dependent Lysosomal Exocytosis. *PloS one* **2010,** *5* (11), e15054.

122. Demais, V.; Barthélémy, A.; Perraut, M.; Ungerer, N.; Keime, C.; Reibel, S.; Pfrieger, F. W., Reversal of Pathologic Lipid Accumulation in NPC1-Deficient Neurons by Drug-Promoted Release of LAMP1-Coated Lamellar Inclusions. *The Journal of neuroscience : the official journal of the Society for Neuroscience* **2016,** *36* (30), 8012-25.

123. Vacca, F.; Vossio, S.; Mercier, V.; Moreau, D.; Johnson, S.; Scott, C. C.; Montoya, J. P.; Moniatte, M.; Gruenberg, J., Cyclodextrin triggers MCOLN1-dependent endo-lysosome secretion in Niemann-Pick type C cells. *Journal of lipid research* **2019,** *60* (4), 832-843.

124. Feltes, M.; Gale, S. E.; Moores, S.; Ory, D. S.; Schaffer, J. E., Monitoring the itinerary of lysosomal cholesterol in Niemann-Pick Type C1-deficient cells after cyclodextrin treatment. *Journal of lipid research* **2020,** *61* (3), 403-412.

125. Váradi, J.; Hermenean, A.; Gesztelyi, R.; Jeney, V.; Balogh, E.; Majoros, L.; Malanga, M.; Fenyvesi, É.; Szente, L.; Bácskay, I.; Vecsernyés, M.; Fehér, P.; Ujhelyi, Z.; Vasvári, G.; Árvai, I.; Rusznyák, Á.; Balta, C.; Herman, H.; Fenyvesi, F., Pharmacokinetic Properties of Fluorescently Labelled Hydroxypropyl-Beta-Cyclodextrin. *Biomolecules* **2019,** *9* (10), 509.

126. Frijlink, H. W.; Visser, J.; Hefting, N. R.; Oosting, R.; Meijer, D. K.; Lerk, C. F., The pharmacokinetics of beta-cyclodextrin and hydroxypropyl-beta-cyclodextrin in the rat. *Pharmaceutical research* **1990,** *7* (12), 1248-52.

127. Calias, P., 2-Hydroxypropyl-β-cyclodextrins and the Blood-Brain Barrier: Considerations for Niemann-Pick Disease Type C1. *Current pharmaceutical design* **2017,** *23* (40), 6231-6238.

128. Tanaka, Y.; Yamada, Y.; Ishitsuka, Y.; Matsuo, M.; Shiraishi, K.; Wada, K.; Uchio, Y.; Kondo, Y.; Takeo, T.; Nakagata, N.; Higashi, T.; Motoyama, K.; Arima, H.; Mochinaga, S.; Higaki, K.; Ohno, K.; Irie, T., Efficacy of 2-Hydroxypropyl-β-cyclodextrin in Niemann-Pick Disease Type C Model Mice and Its Pharmacokinetic Analysis in a Patient with the Disease. *Biological & pharmaceutical bulletin* **2015,** *38* (6), 844-51.

129. Maarup, T. J.; Chen, A. H.; Porter, F. D.; Farhat, N. Y.; Ory, D. S.; Sidhu, R.; Jiang, X.; Dickson, P. I., Intrathecal 2-hydroxypropyl-beta-cyclodextrin in a single patient with Niemann-Pick C1. *Molecular genetics and metabolism* **2015,** *116* (1-2), 75-79.

130. Kost, B.; Brzeziński, M.; Socka, M.; Baśko, M.; Biela, T., Biocompatible Polymers Combined with Cyclodextrins: Fascinating Materials for Drug Delivery Applications. *Molecules* **2020,** *25* (15), 3404.

131. Collins, C. J.; Mondjinou, Y.; Loren, B.; Torregrosa-Allen, S.; Simmons, C. J.; Elzey, B. D.; Ayat, N.; Lu, Z. R.; Thompson, D., Influence of Molecular Structure on the In Vivo Performance of Flexible Rod Polyrotaxanes. *Biomacromolecules* **2016,** *17* (9), 2777-86.

132. Mondjinou, Y. A.; Hyun, S. H.; Xiong, M.; Collins, C. J.; Thong, P. L.; Thompson, D. H., Impact of Mixed beta-Cyclodextrin Ratios on Pluronic Rotaxanation Efficiency and Product Solubility. *ACS Appl Mater Interfaces* **2015,** *7* (43), 23831-6.

133. Collins, C. J.; McCauliff, L. A.; Hyun, S. H.; Zhang, Z.; Paul, L. N.; Kulkarni, A.; Zick, K.; Wirth, M.; Storch, J.; Thompson, D. H., Synthesis, characterization, and evaluation of pluronic-based beta-cyclodextrin polyrotaxanes for mobilization of accumulated cholesterol from Niemann-Pick type C fibroblasts. *Biochemistry* **2013,** *52* (19), 3242-53.

134. Tamura, A.; Nishida, K.; Yui, N., Lysosomal pH-inducible supramolecular dissociation of polyrotaxanes possessing acid-labile N-triphenylmethyl end groups and their therapeutic potential for Niemann-Pick type C disease. *Science and technology of advanced materials* **2016,** *17* (1), 361-374.

135. Collins, C. J.; Loren, B. P.; Alam, M. S.; Mondjinou, Y.; Skulsky, J. L.; Chaplain, C. R.; Haldar, K.; Thompson, D. H., Pluronic based beta-cyclodextrin polyrotaxanes for treatment of Niemann-Pick Type C disease. *Sci Rep* **2017,** *7*, 46737.

136. Kulkarni, A.; Caporali, P.; Dolas, A.; Johny, S.; Goyal, S.; Dragotto, J.; Macone, A.; Jayaraman, R.; Fiorenza, M. T., Linear Cyclodextrin Polymer Prodrugs as Novel Therapeutics for Niemann-Pick Type C1 Disorder. *Scientific Reports* **2018,** *8* (1), 9547.

137. Mouritsen, O. G.; Zuckermann, M. J., What's so special about cholesterol? *Lipids* **2004,** *39* (11), 1101-1113.

138. Radhakrishnan, A.; Goldstein, J. L.; McDonald, J. G.; Brown, M. S., Switch-like control of SREBP-2 transport triggered by small changes in ER cholesterol: a delicate balance. *Cell metabolism* **2008,** *8* (6), 512-21.

139. Das, A.; Goldstein, J. L.; Anderson, D. D.; Brown, M. S.; Radhakrishnan, A., Use of mutant 125I-perfringolysin O to probe transport and organization of cholesterol in membranes of animal cells. *Proceedings of the National Academy of Sciences of the United States of America* **2013,** *110* (26), 10580-5.

140. Olsen, B. N.; Schlesinger, P. H.; Baker, N. A., Perturbations of Membrane Structure by Cholesterol and Cholesterol Derivatives Are Determined by Sterol Orientation. *Journal of the American Chemical Society* **2009,** *131* (13), 4854-4865.

141. Ermilova, I.; Lyubartsev, A. P., Cholesterol in phospholipid bilayers: positions and orientations inside membranes with different unsaturation degrees. *Soft Matter* **2019,** *15* (1), 78-93.

142. Ghysels, A.; Krämer, A.; Venable, R. M.; Teague, W. E.; Lyman, E.; Gawrisch, K.; Pastor, R. W., Permeability of membranes in the liquid ordered and liquid disordered phases. *Nature Communications* **2019,** *10* (1), 5616.

143. Marsh, D., Liquid-ordered phases induced by cholesterol: a compendium of binary phase diagrams. *Biochimica et biophysica acta* **2010,** *1798* (3), 688-99.

144. Weber, L.-W.; Boll, M.; Stampfl, A., Maintaining cholesterol homeostasis: sterol regulatory element-binding proteins. *World J Gastroenterol* **2004,** *10* (21), 3081-3087.

145. Xu, H.; Zhou, S.; Tang, Q.; Xia, H.; Bi, F., Cholesterol metabolism: New functions and therapeutic approaches in cancer. *Biochimica et Biophysica Acta (BBA) - Reviews on Cancer* **2020,** *1874* (1), 188394.

146. Dietschy, J. M.; Turley, S. D., Cholesterol metabolism in the brain. *Current Opinion in Lipidology* **2001,** *12* (2).

147. Bilotta, M. T.; Petillo, S.; Santoni, A.; Cippitelli, M., Liver X Receptors: Regulators of Cholesterol Metabolism, Inflammation, Autoimmunity, and Cancer. *Frontiers in Immunology* **2020,** *11*.

148. Krul, E. S.; Tikkanen, M. J.; Cole, T. G.; Davie, J. M.; Schonfeld, G., Roles of apolipoproteins B and E in the cellular binding of very low density lipoproteins. *J Clin Invest* **1985,** *75* (2), 361-369.

149. Möbius, W.; Van Donselaar, E.; Ohno-Iwashita, Y.; Shimada, Y.; Heijnen, H. F. G.; Slot, J. W.; Geuze, H. J., Recycling Compartments and the Internal Vesicles of Multivesicular Bodies Harbor Most of the Cholesterol Found in the Endocytic Pathway. *Traffic* **2003,** *4* (4), 222-231.

150. Kobayashi, T.; Stang, E.; Fang, K. S.; de Moerloose, P.; Parton, R. G.; Gruenberg, J., A lipid associated with the antiphospholipid syndrome regulates endosome structure and function. *Nature* **1998,** *392* (6672), 193-7.

151. Schoer, J. K.; Gallegos, A. M.; McIntosh, A. L.; Starodub, O.; Kier, A. B.; Billheimer, J. T.; Schroeder, F., Lysosomal Membrane Cholesterol Dynamics. *Biochemistry* **2000,** *39* (26), 7662-7677.

152. Carstea, E. D.; Morris, J. A.; Coleman, K. G.; Loftus, S. K.; Zhang, D.; Cummings, C.; Gu, J.; Rosenfeld, M. A.; Pavan, W. J.; Krizman, D. B.; Nagle, J.; Polymeropoulos, M. H.; Sturley, S. L.; Ioannou, Y. A.; Higgins, M. E.; Comly, M.; Cooney, A.; Brown, A.; Kaneski, C. R.; Blanchette-Mackie, E. J.; Dwyer, N. K.; Neufeld, E. B.; Chang, T. Y.; Liscum, L.; Strauss, J. F., 3rd; Ohno, K.; Zeigler, M.; Carmi, R.; Sokol, J.; Markie, D.; O'Neill, R. R.; van Diggelen, O. P.; Elleder, M.; Patterson, M. C.; Brady, R. O.; Vanier, M. T.; Pentchev, P. G.; Tagle, D. A., Niemann-Pick C1 disease gene: homology to mediators of cholesterol homeostasis. *Science (New York, N.Y.)* **1997,** *277* (5323), 228-31.

153. Davies, J. P.; Ioannou, Y. A., Topological Analysis of Niemann-Pick C1 Protein Reveals That the Membrane Orientation of the Putative Sterol-sensing Domain Is Identical to Those of 3-Hydroxy-3-methylglutaryl-CoA Reductase and Sterol Regulatory Element Binding Protein Cleavage-activating Protein*. *Journal of Biological Chemistry* **2000,** *275* (32), 24367-24374.

154. Gong, X.; Qian, H.; Zhou, X.; Wu, J.; Wan, T.; Cao, P.; Huang, W.; Zhao, X.; Wang, X.; Wang, P.; Shi, Y.; Gao, G. F.; Zhou, Q.; Yan, N., Structural Insights into the Niemann-Pick C1 (NPC1)-Mediated Cholesterol Transfer and Ebola Infection. *Cell* **2016,** *165* (6), 1467-1478.

155. Kwon, H. J.; Abi-Mosleh, L.; Wang, M. L.; Deisenhofer, J.; Goldstein, J. L.; Brown, M. S.; Infante, R. E., Structure of N-terminal domain of NPC1 reveals distinct subdomains for binding and transfer of cholesterol. *Cell* **2009,** *137* (7), 1213-1224.

156. Baker, S. M.; Petukh, M., Effect of pH on the Ability of N-Terminal Domain of Human NPC1 to Recognize, Bind, and Transfer Cholesterol. *ACS Omega* **2020,** *5* (45), 29222-29230.

157. Qian, H.; Wu, X.; Du, X.; Yao, X.; Zhao, X.; Lee, J.; Yang, H.; Yan, N., Structural Basis of Low-pH-Dependent Lysosomal Cholesterol Egress by NPC1 and NPC2. *Cell* **2020,** *182* (1), 98-111.e18.

158. Dubey, V.; Bozorg, B.; Wüstner, D.; Khandelia, H., Cholesterol binding to the sterol-sensing region of Niemann Pick C1 protein confines dynamics of its N-terminal domain. *PLoS Comput Biol* **2020,** *16* (10), e1007554-e1007554.

159. Tang, Y.; Leao, I. C.; Coleman, E. M.; Broughton, R. S.; Hildreth, J. E. K., Deficiency of niemann-pick type C-1 protein impairs release of human immunodeficiency virus type 1 and results in Gag accumulation in late endosomal/lysosomal compartments. *J Virol* **2009,** *83* (16), 7982-7995.

160. Khan, N.; Chen, X.; Geiger, J. D., Role of Endolysosomes in Severe Acute Respiratory Syndrome Coronavirus-2 Infection and Coronavirus Disease 2019 Pathogenesis: Implications for Potential Treatments. *Frontiers in Pharmacology* **2020,** *11*.

161. Herbert, A. S.; Davidson, C.; Kuehne, A. I.; Bakken, R.; Braigen, S. Z.; Gunn, K. E.; Whelan, S. P.; Brummelkamp, T. R.; Twenhafel, N. A.; Chandran, K.; Walkley, S. U.; Dye, J. M., Niemann-pick C1 is essential for ebolavirus replication and pathogenesis in vivo. *mBio* **2015,** *6* (3), e00565.

162. Goldstein, J. L.; Dana, S. E.; Faust, J. R.; Beaudet, A. L.; Brown, M. S., Role of lysosomal acid lipase in the metabolism of plasma low density lipoprotein. Observations in cultured fibroblasts from a patient with cholesteryl ester storage disease. *The Journal of biological chemistry* **1975,** *250* (21), 8487-95.

163. Friedland, N.; Liou, H.-L.; Lobel, P.; Stock, A. M., Structure of a cholesterol-binding protein deficient in Niemann–Pick type C2 disease. *Proceedings of the National Academy of Sciences* **2003,** *100* (5), 2512.

164. Xu, S.; Benoff, B.; Liou, H.-L.; Lobel, P.; Stock, A. M., Structural Basis of Sterol Binding by NPC2, a Lysosomal Protein Deficient in Niemann-Pick Type C2 Disease. *Journal of Biological Chemistry* **2007,** *282* (32), 23525-23531.

165. Okamura, N.; Kiuchi, S.; Tamba, M.; Kashima, T.; Hiramoto, S.; Baba, T.; Dacheux, F.; Dacheux, J. L.; Sugita, Y.; Jin, Y. Z., A porcine homolog of the major secretory protein of human epididymis, HE1, specifically binds cholesterol. *Biochimica et biophysica acta* **1999,** *1438* (3), 377-87.

166. Ko, D. C.; Binkley, J.; Sidow, A.; Scott, M. P., The integrity of a cholesterol-binding pocket in Niemann–Pick C2 protein is necessary to control lysosome cholesterol levels. *Proceedings of the National Academy of Sciences* **2003,** *100* (5), 2518.

167. Body, D. R.; Gray, G. M., The isolation and characterisation of phosphatidylglycerol and a structural isomer from pig lung. *Chemistry and Physics of Lipids* **1967,** *1* (3), 254-263.

168. Kobayashi, T.; Beuchat, M.-H.; Chevallier, J.; Makino, A.; Mayran, N.; Escola, J.-M.; Lebrand, C.; Cosson, P.; Kobayashi, T.; Gruenberg, J., Separation and Characterization of Late Endosomal Membrane Domains *. *Journal of Biological Chemistry* **2002,** *277* (35), 32157-32164.

169. Kolter, T.; Sandhoff, K., Lysosomal degradation of membrane lipids. *FEBS Letters* **2010,** *584* (9), 1700-1712.

170. Showalter, M. R.; Berg, A. L.; Nagourney, A.; Heil, H.; Carraway, K. L.; Fiehn, O., The Emerging and Diverse Roles of Bis(monoacylglycero) Phosphate Lipids in Cellular Physiology and Disease. *International Journal of Molecular Sciences* **2020,** *21* (21), 8067.

171. Liu, N.; Tengstrand, E. A.; Chourb, L.; Hsieh, F. Y., Di-22:6-bis(monoacylglycerol)phosphate: A clinical biomarker of drug-induced phospholipidosis for drug development and safety assessment. *Toxicology and Applied Pharmacology* **2014,** *279* (3), 467-476.

172. Anderson, D. M. G.; Ablonczy, Z.; Koutalos, Y.; Hanneken, A. M.; Spraggins, J. M.; Calcutt, M. W.; Crouch, R. K.; Caprioli, R. M.; Schey, K. L., Bis(monoacylglycero)phosphate lipids in the retinal pigment epithelium implicate lysosomal/endosomal dysfunction in a model of Stargardt disease and human retinas. *Sci Rep* **2017,** *7* (1), 17352.

173. Akgoc, Z.; Sena-Esteves, M.; Martin, D. R.; Han, X.; d'Azzo, A.; Seyfried, T. N., Bis(monoacylglycero)phosphate: a secondary storage lipid in the gangliosidoses. *Journal of lipid research* **2015,** *56* (5), 1006-13.

174. Hein, L. K.; Duplock, S.; Fuller, M., Selective reduction of bis(monoacylglycero)phosphate ameliorates the storage burden in a THP-1 macrophage model of Gaucher disease. *Journal of lipid research* **2013,** *54* (6), 1691-1697.

175. Meikle, Peter J.; Duplock, S.; Blacklock, D.; Whitfield, Phillip D.; Macintosh, G.; Hopwood, John J.; Fuller, M., Effect of lysosomal storage on bis(monoacylglycero)phosphate. *Biochemical Journal* **2008,** *411* (1), 71-78.

176. Brotherus, J.; Renkonen, O.; Herrmann, J.; Fischer, W., Novel stereoconfiguration in lyso-bis-phosphatidic acid of cultured BHK-cells. *Chemistry and Physics of Lipids* **1974,** *13* (2), 178-182.

177. Joutti, A.; Brotherus, J.; Renkonen, O.; Laine, R.; Fischer, W., The stereoconfiguration of newly formed molecules of Bis(monoacylglycero)phosphate in BHK cells. *Biochimica et Biophysica Acta (BBA) - Lipids and Lipid Metabolism* **1979,** *575* (1), 10-15.

178. Joutti, A.; Brotherus, J.; Renkonen, O.; Laine, R.; Fischer, W., The stereochemical configuration of lysobisphosphatidic acid from rat liver, rabbit lung and pig lung. *Biochimica et Biophysica Acta (BBA) - Lipids and Lipid Metabolism* **1976,** *450* (2), 206-209.

179. Tan, H.-H.; Makino, A.; Sudesh, K.; Greimel, P.; Kobayashi, T., Spectroscopic Evidence for the Unusual Stereochemical Configuration of an Endosome-Specific Lipid. *Angewandte Chemie International Edition* **2012,** *51* (2), 533-535.

180. Luquain, C.; Dolmazon, R.; Enderlin, J. M.; Laugier, C.; Lagarde, M.; Pageaux, J. F., Bis(monoacylglycerol) phosphate in rat uterine stromal cells: structural characterization and specific esterification of docosahexaenoic acid. *Biochem J* **2000,** *351 Pt 3* (Pt 3), 795-804.

181. Amidon, B.; Schmitt, J. D.; Thuren, T.; King, L.; Waite, M., Biosynthetic conversion of phosphatidylglycerol to sn-1:sn-1' bis(monoacylglycerol) phosphate in a macrophage-like cell Line. *Biochemistry* **1995,** *34* (16), 5554-5560.

182. Kuipers, O. P.; Dijkman, R.; Pals, C. E. G. M.; Verheij, H. M.; Haas, G. H. d., Evidence for the involvement of tyrosine-69 in the control of stereospecificity of porcine pancreatic phospholipase A2. *Protein Engineering, Design and Selection* **1989,** *2* (6), 467-471.

183. Linderoth, L.; Andresen, T. L.; Jørgensen, K.; Madsen, R.; Peters, G. H., Molecular Basis of Phospholipase A2 Activity toward Phospholipids with sn-1 Substitutions. *Biophysical Journal* **2008,** *94* (1), 14-26.

184. Goursot, A.; Mineva, T.; Bissig, C.; Gruenberg, J.; Salahub, D. R., Structure, Dynamics, and Energetics of Lysobisphosphatidic Acid (LBPA) Isomers. *The Journal of Physical Chemistry B* **2010,** *114* (47), 15712-15720.

185. Hullin-Matsuda, F.; Luquain-Costaz, C.; Bouvier, J.; Delton-Vandenbroucke, I., Bis(monoacylglycero)phosphate, a peculiar phospholipid to control the fate of cholesterol: Implications in pathology. *Prostaglandins, leukotrienes, and essential fatty acids* **2009,** *81* (5-6), 313-24.

186. Hayakawa, T.; Hirano, Y.; Makino, A.; Michaud, S.; Lagarde, M.; Pageaux, J.-F.; Doutheau, A.; Ito, K.; Fujisawa, T.; Takahashi, H.; Kobayashi, T., Differential Membrane Packing of Stereoisomers of Bis(monoacylglycero)phosphate. *Biochemistry* **2006,** *45* (30), 9198-9209.

187. Poorthuis, B. J.; Hostetler, K. Y., Conversion of diphosphatidylglycerol to bis(monoacylglyceryl)phosphate by lysosomes. *Journal of lipid research* **1978,** *19* (3), 309-315.

188. King, R. J.; MacBeth, M. C., Interaction of the lipid and protein components of pulmonary surfactant Role of phosphatidylglycerol and calcium. *Biochimica et Biophysica Acta (BBA) - Biomembranes* **1981,** *647* (2), 159-168.

189. Chen, W.-W.; Chao, Y.-J.; Chang, W.-H.; Chan, J.-F.; Hsu, Y.-H. H., Phosphatidylglycerol Incorporates into Cardiolipin to Improve Mitochondrial Activity and Inhibits Inflammation. *Scientific Reports* **2018,** *8* (1), 4919.

190. Heravi, J.; Waite, M., Transacylase formation of bis(monoacylglycerol)phosphate. *Biochimica et Biophysica Acta (BBA) - Molecular and Cell Biology of Lipids* **1999,** *1437* (3), 277-286.

191. Thornburg, T.; Miller, C.; Thuren, T.; King, L.; Waite, M., Glycerol reorientation during the conversion of phosphatidylglycerol to bis(monoacylglycerol)phosphate in macrophage-like RAW 264.7 cells. *Journal of Biological Chemistry* **1991,** *266* (11), 6834-6840.

192. Cheruku, S. R.; Xu, Z.; Dutia, R.; Lobel, P.; Storch, J., Mechanism of cholesterol transfer from the Niemann-Pick type C2 protein to model membranes supports a role in lysosomal cholesterol transport. *The Journal of biological chemistry* **2006,** *281* (42), 31594-604.

193. Xu, Z.; Farver, W.; Kodukula, S.; Storch, J., Regulation of Sterol Transport between Membranes and NPC2. *Biochemistry* **2008,** *47* (42), 11134-11143.

194. McCauliff, L. A.; Langan, A.; Li, R.; Ilnytska, O.; Bose, D.; Waghalter, M.; Lai, K.; Kahn, P. C.; Storch, J., Intracellular cholesterol trafficking is dependent upon NPC2 interaction with lysobisphosphatidic acid. *eLife* **2019,** *8*.

195. Moreau, D.; Vacca, F.; Vossio, S.; Scott, C.; Colaco, A.; Paz Montoya, J.; Ferguson, C.; Damme, M.; Moniatte, M.; Parton, R. G.; Platt, F. M.; Gruenberg, J., Drug-induced increase in lysobisphosphatidic acid reduces the cholesterol overload in Niemann-Pick type C cells and mice. *EMBO reports* **2019,** *20* (7), e47055.

196. Ilnytska, O.; Lai, K.; Gorshkov, K.; Schultz, M. L.; Tran, B. N.; Jeziorek, M.; Kunkel, T. J.; Azaria, R. D.; McLoughlin, H. S.; Waghalter, M.; Xu, Y.; Schlame, M.; Altan-Bonnet, N.; Zheng, W.; Lieberman, A. P.; Dobrowolski, R.; Storch, J., Enrichment of NPC1-deficient cells with the lipid LBPA stimulates autophagy, improves lysosomal function, and reduces cholesterol storage. *The Journal of biological chemistry* **2021,** *297* (1), 100813.

197. Perrotta, C.; Cervia, D.; De Palma, C.; Assi, E.; Pellegrino, P.; Bassi, M. T.; Clementi, E., The emerging role of acid sphingomyelinase in autophagy. *Apoptosis : an international journal on programmed cell death* **2015,** *20* (5), 635-44.

198. Reagan, J. W.; Hubbert, M. L.; Shelness, G. S., Posttranslational Regulation of Acid Sphingomyelinase in Niemann-Pick Type C1 Fibroblasts and Free Cholesterol-enriched Chinese Hamster Ovary Cells*. *Journal of Biological Chemistry* **2000,** *275* (48), 38104-38110.

199. Devlin, C.; Pipalia, N. H.; Liao, X.; Schuchman, E. H.; Maxfield, F. R.; Tabas, I., Improvement in Lipid and Protein Trafficking in Niemann-Pick C1 Cells by Correction of a Secondary Enzyme Defect. *Traffic* **2010,** *11* (5), 601-615.

200. Taniguchi, M.; Kitatani, K.; Kondo, T.; Hashimoto-Nishimura, M.; Asano, S.; Hayashi, A.; Mitsutake, S.; Igarashi, Y.; Umehara, H.; Takeya, H.; Kigawa, J.; Okazaki, T., Regulation of autophagy and its associated cell death by "sphingolipid rheostat": reciprocal role of ceramide and sphingosine 1-phosphate in the mammalian target of rapamycin pathway. *The Journal of biological chemistry* **2012,** *287* (47), 39898-39910.

201. McCauliff, L. A.; Xu, Z.; Li, R.; Kodukula, S.; Ko, D. C.; Scott, M. P.; Kahn, P. C.; Storch, J., Multiple Surface Regions on the Niemann-Pick C2 Protein Facilitate Intracellular Cholesterol Transport. *The Journal of biological chemistry* **2015,** *290* (45), 27321-27331.

202. McCauliff, L. A.; Xu, Z.; Storch, J., Sterol transfer between cyclodextrin and membranes: similar but not identical mechanism to NPC2-mediated cholesterol transfer. *Biochemistry* **2011,** *50* (34), 7341-7349.

203. Abdul-Hammed, M.; Breiden, B.; Adebayo, M. A.; Babalola, J. O.; Schwarzmann, G.; Sandhoff, K., Role of endosomal membrane lipids and NPC2 in cholesterol transfer and membrane fusion. *Journal of lipid research* **2010,** *51* (7), 1747-60.

204. Berzina, Z.; Solanko, L. M.; Mehadi, A. S.; Jensen, M. L. V.; Lund, F. W.; Modzel, M.; Szomek, M.; Solanko, K. A.; Dupont, A.; Nielsen, G. K.; Heegaard, C. W.; Ejsing, C. S.; Wüstner, D., Niemann-Pick C2 protein regulates sterol transport between plasma membrane and late endosomes in human fibroblasts. *Chemistry and Physics of Lipids* **2018,** *213*, 48-61.

CHAPTER 2. STEREOSPECIFIC SYNTHESIS OF PHOSPHATIDYL GLYCEROL USING A CYANOETHYL PHOSPHORAMIDITE PRECURSOR

This chapter was adapted from Chemistry and Physics of Lipids: Struzik, Z. J.; Weerts, A. N.; Storch, J.; Thompson, D. H., *Chem. Phys. Lipids* **2020,** 231, 104933.

2.1 Abstract

Phosphatidylglycerols (PG) are a family of naturally occurring phospholipids that are responsible for critical operations within cells. PG are characterized by an (R) configuration in the diacyl glycerol backbone and an (S) configuration in the phosphoglycerol headgroup. Herein, we report a synthetic route to provide control over the PG stereocenters as well as control of the acyl chain identity using a symmetric phosphoramidite precursor.

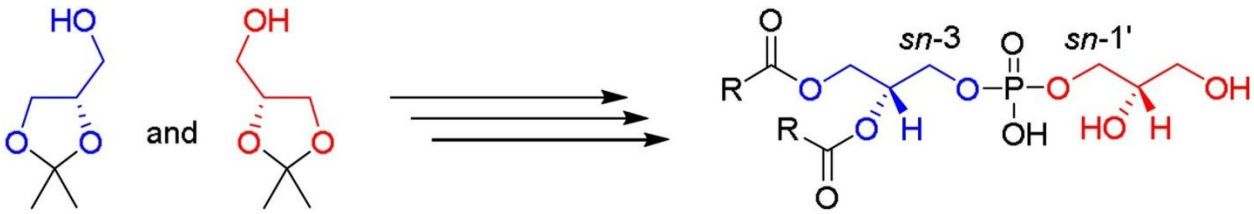

Figure 2.1. Synthesis of PG derived from chiral solketal precursors.

2.2 Introduction

Glycerophospholipids represent a diverse class of biological molecules that play vital roles in all living systems including cell membrane structure, vesicular transport, and intracellular signaling.[1] PL are generally characterized by a glycerol moiety phosphorylated at the *sn*-3 position and fatty acid ester linkages in the *sn*-1 and *sn*-2 positions of the diacylglycerol (DAG) backbone. Deficiencies in PL biogenesis and metabolism have been attributed to a host of inherited and acquired diseases including mitochondrial disorders, breast cancer, neurodegeneration, and

obesity.[2-5] Interestingly, PL have also been used successfully as drug delivery vehicles over the past few decades for numerous anticancer drugs, several of which are FDA approved.[6,7]

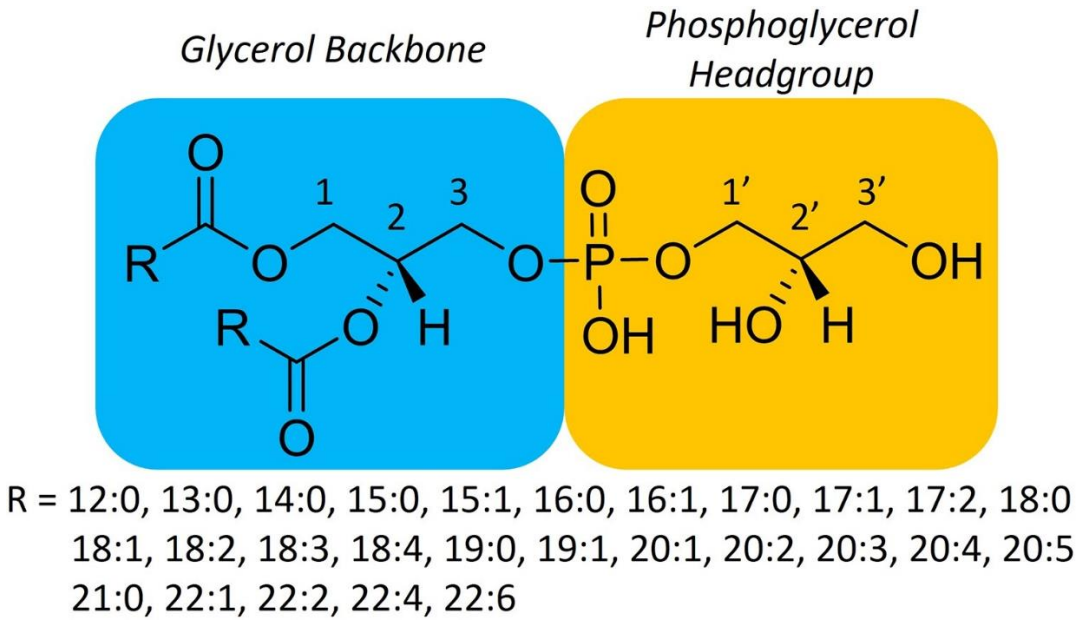

Figure 2.2. General structure of PG with known acyl chain identities as reported in Lipidomics Gateway (2020).[8]

PG are a subset of glycerophospholipids that are distinguished by the presence of an (*R*)-glycerylphosphoester linkage in the lipid headgroup region (Figure 2.2), originally discovered in *Scenedesmus.*[9] PG are suspected as biosynthetic precursors to a range of PL including cardiolipin, bis(monoacylglycero)phosphate (BMP; also known as lysobisphosphatidic acid or LBPA), bacterial proteolipids, lipoteichoic lipids, and other glycophospholipids.[10-12] They are also utilized in other cellular activities such as electron transport in photosynthesis, attenuation of inflammatory responses, lipoprotein maturation, and extracellular stress sensing.[13] This wide use of PG by cells makes it an important PL whose roles in fundamental mechanisms of cellular processes and disease pathology need better elucidation. Naturally occurring PG is phosphorylated at the *sn*-3 and *sn*-1'positions of the two glycerol motifs making enantiomerically pure PG essential for biological

studies. Syntheses of PG has previously been demonstrated.[14-16] Herein, we report an improved synthetic route designed to afford diastereochemically pure PG using two chiral starting materials, (*R*)-solketal and (*S*)-solketal while maintaining control over acyl chain identity.

Our strategy for the synthesis of *sn*-3:*sn*-1' PG **1** was based on a convergent synthesis employing DAG and phosphoglycerol headgroup intermediates, each with stereochemistries that were fixed via the corresponding solketal precursors (Figure 2.3). Global deprotection of protected PG intermediate **2** using a naked fluorine source can be utilized to synthesize **1**. The stereospecific phosphorylation of the DAG **3** and glycerol headgroup **4** can be realized through coupling of the respective glycerol fragments and a P^{III} phosphoramidite reagent commonly employed in DNA oligonucleotide synthesis and other phospholipid syntheses.[17,18] Most recently, the phosphoramidite method has been utilized during the installation of a phosphocholine headgroup.[19] Because this reagent has been used successfully in the synthesis of BMP, a structural isomer of PG, we decided to model our synthetic route closely to this strategy.[20-22] The crucial deprotection of the *p*-methoxybenzyl ether (PMB) group on **3** would expose the stereochemically correct primary alcohol for phosphorylation. One of the challenges commonly encountered in PL synthesis is acyl chain migration that occurs within the glycerol backbone from the *sn*-2 position to the *sn*-1 position under mildly acidic or basic conditions. These adversities have historically been reported with lysophospholipid synthesis[23,24], but are also relevant in synthesizing the DAG in other PL syntheses such as phosphatidylserine[25] and glycosylphosphatidylinositols.[26] Installation of the acyl chains via Steglich esterification of **7** can be employed to afford **5**. Acetonide deprotection of **9** would yield **7**. Protection of (S)-solketal precursor **11** with PMB can be used to synthesize **9**. Following PMB deprotection of the glycerol headgroup, intermediate **6** would correctly expose the primary *sn*-1' alcohol of **4**. TBS protection would allow for

conservation of the *sn*-2' stereocenter in **4** during the latter steps of the synthesis. Prior methods for glycerol backbone synthesis can be used to make the PMB protected, and acetonide deprotected species **8** and **10**, respectively, from the (*R*)-solketal precursor **12**.[22]

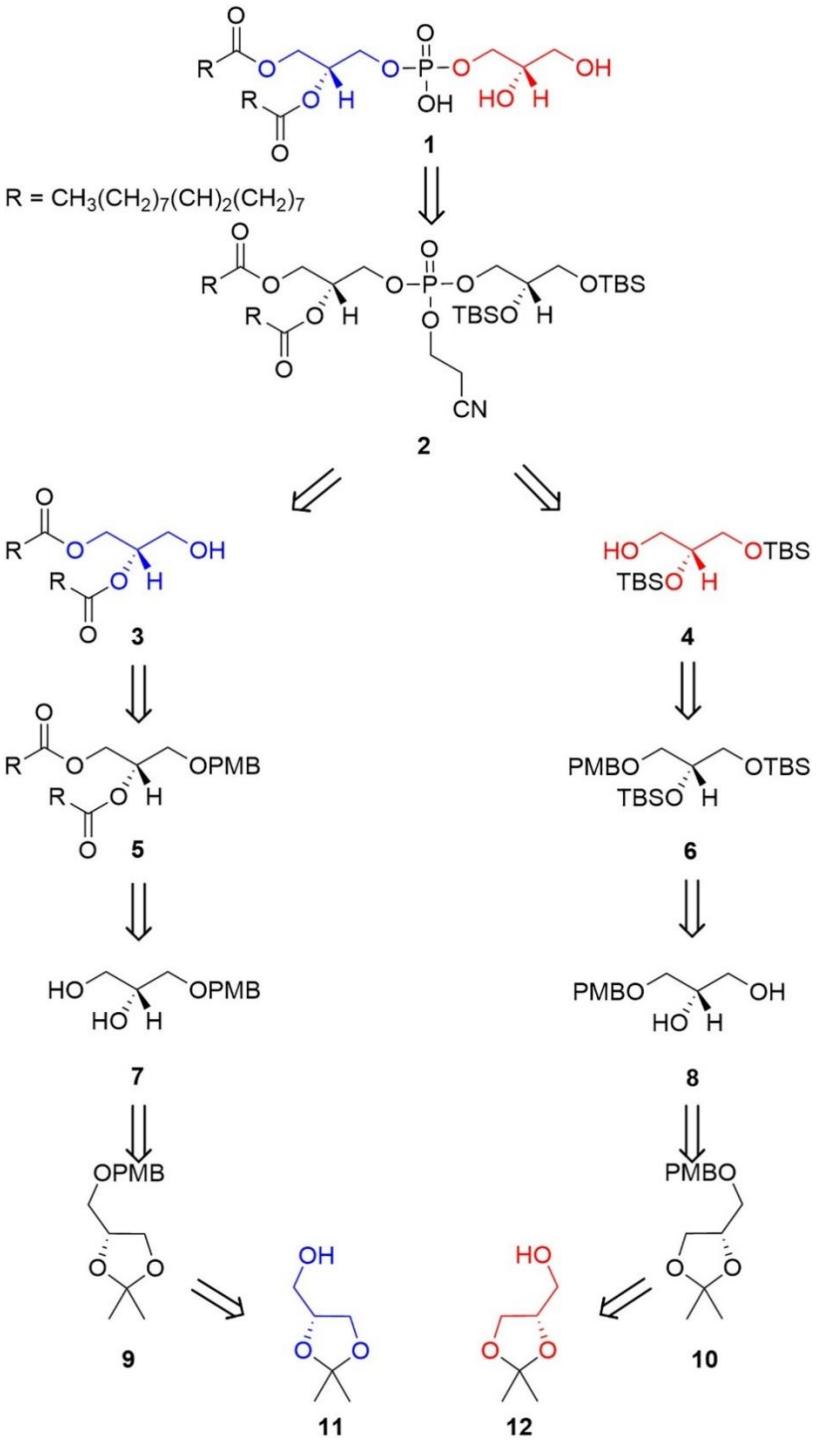

Figure 2.3. Retrosynthetic analysis of 1,2-Dioleyl-sn-glycero-3-phospho-(1'-sn-glycerol).

2.3 Results and Discussion

Protection with PMBCl and NaH of the primary *sn*-1' alcohol of **12** gave **10** in 97% yield. (Figure 2.4). Acetonide deprotection to expose the *sn*-2' and *sn*-3' alcohols of **10** was performed using 1.0 M HCl in THF to afford **8** in 88% yield. We chose to use the bulkier TBS groups instead of TMS groups to protect the 1,2-diol of **8** during the synthesis of **6** to provide increased stability of the glycerol headgroup intermediate throughout the synthetic pathway. Several reported protocols used DCM as the solvent during the silyl protection of intermediate **8** and related compounds.[27,28] Unfortunately, we typically observed yields that were significantly lower than the reported values (20% or less) that most often resulted in partial conversion to the monosilated product. In turn, we set out to identify a more efficient method to protect the *sn*-2' and *sn*-3' alcohols. Patschinski *et al*. examined the effects of solvent and auxiliary base in the Corey silyl ether protection of alcohols.[29] It was found that DMF acted as a catalyst based on the observed turnover of starting material in the absence of imidazole, while the use of DCM resulted in little to no reaction under the same conditions. Furthermore, the addition of non-nucleophilic bases such as Et_3N further enhanced the product yield. This observation was attributed to the regeneration of the imidazole catalyst by the auxiliary base. We, therefore, applied these conditions to our synthesis by reacting the 1,2 - diol with 3.5 equivalencies of TBSCl and imidazole, and 2 equivalents of Et_3N in DMF with heating over 4 h from 24 °C to 50 °C to afford **6** in 93% yield. PMB deprotection of **6** was then inducted with DDQ in a DCM/H_2O mixture to produce **4** in 77% yield.

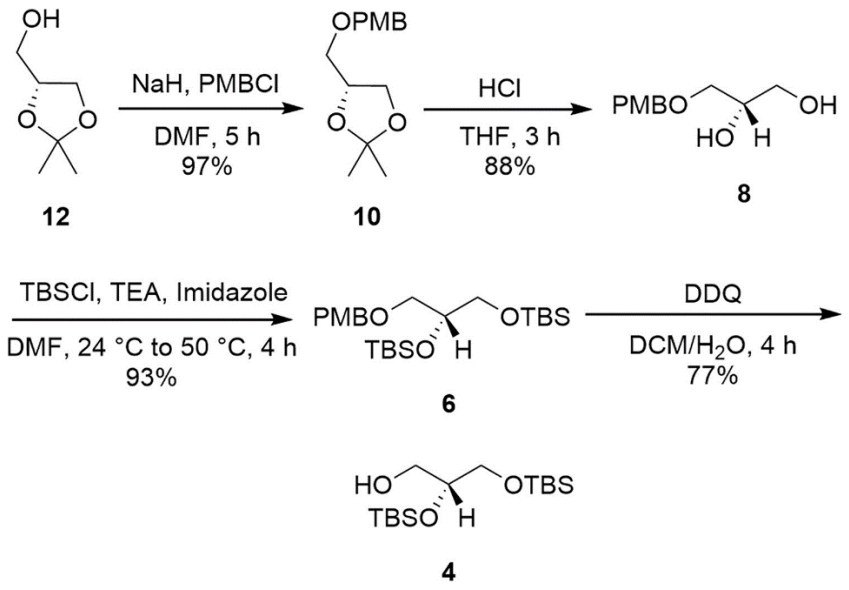

Figure 2.4. Synthesis of the 1'-*sn*-glycerol intermediate **4**.

Next, we synthesized DAG intermediate **3** in a similar manner to that for glycerol intermediate **4** (Figure 2.5). When **11** was mixed with NaH and PMBCl in DMF, **9** was observed in 96% yield. Subsequent acetonide deprotection in 1.0 M HCl exposed the *sn*-2 and *sn*-1 alcohols to give **7** in 90% yield. Steglich esterification was then implemented to install the oleyl acyl chains onto the protected glycerol backbone to give **5**. Formation of DAG **3** was affected via PMB deprotection by DDQ in 82% yield. To minimize the amount of acyl chain migration from the *sn*-2 position to the more thermodynamically stable *sn*-3 position, an optimum reaction time of 4 h is required to produce greater than 99% of the observed esterified product at the *sn*-2 and *sn*-1 positions (Figure 2.6). We base this conclusion on the characteristic ^{1}H NMR peaks observed at 5.08 ppm and 3.73 ppm, corresponding to the methine proton at the esterified *sn*-2 position and methylene protons at the unfunctionalized *sn*-3 position, respectively. Conversely, 38% of the diacyl glycerol product had rearranged after a 24 h reaction time. This product is characterized by the disappearance of the formerly mentioned peaks and the appearance of the unesterified methine proton peak that was shifted up field to 4.09 ppm in **13**.

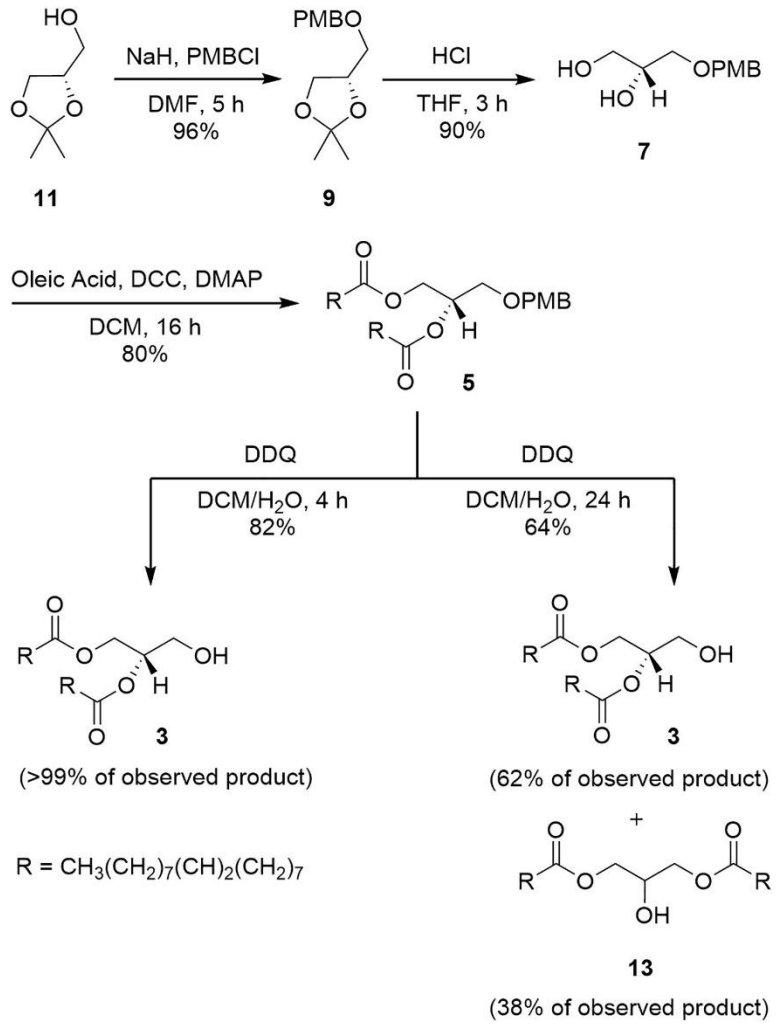

Figure 2.5. Synthesis of the 1,2-Dioleyl-*sn*-glycerol intermediate **3**.

With the glycerol backbone and headgroup intermediates in hand, efforts to phosphorylate and ultimately globally deprotect to yield PG were initiated (Figure 2.7). Our synthesis began with phosphorylation of **4** via coupling with a chloro-substituted phosphoramidite N,N-diisopropylchlorophosphoramidite (PNCl) in the presence of 1-*H* tetrazole. The attractiveness of PNCl was the ability to selectively phosphorylate both the glycerol head group and backbone in separate steps due to the asymmetric nature of the phosphoramidite. However, PNCl proved to be difficult to handle because the product streaked excessively on silica and gave low reaction yields (30% or lower). Multiple byproducts formed due to degradation on the column and hydrolysis of

the excess monochlorophosphoramidite during the workup, consistent with the observations of Ching *et al.*[30], leading us to pursue a different approach with this reagent. We then explored the use of a symmetric phosphoramidite containing two amine substituents, 2-cyanoethyl-N,N,N',N'-

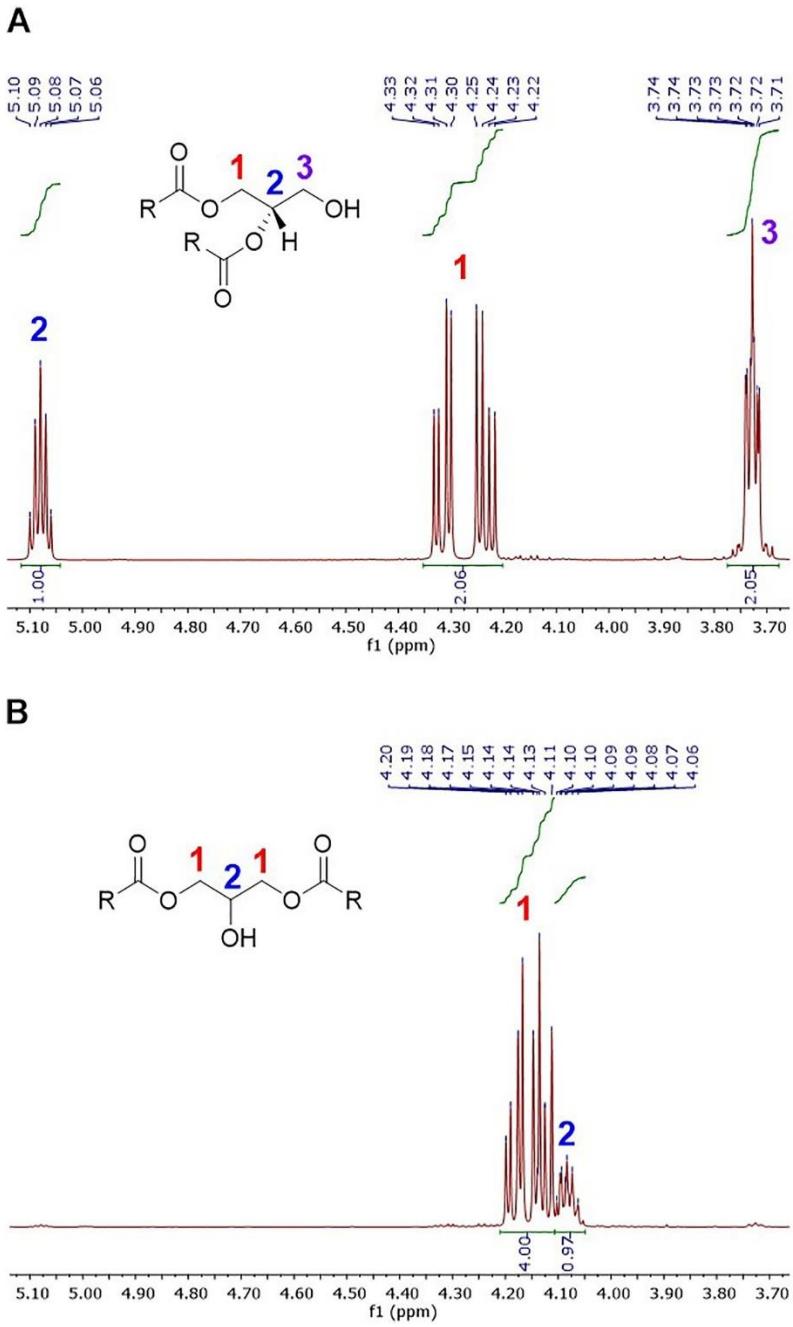

Figure 2.6. ^{1}H NMR comparison of the 1,2-Dioleyl-sn-glycerol product **3** (A) versus the acyl chain migration product **13** (B).

tetraisopropylphosphoramidite (PNN), that is less air and moisture sensitive. Additionally, a diisopropylammonium tetrazolide salt was formed during the reaction that is easily removed by filtration after work-up, thereby simplifying purification. By combining **4** with PNN and 1-*H* tetrazole in MeCN, we were able to obtain **14** in 77% yield**.** A one-pot procedure was used to phosphorylate **3** with phosphoramidite **14** in the presence of 1-*H* tetrazole followed by $P^{III} \rightarrow P^{V}$ oxidation with 70% *t*BuOOH to give **2** in 74% yield. Our global deprotection strategy was adopted from Chevallier *et al*. who also utilized a naked fluorine source to remove both the cyanoethyl and silyl ether protecting groups in a single step.[20] Phospholipid precursor **2** was mixed with TBAF and an equivalent amount of acetic acid to neutralize the mildly basic fluorine in THF, giving **1** in 42% yield after silica chromatography and ion exchange chromatography using Sephadex C-25.

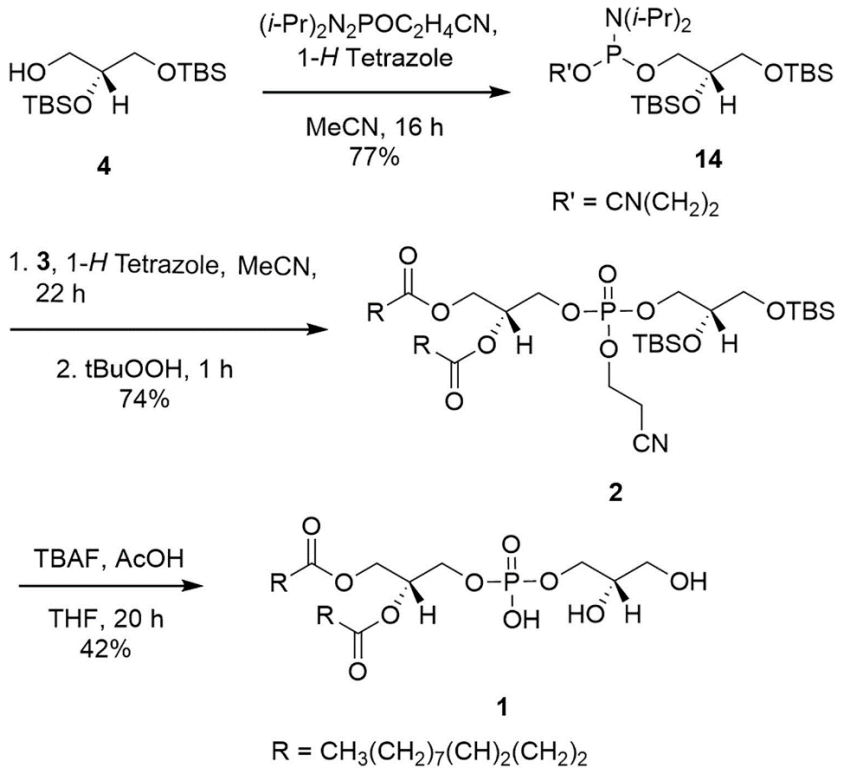

Figure 2.7. Synthesis of 1,2-Dioleyl-*sn*-glycero-3-phospho-(1'-*sn*-glycerol) (**1**).

To validate our synthetic protocol, we compared our diastereochemically pure PG **1** to the racemic PG that is commercially available from MilliporeSigma using hydrophilic interaction liquid chromatography coupled to tandem mass spectrometry (HILIC-MS/MS) (Figure 2.8). The racemic compound had a retention time of 7.5 min similar to that observed for **1** at 7.6 min in HILIC-MS/MS. The ^{1}H NMR spectra share similar chemical shifts positions and integrations at key points such as the methine peak at 5.22 ppm that integrates to 1.00 indicating that acyl chain migration did not occur (Figure 2.21). Additionally, the peak pattern in the glycerol region is consistent between the two samples for peaks appearing at 3.38, 3.61, 3.65, 4.16, and 4.39 ppm, further indicating esterifcations at the *sn*-2 and *sn*-1 positions. While the peaks belonging to PG are similar between the commercial standard and synthesized sample, a significant difference between the two spectra is a broad singlet appearing at 2.41 ppm that integrates to 5.83 protons in the commercial source that does not appear to belong to PG. ^{31}P NMR data collected for **1** as a tetrabutyl ammonium salt further validates the structure as the PG since a single peak at 1.77 ppm was observed in $CDCl_3$, whereas a single signal at 1.68 ppm was observed for commercial PG (Figure 2.22), thus confirming that the synthesized PG belongs to the same lipid class as the commercial standard. While the goal of the ion exchange step was to obtain the sodium salt of PG, the $CHCl_3$/MeOH/H_2O extraction required after chromatography prevented salt formation entirely and thus resulted in a broad ^{31}P NMR spectrum most likely due to self-assembly of the lipid into higher ordered structures.[31]

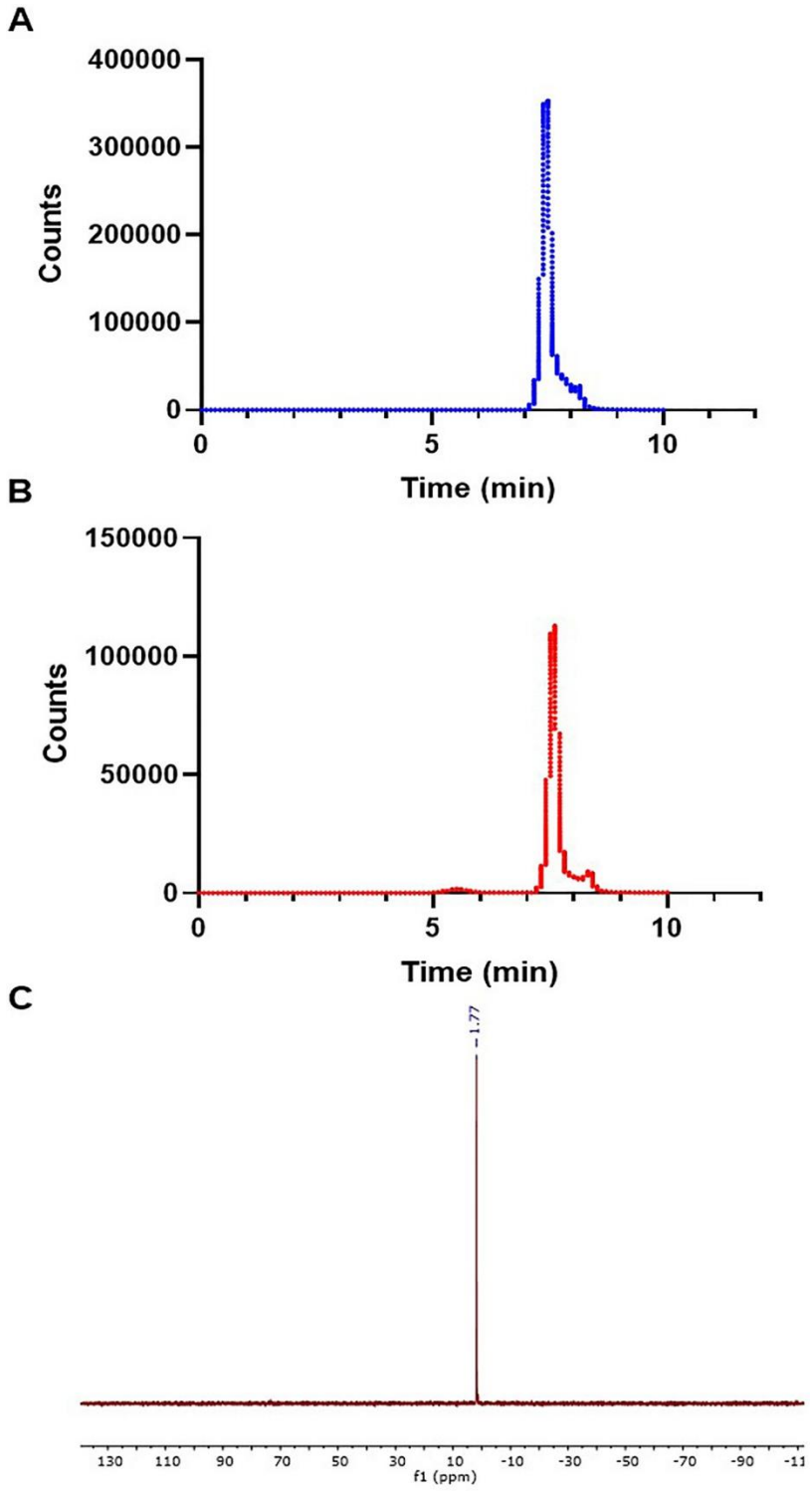

Figure 2.8. HILIC-MS/MS of racemic (A) and stereospecific PG (B).^{31}P NMR of **1** as a tetrabutylammonium salt (C).

In summary, we have successfully developed a synthetic protocol to make stereochemically pure PG from two chiral solketal precursors. The DAG was synthesized without acyl chain migration by quenching the reaction at 4 h; significant acyl chain migration was observed for reaction times longer than 4 h. The globally protected PG was synthesized by coupling the protected glycerol headgroup and glycerol backbone to a symmetric phosphoramidite using methodology adapted from DNA oligonucleotide synthesis. Finally, a naked fluorine source was used to remove the silyl and cyanoethyl protecting groups to yield diastereochemically pure PG after silica and ion exchange chromatography.

2.4 Materials and Methods

2.4.1 General Information

Commercial reagents were used as purchased from TCI Chemicals and MilliporeSigma. Organic solvents used were reagent grade purchased from Fisher Scientific. Dry solvents were purified using a Glass Contour Solvent System from Pure Process Technology, LLC, with Fisher HPLC grade DCM, Aldrich anhydrous DMF, and Fisher HPLC/ACS grade THF. Reactions were monitored by thin-layer chromatography carried out on silica gel 60 F254 plates (Merck). UV light (254 nm) and staining with aqueous $KMnO_4$ was used to visualize the developed chromatograms. Flash chromatography was performed using a Biotage instrument (SP4 A2A0) with RediSep Rf silica flash columns (12 g, 60 mg-1.2g sample size) and collected in 9 mL fraction volumes or performed via manual silica column chromatography using silica gel 60 (MilliporeSigma, 0.040-0.063 MM). Compounds purified via automatic flash chromatography are accompanied with a gradient table. All ^{1}H, ^{13}C and ^{31}P NMR spectra were recorded on a Bruker-AV-III-500-HD instrument. Chemical shifts (δ) are reported in parts per million relative to $CDCl_3$ (^{1}H NMR

residual peak at δ = 7.26 ppm, ^{13}C NMR residual peaks at δ = 77.3, 77.0, 76.8 ppm) and coupling constants (J) are given in Hz. Unless otherwise stated, all reactions occurred at 24 °C. Reported yields in figures are given as averages over the three most successful trials.

2.4.2 HPLC/MS-MS Analysis

The method used was based on a previously reported protocol.[32] Separation was performed on an Agilent Rapid Res 1200 HPLC system using a HILICON iHILIC-Fusion (2.1 x 150 mm, 3.5 µm) column. Mobile phase A was water with 35 mM NH_4OH, pH 5.75 and mobile phase B was ACN. Initial conditions were 3:97 A:B, held for 0.5 minute, followed by a linear gradient to 25:75 at 26.5 min, 40:60 at 27 min, and held until 33 min. Column re-equilibration was performed by returning to 3:97 A:B at 35 min and held until 45 min. Column flow rate was 0.3 mL/min. The retention time for PG was 7.5 min. Analytes were detected by MS/MS, based on multiple reaction monitoring, utilizing an Agilent 6460 triple quadrupole mass spectrometer. Electrospray ionization in negative mode was used with a transition of 773.4 to 281.2, with a collision energy of 45 V, for both BMP and PG. A fragmentor energy of 100 V and a dwell time of 200 ms was used. Source parameters were as follows: nitrogen gas temperature = 325 °C and flow rate = 9 L/min, nebulizer pressure = 40 psi, sheath gas temperature = 250 °C, sheath gas flow rate = 7 L/min, and capillary potential = 3.8 kV. All data were collected and analyzed with Agilent MassHunter B.03 software.

2.4.3 Procedure for the synthesis of 1,2-dioleyl-sn-glycero-3-phospho-(1'-sn-glycerol) (1)

In an oven dried 2-neck flask equipped with a magnetic stir bar was placed **2** (0.200 g, 0.19 mmol). The flask was dried via Schlenk techniques and equipped with an Ar balloon. Dry THF (3 mL) was then placed in the flask to dissolve **2**, followed by the addition of AcOH (0.227 g, 3.79 mmol). TBAF (1.0 M in dry THF) (0.990 g, 3.79 mmol) was subsequently added to the flask, and

the reaction was allowed to stir for 24 h at 23 °C before removal of the solvent *in vacuo*. The reaction mixture was then dissolved in 30 mL of $CHCl_3$ and placed directly into a separatory funnel followed by the addition of 20 mL of MeOH, and then 10 mL of water. After shaking, the organic layer separated, dried with anhydrous Na_2SO_4, and was concentrated *in vacuo*. The crude product was purified on a Biotage flash purification system (DCM:MeOH). After two rounds of silica chromatography (both followed the same gradient), the tetrabutyl ammonium salt of the product was removed by passage through 10 g of SP-Sephadex C-25 ion exchange medium that was swelled in 0.22 M NaCl over 2 d. After elution (MeOH:H_2O, 1:1), the pure product was removed from water by using a similar extraction to that of the crude product. Here, the fractions containing **1** were added to 30 mL of $CHCl_3$ placed in a separatory funnel followed by the addition of 20 mL of MeOH, and then 10 mL of water. Occasionally, centrifugation (7000 rpm for 5 min) was required to separate the layers. After shaking and/or centrifugation, the organic layer was collected and concentrated under reduced pressure to afford **1** as a clear colorless oil in 56% yield (0.082 g); $[\alpha]_D^{27}$ +0.975 (*c* 0.003, $CHCl_3$); *Rf* = 0.46 (DCM:MeOH:H_2O, 80:18:2); ^{1}H NMR (500 MHz, $CDCl_3$) δ 5.33 (q, *J* = 5.0, 4.5 Hz, 4H), 5.23 (dq, *J* = 8.8, 5.1 Hz, 1H), 4.43 – 4.34 (m, 1H), 4.15 (dd, *J* = 12.1, 6.8 Hz, 1H), 4.00 – 3.83 (m, 5H), 3.71 – 3.56 (m, 2H), 2.29 (dt, *J* = 14.7, 7.5 Hz, 4H), 2.00 (q, *J* = 6.4 Hz, 8H), 1.57 (t, *J* = 7.1 Hz, 4H), 1.38 – 1.17 (m, 42H), 0.88 (t, *J* = 6.7 Hz, 7H); ^{13}C NMR (126 MHz, $CDCl_3$) δ 130.0, 129.6, 77.3, 77.0, 76.8, 34.3, 34.1, 31.9, 29.8, 29.6, 29.3, 27.2, 24.9, 24.9, 22.7, 14.1; ^{31}P NMR (203 MHz, $CDCl_3$) δ 1.45; QTOF-HRMS (ESI) for $C_{42}H_{79}O_{10}P$ [M+Na^+]: found 797.5303, calcd 797.5303.

2.4.4 Procedure for the one-pot synthesis of (2R)-3-((((S)-2,3-bis((tert-butyldimethylsilyl)oxy)propoxy)(2-cyanoethoxy)phosphoryl)oxy)propane-1,2-diyl dioleate (2)

In an oven dried three-neck 25 mL round bottom flask was placed **3** (1.2 eq., 0.5 mmol). Schlenk techniques were used and the flask before it was equipped with an Ar balloon. 1-*H* tetrazole (3.0 eq., 1 mmol) and dry DCM (1.5 mL) was added and stirred until dissolved. A solution of **14** (1.0 eq, 0.4 mmol) in dry DCM (1.5 mL) was added dropwise to the reaction flask and stirred for 16 h. Then, under an open atmosphere, t-BuOOH (4.0 eq., 2 mmol, 70% in H_2O) was added. After mixing for 1 h, the reaction mixture was diluted with ethyl acetate (30 mL) and washed with saturated $NaHCO_3$ solution (2x20 mL). The combined aqueous washes were rinsed with ethyl acetate (2x25 mL) and all organic fractions were combined, dried with anhydrous Na_2SO_4 and concentrated under reduced pressure. The resulting crude product was purified on a Biotage flash purification system (hexane:EtOAc) to give the purified product as a clear colorless oil in 71% yield (0.29 g); $[\alpha]_D^{27}$ +2.73 (*c* 0.01, $CHCl_3$); R_f = 0.51 (DCM:MeOH, 96:4); ^{1}H NMR (500 MHz, $CDCl_3$) δ 5.37 – 5.30 (m, 4H), 5.24 (h, *J* = 4.8 Hz, 1H), 4.33 (ddd, *J* = 11.9, 9.4, 4.4 Hz, 1H), 4.28 – 4.11 (m, 6H), 3.99 (dq, *J* = 10.1, 5.7 Hz, 1H), 3.89 – 3.83 (m, 1H), 3.59 – 3.51 (m, 2H), 2.76 (td, *J* = 6.4, 2.8 Hz, 2H), 2.32 (dt, *J* = 11.4, 7.6 Hz, 4H), 2.01 (q, *J* = 6.4 Hz, 8H), 1.60 (p, *J* = 6.8 Hz, 4H), 1.29 (dd, *J* = 19.1, 5.5 Hz, 42H), 0.88 (d, *J* = 4.6 Hz, 24H), 0.09 (d, *J* = 3.8 Hz, 6H), 0.06 (s, 6H); ^{13}C NMR (126 MHz, $CDCl_3$) δ 173.1, 172.7, 116.1, 77.3, 77.0, 76.8, 71.8, 71.8, 69.6, 69.3, 65.8, 63.9, 63.8, 91.9, 61.5, 34.1, 34.0, 31.9, 29.7, 29.5, 29.3, 29.2, 29.1, 27.2, 27.2, 25.9, 25.7,24.8, 22.7, 19.6, 19.6, 18.3, 18.1, 14.1, -4.7, -4.76; ^{31}P NMR (203 MHz, $CDCl_3$) δ -1.37, -1.50; QTOF-HRMS (ESI) for $C_{57}H_{110}NO_{10}P$ [M+Na$^+$]: found 1078.7299.5303, calcd 1078.7297.

2.4.5 Procedure for the synthesis of (S)-3-hydroxypropane-1,2-diyl dioleate (3)

This protocol was based a previously reported method.[21] In a 100 mL round bottom flask was placed **5** (1.0 eq., 2 mmol) and DCM/H_2O (15 mL, 5% H_2O). Following the addition of DDQ (1.5 eq., 3 mmol) the reaction flask was completely wrapped in aluminum foil and stirred at 20 ºC for 4 h. The reaction mixture turned from dark green to a dark shade of red. The mixture was diluted with DCM and vacuum filtered through a coarse glass frit with celite. The collected filtrate was washed with saturated $NaHCO_3$ solution (40 mL), swirling gently to mix. The organic layer was washed again with $NaHCO_3$ (80 mL) and swirled vigorously to mix. Again the organic layer was washed with $NaHCO_3$ (2x100 mL), this time shaken to combine. The resulting organic solution was dried with anhydrous Na_2SO_4 concentrated under reduced pressure. The crude product was purified on a Biotage flash purification system (hexane:EtOAc) to yield the desired product as a clear colorless oil in an 84% yield (1.1 g); $[\alpha]_D^{26}$ +3.0 (*c* 0.016, EtOAc); R_f = 0.08 (Hexane:EtOAc, 9:1); ^{1}H NMR (500 MHz, $CDCl_3$) δ 5.38 – 5.30 (m, 4H), 5.08 (p, *J* = 5.0 Hz, 1H), 4.34 – 4.21 (m, 2H), 3.73 (ddd, *J* = 6.8, 4.9, 1.7 Hz, 2H), 2.33 (dt, *J* = 11.0, 7.5 Hz, 4H), 2.05 – 1.98 (m, 9H), 1.61 (p, *J* = 7.3 Hz, 4H), 1.35 – 1.23 (m, 41H), 0.88 (t, *J* = 6.9 Hz, 6H); ^{13}C NMR (126 MHz, $CDCl_3$) δ 173.8, 173.4, 130.0, 129.7, 77.3, 77.0, 76.8, 72.1, 62.0, 61.5, 34.3, 34.1, 31.9, 29.8, 29.7, 29.5, 29.3, 29.2, 29.1, 27.21, 27.16, 24.9, 22.7, 14.1; HRMS (ESI) $C_{39}H_{72}O_5$ [M+Na^+]: found 643.5262, calcd 643.5272.

2.4.6 Procedure for the synthesis of (R)-2,3-bis((tert-butyldimethylsilyl)oxy)propan-1-ol (4)

This protocol was based a previously reported method.[27] In a 100 mL round bottom flask was placed **6** (1.0 eq., 3 mmol) and DCM:H_2O (15 mL, 5% H_2O). Following the addition of DDQ (1.5 eq., 5 mmol) the reaction flask was completely wrapped in aluminum foil and stirred at 20 ºC

for 4 h. The reaction mixture turned from dark green to a dark shade of red. The mixture was diluted with DCM and vacuum filtered through a coarse glass frit with celite. The collected filtrate was washed with saturated $NaHCO_3$ solution (40 mL), swirling gently to mix. The organic layer was washed again with $NaHCO_3$ (80 mL), swirled vigorously to mix. Again, the organic layer was washed with $NaHCO_3$ (2x120 mL), this time shaken to combine. The resulting organic solution was dried with anhydrous Na_2SO_4 and concentrated under reduced pressure. The crude product was purified using a Biotage flash purification system (hexane:EtOAc) to give the desired product as a clear colorless oil in 78% yield (0.85g); $[\alpha]_D^{25}$ +9.45 (*c* 0.005, EtOAc); R_f = 0.35 (hexane:EtOAc, 9:1); ^{1}H NMR (500 MHz, $CDCl_3$) δ 3.78 – 3.73 (m, 1H), 3.66 – 3.54 (m, 4H), 2.17 (dd, *J* = 7.5, 4.9 Hz, 1H), 0.88 (d, *J* = 1.6 Hz, 18H), 0.08 (d, *J* = 2.4 Hz, 6H), 0.05 (d, *J* = 1.9 Hz, 6H); ^{13}C NMR (126 MHz, $CDCl_3$) δ 72.6, 64.9, 64.8, 25.9, 25.8, 18.3, 18.1, -4.6, -4.9, -5.5, -5.5; HRMS (ESI) for $C_{15}H_{36}O_3Si_2$ [M+Na$^+$]: found 321.2280, calcd 321.2276.

2.4.7 Procedure for the synthesis of (S)-3-((4-methoxybenzyl)oxy)propane-1,2-diyl dioleate (5)

This protocol was based a previously reported method.[33] In an oven dried 100 mL three-neck round bottom flask was placed **7** (1.0 eq., 5 mmol) and oleic acid (2.1 eq., 10 mmol). The contents of the flask were dried using Schlenk techniques, the flask was equipped with an Ar balloon and dry DCM (15 mL) was added. A solution of DCC (2.3 eq., 11 mmol) and DMAP (2.3 eq., 11 mmol) in dry DCM (15 mL) was prepared in a separate 100 mL round bottom flask and equipped with an Ar balloon. This solution was transferred to the three-neck reaction flask via a cannula and stirred at 20 ºC for 16 h. The formed salt was removed by vacuum filtration through a coarse glass frit containing celite and the resulting filtrate was collected and concentrated under reduced pressure. To the crude product was added a minimal amount of hexane and the mixture

was sonicated to dissolve the solid. The resulting solution was purified on a 4 cm diameter, 32 cm long silica gel column (hexane:EtOAc) to yield the desired product clear colorless oil in 82% yield (2.9 g). The use of a shorter column resulted in co-elution of oleic acid; $[\alpha]_D^{26}$ +7.08 (*c* 0.029, EtOAc); R_f = 0.32 (hexane:EtOAc, 9:1); ^{1}H NMR (500 MHz, $CDCl_3$) δ 7.25 – 7.20 (m, 2H), 6.90 – 6.84 (m, 2H), 5.38 – 5.30 (m, 4H), 5.24 – 5.20 (m, 1H), 4.46 (q, *J* = 11.7 Hz, 2H), 4.33 (dd, *J* = 11.9, 3.8 Hz, 1H), 4.17 (dd, *J* = 11.9, 6.4 Hz, 1H), 3.80 (s, 3H), 3.55 (dd, *J* = 5.2, 1.9 Hz, 2H), 2.29 (dt, *J* = 20.5, 7.5 Hz, 4H), 2.01 (q, *J* = 6.6 Hz, 8H), 1.64 – 1.55 (m, 4H), 1.29 (td, *J* = 13.2, 5.2 Hz, 40H), 0.88 (t, *J* = 6.9 Hz, 6H); ^{13}C NMR (126 MHz, $CDCl_3$) δ 173.4, 173.1, 159.3, 130.0, 129.8, 129.7, 129.3, 113.8, 72.9, 70.0, 67.9, 62.7, 55.3, 34.3, 34.1, 31.9, 29.8, 29.7, 29.5, 29.3, 29.2, 29.1, 29.1, 29.1, 27.2, 27.2, 24.9, 24.9, 22.7, 14.1; HRMS (ESI) for $C_{47}H_{80}O_6$ [M+Na$^+$]: found 763.5837, calcd 763.5847.

2.4.8 Procedure for the synthesis of (R)-5-(((4-methoxybenzyl)oxy)methyl)-2,2,3,3,8,8,9,9-octamethyl-4,7-dioxa-3,8-disiladecane (6)

In an oven dried 100 mL three-neck round bottom flask was placed **8** (4 eq., 19 mmol), and TBSCl (4 eq., 19 mmol). The contents were dried using Schlenk techniques and the closed flask was equipped with an Ar balloon. The contents were dissolved in dry DMF (15 mL) and the reaction was heated to 50 ºC in an oil bath. Et_3N (2.4 eq., 11 mmol) was added and stirred at 50 ºC for 4 h. After completion the reaction was quenched with water (60 mL) and extracted with EtOAc (3x80 mL). The combined organic layers were washed with water (3x 50 mL) and brine (2x25 mL) before being dried with anhydrous Na_2SO_4 and concentrated under reduced pressure. The crude product was purified using a Biotage flash purification system (hexane:EtOAc) to give the desired product as a clear colorless oil in 96% yield (2.0 g); $[\alpha]_D^{26}$ +4.39 (*c* 0.006, EtOAc); R_f = 0.49 (hexane:EtOAc, 9:1); ^{1}H NMR (500 MHz, $CDCl_3$) δ 7.25 (d, *J* = 7.9 Hz, 2H), 6.89 – 6.85

(m, 2H), 4.46 (s, 2H), 3.84 (qd, J = 5.6, 4.7 Hz, 1H), 3.80 (s, 3H), 3.60 (dd, J = 10.2, 5.8 Hz, 1H), 3.56 – 3.48 (m, 2H), 3.39 (dd, J = 9.9, 5.5 Hz, 1H), 0.88 (s, 18H), 0.06 (d, J = 1.2 Hz, 6H); ^{13}C NMR (126 MHz, $CDCl_3$) δ 159.1, 130.7, 129.2, 113.7, 73.0, 72.8, 71.9, 65.1, 55.3, 26.0, 25.9, 18.4, 18.2, 1.0, -4.6, -4.7, -5.3, -5.4; HRMS (ESI) for $C_{23}H_{44}O_4Si_2$ [M+Na$^+$]: found 463.2670, calcd 463.2657.

2.4.9 Procedure for the synthesis of (R)-3-((4-methoxybenzyl)oxy)propane-1,2-diol (7)

This protocol was based a previously reported method.[22] To a 100 mL round bottom flask containing a solution of **9** (1.0 eq., 8 mmol) in 21 mL THF was added aquesous HCl (1M, 2.8 eq., 22 mmol). The reaction mixture was stirred at 20 ºC for 2 h. Saturated $NaHCO_3$ solution was then added to quench the reaction and the reaction mixture was extracted with ethyl acetate (3x100 mL). The combined organic extracts were dried with anhydrous Na_2SO_4 and concentrated under reduced pressure. The crude product was purified on a Biotage flash purification system (DCM:MeOH) to give a white solid in 90 % yield (1.5 g); $[\alpha]_D^{25}$ +3.77 (c 0.009, EtOAc); R_f = 0.13 (DCM:MeOH, 98:2); ^{1}H NMR (500 MHz, $CDCl_3$) δ 7.26 – 7.22 (m, 2H), 6.89 – 6.85 (m, 2H), 4.46 (s, 2H), 3.85 (td, J = 6.0, 3.0 Hz, 1H), 3.79 (s, 3H), 3.67 – 3.55 (m, 2H), 3.49 (qd, J = 9.7, 5.2 Hz, 2H), 3.08 (s, 1H), 2.69 (s, 1H); ^{13}C NMR (126 MHz, $CDCl_3$) δ 159.4, 129.8, 129.5, 113.9, 73.2, 71.5, 70.7, 64.1, 55.3; HRMS (ESI) for $C_{11}H_{16}O_4$ [M+Na$^+$]: found 235.0940, calcd 235.0941.

2.4.10 Procedure for the synthesis of (S)-3-((4-methoxybenzyl)oxy)propane-1,2-diol (8)

This protocol was based a previously reported method.[21] To a 100 mL round bottom flask containing a solution of **10** (1.0 eq., 8 mmol) in 21 mL THF was added aqueous HCl (1M, 2.77 eq., 22 mmol). The reaction mixture was allowed to react at 20 ºC for 2 h. Saturated $NaHCO_3$ solution was added to quench the reaction and the reaction mixture was extracted with EtOAc

(3x100 mL). The combined organic extracts were dried with anhydrous Na_2SO_4 and concentrated under reduced pressure. The crude product was purified on a Biotage flash purification system (DCM:MeOH) to yield the product as a white solid in 93% yield (1.6 g); $[\alpha]_D^{25}$ -3.24 (*c* 0.010, EtOAc); R_f = 0.13 (DCM:MeOH, 98:2); ^{1}H NMR (500 MHz, $CDCl_3$) δ 7.25 – 7.22 (m, 2H), 6.89 – 6.86 (m, 2H), 4.47 (s, 2H), 3.86 (q, *J* = 5.6 Hz, 1H), 3.80 (s, 3H), 3.69 – 3.56 (m, 2H), 3.50 (qd, *J* = 9.7, 5.2 Hz, 2H), 2.96 (d, *J* = 4.8 Hz, 1H), 2.54 (t, *J* = 6.0 Hz, 1H); ^{13}C NMR (126 MHz, $CDCl_3$) δ 159.4, 129.8, 129.5, 113.9, 73.2, 71.5, 70.7, 64.1, 55.3; HRMS (ESI) for $C_{11}H_{16}O_4$ [M+Na$^+$]: found 235.0945, calcd 235.0941.

2.4.11 Procedure for the synthesis of (S)-4-(((4-methoxybenzyl)oxy)methyl)-2,2-dimethyl-1,3-dioxolane (9)

This protocol was based a previously reported method.[21] To an oven dried 250 mL multineck round bottom flask was added NaH (3.0 eq., 113 mmol). Schlenk techniques were utilized to evacuate the flask and dry DMF (50 mL) was added. The flask was maintained under an Ar atmosphere for the duration of the reaction. The reaction flask was lowered into an ice bath and (*S*)-solketal (1.0 eq., 38 mmol) was added dropwise and allowed to react with vigorous stirring at 5 ºC for 45 min. PMBCl (1.1 eq., 42 mmol) was added and stirred at 20 ºC for 4 h. The completed reaction was quenched slowly with saturated NH_4Cl solution and extracted with EtOAc (3x150 mL). The combined organic extracts were washed with water (2x150 mL), washed with brine (2x150 mL), dried over anhydrous Na_2SO_4, and concentrated under reduced pressure. The crude product was purified on a 5 cm diameter silica gel column (DCM:MeOH 98:2) to yield the desired product as a yellow oil in 96% yield (9.2 g); $[\alpha]_D^{25}$ +39.85 (*c* 0.001, EtOAc); R_f = 0.50 (DCM:MeOH, 98:2); ^{1}H NMR (500 MHz, $CDCl_3$) δ 7.28 – 7.23 (m, 2H), 6.90 – 6.85 (m, 2H), 4.50 (q, *J* = 11.7 Hz, 2H), 4.28 (p, *J* = 6.0 Hz, 1H), 4.04 (dd, *J* = 8.3, 6.4 Hz, 1H), 3.80 (s, 3H),

3.72 (dd, J = 8.3, 6.3 Hz, 1H), 3.48 (ddd, J = 43.4, 9.8, 5.7 Hz, 2H), 1.42 (s, 3H), 1.36 (s, 3H); ^{13}C NMR (126 MHz, $CDCl_3$) δ 159.3, 130.0, 129.4, 113.8, 109.4, 74.8, 73.2, 70.8, 66.9, 55.3, 26.8, 25.4. HRMS (ESI) for $C_{14}H_{20}O_4$ [M+Na$^+$]: found 275.1252, calcd 275.1254.

2.4.12 Procedure for the synthesis of (R)-4-(((4-methoxybenzyl)oxy)methyl)-2,2-dimethyl-1,3-dioxolane (10)

To an oven dried 250 mL multineck round bottom flask was added NaH (3.0 eq., 113 mmol). Schlenk techniques were utilized to evacuate the flask and dry DMF (50 mL) was added. The flask was maintained under a continuous Ar atmosphere for the duration of the reaction. The reaction flask was lowered into an ice bath and (*R*)-solketal (1.0 eq., 38 mmol) was added dropwise and allowed to stir vigorously at 0 ºC for 45 min. PMBCl (1.1 eq., 42 mmol) was added and stirred at 20 ºC for 4 h. The completed reaction was quenched slowly with saturated NH_4Cl solution and extracted with ethyl acetate (3x150 mL). Combined organic extracts were washed with water (2x150 mL), washed with brine (2x150 mL), dried over anhydrous Na_2SO_4, and concentrated under reduced pressure. The crude product was purified on a 5 cm silica gel column (DCM:MeOH, 98:2) to yield the desired product as a yellow oil in 99% yield (9.5 g); $[\alpha]_D^{25}$ -14.22 (*c* 0.025, EtOAc); R_f = 0.50 (DCM:MeOH, 98:2); ^{1}H NMR (500 MHz, $CDCl_3$) δ 7.28 – 7.22 (m, 2H), 6.89 – 6.84 (m, 2H), 4.50 (q, J = 11.7 Hz, 2H), 4.31 – 4.24 (m, 1H), 4.04 (dd, J = 8.3, 6.4 Hz, 1H), 3.79 (s, 3H), 3.72 (dd, J = 8.3, 6.3 Hz, 1H), 3.48 (ddd, J = 43.3, 9.8, 5.7 Hz, 2H), 1.38 (d, J = 29.6 Hz, 6H); ^{13}C NMR (126 MHz, $CDCl_3$) δ 159.3, 130.1, 129.4, 113.8, 109.4, 74.8, 73.2, 70.8, 66.9, 55.3, 26.8, 25.4; HRMS (ESI) for $C_{14}H_{20}O_4$ [M+Na$^+$]: found 275.1257, calcd 275.1254.

2.4.13 Procedure for the synthesis of (S)-2,3-bis((tert-butyldimethylsilyl)oxy)propyl(2-cyanoethyl) diisopropylphosphoramidite (14)

This method was based on previously reported protocol.[30] In dry 25 mL round bottom flask was placed **4** (1.0 eq., 0.6 mmol). The flask was dried with Schlenk techniques and fitted with an Ar balloon. To the flask was added 1-*H* tetrazole (1.5 eq., 0.8 mmol) and dry ACN (2 mL). Phosphoramidite (2.0 eq., 1 mmol) was added to the reaction flask dropwise at a rapid rate and stirred at 20 ºC for 18 h. Then, the reaction mixture was diluted with EtOAc (10 mL) and filtered through a coarse glass frit. The collected filtrate was washed with saturated $NaHCO_3$ solution (15 mL), after which it was dried with anhydrous Na_2SO_4 and the solvent removed under reduced pressure. A Biotage flash purification system was used to purify the crude product to give the desired product in 79% yield (0.23 g); clear colorless liquid; $[\alpha]_D^{27}$ +6.26 (*c* 0.009, $CHCl_3$) R_f = 0.55 (Hexane:EtOAc, 9:1); ^{1}H NMR (500 MHz, $CDCl_3$) δ 3.88 – 3.77 (m, 3H), 3.69 – 3.47 (m, 6H), 2.63 (tdd, *J* = 6.3, 3.3, 2.0 Hz, 2H), 1.20 – 1.16 (m, 12H), 0.89 (d, *J* = 2.7 Hz, 18H), 0.09 – 0.04 (m, 12H); ^{13}C NMR (126 MHz, $CDCl_3$) δ 127.3, 77.3, 77.0, 76.8, 65.0, 64.8, 58.5, 43.04, 26.0, 25.9, 25.7, 24.7, 24.6, 20.4, 18.4, 18.2, -4.6, -4.7, -5.4, -5.4 ; ^{31}P NMR (203 MHz, $CDCl_3$) δ 148.48, 147.88; QTOF-HRMS (ESI) for $C_{24}H_{53}N_2O_4PSi_2$ $[M+Na^+]$: found 521.3339, calcd 521.3354.

2.5 Supporting Information

2.5.1 Gradient Tables Used for Column Chromatography

Table 2.1. Purification of **1**.

Flow Rate	Apolar:Polar Solvent	Product Appearance	Gradient Steps (in % MeOH)		
			Start (%)	End (%)	Length (mL)
17 mL/min	DCM:MeOH	Fractions [80-96]	1	1	90
			1	2	72
			2	2	72
			2	3	72
			3	3	72
			3	4	72
			4	4	72
			4	5	72
			5	5	72
			5	6	72
			6	6	72
			6	7	72
			7	7	72
			7	8	72
			8	10	72
			10	15	288

Table 2.2. Purification of **2**.

Flow Rate	**Apolar:Polar Solvent**	**Product Appearance**	**Gradient Steps (in %EtOAc)**		
			Start (%)	End (%)	Length (mL)
			5%	5	72
			5%	5	72
			5%	7	72
			7%	9	72
			9%	10	72
17 mL/min	Hexane:EtOAc	Fractions 65-80	10%	10	72
			10%	10	72
			10%	10	72
			10%	20	72
			20%	25	72
			25%	25	72
			25%	30	72
			30%	30	72

Table 2.3. Purification of **3**

Flow Rate	**Apolar:Polar Solvent**	**Product Appearance**	**Gradient Steps (in %EtOAc)**		
			Start (%)	End (%)	Length (mL)
			0%	0	90
			0%	0	72
			0%	1	72
			1%	2	72
15 mL/min	Hexane:EtOAc	Fractions 53-80	2%	3	72
			3%	4	72
			4%	5	72
			5%	6	72
			6%	10	72
			10%	10	144

Table 2.4. Purification of **4**.

Flow Rate	**Apolar:Polar Solvent**	**Product Appearance**	**Gradient Steps (in %EtOAc)**		
			Start (%)	End (%)	Length (mL)
15 mL/min	Hexane:EtOAc	Fractions 22-30	0%	0	90
			0%	0	72
			0%	1	72
			1%	2	72
			2%	3	72
			3%	4	72
			4%	5	72
			5%	6	72
			6%	10	72

Table 2.5. Purification of **6**.

Flow Rate	**Apolar:Polar Solvent**	**Product Appearance**	**Gradient Steps (in %EtOAc)**		
			Start (%)	End (%)	Length (mL)
20 mL/min	Hexane:EtOAc	Fractions 2-12	0%	0	135
			0%	0	72
			0%	1	72
			1%	1	72
			1%	2	72
			2%	2	72
			2%	3	72
			3%	5	72
			5%	5	72

Table 2.6. Purification of **7**.

Flow Rate	**Apolar:Polar Solvent**	**Product Appearance**	**Gradient Steps (in %MeOH)**		
			Start (%)	End (%)	Length (mL)
			0	0	135
			0	0	72
17 mL/min	DCM:MeOH	Fractions 20-38	0	1	72
			1	1	72
			1	8	72
			8	8	504

Table 2.7. Purification of **8**.

Flow Rate	**Apolar:Polar Solvent**	**Product Appearance**	**Gradient Steps (in %MeOH)**		
			Start (%)	End (%)	Length (mL)
			0	0	135
			0	0	72
17 mL/min	DCM:MeOH	Fractions 6-38	0	1	72
			1	1	72
			1	8	72
			8	8	504

Table 2.8. Purification of **14**.

Flow Rate	**Apolar:Polar Solvent**	**Product Appearance**	**Gradient Steps (in %EtOAc)**		
			Start (%)	End (%)	Length (mL)
17 mL/min	Hexane:EtOAc	Fractions 3-7	5%	5	90
			5%	10	72
			10%	10	72
			10%	15	72
			15%	15	72

2.5.2 NMR Spectra of All Compounds

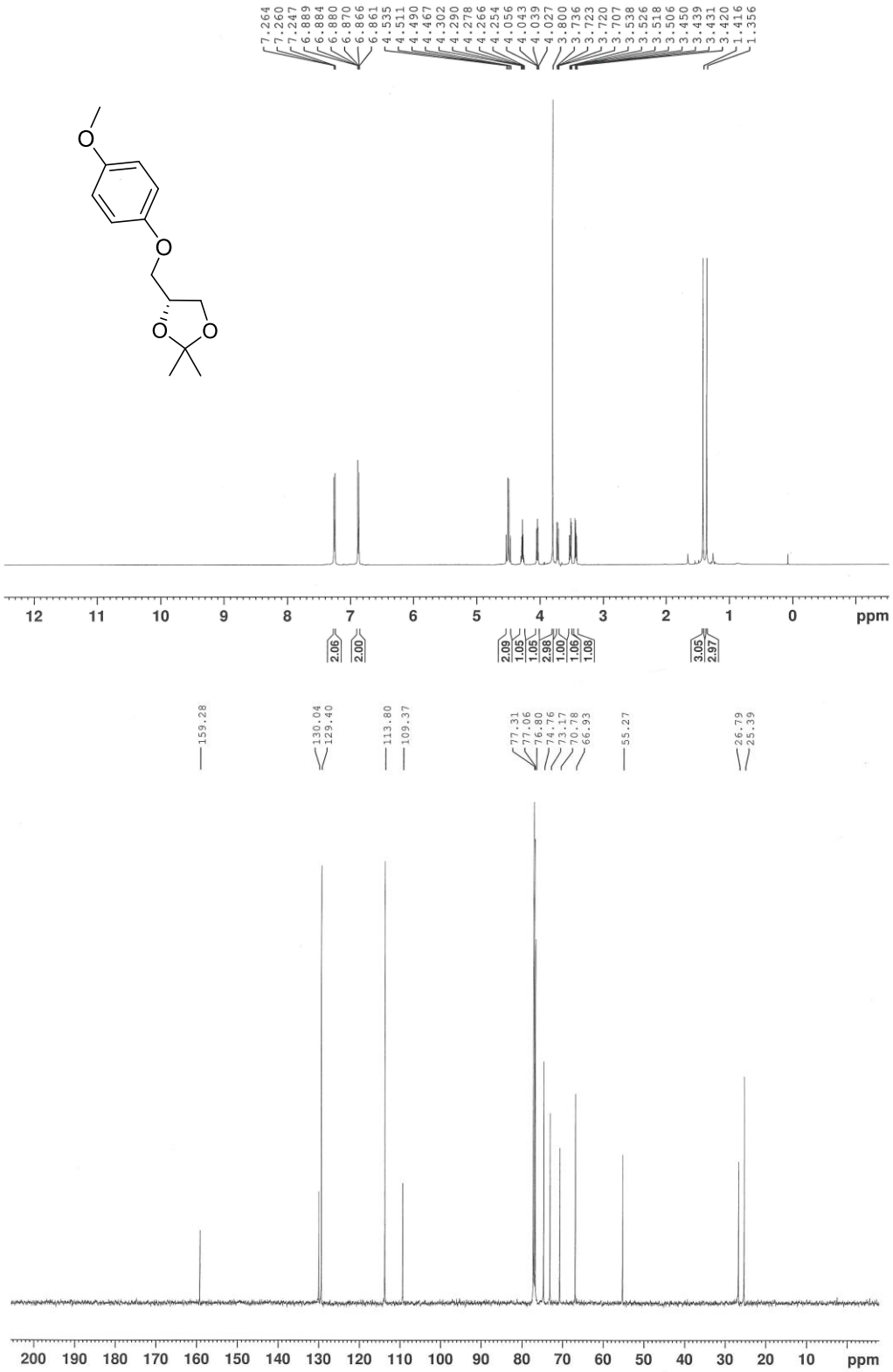

Figure 2.9. ^{1}H NMR and ^{13}C NMR of **10**.

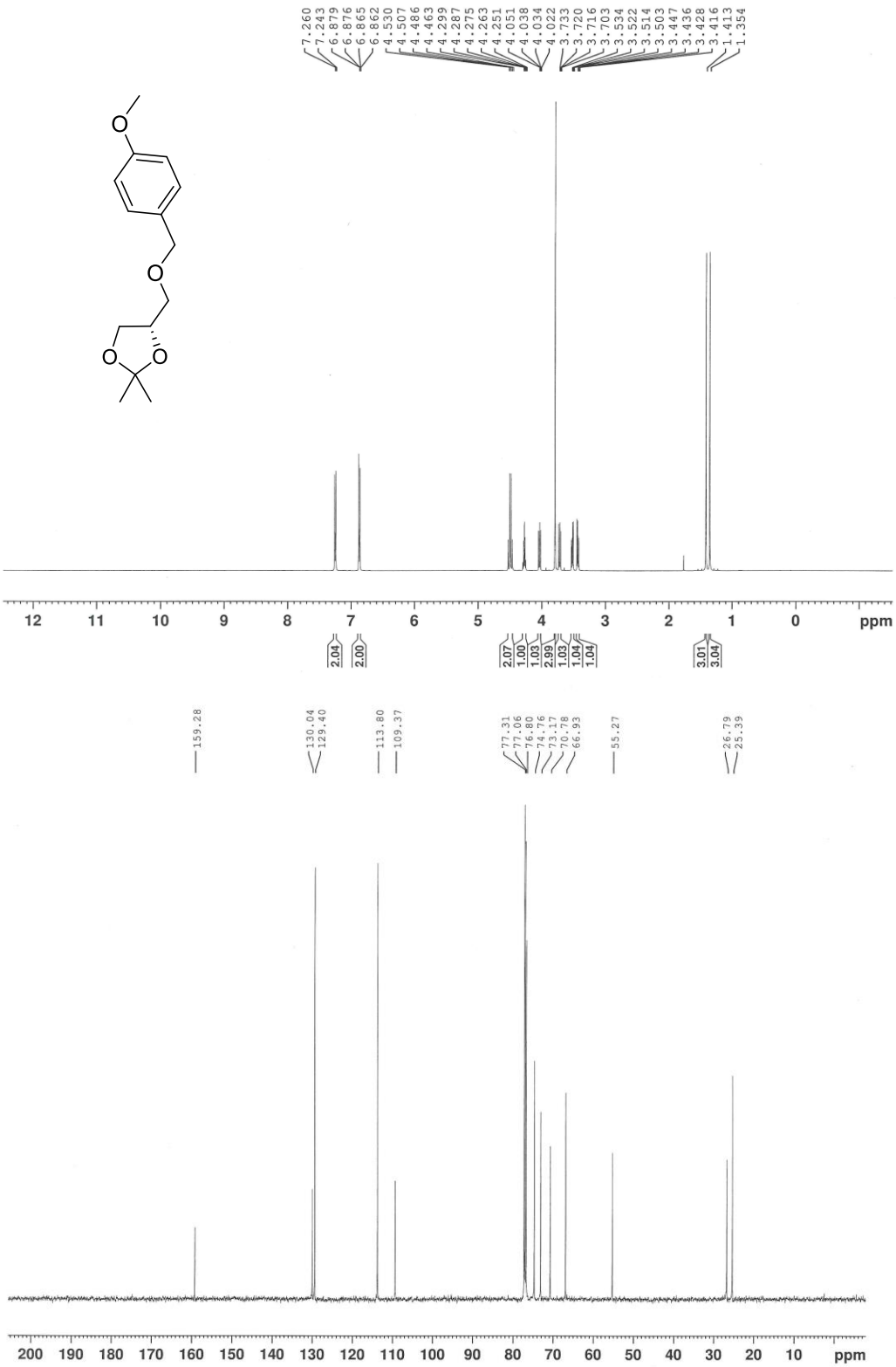

Figure 2.10. ^{1}H and ^{13}C NMR of **9**.

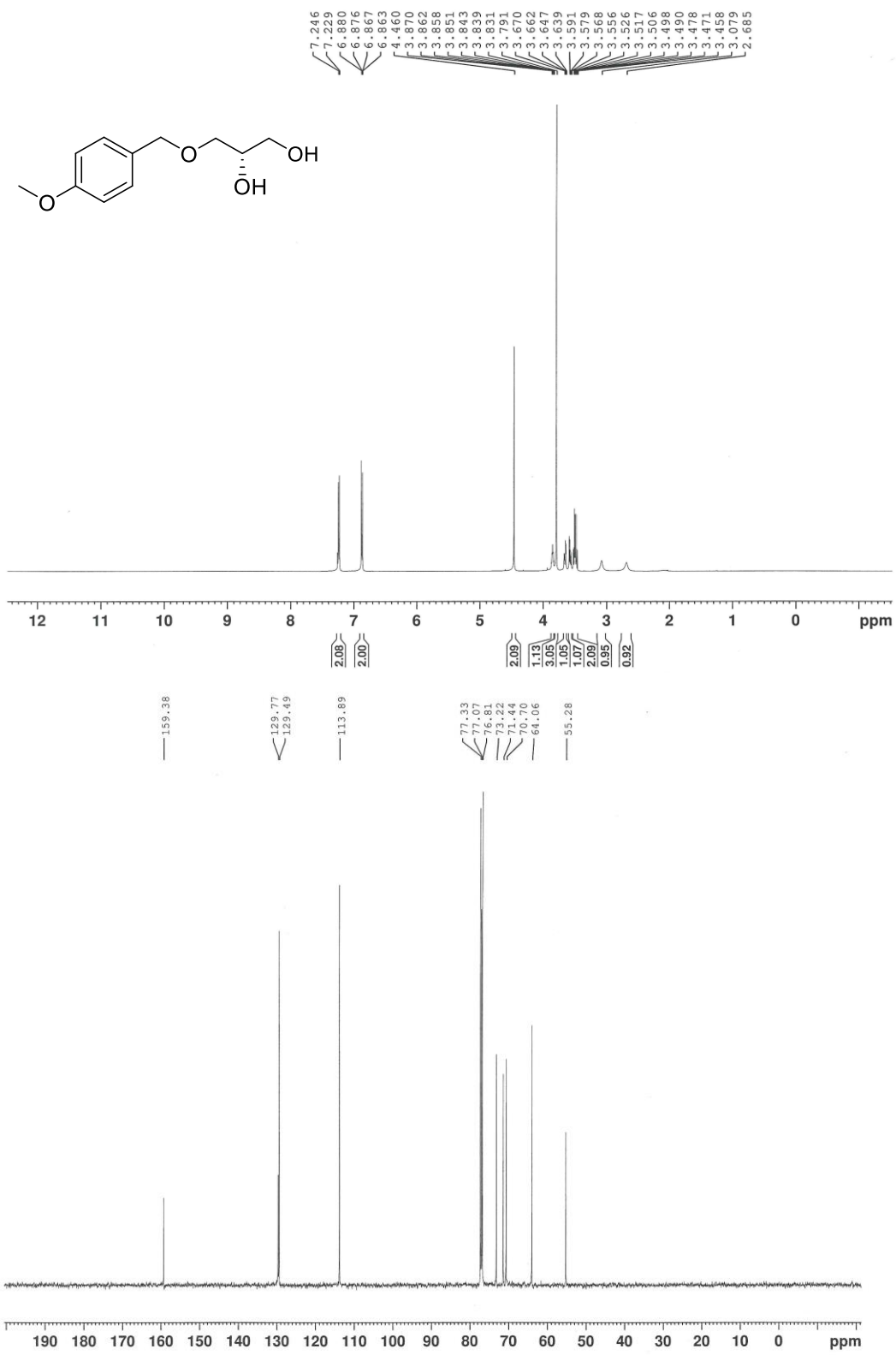

Figure 2.11. ^{1}H and ^{13}C NMR of **8**.

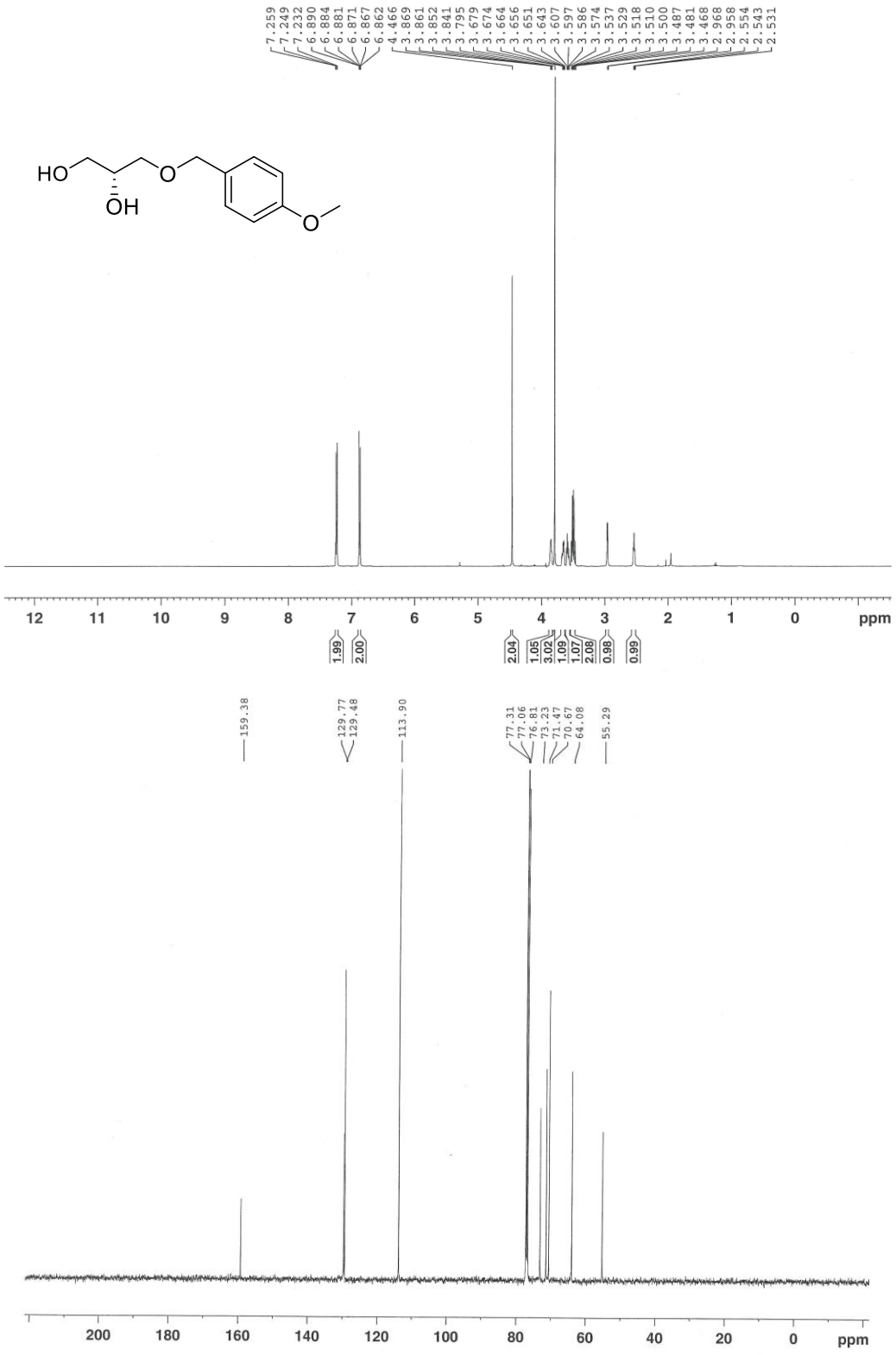

Figure 2.12. ^{1}H and ^{13}C NMR of **7**.

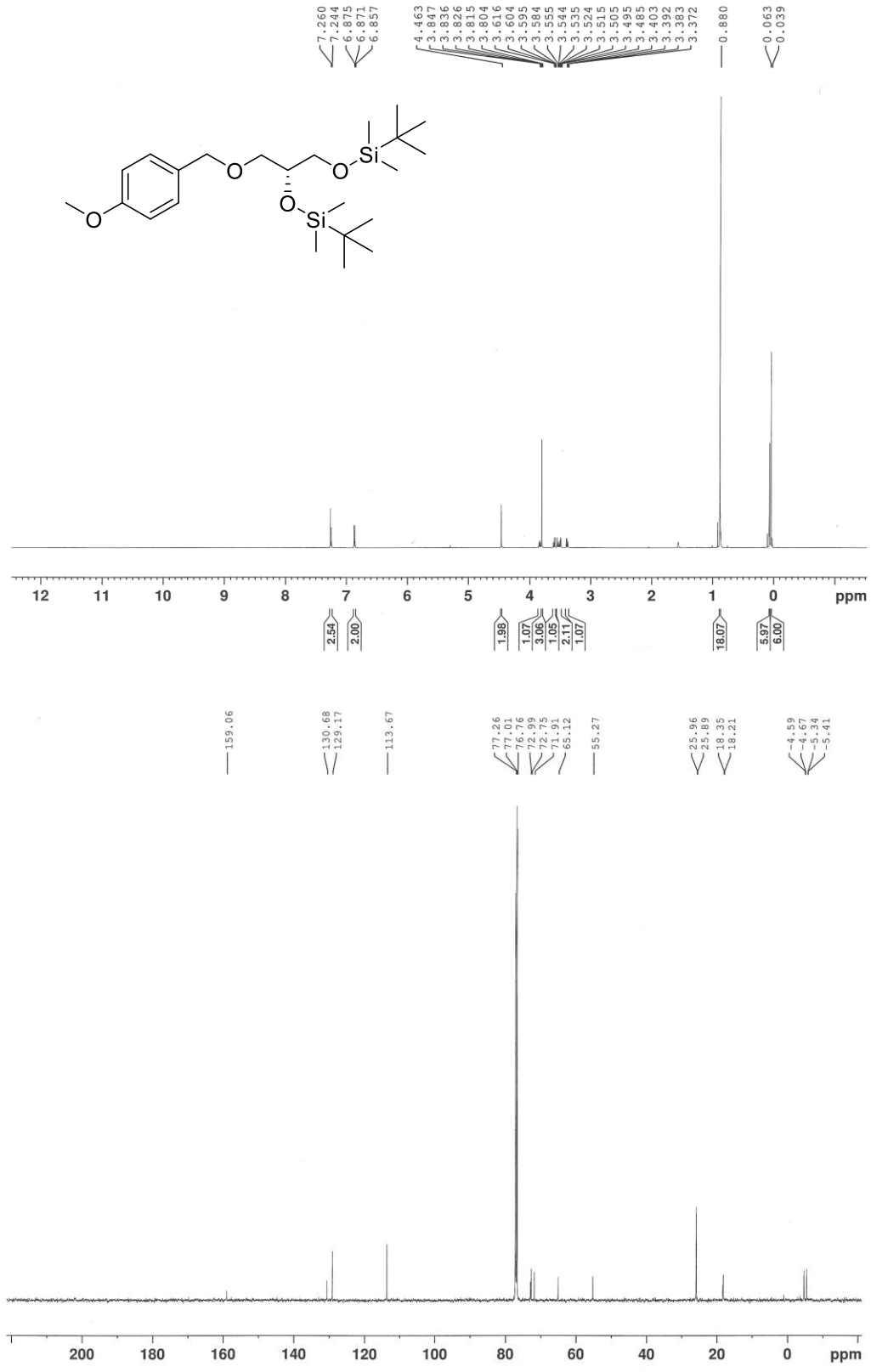

Figure 2.13. ^{1}H and ^{13}C NMR of **6**.

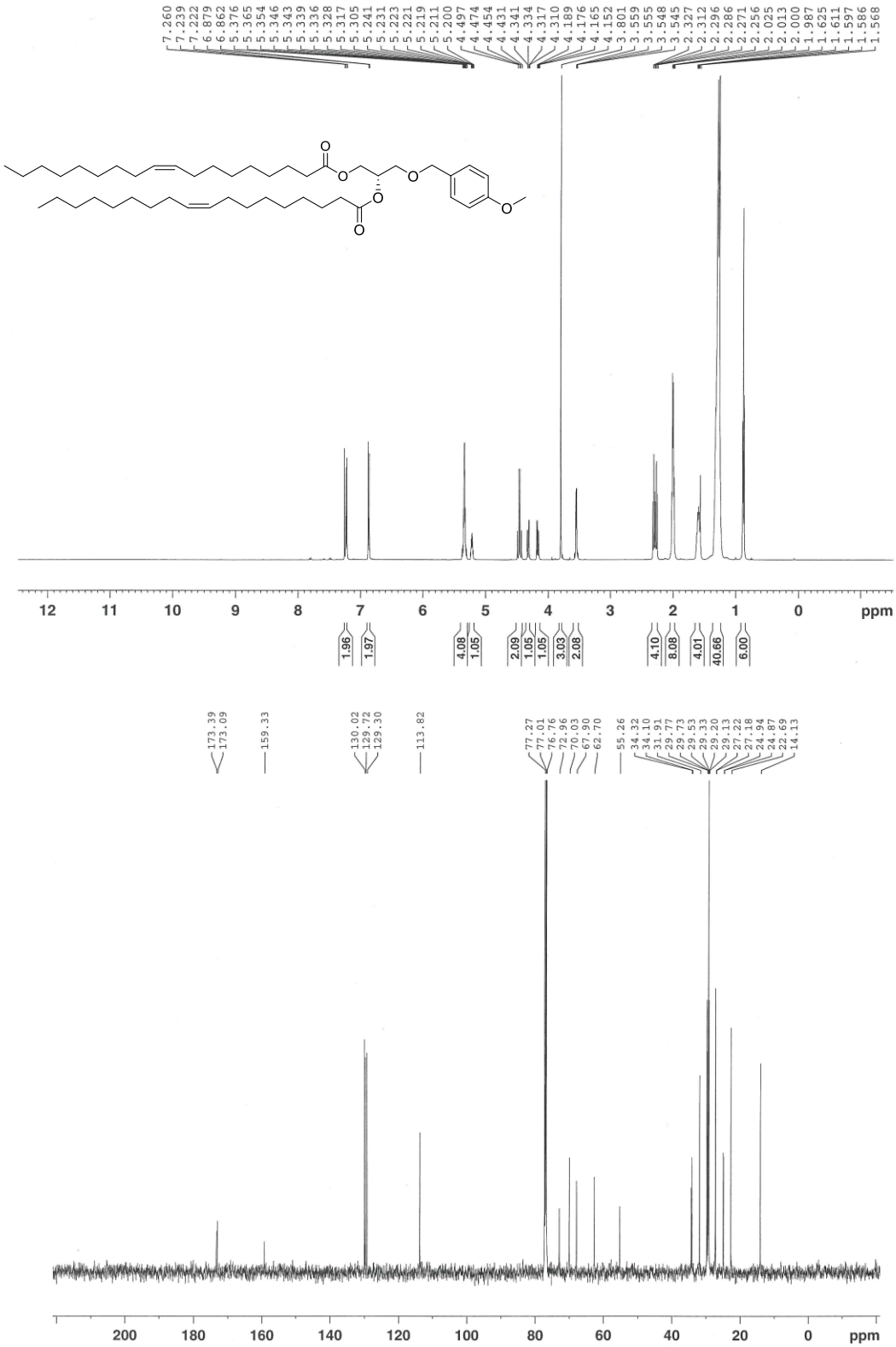

Figure 2.14.^{1}H and ^{13}C NMR of **5**.

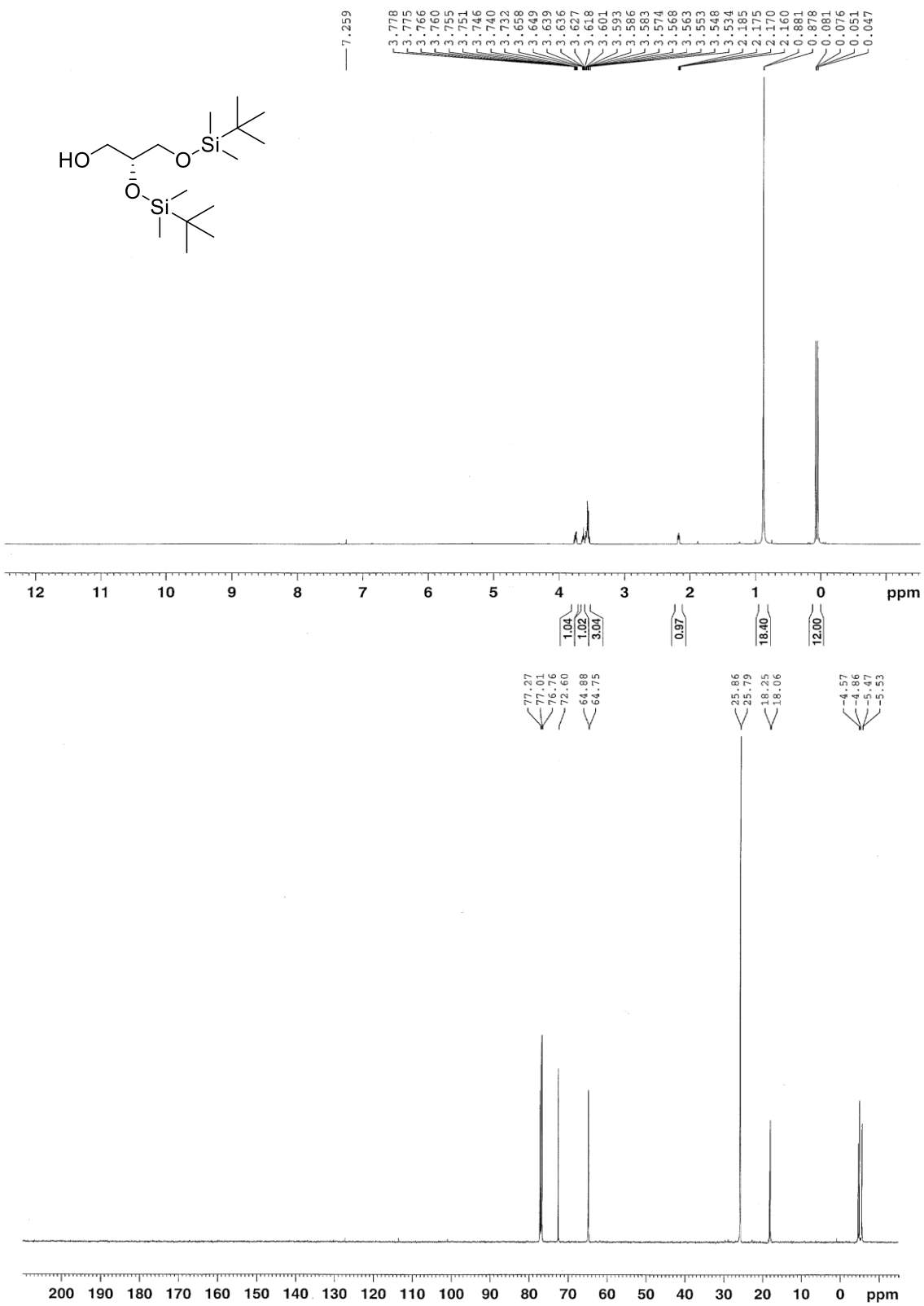

Figure 2.15. ^{1}H and ^{13}C NMR of **4**.

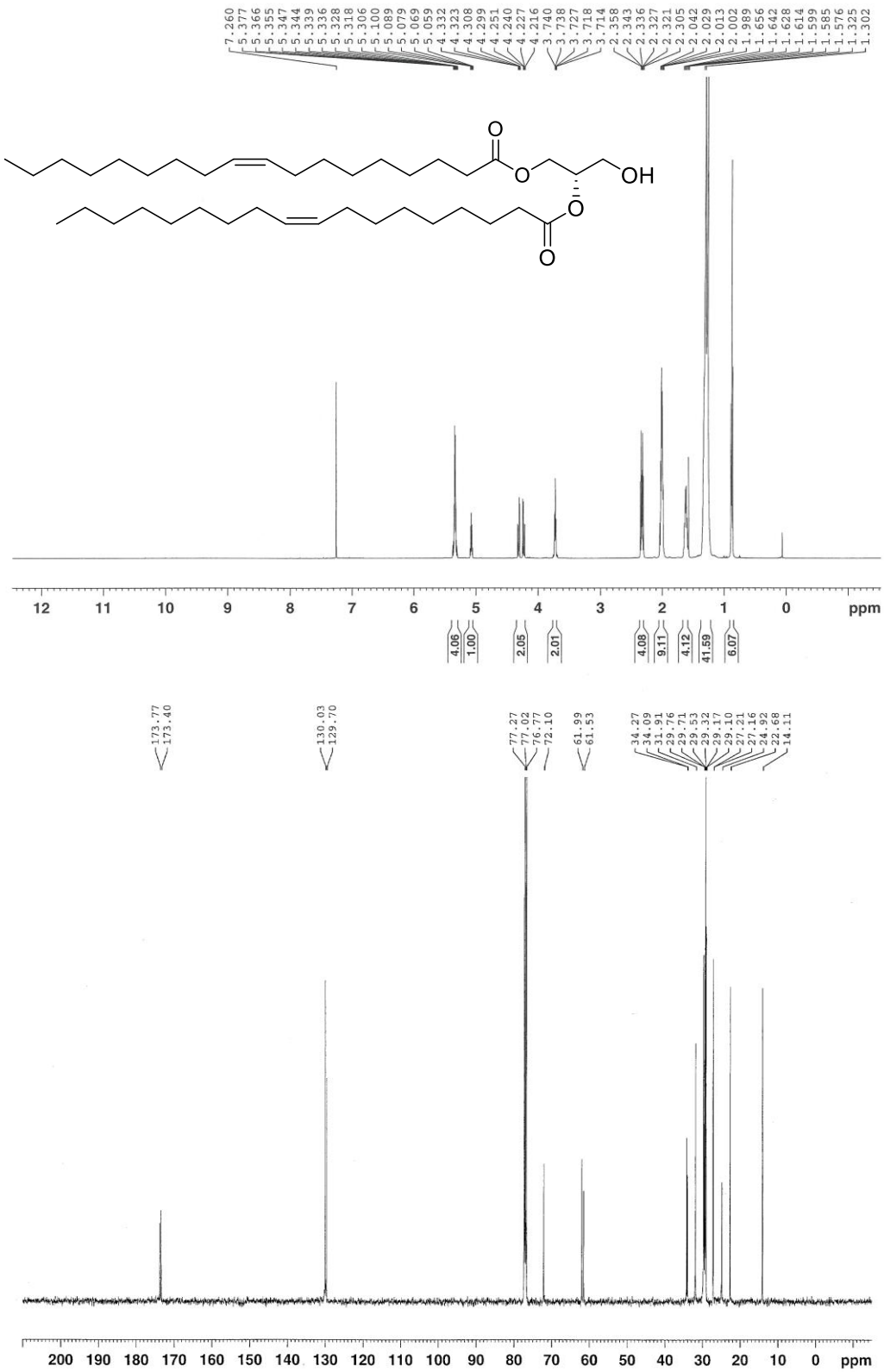

Figure 2.16. ^{1}H and ^{13}C NMR of **3**.

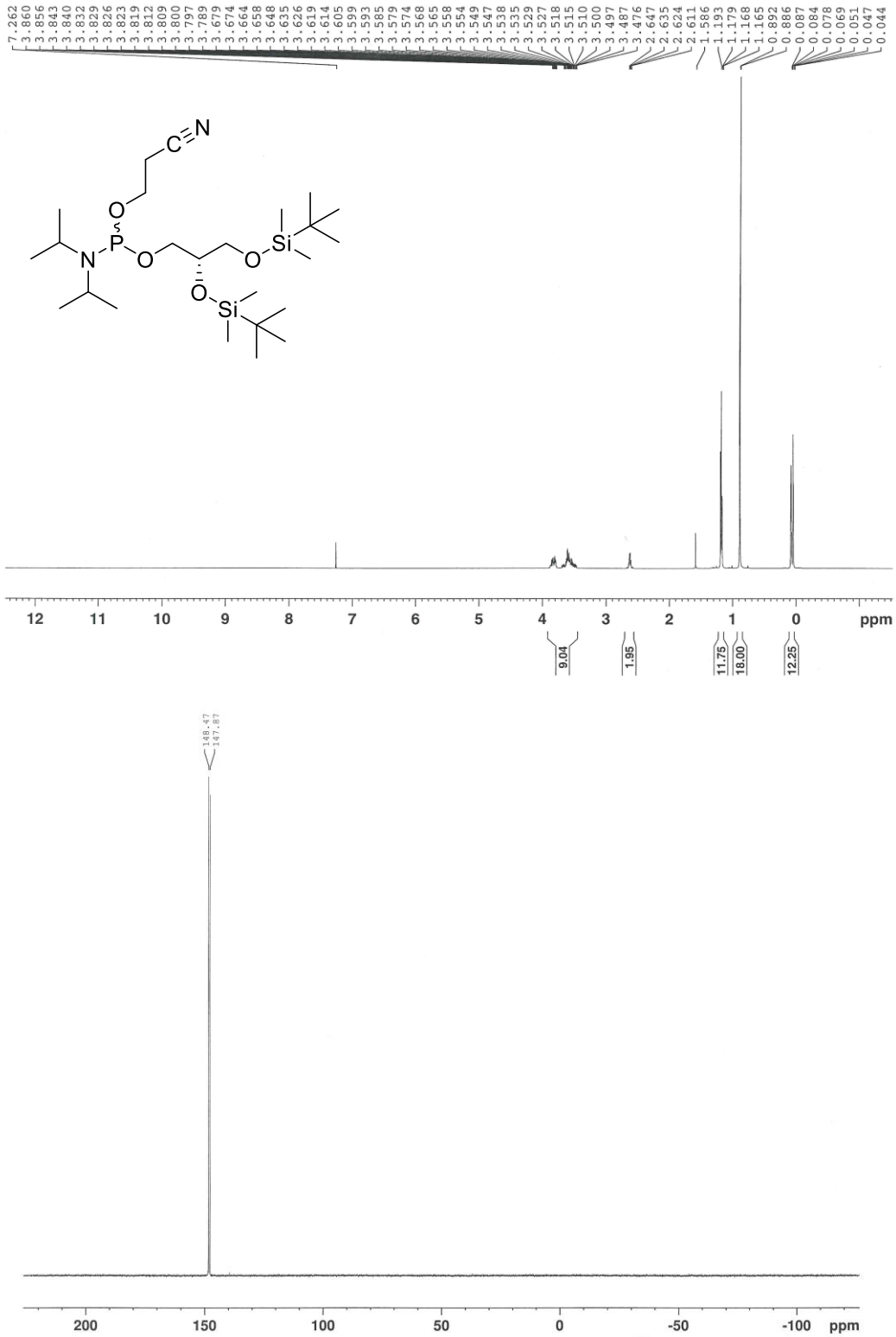

Figure 2.17. ^{1}H,^{13}C, and ^{31}P NMR of **14**.

Figure 2.17 continued.

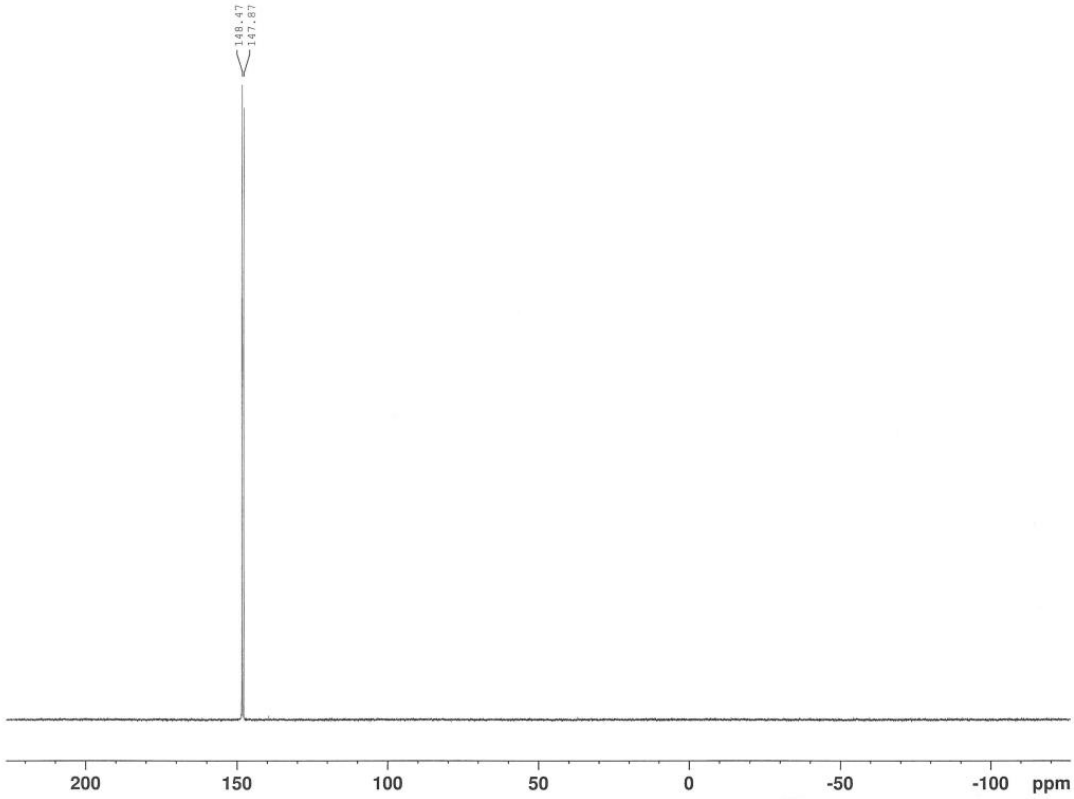

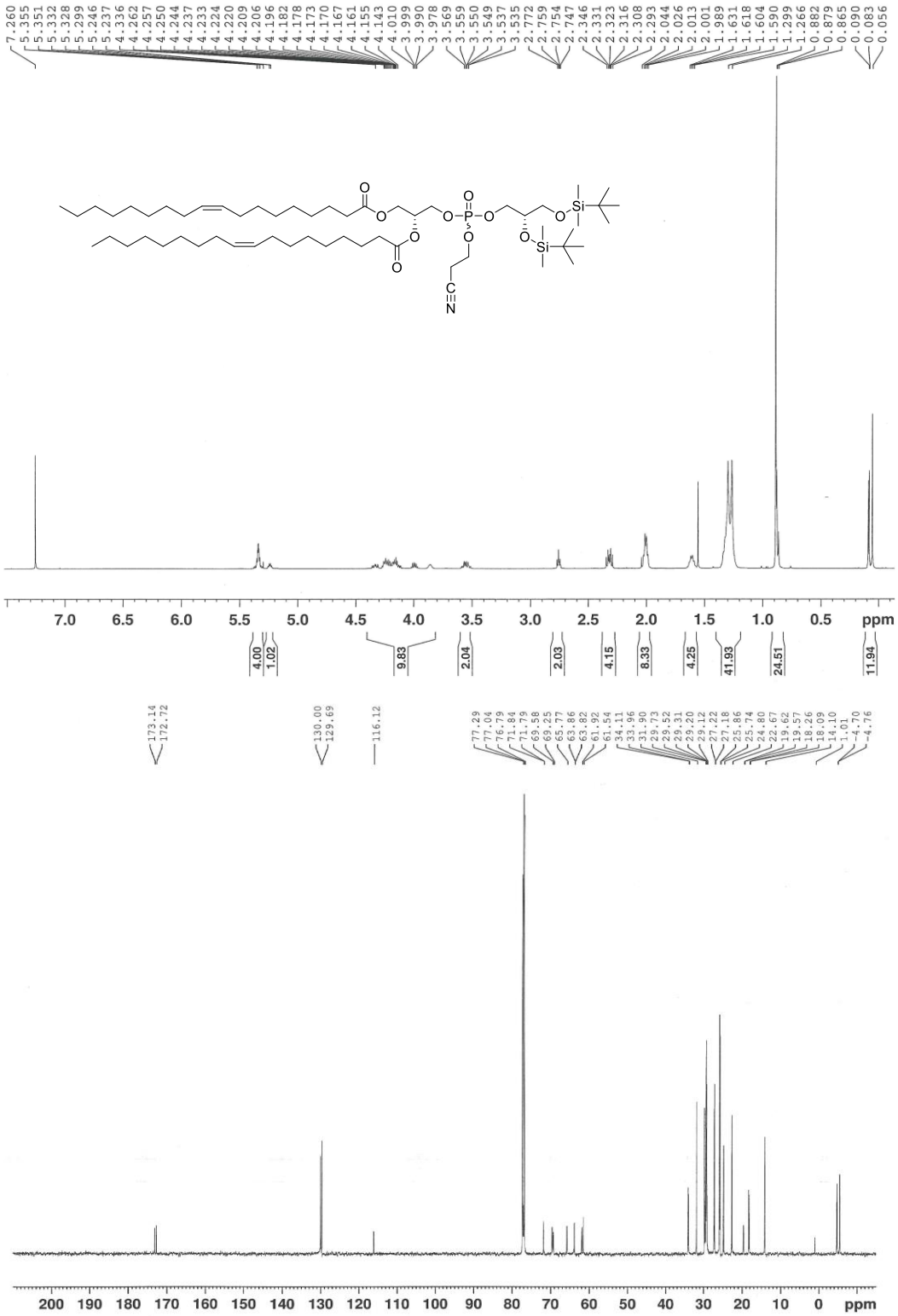

Figure 2.18. ^{1}H,^{13}C, and ^{31}P NMR of **2**.

Figure 2.18 continued.

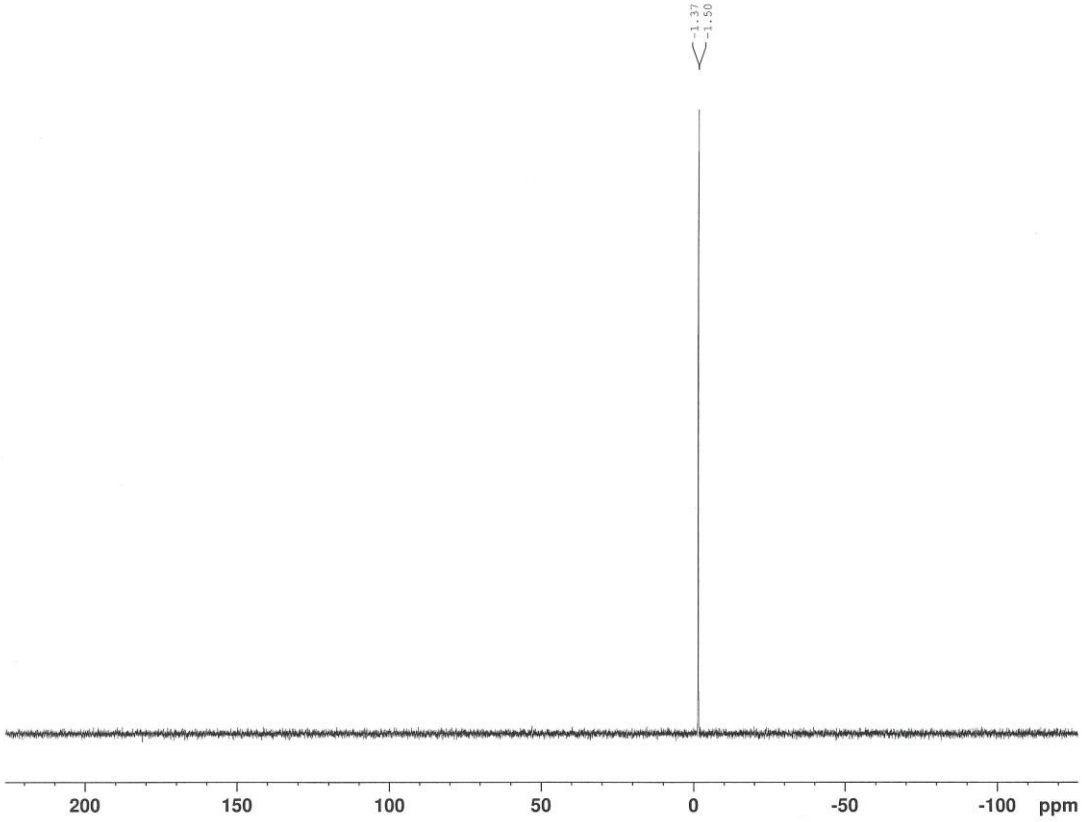

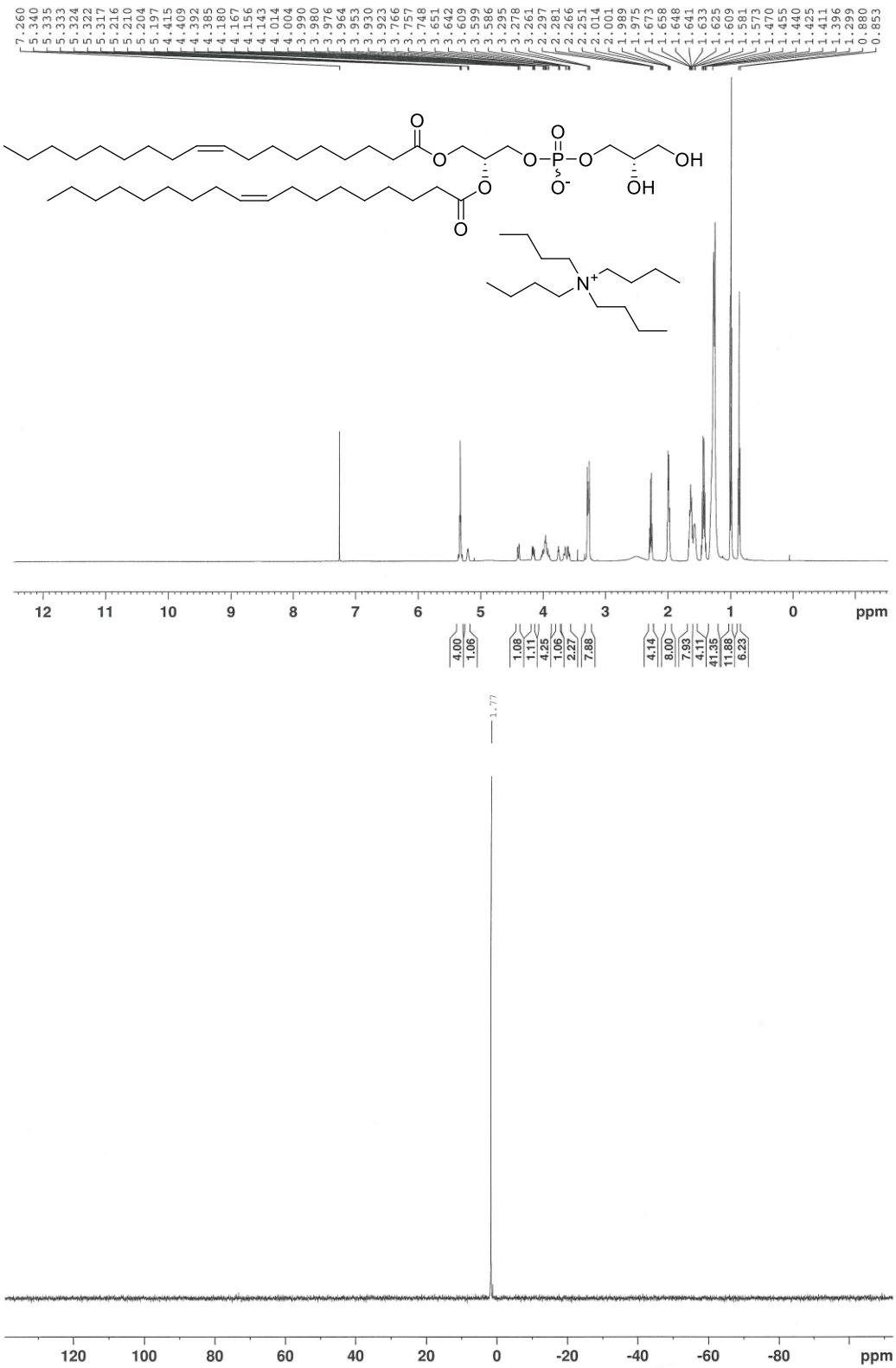

Figure 2.19. ^{1}H and ^{31}P NMR of the tetrabutylammonium salt of **1**.

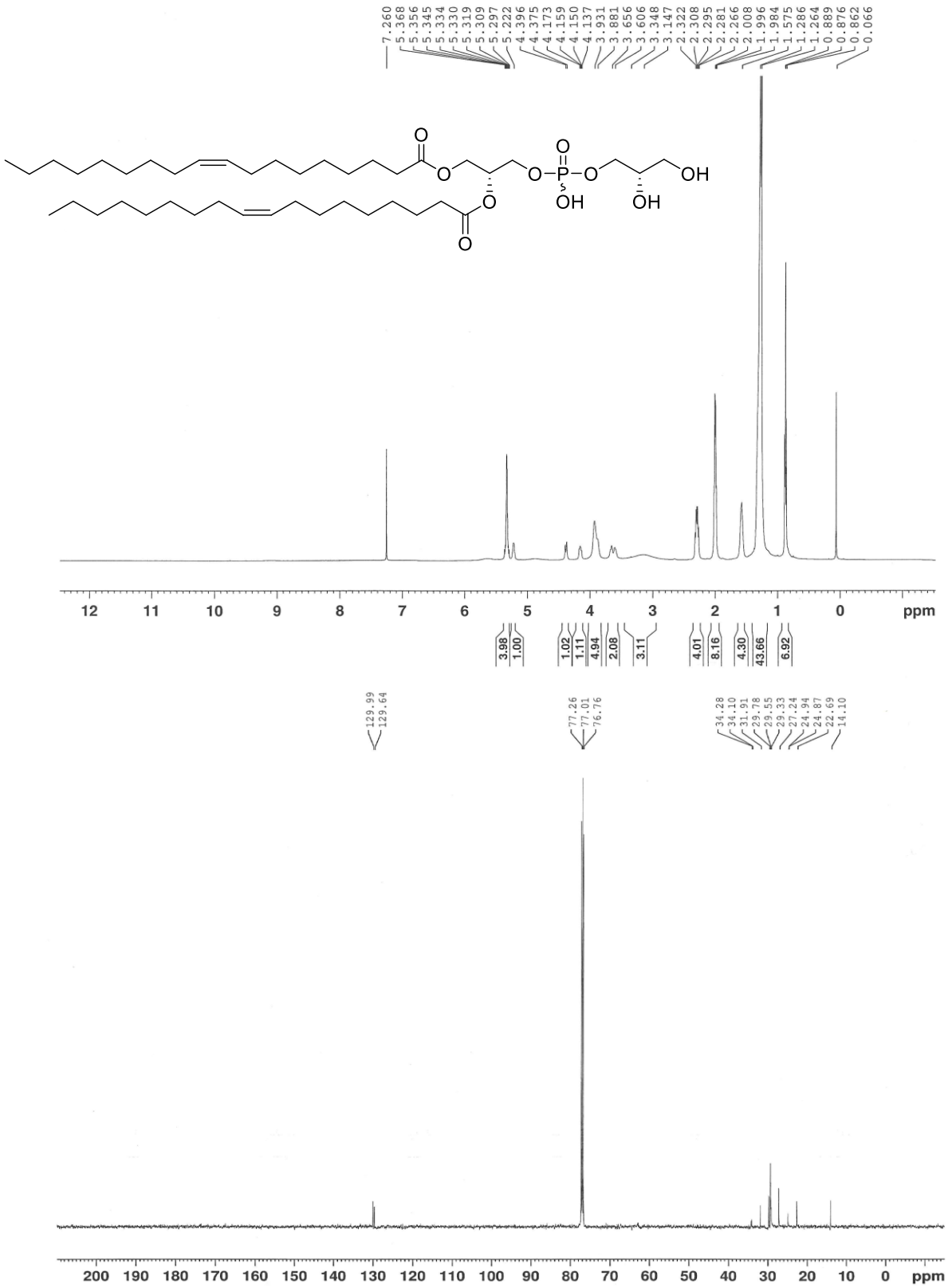

Figure 2.20. ^{1}H and ^{13}C NMR of **1**.

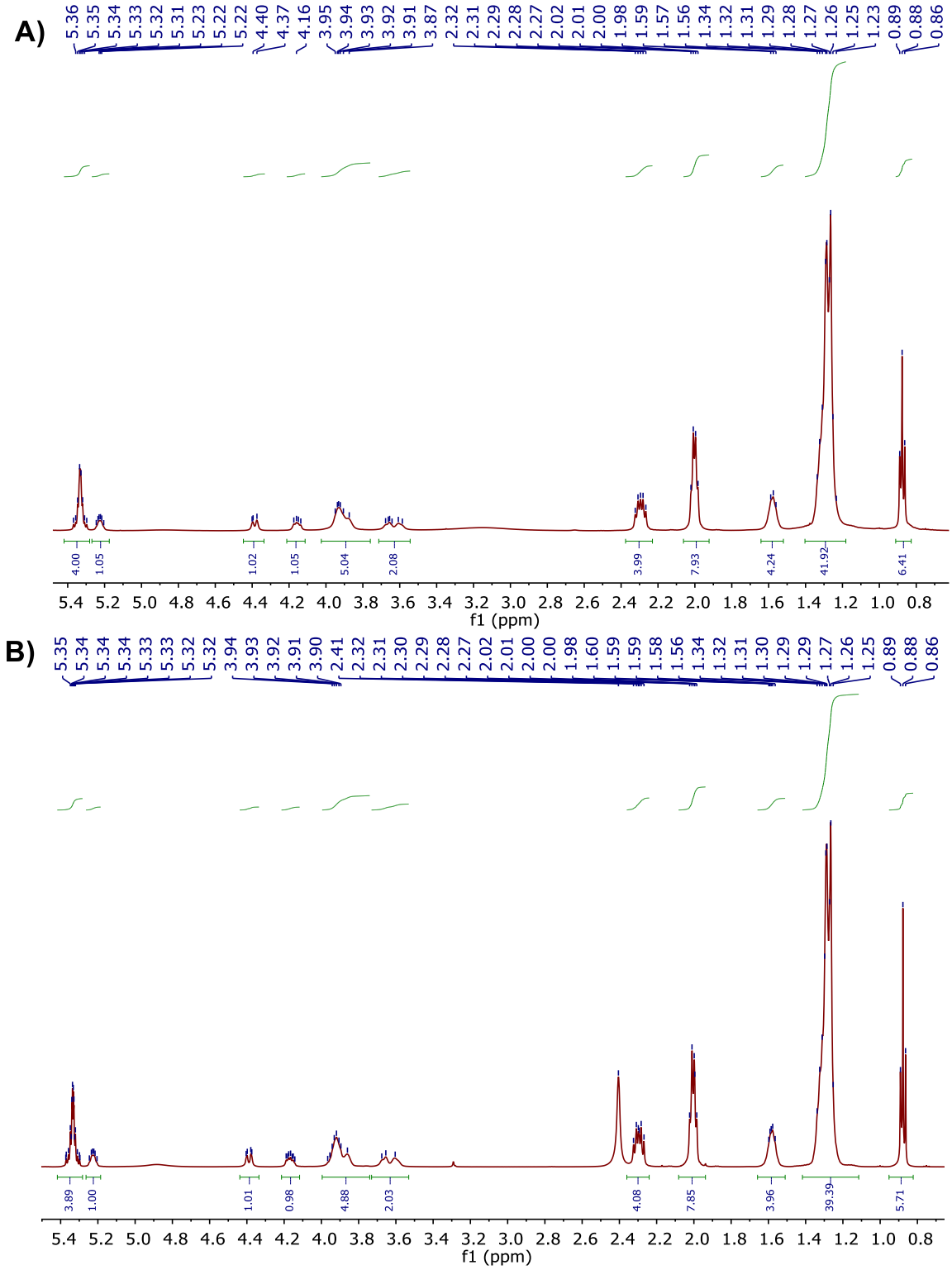

Figure 2.21. ^{1}H NMR comparison of synthesized PG (A) and commercial PG (B).

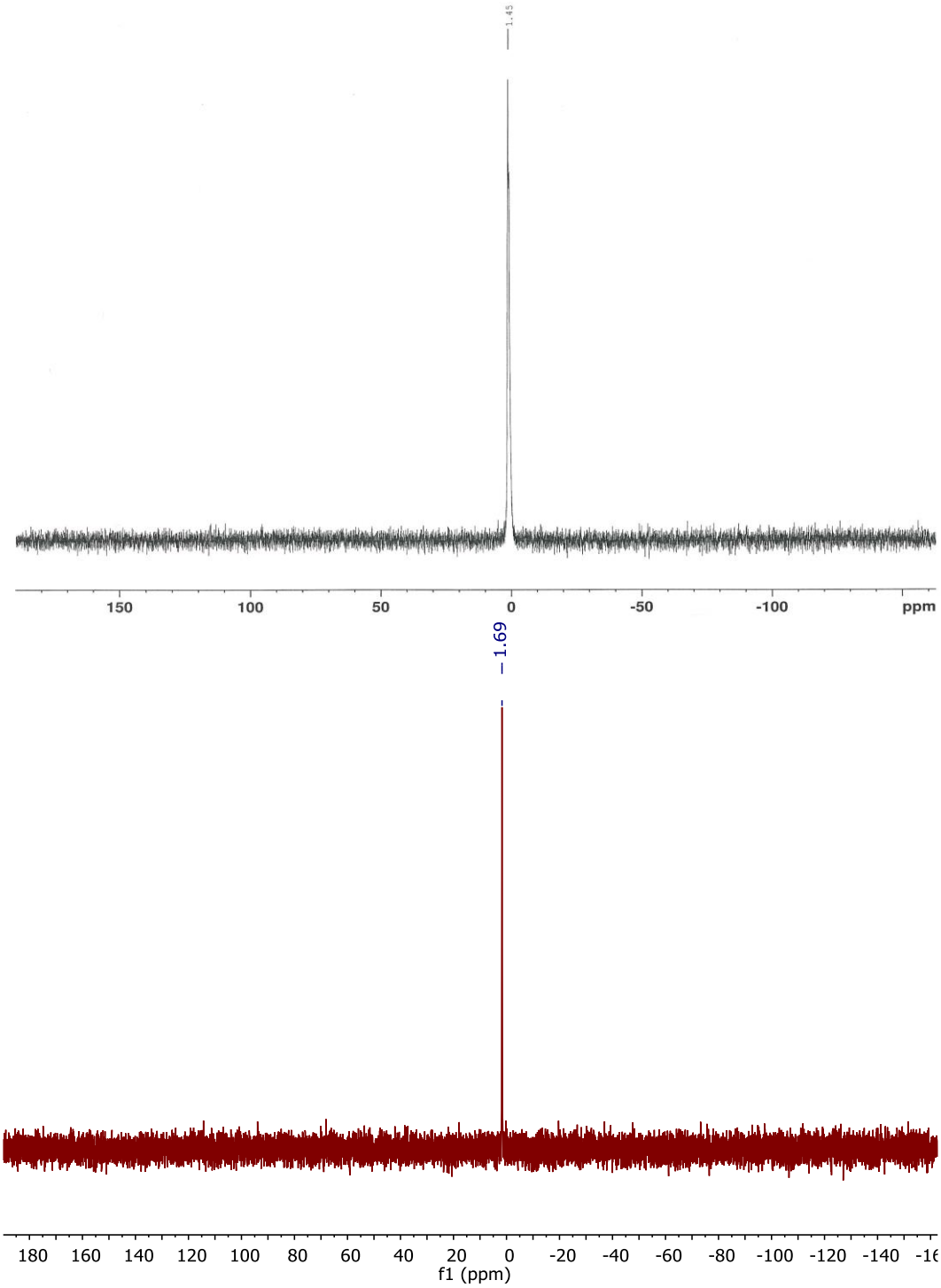

Figure 2.22. ^{31}P NMR of **1** (top) and commercial PG (bottom).

2.6 References

1. Dowhan, W.; Bogdanov, M.; Mileykovskaya, E., CHAPTER 1 - Functional roles of lipids in membranes. In *Biochemistry of Lipids, Lipoproteins and Membranes (Fifth Edition)*, Vance, D. E.; Vance, J. E., Eds. Elsevier: San Diego, 2008; pp 1-37.

2. Anjani, K.; Lhomme, M.; Sokolovska, N.; Poitou, C.; Aron-Wisnewsky, J.; Bouillot, J. L.; Lesnik, P.; Bedossa, P.; Kontush, A.; Clement, K.; Dugail, I.; Tordjman, J., Circulating phospholipid profiling identifies portal contribution to NASH signature in obesity. *J Hepatol* **2015,** *62* (4), 905-12.

3. Lu, Y.-W.; Claypool, S. M., Disorders of phospholipid metabolism: an emerging class of mitochondrial disease due to defects in nuclear genes. *Frontiers in Genetics* **2015,** *6*.

4. Mesa-Herrera, F.; Taoro-González, L.; Valdés-Baizabal, C.; Diaz, M.; Marín, R., Lipid and Lipid Raft Alteration in Aging and Neurodegenerative Diseases: A Window for the Development of New Biomarkers. *Int J Mol Sci* **2019,** *20* (15).

5. Yang, L.; Cui, X.; Zhang, N.; Li, M.; Bai, Y.; Han, X.; Shi, Y.; Liu, H., Comprehensive lipid profiling of plasma in patients with benign breast tumor and breast cancer reveals novel biomarkers. *Analytical and bioanalytical chemistry* **2015,** *407* (17), 5065-77.

6. Savla, R.; Browne, J.; Plassat, V.; Wasan, K. M.; Wasan, E. K., Review and analysis of FDA approved drugs using lipid-based formulations. *Drug development and industrial pharmacy* **2017,** *43* (11), 1743-1758.

7. Yingchoncharoen, P.; Kalinowski, D. S.; Richardson, D. R., Lipid-Based Drug Delivery Systems in Cancer Therapy: What Is Available and What Is Yet to Come. *Pharmacological reviews* **2016,** *68* (3), 701-87.

8. Sud, M.; Fahy, E.; Cotter, D.; Dennis, E. A.; Subramaniam, S., LIPID MAPS-Nature Lipidomics Gateway: An Online Resource for Students and Educators Interested in Lipids. *Journal of Chemical Education* **2012,** *89* (2), 291-292.

9. Benson, A. A.; Maruo, B., Piant phospholipids. I. Identification of the phosphatidyl glycerols. *Biochimica et biophysica acta* **1958,** *27* (1), 189-95.

10. Emdur, L.; Chiu, T.-h., The role of phosphatidylglycerol in the in vitro biosynthesis of teichoic acid and lipoteichoic acid. *FEBS Letters* **1975,** *55* (1-2), 216-219.

11. Poorthuis, B.; Hostetler, K. Y., Biosynthesis of bis(monoacylglyceryl)phosphate and acylphosphatidylglycerol in rat liver mitochondrial. *The Journal of biological chemistry* **1975,** *250* (9), 3297-302.

12. Stillwell, W. *An Introduction to Biological Membranes (Second Edition)*, Stillwell, W., Ed. Elsevier: 2016.

13. Dugail, I.; Kayser, B. D.; Lhomme, M., Specific roles of phosphatidylglycerols in hosts and microbes. *Biochimie* **2017,** *141*, 47-53.

14. Burugupalli, S.; Richardson, M. B.; Williams, S. J., Total synthesis and mass spectrometric analysis of a Mycobacterium tuberculosis phosphatidylglycerol featuring a two-step synthesis of (R)-tuberculostearic acid. *Organic & Biomolecular Chemistry* **2017,** *15* (35), 7422-7429.

15. Murakami, K.; Molitor, E. J.; Liu, H.-w., An Efficient Synthesis of Unsymmetrical Optically Active Phosphatidyl Glycerol. *The Journal of Organic Chemistry* **1999,** *64* (2), 648-651.

16. Sato, R.; Itabashi, Y.; Fujishima, H.; Okuyama, H.; Kuksis, A., Simple synthesis of diastereomerically pure phosphatidylglycerols by phospholipase D-catalyzed transphosphatidylation. *Lipids* **2004,** *39* (10), 1025-1030.

17. Hughes, R. A.; Ellington, A. D., Synthetic DNA Synthesis and Assembly: Putting the Synthetic in Synthetic Biology. *Cold Spring Harb Perspect Biol* **2017,** *9* (1), a023812.

18. Keith, D. J.; Townsend, S. D., Total Synthesis of the Congested, Bisphosphorylated Morganella morganii Zwitterionic Trisaccharide Repeating Unit. *Journal of the American Chemical Society* **2019,** *141* (32), 12939-12945.

19. Xu, L. L.; Berg, L. J.; Jamin Keith, D.; Townsend, S. D., An effective reagent to functionalize alcohols with phosphocholine. *Organic & biomolecular chemistry* **2020,** *18* (4), 767-770.

20. Chevallier, J.; Sakai, N.; Robert, F.; Kobayashi, T.; Gruenberg, J.; Matile, S., Rapid Access to Synthetic Lysobisphosphatidic Acids Using PIII Chemistry. *Organic Letters* **2000,** *2* (13), 1859-1861.

21. Jiang, G.; Xu, Y.; Falguières, T.; Gruenberg, J.; Prestwich, G. D., Concise Synthesis of Ether Analogues of Lysobisphosphatidic Acid. *Organic Letters* **2005,** *7* (18), 3837-3840.

22. Jiang, G.; Xu, Y.; Prestwich, G. D., Practical Enantiospecific Syntheses of Lysobisphosphatidic Acid and Its Analogues. *The Journal of Organic Chemistry* **2006,** *71* (3), 934-939.

23. D'Arrigo, P.; Servi, S., Synthesis of lysophospholipids. *Molecules* **2010,** *15* (3), 1354-77.

24. Plueckthun, A.; Dennis, E. A., Acyl and phosphoryl migration in lysophospholipids: importance in phospholipid synthesis and phospholipase specificity. *Biochemistry* **1982,** *21* (8), 1743-1750.

25. Mallik, S.; Prasad, R.; Bhattacharya, A.; Sen, P., Synthesis of Phosphatidylserine and Its Stereoisomers: Their Role in Activation of Blood Coagulation. *ACS Medicinal Chemistry Letters* **2018,** *9* (5), 434-439.

26. Guo, Z., Synthetic Studies of Glycosylphosphatidylinositol (GPI) Anchors and GPI-Anchored Peptides, Glycopeptides, and Proteins. *Current Organic Synthesis* **2013,** *10* (3), 366-383.

27. Abe, M.; Kitsuda, S.; Ohyama, S.; Koubori, S.; Murai, M.; Miyoshi, H., Concise procedure for the synthesis of cardiolipins having different fatty acid combinations. *Tetrahedron Letters* **2010,** *51* (15), 2071-2073.

28. Abe, M.; Nakano, M.; Kosaka, A.; Miyoshi, H., Syntheses of photoreactive cardiolipins for a photoaffinity labeling study. *Tetrahedron Letters* **2015,** *56* (17), 2258-2261.

29. Patschinski, P.; Zhang, C.; Zipse, H., The Lewis Base-Catalyzed Silylation of Alcohols—A Mechanistic Analysis. *The Journal of Organic Chemistry* **2014,** *79* (17), 8348-8357.

30. Ching, S. M.; Tan, W. J.; Chua, K. L.; Lam, Y., Synthesis of cyclic di-nucleotidic acids as potential inhibitors targeting diguanylate cyclase. *Bioorganic & Medicinal Chemistry* **2010,** *18* (18), 6657-6665.

31. Filippov, A. V.; Khakimov, A. M.; Munavirov, B. V., Chapter Two - 31P NMR Studies of Phospholipids. In *Annual Reports on NMR Spectroscopy*, Webb, G. A., Ed. Academic Press: 2015; Vol. 85, pp 27-92.

32. Vosse, C.; Wienken, C.; Cadenas, C.; Hayen, H., Separation and identification of phospholipids by hydrophilic interaction liquid chromatography coupled to tandem high resolution mass spectrometry with focus on isomeric phosphatidylglycerol and bis(monoacylglycero)phosphate. *Journal of Chromatography A* **2018,** *1565*, 105-113.

33. Abe, M.; Niibayashi, R.; Koubori, S.; Moriyama, I.; Miyoshi, H., Molecular Mechanisms for the Induction of Peroxidase Activity of the Cytochrome c–Cardiolipin Complex. *Biochemistry* **2011,** *50* (39), 8383-8391.

CHAPTER 3. SYNTHESIS OF PHOSPHATIDYL GLYCEROL CONTAINING UNSYMMETRIC ACYL CHAINS USING H-PHOSPHONATE METHODOLOGY

This chapter was adapted from Molecules: Struzik, Z. J.; Biyani, S.; Grotzer, T.; Storch, J.; Thompson, D. H., Synthesis of Phosphatidyl Glycerol Containing Unsymmetric Acyl Chains Using H-Phosphonate Methodology. *Molecules* **2022**, *27* (7), 2199.

3.1 Abstract

Naturally occurring phospholipids, such as phosphatidyl glycerol (PG), are gaining interest due to the roles they play in disease mechanisms. To elucidate the metabolism of PG, an optically pure material is required, but this is unfortunately not commercially available. Our previous PG synthesis route utilized phosphoramidite methodology that addressed issues surrounding fatty acid substrate scope and glycerol backbone modifications prior to headgroup phosphorylation, but faltered in the reproducibility of the overall pathway due to purification challenges. Herein, we present a robust pathway to optically pure PG in fewer steps, utilizing H-phosphonates that features a chromatographically friendly and stable triethyl ammonium H-phosphonate salt. Our route is also amendable to the simultaneous installation of different acyl chains, either saturated or unsaturated, on the glycerol backbone.

3.2 Introduction

Naturally occurring phospholipids (PLs) are biological molecules that are a major component of cell membranes. PLs contain a polar headgroup and glycerol backbone bearing two fatty acyl chains usually located on the *sn*-1 and *sn*-2 positions of the *sn*-3-phosphoglycerol backbone. The most common headgroups of PL are choline, ethanolamine, serine, inositol, and glycerol.[1] Bis(monoacylglycero)phosphate (BMP), also known as lysobisphosphatidic acid

(LBPA), is an isomer of phosphatidylglycerol (PG) that comprises less than 1% of the total cellular membrane PL, but about 15% of the lysosomal PL, and is considered a lysosome specific phospholipid.[2-3] BMP contains an unusual structure wherein the phosphoglycerol backbone is phosphorylated at the *sn*-1 position instead of the usual *sn*-3 position (Figure 3.1).[4-5] Several studies have suggested that PG is the biosynthetic precursor to BMP[6-8], however, the underlying metabolic pathway(s) are not known, nor has the catabolic metabolism of PG been reported. As an initial step to elucidate the conversion of PG to BMP, we sought the preparation of optically pure PG.

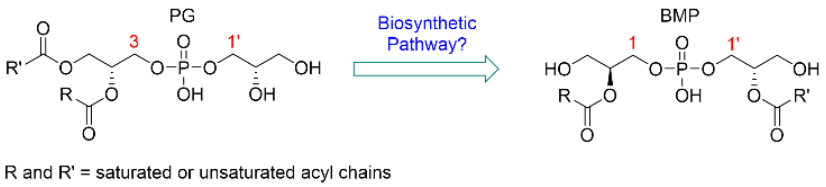

Figure 3.1. PG as a postulated precursor to BMP.

This challenge requires an efficient route to make PG bearing unsymmetric acyl chains to enable the chemical dissection of the BMP biosynthetic pathway. Unfortunately, optically pure derivatives of unsymmetric PG are not commercially available. We previously reported on the synthesis of diastereochemically pure PG[9] using phosphoramidite precursors that are commonly utilized in oligonucleotide synthesis (Figure 3.2).[10] This strategy addressed issues regarding the previous syntheses of PG[11-13] such as the ability to incorporate unsaturated acyl chains without concern of olefin reduction and allowed for early modification of glycerol headgroup alcohols prior to generation of the phosphoglycerol diester. While **1** was synthesized in modest yield, the use of an aliphatic ammonium fluoride source such as TBAF in the final global deprotection step to simultaneously remove the bulky silyl ethers of the phosphoglycerol headgroup and the cyanoethyl protecting group of the phosphate resulted in batch-to-batch inconsistencies and

suboptimal yields. Our experience has shown that this can be attributed to the necessity for rigorous chromatographic conditions for final product isolation; specifically, highly polar (aqueous) mobile phases on silica flash columns[14], an ion exchange column[15-16], and a prep HPLC separation.[17] Additionally, this routing does not allow for the installation of different acyl chains. Given these significant limitations, a more efficient and consistent path to enable manipulation of any segment of the PG structure was sought. To avoid the inconsistency and chromatographic burden of the previous synthesis, we now report a novel route to PG that takes advantage of H-phosphonate methodology via diphenyl phosphite[18-24] as the phosphorylating agent. This approach features a bench and air stable H-phosphonate salt intermediate developed during the synthesis of phosphatidyl serine[20] that simplifies subsequent phosphorylation reactions and purification conditions. Additionally, we were able to reduce the number of synthetic steps from eleven to eight by directly installing an acetonide protected glycerol headgroup without further modification of the primary and secondary alcohols, an effort that was previously needed to retain the desired stereochemistry of the PG product.

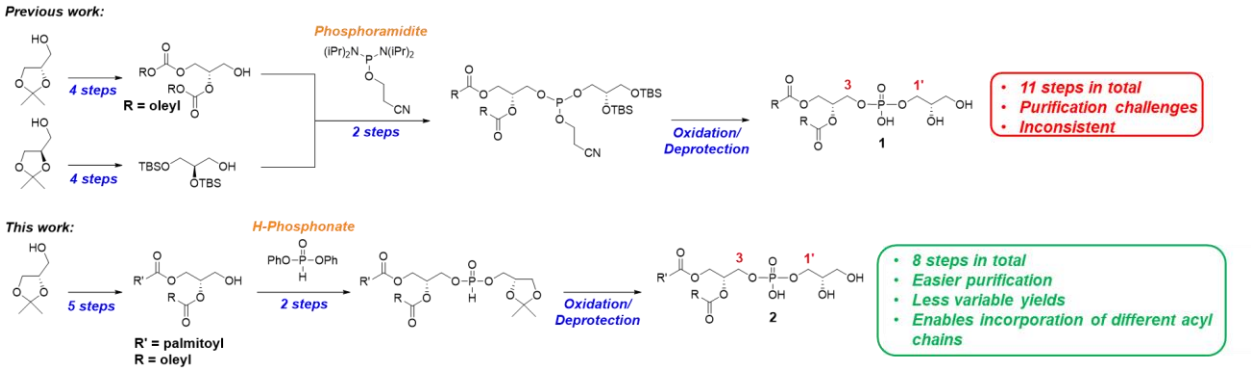

Figure 3.2. PG has been previously synthesized using phosphoramidite methodology (top). A more efficient route has been developed by incorporating H-phosphonates as the phosphonylating agent (bottom).

3.3 Results and Discussion

Initial efforts to improve the synthetic route involved substituting fluoride sources[25-27] in the deprotection step and substituting diphenylmethylsilyl ethers (DPMS)[28] on the phosphoglycerol headgroup instead of TBS ethers. Through a series of high-throughput experiments using desorption electrospray ionization mass spectrometry [29-30], modification of solketal protection from p-methoxybenzyl ether (PMB)[31-32] to a phenyl acyl ester, and translation to flow chemistry[33], we were able to successfully phosphorylate the protected phosphoglycerol head group on the gram scale allowing us to upscale the synthesis of phosphoramidite intermediate in higher yields compared to the batch methods. Unfortunately, subsequent acyl chain migration and deprotection of the labile DPMS groups prevented us from moving forward with the phosphoramidite approach. For a more complete discussion of these efforts, please see the Supporting information. Despite multiple attempts to perform the desired transformation using phosphoramidites, we abandoned this approach and began to explore other phosphonylation strategies to achieve a robust and reproducible method for PG synthesis. H-phosphonates are a class of phosphonylated intermediates that have been used in the syntheses of other glycerophospholipids including phosphatidyl inositols[34-37], phosphatidyl ethanolamine[38], phosphatidyl choline[38], and phosphatidyl serine[20, 38]. They have also been used in the total synthesis of glycophospholipids[39-41] as well as nucleoside-based phospholipids[24] and drugs[42]. To our surprise, they have not, however, been utilized in the synthesis of PG. The attractiveness of this methodology was based on the ability to obtain a phosphonylated intermediate in the form of an organic salt that can be readily purified by chromatography on polar stationary phases such silica or alumina. Another advantage of this strategy is that the phosphite precursor to H-phosphonates can undergo transesterifications reactions under basic conditions with alcohols, a

circumstance that is ideal for installation of the phosphorous species on the glycerol backbone to prevent acyl chain migration from the *sn*-2 to the *sn*-1 position. A third advantage is that H-phosphonate monoesters such as **9** are less susceptible to air oxidation as well as base- and acid-catalyzed hydrolysis due to the large electron density associated with the anionic form of the phosphonate, whereas the phosphonate proton needs to be removed before undergoing nucleophilic attack.[18, 43-47] Once activated, H-phosphonates have exhibited high rates of condensation with alcohols approaching 10^5 M s^{-1} [47-48], further supporting the case for their use. In most of the examples listed previously, the H-phosphonate intermediates were synthesized by reacting the alcohol substrate with PCl_3 and imidazole, followed by introduction of the second glycerol derivative with a coupling agent such as pivaloyl chloride.[38] Due to the air and moisture sensitivity of PCl_3, we employed a strategy by Mallik *et al.* utilizing low cost diphenyl phosphite as the phosphonylation reagent for quantitative conversion of substrate.[20] Additionally, the electron-withdrawing phenol group further enhances transesterification.[47]

In our previous synthesis of PG[9], we designed the phosphoglycerol headgroup such that the final deprotection step avoided the use of functional groups that required acid deprotection to obviate potential acyl chain migration side reactions. Additionally, it was convenient to remove the cyanoethyl group and silyl groups simultaneously under mildly basic fluoride conditions to avoid multiple purification steps after formation of the phosphate. Thus, we replaced the acetonide of solketal with silyl groups that could be removed in the presence of TBAF. Encouraged by the robustness of H-phosphonates in our hands, we were curious as to how much of a concern the use of harsh acidic conditions would be for discovering an efficient PG route. To probe this question, we decided to phosphonylate solketal precursor **10** directly after the installation of the backbone (Figure 3.3). If the acetonide could be removed in the presence of acid without acyl chain migration

or other major obstacles that would negatively impact overall yield, this would streamline the synthesis by four steps from the phosphoramidite route.[9] We also wanted to determine the scope of conditions that would be successful for the installation of asymmetric acyl chains on the *sn*-1 and *sn*-2 positions of the glycerol backbone. We were pleased to observe chemoselective control of each **5** alcohol esterification simply by limiting the fatty acid stoichiometry in the reaction. The formation of the diesterified product comprised only about 5% of the yield. While the esterification of the primary hydroxyl may seem obvious, we were unsure about how much the secondary hydroxyl group would affect the product distribution. Thus, we were able to successfully synthesize **6** and **7** using standard Steglich esterification conditions in 78% and 82% yields, respectively. Deprotection of the PMB ether with DDQ afforded **8** in 84% yield without substantial acyl chain migration of either the symmetrical or asymmetrical acyl chain versions of the target. We were able to successfully phosphorylate **8** with diphenyl phosphite (6 equivalents) in pyridine at 0 °C and subsequent quenching in aqueous. conditions to give an easy-to-handle phosphonate salt **9** in 87% yield. The acetonide protected head-group was esterified with 10 upon coupling with pivaloyl chloride in pyridine at 0 °C to afford 11 in 75% yield. While protocols using this chemistry generally call for 3-6 equivalents of the coupling agent, we found that using the lower end of that range (~3 equivalents) resulted in fewer by-products, a higher yield, and simplified purification since homocoupled pyrophosphates generated by condensation of H-phosphonates and pivalic acid after transesterification with an alcohol were found to be problematic at higher equivalencies. Finally, oxidation of the H-phosphonate from P(III) to P(V) was conducted in the usual manner with I_2 in a pyridine/water mixture. Once the solvent was removed in vacuo, the crude product was be placed directly in a 5:1:0.5 $CHCl_3$:TFA:MeOH mixture to remove the acetonide of **11** to provide PG **1** and **2** in 73% yield. While this reaction can be performed in this manner without a

purification step between the oxidation and acetonide deprotection, we recommend a chromatographic purification between each step. The product was consistently cleaner by ^{1}H and ^{31}P NMR analysis, and the yield of **1** and **2** did not vary significantly, by incorporating an additional purification step.

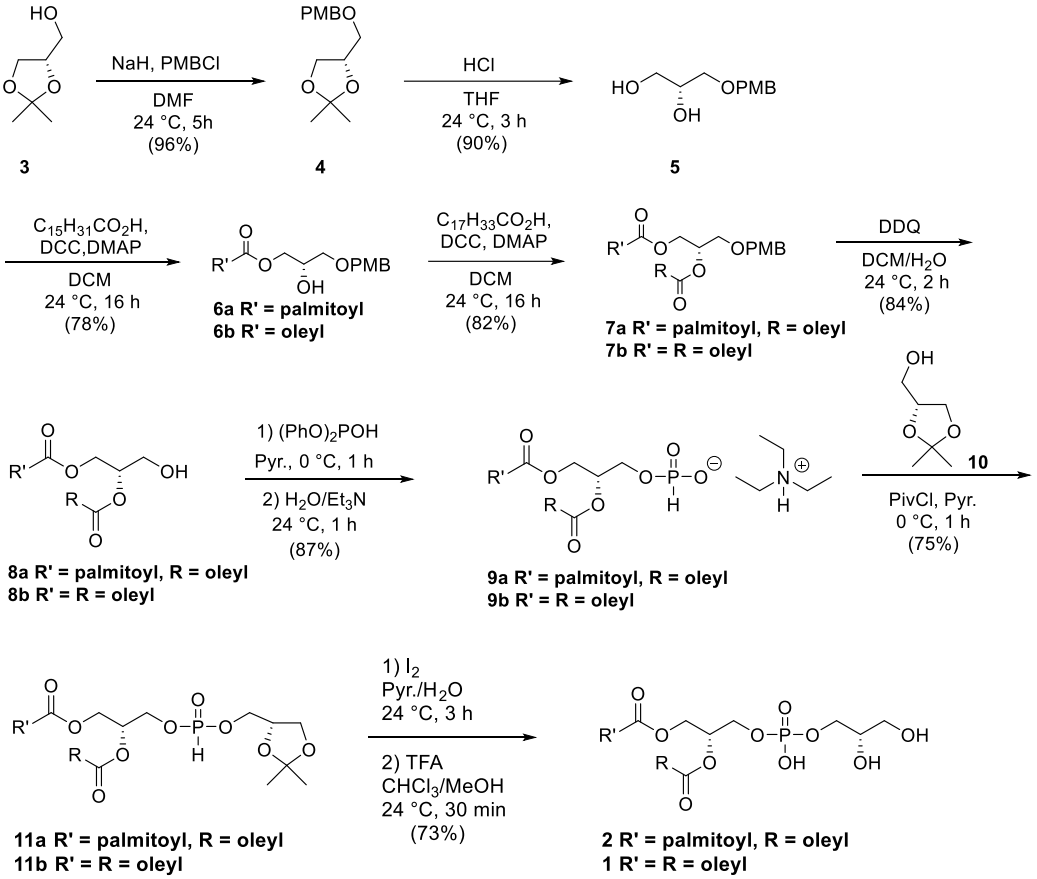

Figure 3.3. Synthesis of PG containing different acyl chains using H-phosphonates.

We have demonstrated the synthesis of diastereochemically pure PG containing both symmetric and asymmetric acyl chains using H-phosphonate methodology. Due to the simpler purification procedure and handling of the phosphonylated intermediates via the use of diphenyl phosphite, this approach gave PG in higher isolated yields with more consistent results than the

phosphoramidite approach. Moving forward, we hope to be able to apply this chemistry for the investigation of PG metabolism.

3.4 Materials and Methods

3.4.1 General Information

Commercial reagents were used as purchased from TCI Chemicals (Portland, OR, USA) and MilliporeSigma (Burlington, MA, USA). Organic solvents used were reagent grade, purchased from Fisher Scientific (Hampton, NH, USA). Dry solvents were purified using a Glass Contour Solvent System from Pure Process Technology, LLC (Nashua, NH, USA), with Fisher HPLC grade DCM, Aldrich anhydrous DMF, and Fisher HPLC/ACS grade THF. Reactions were monitored by thin-layer chromatography using silica gel 60 F254 plates (Merck, Darmstadt, Germany). UV light (254 nm) and staining with aqueous $KMnO_4$ was used to visualize the developed chromatograms. Flash chromatography was performed using a Biotage SP4 A2A0 with RediSep Rf silica flash columns (12 g, 60 mg– 1.2 g sample size) and collected in 9 mL fraction volumes or performed via manual silica column chromatography using silica gel 60 (MilliporeSigma, Burlington, MA, USA). Compounds purified via automatic flash chromatography are accompanied by a gradient table in the Supplementary Material. All ^{1}H, ^{13}C and ^{31}P NMR spectra were recorded on a Bruker-AV-III-500-HD instrument. Chemical shifts (δ) are reported in parts per million, relative to $CDCl_3$ (^{1}H NMR residual peak at δ = 7.26 ppm, ^{13}C NMR residual peak at δ = 77.0 ppm), and coupling constants (J) are given in Hz. High-resolution mass measurements were acquired on an Agilent 6550 iFunnel LC/Q-TOF mass spectrometer (Agilent Technologies, Santa Clara, CA, USA).

3.4.2 Synthesis of (S)-4-(((4-methoxybenzyl)oxy)methyl)-2,2-dimethyl-1,3-dioxolane (4).

NaH (2.71 g, 113 mmol) was added to an oven-dried, 250-mL, multi-neck, roundbottom flask. Schlenk techniques were utilized to evacuate the flask, and then dry DMF (50 mL) was added. The flask was maintained under a continuous Ar atmosphere for the duration of the reaction. The reaction flask was lowered into an ice bath and (S)-solketal (5.0 g, 38 mmol) was added dropwise and stirred vigorously at 0 °C for 45 min. 4-Methoxybenzyl chloride (6.6 g, 42 mmol) was added and stirred at 20 °C for 4 h. The completed reaction was slowly quenched with saturated NH_4Cl solution and extracted with ethyl acetate (3 × 150 mL). Combined organic extracts were washed with water (2 × 150 mL), washed with brine (2 × 150 mL), dried over anhydrous Na_2SO_4, and concentrated under reduced pressure. The crude product was purified on a 5 cm silica gel column (100:0 to 98:2 DCM:MeOH) to yield the desired product as a yellow oil in 99% yield; $[\alpha]_D^{27}$ + 205 (c 0.049, $CHCl_3$); R_f = 0.50 (DCM:MeOH); ^{1}H NMR (500 MHz, $CDCl_3$) δ 7.28–7.23 (m, 2H), 6.91–6.84 (m, 2H), 4.50 (q, J = 11.7 Hz, 2H), 4.28 (p, J = 6.0 Hz, 1H), 4.04 (dd, J = 8.3, 6.4 Hz, 1H), 3.80 (s, 3H), 3.72 (dd, J = 8.3, 6.3 Hz, 1H), 3.52 (dd, J = 9.8, 5.7 Hz, 1H), 3.44 (dd, J = 9.8, 5.6 Hz, 1H), 1.42 (s, 3H), 1.36 (s, 3H); ^{13}C NMR (126 MHz, $CDCl_3$) δ 159.3, 130.1, 129.4, 113.8, 109.4, 77.3, 77.1, 76.8, 74.8, 73.2, 70.8, 77.0, 55.3, 26.8, 25.4. QTOF-HRMS (ESI) for $C_{14}H_{20}O_4$ [M+Na+]: found 275.1255, calcd 275.1254.

3.4.3 Synthesis of (R)-3-(benzyloxy)propane-1,2-diol (5).

Aqueous 1M HCl (21 mL) was added to a 100-mL, round-bottom flask containing a solution of **4** (1.46 g, 8 mmol) in 21 mL THF. The reaction mixture was allowed to react at 20 °C for 2 h. Saturated $NaHCO_3$ solution was added to quench the reaction and the reaction mixture was extracted with EtOAc (3 × 100 mL). The combined organic extracts were dried with anhydrous Na_2SO_4 and concentrated under reduced pressure. The crude product was purified on a Biotage

flash purification system (DCM:MeOH) to yield the product as a white solid in 93% yield (refer to Table 3.8 for gradient); $[\alpha]_D^{27}$-12.1 (c 0.025, $CHCl_3$); R_f = 0.13 (DCM:MeOH 98:2); ^{1}H NMR (500 MHz, $CDCl_3$) δ 7.25–7.20 (m, 2H), 6.89–6.83 (m, 2H), 4.45 (s, 2H), 3.84 (tt, J = 6.1, 4.0 Hz, 1H), 3.78 (s, 3H), 3.63 (dd, J = 11.5, 3.7 Hz, 1H), 3.55 (dd, J = 11.5, 5.9 Hz, 1H), 3.51–3.42 (m, 2H), 3.10 (s, 2H). ^{13}C NMR (126 MHz, $CDCl_3$) δ 159.4, 129.8, 129.7, 129.6, 129.5, 114.0, 113.9, 77.4, 77.1, 76.9, 73.2, 71.4, 70.8, 64.1, 55.3. QTOF-HRMS (ESI) for $C_{11}H_{16}O_4$ [M+Na+]: found 235.0943., calcd 235.0941.

3.4.4 Synthesis of (S)-2-hydroxy-3-((4-methoxybenzyl)oxy)propyl palmitate (6a).

Palmitic acid (1.09 g, 4.8 mmol) and **5a** (1.06 g, 5 mmol) were placed in an oven-dried, 100-mL, three-neck, round-bottom flask. The contents of the flask were cycled three times with vacuum/Ar, and the flask was equipped with an Ar balloon and dry DCM (15 mL) was added. A solution of DCC (0.97 g, 4.7 mmol) and DMAP (0.58 g, 4.7 mmol) in dry DCM (15 mL) was prepared in a separate 100-mL, round-bottom flask and equipped with an Ar balloon. This solution was transferred to the three-neck reaction flask via a cannula and stirred at 20 °C for 16 h. The salt was removed by vacuum filtration through a coarse glass frit containing Celite, and the resulting filtrate was collected and concentrated under reduced pressure. A minimal amount of hexane was added to the crude product, and the mixture was sonicated to dissolve the solid. The resulting solution was purified on a Biotage flash purification system (Hexane:EtOAc) to yield the desired product as a clear white solid with 78% yield (refer to Table 3.9 for gradient); $[\alpha]_D^{25}$ +19.1 (c 0.038, $CHCl_3$) R_f = 0.25 (Hexane:EtOAc, 8:2); ^{1}H NMR (500 MHz, $CDCl_3$) δ 7.27–7.22 (m, 2H), 6.91–6.84 (m, 2H), 4.48 (s, 2H), 4.20–4.07 (m, 2H), 4.01 (tt, J = 6.1, 4.4 Hz, 1H), 3.80 (s, 3H), 3.55–3.41 (m, 2H), 2.31 (t, J = 7.6 Hz, 2H), 1.60 (p, J = 7.3 Hz, 2H), 1.25 (s, 24H), 0.88 (t, J = 6.9 Hz, 3H); ^{13}C NMR (126 MHz, $CDCl_3$) δ 174.0, 159.4, 129.8, 129.4, 113.9, 77.3, 77.3, 77.1, 76.8, 73.2,

73.0, 70.6, 68.9, 68.7, 65.4, 55.3, 34.2, 31.9, 29.7, 29.7, 29.6, 29.5, 29.4, 29.3, 29.2, 24.9, 22.7, 14.1. QTOF-HRMS (ESI) for $C_{27}H_{46}O_5$ [M+Na+]: found 473.3235, calcd 473.3237.

(S)-2-Hydroxy-3-((4-methoxybenzyl)oxy)propyl oleate (6b). Clear oil in 76% yield; $[\alpha]_D^{25}$ +27 (*c* 0.011, $CHCl_3$) R_f=0.18 (Hexane:EtOAc, 8:2); ^{1}H NMR (500 MHz, $CDCl_3$) δ 7.26 – 7.22 (m, 2H), 6.91 – 6.85 (m, 2H), 5.39 – 5.30 (m, 2H), 4.48 (s, 2H), 4.20 – 4.08 (m, 2H), 4.01 (tt, *J* = 6.2, 4.4 Hz, 1H), 3.80 (s, 3H), 3.55 – 3.42 (m, 2H), 2.31 (t, *J* = 7.6 Hz, 2H), 2.04 – 1.97 (m, 4H), 1.61 (p, *J* = 7.3 Hz, 2H), 1.38 – 1.17 (m, 26H), 0.88 (t, *J* = 6.9 Hz, 3H); ^{13}C NMR (126 MHz, $CDCl_3$) δ 173.9, 159.4, 130.0, 129.8, 129.4, 113.9, 77.3, 77.1, 76.8, 73.2, 70.6, 68.9, 65.4, 55.3, 34.2, 31.9, 29.8, 29.7, 29.5, 29.4, 29.3, 29.2, 29.1, 27.2, 27.2, 27.1, 24.9, 22.7, 14.14. QTOF-HRMS (ESI) for $C_{29}H_{48}O_5$ [M+Na^+]: found 499.3391, calcd 499.3394.

3.4.5 Synthesis of (S)-3-((4-methoxybenzyl)oxy)propane-1,2-diyl dioleate (7b).

Oleic acid (2.82 g, 10 mmol) and **6b** (2.38 g, 5 mmol) were placed in an oven-dried, 100-mL, three-neck, round-bottom flask. The contents of the flask were treated with three cycles of vacuum/Ar, the flask was equipped with an Ar balloon, and dry DCM (15 mL) was added. A solution of DCC (2.3 g, 11 mmol) and DMAP (1.3 g, 11 mmol) in dry DCM (15 mL) was prepared in a separate, 100-mL, round-bottom flask equipped with an Ar balloon. This solution was transferred to the three-neck reaction flask via a cannula and stirred at 20 °C for 16 h. The formed salt was removed by vacuum filtration through a coarse glass frit containing Celite, and the resulting filtrate was collected and concentrated under reduced pressure. A minimal amount of hexane was added to the crude product, and the mixture was sonicated to dissolve the solid. The resulting solution was purified on a 4-cm-diameter, 32-cm-long manual silica gel column (hexane:EtOAc) to yield the desired product as a clear, colorless oil in 82% yield. The use of a shorter column resulted in the co-elution of oleic acid. A Biotage method was also developed for

this procedure (hexane:EtOAc) (refer to Table 3.10 for gradient); $[\alpha]_D^{25}$ +51 (c 0.020, $CHCl_3$); R_f = 0.63 (Hexane:EtOAc, 8:2); 1H NMR (500 MHz, $CDCl_3$) δ 7.25–7.20 (m, 2H), 6.89–6.84 (m, 2H), 5.39– 5.29 (m, 4H), 5.22 (dtd, J = 6.5, 5.2, 3.7 Hz, 1H), 4.53–4.41 (m, 2H), 4.33 (dd, J = 11.8, 3.8 Hz, 1H), 4.17 (dd, J = 11.9, 6.4 Hz, 1H), 3.80 (s, 3H), 3.55 (dd, J = 5.2, 1.9 Hz, 2H), 2.29 (dt, J = 20.5, 7.5 Hz, 4H), 2.05–1.96 (m, 8H), 1.66–1.57 (m, 4H), 1.38–1.21 (m, 42H), 0.88 (t, J = 6.9 Hz, 6H). ^{13}C NMR (126 MHz, $CDCl_3$) δ 173.4, 173.1, 159.3, 130.0, 129.8, 129.7, 129.3, 113.8, 77.3, 77.0, 76.8, 73.0, 70.0, 67.9, 62.7, 55.3, 34.3, 34.1, 31.9, 29.8, 29.7, 29.5, 29.3, 29.2, 29.2, 29.1, 29.1, 27.2, 27.2, 25.0, 24.9, 22.7, 14.1. QTOF-HRMS (ESI) for $C_{47}H_{80}O_6$ [M+H+]: found 741.6027, calcd 741.6027.

(S)-1-((4-Methoxybenzyl)oxy)-3-(palmitoyloxy)propan-2-yl oleate (7a). Clear oil in 80% yield. $[\alpha]_D^{24}$ +57.8 (c 0.017, $CHCl_3$); R_f=0.68 (Hexane:EtOAc, 8:2); ^1H NMR (500 MHz, $CDCl_3$) δ 7.25 – 7.21 (m, 2H), 6.90 – 6.85 (m, 2H), 5.38 – 5.30 (m, 2H), 5.25 – 5.19 (m, 1H), 4.47 (q, J = 11.7 Hz, 2H), 4.33 (dd, J = 11.9, 3.8 Hz, 1H), 4.17 (dd, J = 11.9, 6.4 Hz, 1H), 3.80 (s, 3H), 3.55 (dd, J = 5.2, 1.9 Hz, 2H), 2.29 (dt, J = 20.6, 7.5 Hz, 4H), 2.06 – 1.96 (m, 4H), 1.60 (dp, J = 14.4, 7.3 Hz, 4H), 1.37 – 1.19 (m, 47H), 0.88 (t, J = 6.9 Hz, 6H). ^{13}C NMR (126 MHz, $CDCl_3$) δ 173.4, 173.1, 159.3, 130.0, 129.8, 129.7, 129.3, 113.8, 77.3, 77.0, 76.8, 73.0, 70.0, 67.9, 62.7, 55.3, 34.3, 34.1, 32.0, 29.8, 29.7, 29.7, 29.7, 29.6, 29.5, 29.4, 29.3, 29.3, 29.2, 29.2, 29.1, 27.2, 27.2, 25.0, 24.9, 22.7, 14.1; QTOF-HRMS (ESI) for $C_{45}H_{78}O_6$ [M+H+]: found 715.5872, calcd 715.5871.

3.4.6 Synthesis of (S)-3-Hydroxypropane-1,2-diyl dioleate (8b).

DCM/H_2O (15 mL, 5% H_2O) and **7b** (1.48 g, 2 mmol) were placed in a 100-mL, roundbottom flask. Following the addition of DDQ (0.68 g, 3 mmol), the reaction flask was completely wrapped in aluminum foil and stirred at 20 °C for 1 h. The reaction mixture turned from dark green to a dark shade of red. The mixture was diluted with DCM and vacuum filtered

through a coarse glass frit with Celite. The collected filtrate was washed with saturated $NaHCO_3$ solution (40 mL), swirling gently to mix. The organic layer was washed again with $NaHCO_3$ (80 mL) and swirled vigorously to mix. Again, the organic layer was washed with $NaHCO_3$ (2 × 100 mL), and then shaken to combine. The resulting organic solution was dried with anhydrous Na_2SO_4 before concentration under reduced pressure. The crude product was purified on a Biotage flash purification system (hexane:EtOAc) to yield the desired product as a clear, colorless oil with an 84% yield (refer to Table 3.11 for gradient); $[\alpha]_D^{25}$ −21 (c 0.024, $CHCl_3$); R_f=0.36 (Hexane:EtOAc, 8:2); ^{1}H NMR (500 MHz, $CDCl_3$) δ 5.39–5.29 (m, 4H), 5.08 (p, J = 5.0 Hz, 1H), 4.32 (dd, J = 11.9, 4.5 Hz, 1H), 4.23 (dd, J = 12.0, 5.7 Hz, 1H), 3.72 (dd, J = 5.0, 1.6 Hz, 2H), 2.33 (dt, J = 11.1, 7.5 Hz, 4H), 2.05–1.96 (m, 8H), 1.62 (h, J = 7.3 Hz, 5H), 1.37–1.20 (m, 42H), 0.88 (t, J = 6.9 Hz, 6H). ^{13}C NMR (126 MHz, $CDCl_3$) δ 173.8, 173.4, 130.0, 129.7, 77.3, 77.0, 76.8, 72.1, 62.0, 61.6, 34.3, 34.1, 31.9, 29.8, 29.7, 29.5, 29.3, 29.2, 29.1, 29.1, 27.2, 27.2, 24.9, 24.9, 22.7, 14.1. QTOF-HRMS (ESI) for $C_{39}H_{72}O_5$ [M+H+]: found 621.5452, calcd 621.5452.

(S)-1-Hydroxy-3-(palmitoyloxy)propan-2-yl oleate (8a). White semi-solid in 81% yield; $[\alpha]_D^{25}$ -27.2 (*c* 0.021, $CHCl_3$); R_f=0.36 (Hexane:EtOAc, 8:2); ^{1}H NMR (500 MHz, $CDCl_3$) δ 5.40 – 5.29 (m, 2H), 5.08 (p, *J* = 5.0 Hz, 1H), 4.32 (dd, *J* = 11.9, 4.5 Hz, 1H), 4.23 (dd, *J* = 11.9, 5.6 Hz, 1H), 3.73 (dd, *J* = 5.0, 1.6 Hz, 2H), 2.33 (dt, *J* = 11.4, 7.5 Hz, 4H), 2.01 (q, *J* = 6.3 Hz, 4H), 1.62 (h, *J* = 7.6 Hz, 4H), 1.40 – 1.18 (m, 46H), 0.88 (t, *J* = 6.9 Hz, 6H). ^{13}C NMR (126 MHz, $CDCl_3$) δ 173.8, 173.4, 130.1, 129.7, 77.3, 77.0, 76.8, 72.1, 62.0, 61.6, 34.3, 34.1, 31.9, 29.8, 29.7, 29.7, 29.6, 29.5, 29.5, 29.4, 29.3, 29.3, 29.2, 29.1, 29.1, 27.2, 27.2, 24.9, 24.9, 22.7, 14.1. QTOF-HRMS (ESI) for $C_{37}H_{70}O_4$ [M+H$^+$]: found 595.5296, calcd 595.5295.

3.4.7 Synthesis of (R)-2,3-Bis(oleoyloxy)propyl phosphonate (9b).

The synthesis of **9** was performed according to a previously reported protocol.[20] Alcohol 8b (0.248 g, 0.4 mmol) was placed in an oven-dried, 10-mL, two-neck, round-bottom flask equipped with a stir bar. The flask was then dried using Schlenk techniques followed by the attachment of an Ar balloon. The starting material was then dissolved in dry pyridine (4 mL) and the solution was cooled to 0 °C in an ice bath. Diphenyl phosphite (0.46 mL, 2.5 mmol) was added dropwise and the solution was stirred for 1 h. The solution was then allowed to warm to room temperature where a 1:1 H_2O:Et_3N solution (5 mL) was added to the round-bottom flask, where it was stirred for an additional 1 h. The pyridine was removed from the solution under reduced pressure by azeotropically drying three times with toluene. The crude oil was then dissolved with DCM (30 mL) and washed with saturated $NaHCO_3$ (3 × 15 mL), where it was dried with anhydrous Na_2SO_4 and concentrated under reduced pressure. The product was purified using a silica gel column to yield a white semi-solid with 75% yield (gradient from 100:0 to 95:5 $CHCl_3$:MeOH containing 0.5% Et_3N); $[\alpha]_D^{27}$ +25.5 (c 0.032, $CHCl_3$); R_f = 0.23 (Hexane:EtOAc, 8:2); ^{1}H NMR (500 MHz, $CDCl_3$) δ 5.37–5.28 (m, 4H), 5.20 (qd, J = 5.3, 3.6 Hz, 1H), 4.35 (dd, J = 11.9, 3.7 Hz, 1H), 4.16 (dd, J = 11.9, 6.3 Hz, 1H), 4.00 (dd, J = 8.1, 5.2 Hz, 2H), 3.06 (qd, *J* = 7.3, 4.2 Hz, 6H), 2.32–2.23 (m, 4H), 1.99 (qd, J = 6.2, 2.7 Hz, 8H), 1.58 (tq, J = 7.0, 3.6 Hz, 4H), 1.37– 1.19 (m, 50H), 0.86 (t, J = 6.9 Hz, 6H). ^{13}C NMR (126 MHz, $CDCl_3$) δ 173.4, 173.0, 130.0, 129.7, 77.3, 77.1, 76.8, 70.3, 70.3, 62.4, 62.1, 62.1, 45.6, 34.3, 34.1, 31.9, 29.8, 29.7, 29.5, 29.3, 29.2, 29.2, 29.1, 27.2, 27.2, 24.9, 22.7, 14.1, 8.5. ^{31}P NMR (203 MHz, $CDCl_3$) δ 4.55. QTOF-HRMS (ESI) for $C_{39}H_{72}O_7P$ [M+Na+]: found 707.4986, calcd 707.4986.

(R)-2-(Oleoyloxy)-3-(palmitoyloxy)propyl phosphonate (9a). White semi-solid in 78% yield $[\alpha]_D^{27}$ +18.5 (*c* 0.029, $CHCl_3$); R_f=0.23 (Hexane:EtOAc, 8:2); ^{1}H NMR (500 MHz, $CDCl_3$) δ 5.38 – 5.29 (m, 2H), 5.21 (qd, *J* = 5.2, 3.6 Hz, 1H), 4.36 (dd, *J* = 11.9, 3.8 Hz, 1H), 4.17 (dd, *J* = 11.9,

6.3 Hz, 1H), 4.03 (dd, J = 8.2, 5.1 Hz, 2H), 3.08 (qd, J = 7.3, 4.4 Hz, 5H), 2.30 (dt, J = 9.9, 7.6 Hz, 4H), 2.04 – 1.96 (m, 4H), 1.59 (h, J = 6.7 Hz, 5H), 1.40 – 1.19 (m, 55H), 0.87 (t, J = 6.9 Hz, 7H); ^{13}C NMR (126 MHz, $CDCl_3$) δ 173.4, 173.00, 130.0, 129.7, 77.3, 77.0, 76.8, 70.2, 62.3, 45.6, 34.3, 34.1, 32.0, 29.8, 29.8, 29.7, 29.7, 29.5, 29.4, 29.3, 29.2, 29.2, 29.1, 27.2, 27.2, 24.9, 22.7, 14.1, 8.6; ^{31}P NMR (203 MHz, $CDCl_3$) δ 4.59. QTOF-HRMS (ESI) for $C_{37}H_{70}O_7P$ [M+Na$^+$]: found 681.4826, calcd 681.4829.

3.4.8 Synthesis of (2R)-3-(((S)-2,2-dimethyl-1,3-dioxolan-4-yl)methoxy)propane-1,2-dioleyl phosphonate (11b).

Compound **9b** (0.235 g, 0.3 mmol) was added to an oven-dried, 10-mL, two-neck, round-bottom flask equipped with a stir bar. The flask was cycled three times with vacuum/Ar, and a balloon was attached. Dry pyridine (5 mL) was then added, followed by solketal (0.05 mL, 0.4 mmol). The reaction temperature was lowered to 0 °C via an ice bath and pivaloyl chloride (0.22 mL, 1.7 mmol) was subsequently added dropwise to the reaction. The solution changed from transparent to a violet. The reaction was stirred for 1 h and then warmed slowly to room temperature. Pyridine was then azeotropically stripped from the solution with toluene under reduced pressure. The crude oil was then redissolved in DCM (30 mL), and the solution was washed with saturated $NaHCO_3$ (2 × 10 mL). The organic layer was then dried with anhydrous Na_2SO_4 and concentrated under reduced pressure. The crude product was purified on a silica gel column to yield a colorless oil (gradient of 100:0 to 98:2 DCM:MeOH); $[\alpha]_D^{26}$ +12.9 (c 0.023, $CHCl_3$); R_f = 0.34 (Hexane:EtOAc, 8:2); ^{1}H NMR (500 MHz, $CDCl_3$) δ 5.39–5.29 (m, 4H), 5.23 (h, J = 5.2 Hz, 1H), 4.38–4.00 (m, 10H), 3.85–3.70 (m, 2H), 2.37–2.27 (m, 4H), 2.05–1.97 (m, 8H), 1.61 (h, J = 7.1 Hz, 4H), 1.44 (d, J = 3.5 Hz, 4H), 1.39–1.20 (m, 51H), 0.88 (t, J = 6.8 Hz, 6H); ^{13}C NMR (126 MHz, $CDCl_3$) δ 173.8, 173.4, 130.1, 129.7, 77.3, 77.0, 76.8, 72.1, 62.0, 61.6,

34.3, 34.1, 31.9, 29.8, 29.7, 29.7, 29.6, 29.5, 29.5, 29.4, 29.3, 29.3, 29.2, 29.1, 29.1, 27.2, 27.2, 24.9, 24.9, 22.7, 14.1; 31P NMR (203 MHz, $CDCl_3$) δ 8.62, 8.52 QTOF-HRMS (ESI) for $C_{45}H_{83}O_9P$ [M+Na+]: found 821.5666, calcd 821.5667.

(2R)-1-(((S)-2,2-Dimethyl-1,3-dioxolan-4-yl)methoxy)(hydroxy)-3-(palmitoyloxy)propan-2-oleyl phosphonate (11a). Clear oil in 72% yield; $[\alpha]_D^{26}$ -1.90 (*c* 0.023, $CHCl_3$); R_f=0.35 (Hexane:EtOAc, 8:2); ^{1}H NMR (500 MHz, $CDCl_3$) δ 5.39 – 5.29 (m, 2H), 5.26 – 5.20 (m, 1H), 4.37 – 4.00 (m, 8H), 3.85 – 3.70 (m, 2H), 2.39 – 2.27 (m, 4H), 2.05 – 1.95 (m, 4H), 1.67 – 1.55 (m, 4H), 1.46 – 1.14 (m, 54H), 0.88 (t, *J* = 6.8 Hz, 6H). ^{13}C NMR (126 MHz, $CDCl_3$) δ 173.4, 173.0, 130.0, 129.7, 77.3, 77.1, 76.8, 70.3, 70.3, 62.4, 62.1, 62.1, 45.6, 34.3, 34.1, 31.9, 29.8, 29.7, 29.5, 29.3, 29.2, 29.2, 29.1, 27.2, 27.2, 24.9, 22.7, 14.1; ^{31}P NMR (203 MHz, $CDCl_3$) δ 8.63, 8.52. QTOF-HRMS (ESI) for $C_{43}H_{81}O_9P$ [M+Na^+]: found 795.5512, calcd 795.5510.

3.4.9 Synthesis of (2R)-3-((((S)-2,3-dihydroxypropoxy)(hydroxy)phosphoryl)oxy)propane-1,2-diyl dioleate (1).

H-phosphonate **11** (0.160 g, 0.20 mmol) was added to a 10-mL, round-bottom flask. A 9:1 v/v of H_2O/Pyr. (5 mL) was added to flask, and the temperature was lowered to 0 °C. I2 was then added, and the reaction was warmed to 24 °C with stirring for 3 h. The pyridine was then removed from the solution by azeotropically drying three times with toluene. The resulting oil was diluted with 45 mL of DCM and washed with a solution of saturated Na_2SO_3 (2 × 10 mL) and once with brine (10 mL). The organic layer was then dried with anhydrous Na_2SO_4 and concentrated under reduced pressure. The crude product was purified on a manual silica gel column (gradient of 98:2 $CHCl_3$:MeOH to 65:25:4 $CHCl_3$:MeOH:H_2O) (refer to Table 3.4 for gradient). Fractions were collected in 13 × 100 mm cell culture tubes, with 72 mL intervals between each change, in a mobile

phase composition (9 mL/fraction). Product appeared from fractions 25–32. The isolated product was concentrated under reduced pressure in a 20 mL scintillation vial, and then $CHCl_3$ (5 mL) was added to dissolve the oil. After cooling the solution to 0 °C in an ice bath, MeOH (0.1 mL) and TFA (0.5 mL dropwise) were added to the reaction mixture. The reaction was allowed to stir for 30 min at room temperature. Saturated $NaHCO_3$ was then added, and the solution was diluted with $CHCl_3$ (30 mL). The mixture was transferred to a separatory funnel, where MeOH (20 mL) and then H_2O (10 mL) were added, followed by shaking. The organic layer was collected, dried with anhydrous Na_2SO_4, and concentrated under reduced pressure. The crude product was then purified using a gradient of 98:2 $CHCl_3$:MeOH to 65:25:4 $CHCl_3$:MeOH:H_2O to yield a clear oil in 73% yield. $[\alpha]_D^{27}$ −16 (c 0.011, $CHCl_3$); Rf = 0.46 ($CHCl_3$:MeOH:H_2O, 65:25:4); ^{1}H NMR (500 MHz, $CDCl_3$) δ 5.26 (tt, J = 5.7, 3.3 Hz, 4H), 5.12 (qd, J = 5.8, 3.0 Hz, 1H), 4.28 (dt, J = 12.1, 3.1 Hz, 1H), 4.10–4.00 (m, 1H), 3.93–3.75 (m, 5H), 3.66–3.50 (m, 3H), 3.43 (d, J = 6.0 Hz, 5H), 2.23 (td, J = 8.8, 4.8 Hz, 4H), 1.93 (q, J = 7.1 Hz, 8H), 1.51 (td, J = 7.9, 3.9 Hz, 4H), 1.33–1.14 (m, 42H), 0.80 (td, J = 6.9, 3.0 Hz, 6H). ^{13}C NMR (126 MHz, $CDCl_3$) δ 174.0, 173.8, 162.5, 130.0, 129.6, 117.5, 77.3, 77.1, 76.8, 70.4, 62.5, 62., 49.5, 49.4, 49.2, 49.0, 48.9, 48.7, 48.5, 34.1, 33.9, 31.8, 29.7, 29.4, 29.2, 29.2, 29.1, 29.0, 29.00, 27.1, 27.1, 24.7, 22.6, 14.0, 0.9. ^{31}P NMR (203 MHz, $CDCl_3$) δ -2.67. QTOF-HRMS (ESI) for $C_{42}H_{79}O_{10}P$ [M+Na+]: found 797.5300, calcd 797.5303.

(2R)-1-((((S)-2,3-Dihydroxypropoxy)(hydroxy)phosphoryl)oxy)-3-(palmitoyloxy)propan-2-yl oleate (2). A waxy solid in 70% yield. $[\alpha]_D^{27}$ -7.4 (*c* 0.088, $CHCl_3$); ^{1}H NMR (500 MHz, $CDCl_3$) δ 5.39 – 5.28 (m, 2H), 5.17 (s, 1H), 4.38 (d, *J* = 11.4 Hz, 1H), 4.11 (dd, *J* = 12.6, 6.8 Hz, 1H), 3.98 – 3.74 (m, 5H), 3.73 – 3.50 (m, 3H), 2.37 – 2.21 (m, 4H), 2.00 (q, *J* = 6.5 Hz, 4H), 1.66 – 1.49 (m, 4H), 1.38 – 1.14 (m, 43H), 0.88 (t, *J* = 6.9 Hz, 6H). ^{13}C NMR (126 MHz, $CDCl_3$) δ 174.2, 174.1, 130.0, 129.7, 117.8, 115.4, 77.3, 77.0, 76.78, 70.7, 62.8, 34.2,

34.1, 32.0, 31.9, 29.8, 29.8, 29.7, 29.7, 29.6, 29.4, 29.4, 29.3, 29.3, 29.2, 27.3, 24.9, 24.8, 22.7, 14.1, 1.0. ^{31}P NMR (203 MHz, $CDCl_3$) δ 0.93. QTOF-HRMS (ESI) for $C_{40}H_{77}O_{10}P$ [M+Na^+]: found 771.5145, calcd 771.5146.

3.5 Supporting Information

3.5.1 Initial Studies to Simultaneously Deprotect the Cyanoethyl Groups and Silyl Groups

Initial attempts to improve the phosphorylation conditions began by exploring more polar fluoride sources to deprotect the TBS ethers in an attempt to simplify the product isolation procedure (Table 3.1). Many of the organic and inorganic naked fluorine sources we tested led to low conversion of starting material (e.g. Me_4NF[25], KF•H_2O[27], or NaF[26]). Interestingly, ^{1}H and ^{31}P NMR revealed that the cyanoethyl protecting group remained intact during TBS deprotection efforts with KF•H_2O and 18-crown-6 ether. Unfortunately, similar purification issues to TBAF arose since mobile phases in phospholipid chromatography are typically aqueous ion pairing media such as $CHCl_3$:MeOH:aq. NH_4Cl[14] that can lead to streaking of compounds like crown ethers on polar stationary phases. Since our goal was to create a route with a simplified purification scheme, we sought a different approach.

Table 3.1 Summary of attempts to perform a global deprotection step with alternative fluoride sources. [a] Conversion of starting material (SM) determined qualitatively by TLC.

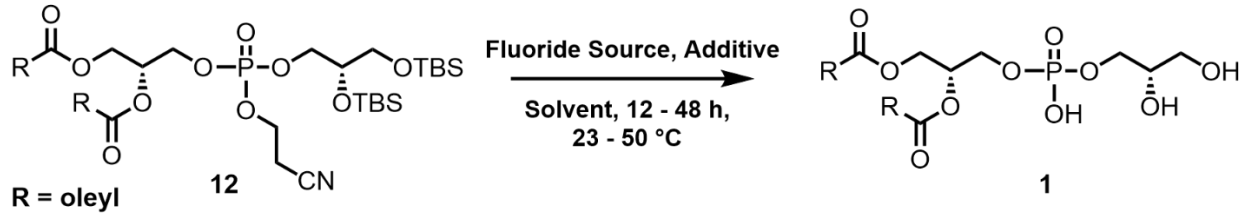

Entry	Fluoride Source	Solvent	Additive	Time (h)	Temperature (°C)	Conversion of SM[a]
1	NaF	3:2:1 THF:H_2O:MeOH	AcOH	24	23	None
2	TMAF	3:1 THF:MeOH	AcOH	12	23	None
3	TMAF	3:1 THF:MeOH	AcOH	48	23	None
4	KF•2H_2O	1.5:1 THF:MeOH	-	24	23	Slight
5	KF•2H_2O	1.5:1 THF:MeOH	AcOH	12	23	Slight
6	KF•2H_2O	1.5:1 THF:MeOH	AcOH	24	35	Slight
7	KF•2H_2O	1.5:1 THF:MeOH	AcOH + 18-c-6	36	23	Slight
8	Benzylsulfonyl Fluoride	4:1 THF:H_2O	-	12	23	No
9	Benzylsulfonyl Fluoride	4:1 THF:H_2O	-	12	50	No

In a 25 mL round bottom flask equipped with a magnetic stir bar was placed **12** (0.1 g, 0.95 mmol) and fluoride source (19 mmol). The contents were dissolved in the specified solvent (10 mL) and the additive was subsequently added (19 mmol). Reactions conducted above 23 °C were heated using a temperature controlled oil bath. Reaction times varied between 12 – 48 h. Conversion of starting material was monitored by the disappearance of **12** that was synthesized according to a previously published protocol. Upon initial investigation of naked fluorine sources utilized to deprotect both of the silyl groups as well as the cyanoethyl group of the phosphate simultaneously, solubility of both the substrate and the fluorine salt proved to be a challenge. For example, an inorganic salt such as NaF was not soluble in any of the aqueous/organic solvent systems tested. On the other hand, the substrate was also not soluble in a pure aqueous system. This led to no conversion of the starting material as determined by TLC. Even the addition of an organic acid in a purely aqueous system led to precipitation of the salt. Due to the risk of acyl chain migration of the phosphoglycerol backbone to the glycerol head group, we avoided heating these

reaction mixtures to high temperatures (> 50 °C). However, gentle heating of the solution below this temperature still appeared to be ineffective at global deprotection. To alleviate this issue, we hypothesized that using a less hydrophobic ammonium fluoride such as tetramethyl ammonium fluoride (TMAF) instead of TBAF would not only improve the solubility of the fluoride source in organic solvents, but it also might make the separation of the product and TMAF more facile. Unfortunately, similar solubility issues arose between the substrate and TMAF that forced us to explore other fluoride reagents.

While NaF has shown little solubility in organic/aqueous systems, $KF{\cdot}2H_2O$ has shown moderate solubility in these same solvent ratios. We were able to observe conversion of the substrate by TLC and were able to isolate the product after column chromatography. The presence of the silyl groups were still present on our substrate as observed by the ^{1}H NMR shifts between 0.87-0.81 and 0.07 – 0.02 ppm (Figure 3.4). However, the α protons to the cyano group of the phosphotriester had disappeared. Additionally, the absence of the cyanotheyl carbon peaks corresponding to the cyano carbon as well as the α carbon at ~19 and 117 ppm, respectively, also indicated that cyanoethyl group was removed. Finally, ^{31}P NMR revealed a single peak at -0.54 ppm which can be attributed to a phosphate diester. Encouraged by these results, we attempted to remove the silyl group by adding a weak acid such as acetic acid to promote the hydrolysis of the silyl groups. Unfortunately, addition of AcOH hindered the solubility, thereby limiting the hydrolysis to only one of the silyl groups. It has been reported that the use of crown ethers can help the solubility of the KF salt. While the solubility of the substrate and salt appeared to increase upon addition of the crown ether in the presence of an acid, the conversion of the substrate did not appear to increase.

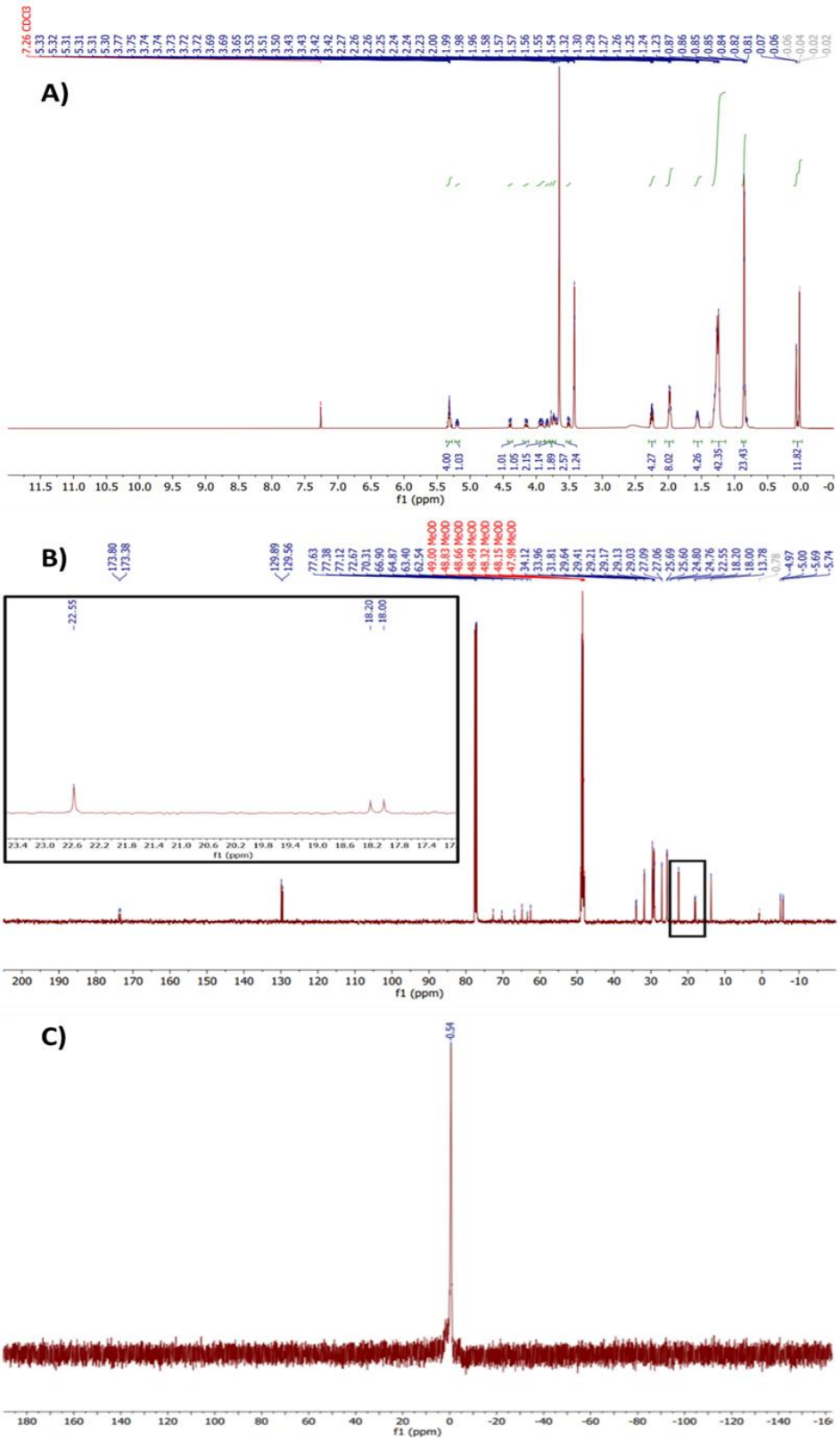

Figure 3.4. ^{1}H (A), ^{13}C (B), and ^{31}P (C) NMR of partially converted substrate by $KF{\cdot}2H_2O$.

3.5.2 High-throughput Experimentation of Diphenylmethylsilyl Deprotection

Catalytic amounts of sulfonyl fluoride reportedly can selectively deprotect diphenyl methyl silyl (DPMS) ethers in the presence of an aqueous surfactant such as TPGS 750-M.[28] Unfortunately, these conditions failed to deprotect our TBS modified substrate under surfactant free conditions (i.e., we did not want to further complicate product chromatographic purification). We then replaced the headgroup protection to enable the use of DPMS ethers instead of TBS ethers to accommodate for the use of benzylsulfonyl fluoride (BSF) as a deprotection agent (Table 3.2). Before applying this strategy to the final deprotection steps, we optimized the deprotection conditions using a model substrate **13** bearing DPMS protecting groups published according to a previously reported protocol using DPMSCl instead of TBSCl[9], and a PMB group that was expected to remain inert to the BSF. Upon completion of pilot experiments, we observed trace amounts of **14** under almost all conditions. Entry 1 seemed to be the only set of conditions that resulted in no reaction despite these conditions being optimal in the substrates tested by Akproji *et al*.[28]

Table 3.2 Initial attempts to remove DPMS silyl ethers using BSF. [a] Conversion of starting material (SM) determined qualitatively by TLC.

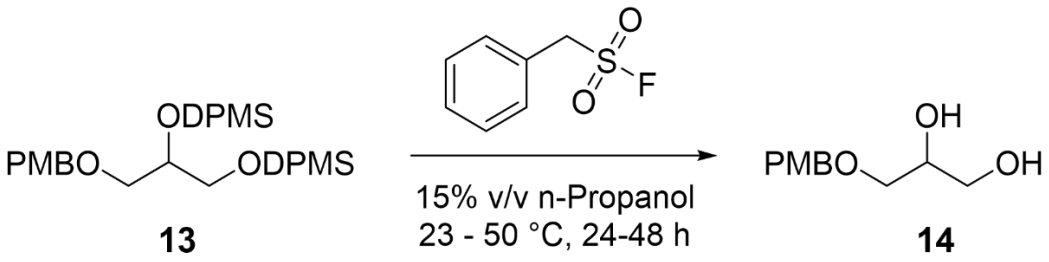

Entry	Eq. BSF	TPGS 750-M	Solvent	Time (h)	Temp. (°C)	Conversion of 3[a]
1	0.3	Yes	H_2O	48	50	No
2	0.5	No	THF	24	23	Slight
3	0.5	No	THF	48	50	Slight
4	0.3	No	THF	24	23	Slight
5	0.3	No	THF	48	50	Slight
6	1	No	THF	24	23	Slight
7	1	No	THF	48	50	Slight

We then chose to explore a larger reaction landscape needed to identify optimal reaction conditions. We turned to a recently reported high throughput experimentation system (HTE) to rapidly screen reaction conditions by using a liquid handling robot in tandem with desorption electrospray ionization mass spectrometry (DESI-MS) (Figure 3.5).[29] From this experiment, we were able to examine 84 unique reaction conditions including 7 solvents and 6 BSF catalyst stoichiometries (Figure 3.6). In this semi-automated system, we were able to simultaneously examine each set of reaction conditions at 20 °C and 50 °C in sealed, 96 well microtiter plates. The results from this experiment indicate that the temperatures examined do not play a significant role on the reaction progress. They do, however, indicate that catalytic amounts of BSF appear to be more efficient than stoichiometric amounts of reagents. Additionally, a 3:1 THF/Water solution appeared to be far superior to many of the other solvent systems tested, although the organic/water solvent systems in general seem to outperform the purely organic solvents. Armed with these

preferred conditions identified by HTE, we attempted the synthesis of the newly designed phosphoglycerol headgroup. Unfortunately, standard deprotection conditions of PMB ether **13** with DDQ[32] produced an acidic hemiacetal byproduct that promoted hydrolysis of the DPMS ether protecting groups of **13** (Figure 3.7A) in spite of modifying the protocol with respect to time, temperature, and DDQ stoichiometry. Even implementing protocols that suggested more mild approaches such as the use of an Ag(I) catalyst in the presence of 1,3,5-trimethoxybenzene[31], we were unable to produce the desired product. Fortunately, we were able to circumvent this issue by replacing the PMB ether with a phenyl acyl ester that could be cleared by DIBAL-H reduction (Figure 3.7B). We were able to obtain **18** in 88% yield by reacting **17** with phenylacetyl chloride in the presence of Et_3N. The acetonide was successfully removed to afford **19** using a 2M HCl/THF solution in 94% yield without significant hydrolysis of the ester. Installation of the DPMS groups to give **20** in an 89% yield was carried out by using DPMSCl in the presence of imidazole and Et_3N. Finally, **21** was afforded in 79% after DIBAL-H treatment.

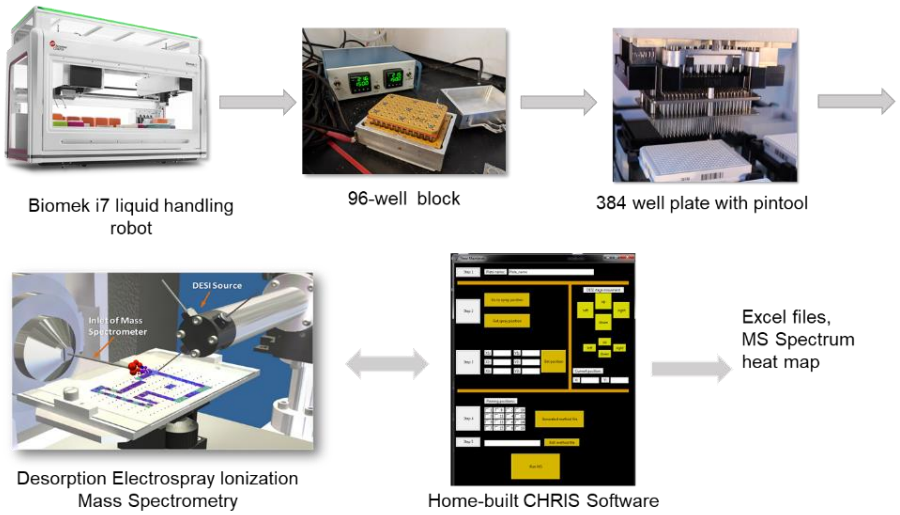

Figure 3.5. General workflow for High Throughput Experimentation.

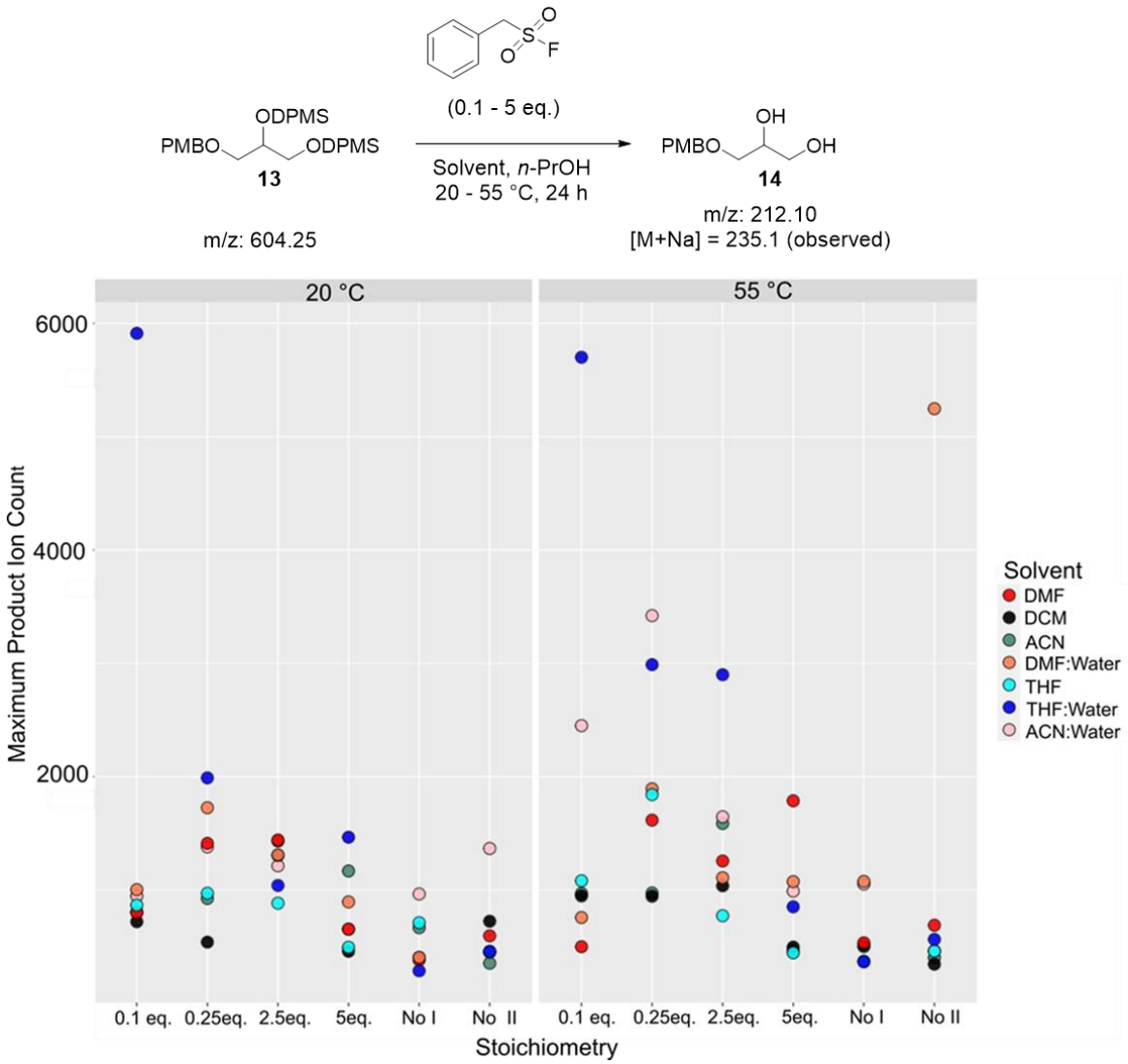

Figure 3.6. HTE screening of DPMS ether deprotection of BSF. The y-axis is the average maximum product ion intensity for each reaction. Each set of conditions was run in quadruplicates. The x-axis is the BSF catalyst loadings. "No I" and "No II" refer to negative controls where reactions contain no substrate (**13**) or no catalyst, respectively.

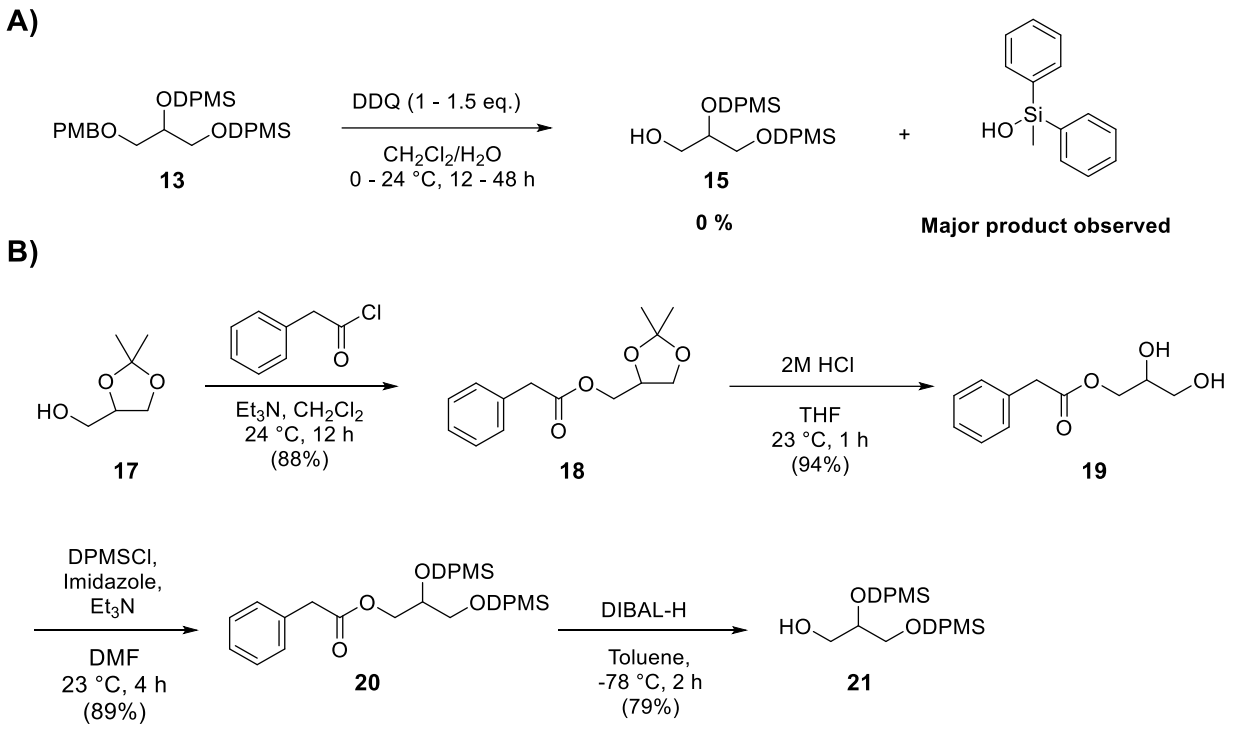

Figure 3.7. (A) Hydrolysis of DPMS ethers upon reaction with DDQ. (B) Alternative protection/deprotection strategy employing a solketal phenyl ester intermediate.

3.5.3 Development of Phosphorylated Intermediates via High-throughput Experimentation and Flow Chemistry

Before employing this transformation in flow, we deployed a round of HTE to determine the most promising reaction conditions. Ideally, we preferred the use of the asymmetric NCP reagent and rationalized the enhanced mixing in flow might not only improve the scaling issues, but also reduce the number of hydrolyzed byproducts since the phosphoramidite could be run closer to the 1:1 stoichiometry than the 2:1 stoichiometry that we previously used. In this experiment, we used a 2^3 factorial design of experiments with time, base, and phosphoramidite stoichiometry as variables (Figures 3.8, 3.9, and 3.10). Interestingly, our desired mass peak from phosphoramidite **22** at an *m/z* of 684.3 did not appear in any of our reactions. Instead, we were observing a significant amount of an *m/z* of 239.1 corresponding to a methoxylated phosphotriester. We infer from these findings that **22** was undergoing substitution with methanol

and cleaving the DPMS ethers in the acidic DESI-MS spray solvent. This hypothesis is consistent with Kele et al.[30] and supported by synthesizing **22** and observing a similar spectrum to that of the HTE experiment (Figure 3.11), suggesting that **22** degrades under the conditions of the DESI-MS analysis.

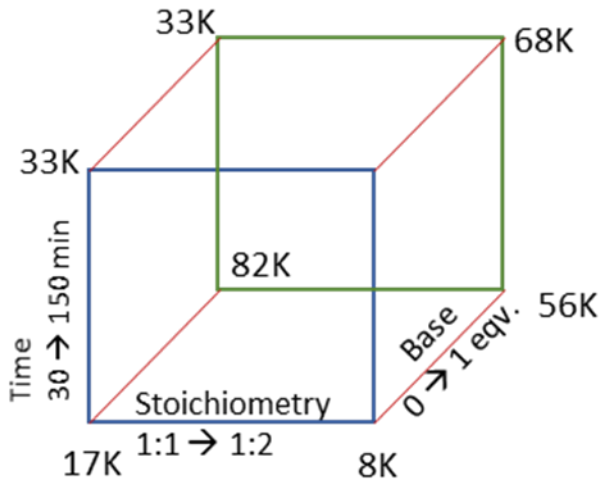

Figure 3.8. A 2^3 full factorial design with time, stoichiometry (where phosphoramidite is in excess), and base at lower and higher values each. The numbers on the edge of the cube (17K, 33K, etc.) corresponds to the DESI-MS average ion count response.

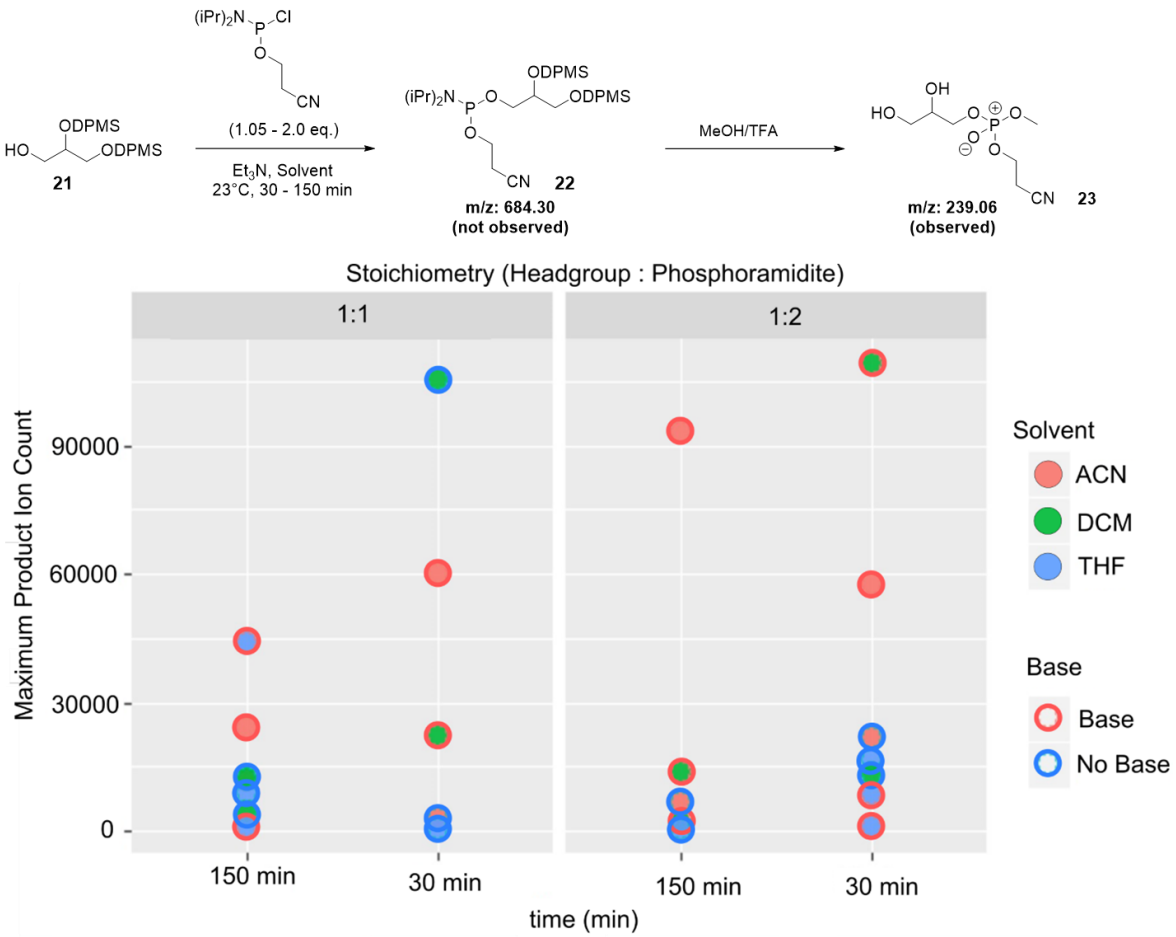

Figure 3.9. .HTE of phosphoglycerol headgroup phosphorylation campaign with NCP using DESI-MS analysis.

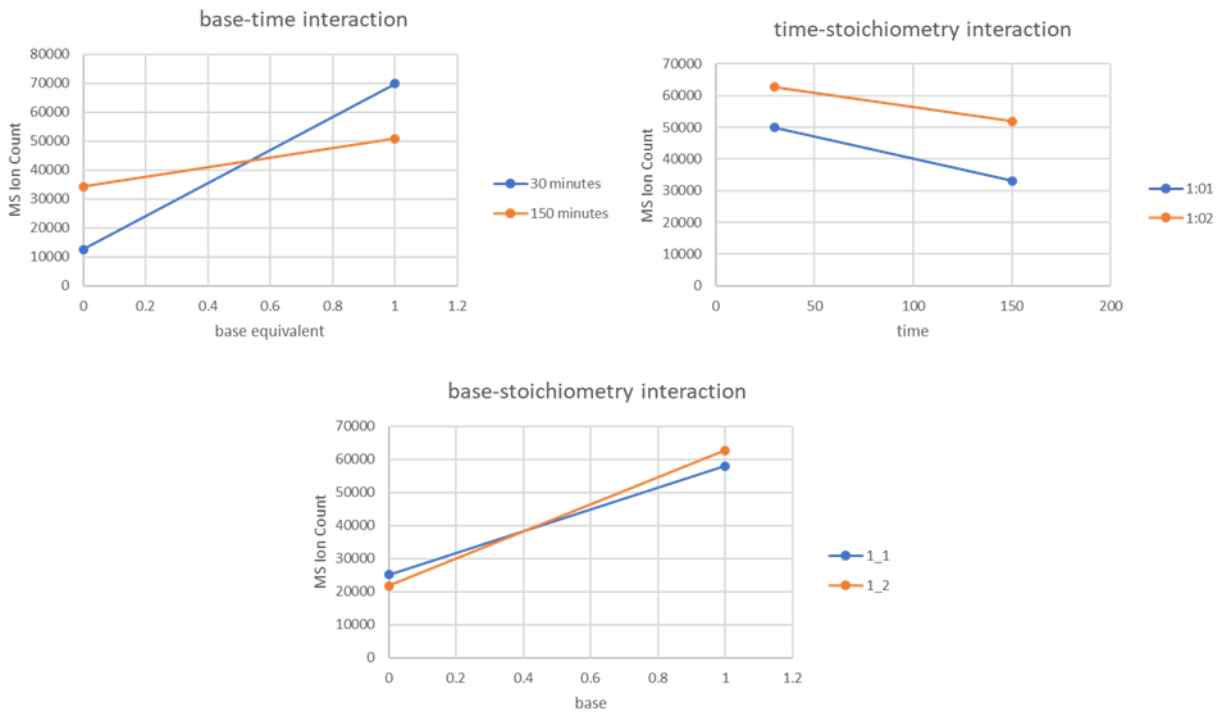

Figure 3.10. Interaction effects plot. Y-axis corresponds to the DESI-MS Ion Count Response and interaction plot between base-time (top-left), time-stoichiometry (top-right), and base-stoichiometry (bottom) is indicated.

The results demonstrated that a 2-fold excess of NCP yielded a larger amount of desired product than a 1:1 stoichiometry. However, our HTE system is not currently conducive for air-sensitive reactions such as this one. Therefore, it might not be rational to conclude that a 2-fold excess of NCP is necessary especially when precautions are implemented to prevent air and moisture entrance to the reaction can be taken at the bench. As expected, the presence of a base such as Et_3N appears to be beneficial for the reaction by buffering HCl liberation after substitution, thereby inhibiting DPMS hydrolysis. After optimization of the glycerol headgroup phosphorylation conditions, we translated these results to a flow on a 100 mg scale (Figure 3.12). For these experiments, we used a 10 µL microchip Chemtrix reactor (Figure 3.13) containing two staggered-oriented ridge (SOR) mixers prior to entering the reaction zone. Based on the HTE data, it was imperative that the phosphoramidite and the base are homogenized before introduction of the protected phosphoglycerol headgroup **21** to avoid hydrolysis of the DPMS ethers. We achieved this by mixing NCP and Et_3N in the first SOR mixer, followed by the introduction of **21** in the second SOR mixer. A residence time of 1 min at 30 °C was optimal for producing phosphoramidite intermediate **22** in 73% yield compared to a 40% yield for the batch reaction. Longer residence times and lower temperatures resulted in formation of the hydrolysis product and incomplete conversion of starting material, respectively, as observed by TLC. Additionally, the need for only a slight excess of NCP compared to the 2 more equivalents required for batch conditions greatly simplified the purification process by only requiring an aqueous extraction for workup.

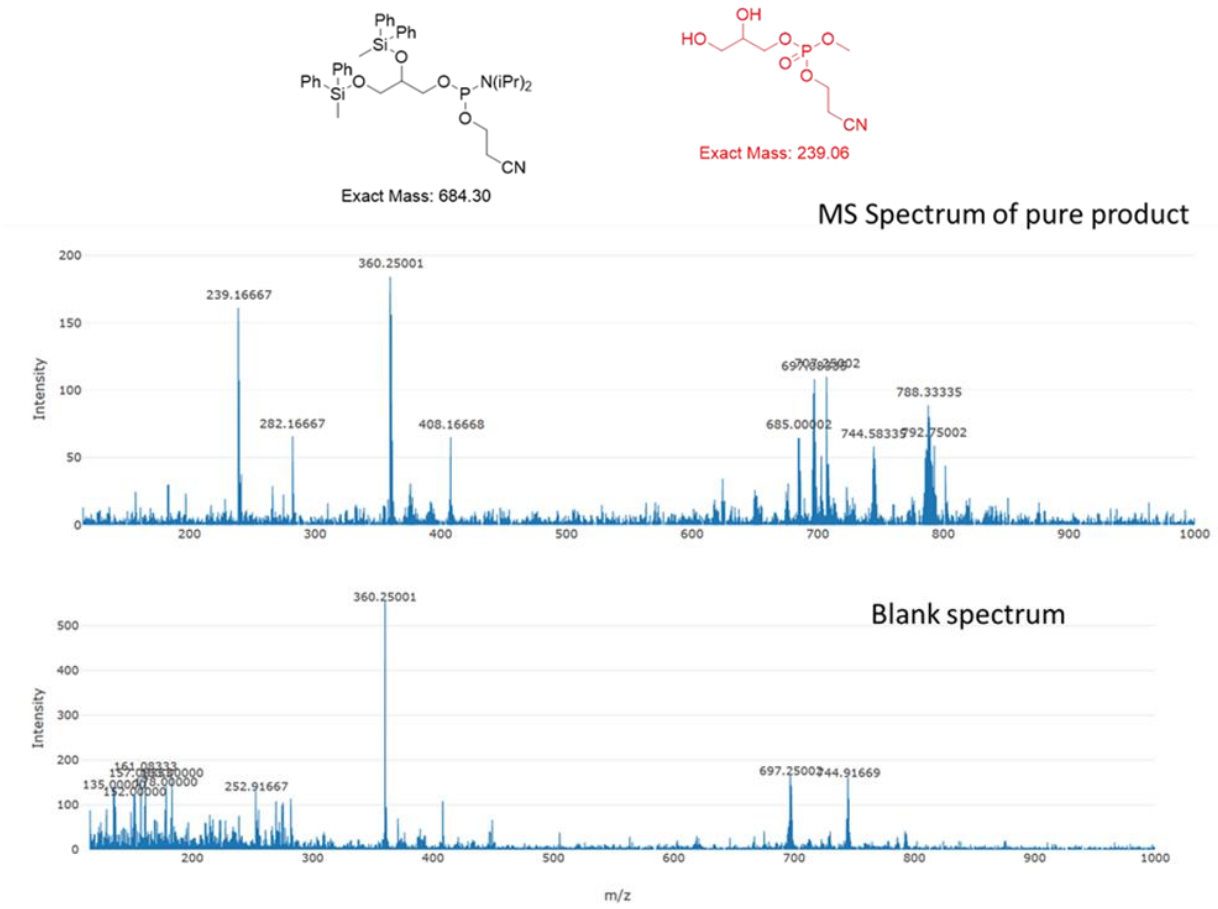

Figure 3.11. DESI-MS Spectrum for the authentic product which has been characterized by NMR (top) and the blank spectrum where nothing was pinned. The desired product [M+H] is 685 however the most abundant peak is at m/z 239.1. We attribute the peak at m/z 239.16 to the structure shown in red.

Next, we set out to increase the scale of the reaction from 100 mg to greater than 1 g. The order of addition was conducted similarly to the small-scale experiments by using a T-mixer followed by a static T-mixer for increased mixing upon the introduction of **21** to induce turbulent flow before entering the temperature controlled coiled reactor (Figure S15). Flow rates were 0.5 mL/min for each syringe, translating to a total residence time of 1 min. The stoichiometries of NCP and Et_3N were 1.1 and 2, respectively. To our delight, we were able to obtain 1.1 g of our desired product **22** in a 75% isolated yield with this reactor configuration.

With phosphoramidite intermediate **22** in hand, we proceeded to phosphorylate the glycerol backbone. Unlike the phosphorylation of **21**, the reaction with the backbone proved to be more challenging as the substitution of the diisopropylamine substituent is catalyzed by mildly acidic conditions. We again went back to small scale pilot experiments in both flow and batch to optimize these reaction conditions (Table 3.3). Unfortunately, all conditions tested resulted in significant acyl chain migration of the glycerol backbone wherein the acyl chain transesterified to the more thermodynamically stable primary position from the secondary position. No desired product **22** formation was observed by TLC.

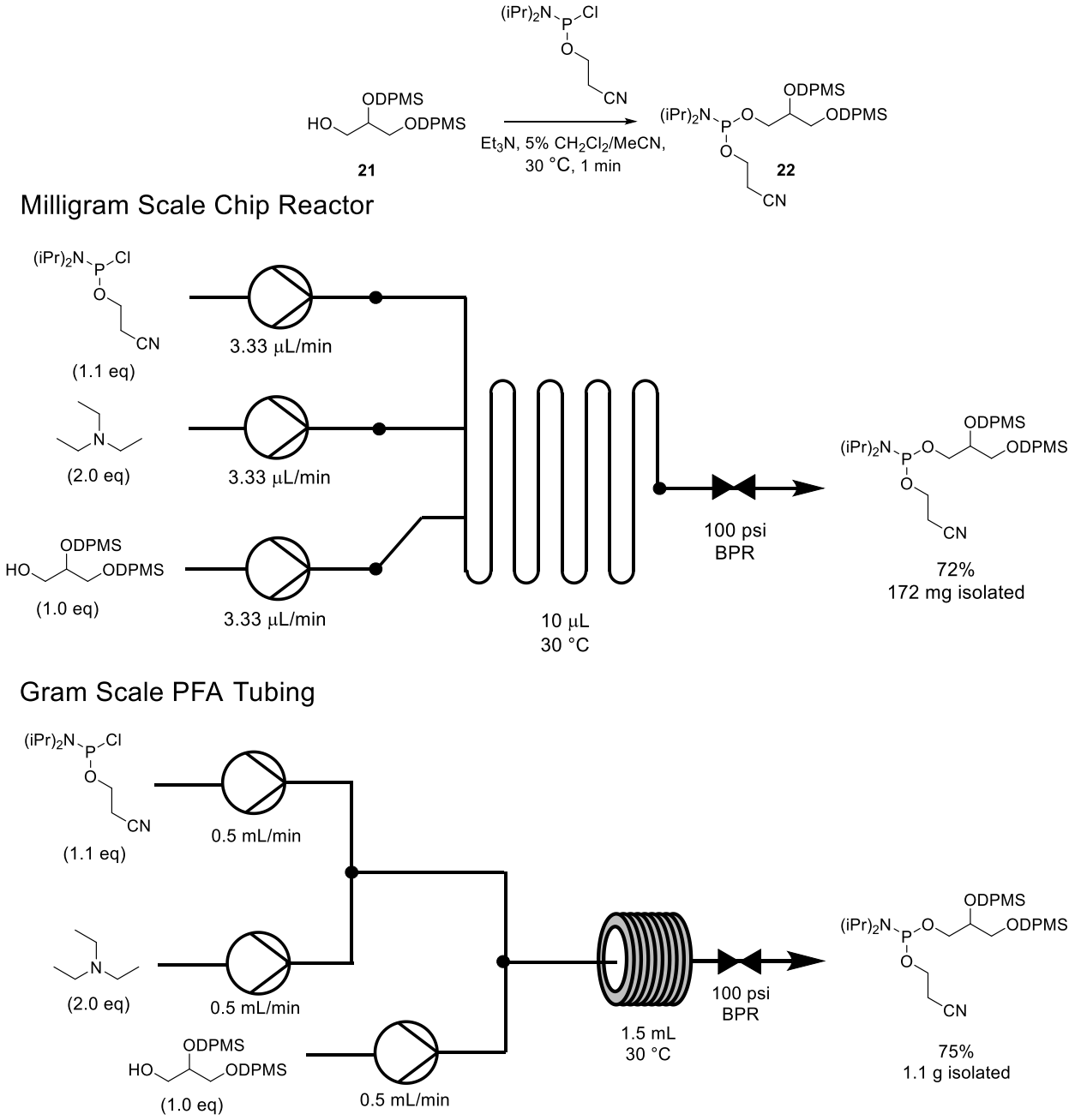

Figure 3.12. Small scale flow schematic using a microfludidic chip (top). Gram scale reaction using PFA tubing (bottom).

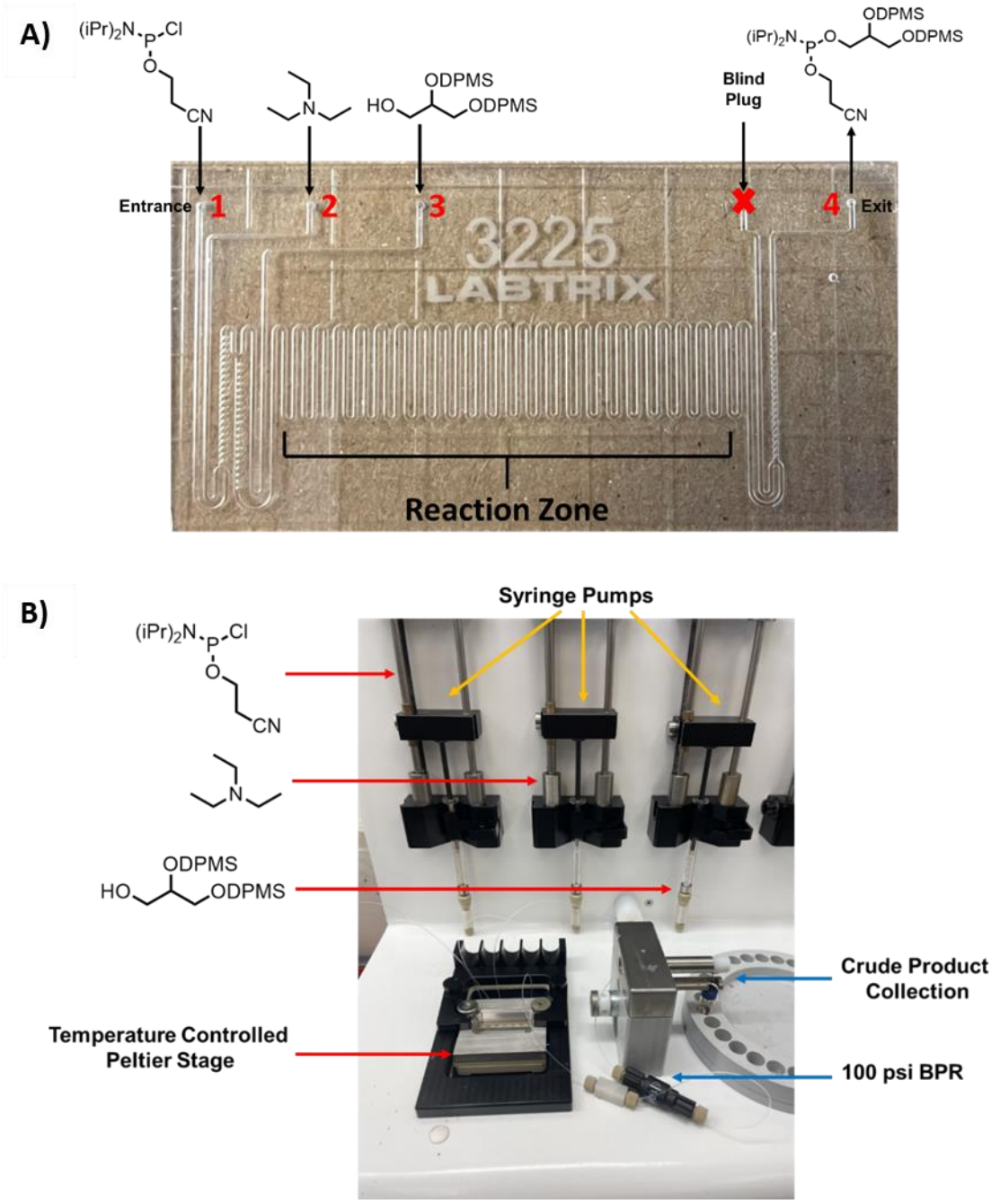

Figure 3.13. Arrangement of reagents as they enter and exit the microfluidic reactor (A). The "reaction zone" is comprised of the region between the last SOR mixer of the entrance, and the SOR mixer prior to the exit of the chip. Tubing assembly and arrangement of syringes of on the S1 (B).

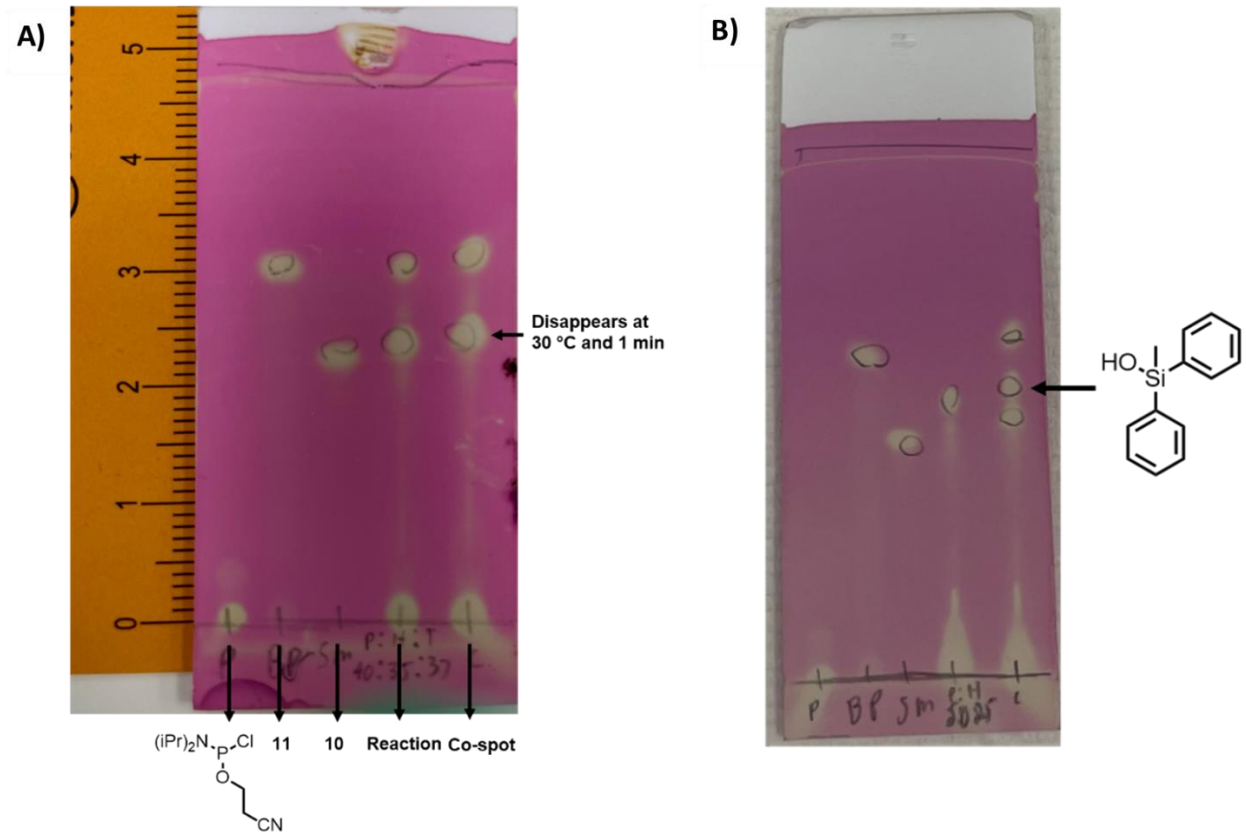

Figure 3.14. Example of a TLC at a residence time of 30 s and at 23 °C with the addition of Et_3N (A). Example of a TLC showing silyl hydrolysis product without the addition of Et_3N most likely due to the formation of HCl (B). The order of analytes from left to right on the TLC plate in B is the same as in A.

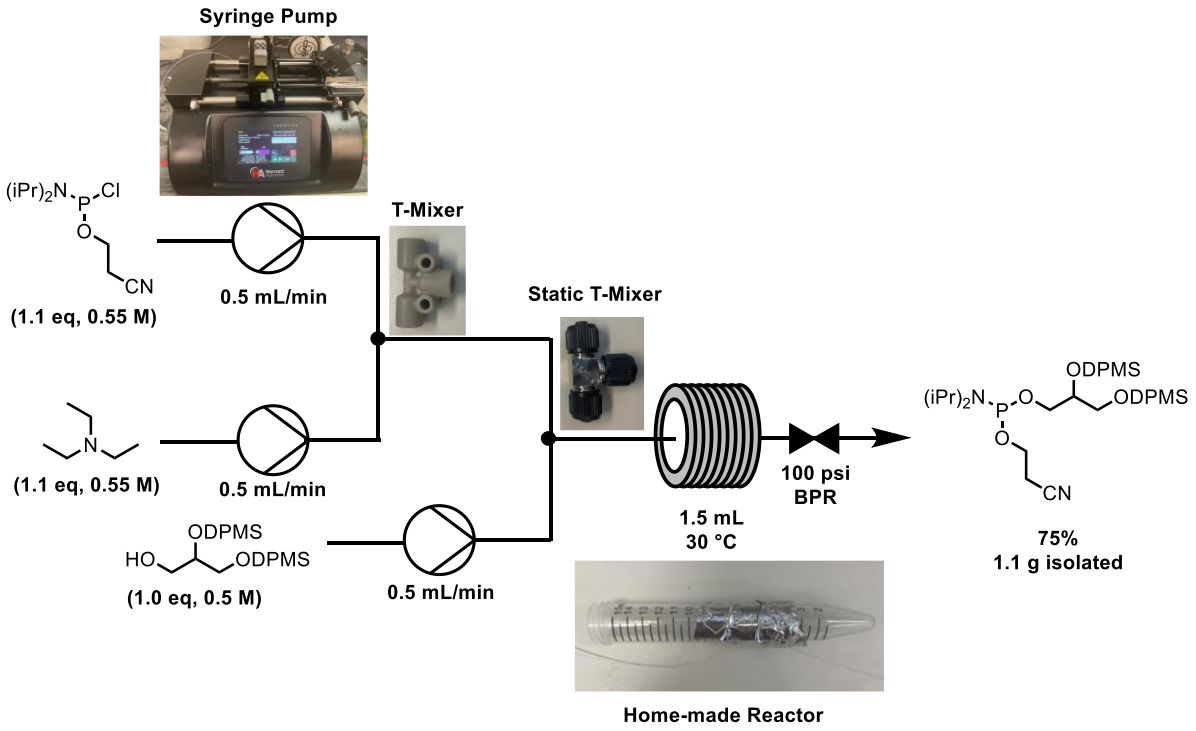

Figure 3.15. Flow schematic of gram scale reactions containing concentration of reagents and images of components.

Table 3.3. Attempts to phosphorylate the *sn*-3 phosphoglycerol backbone under acidic conditions. [a]Acyl chain migration observed by TLC.

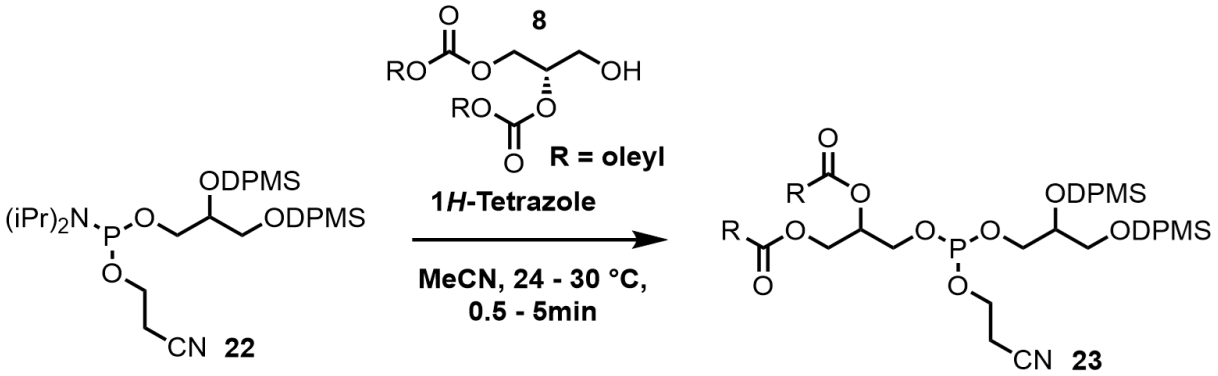

Entry	Eq. of 12	Residence Time (min)	Temperature (°C)	Acyl Chain Migration[a]
1	1.1	0.5	23	No
2	1.25	0.5	30	No
3	1.1	1	23	Yes
4	1.25	1	30	Yes
5	1.1	5	23	Yes
6	1.25	5	30	Yes

3.5.4 Methods for Supporting Information

High Throughput Experimentation General Workflow. The desorption electrospray ionization-mass spectrometry (DESI-MS) experiments were performed using the previously published protocol by Wleklinski et al.[7] along with the Chemical Reaction Screening (CHRIS) module[7], a user-friendly in-teractive home-built software. The reagent stock solutions were prepared and transferred into the reservoirs on the deck of the liquid handling robot (Biomek, i7, Beckman Coulter) and then transferred using the multi-channel pod and the span-8 pod to prepare the 96 well plates. The 96 well block (Analytical Sales, Inc) was comprised of glass vials inserted into an aluminum block. Once the vials were charged with reagents, the plate was sealed and heated to the desired temperature between using custom-made aluminum 100 W cartridge heaters

fabricated in-house (Amy Facility, Purdue University) or placed on the orbital shaker at room temperature. The reaction mixtures were then transferred to 384 well plates and then spotted onto DESI-MS plate without any further purification. The DESI-MS plate is comprised of a porous PTFE sheet (EMDMillipore, Saint Go-bain) mounted onto a glass support (Foxx Life Sciences) via Scotch spray mount (3M). Spotting was done using the 50 nL magnetic slotted transfer pin-tool mounted onto the liquid han-dling robot. The data acquisition for DESI-MS was performed using a linear ion trap mass spectrometer (LTQ, Thermo Scientific) fitted with a DESI Imaging source that is commercially available (2D Prosolia DESI stage, Waters Corporation). Analysis of the data was performed using the csv files obtained from the CHRIS created workflow. CHRIS allows DESI-MS operation and analysis of the DESI-MS plates by monitoring the product ion counts of selected m/z values of interest for the starting material, product, and by-products. The product ion counts for the expected m/z values for the product were analyzed by creating data visualization in R studio, excel and JMP Pro.

High Throughput Experimentation of Glycerol Head-group Phosphorylation. We chose a design of experiments (DoE) with 23 full factorial design for our phosphorylation ex-periment with times of 30 minutes and 150 minutes, stoichi-ometries of phorphoramidites at 1:1 and 1:2, and Et3N at 0 and 1 equiv. We prepared 1 mL stock solutions of 0.125 M & 0.25 M 3-((chloro(diisopropylamino)phosphaneyl)oxy)propaneni-trile (Phosphoramidite) and 0.125 M Et_3N in DCM, THF and MeCN. From these stocks solution, respective volumes of each reagent were transferred using the Biomek i7 liquid handling robotic system to the individual well in two different 96 well block (Analytical Sales, Inc.) to get the final concentration of 0.03M of Headgroup, 0.03 M & 0.06 M (1 equiv. & 2 equiv. respectively) of Phosphoramidite and 0.03 M (1 equiv.) of Et_3N with a final volume of 150 µL of the solution. The 96 well blocks were placed

on the orbital shaker for 30 or 150 minutes each. The reaction solution (60 µL) was then transferred into polypropylene 384 well plates. As a control, 60 µL of the pure product (synthesized in flow and characterized by NMR) was transferred in one of the wells manually in the 384 well plate. An aliquot of the solution (50 nL) was then drawn out using the 384 pin-tool from the 384 well plate and then stamped onto a porous PTFE surface glued to glass (DESI-slide) with 4 repli-cates. DESI-MS was performed using MeOH + 0.1% formic acid as the spray solvent and the average product ion count was generated using home-built CHRIS software which was coupled to the DESI-MS readout. The average product ion intensities were used to perform the further analysis using R programming & Excel.

Milligram Scale Synthesis of 2,3-bis((methyldiphenylsilyl)oxy)propyl(2-cyanoethyl)diisopropylphosphoramidite (22). A flow schematic can be seen in Figure 3.12. Reactions for the translation of HTE data to small scale pilot flow experiments were carried out using three 1 mL gas tight syringes on a Chemtrix Labtrix S1 system (S1) that were connected to a Chemtrix Labtrix 3225 glass microfluidic reactor chip (Figure 3.13). Each syringe filled with reagent solution was attached to its own individual pump on the S1. The solutions were all made in 5% DCM in dry MeCN where the phosphoramidite concentration was 0.06 – 0.38 M, Et_3N concentration was 0.1 – 0.7 M, and alcohol **10** was 0.05 – 0.35 M. SOR mixers in these chips serve to induce turbulent flow of the reagents to ensure adequate mixing. PFA tubing was used to connect the microfluidic chip to the syringes and collection vial. The phosphoramidite and the Et_3N solutions were mixed upon entering the chip through ports 1 and 2. After passage through the first SOR mixer, 10 was introduced into port 3 prior to the second SOR mixer and the reaction zone. The residence time (T_r) expressed in min can be calculated by using the following equation:

$$T_r = \frac{V_r}{V_f} \qquad (1)$$

where V_r is the total volume of the reactor in mL, and V_f is the volumetric flow rate in μL/min. Residence times and temperature were controlled by adjusting the flow rates and heat delivered to the Peltier stage, respectively, using the Chemtrix Labtrix software. Residence times were evaluated between 10 s^{-1} min, and evaluated by TLC. The temperature varied between 23 and 30 °C is required by the experiment. Samples were collected in 20 mL glass scintillation vials capped with a rubber septum. The vials were purged and maintained under an Ar atmosphere via an Ar ballon during collection. Complete disappearance of the starting material by TLC did not occur until the concentrations of each reactant were raised 7-fold from the initial concentrations at a residence time of 1 min at 30 °C. The tubing used before and after the glass reactor chip consisted of FEP (0.8 mm OD x 0.25 mm ID). The 100 psi back pressure regulator was installed after the crude product exited the microfluidic chip. Check valves were attached to the male ends of each syringe to prevent backflow. After the reaction conditions were optimized, a prep-scale run (172 mg) was conducted by continuously collecting crude product solution until all three of the syringes were depleted. The crude reaction mixture was then diluted with 30 mL of DCM and washed with saturated $NaHCO_3$ (3 x 10 mL). The combined organic extracts were then dried with anhydrous Na_2SO_4 and concentrated in vacuo. The crude oil was then purified using a Biotage flash purification system (hexane:EtOAc). The product was isolated as a clear oil in 75% yield (Refer to Table 3.7 for gradient); R_f=0.27 (DCM:MeOH, 98:2); ^{1}H NMR (500 MHz, $CDCl_3$) δ 7.66 – 7.47 (m, 8H), 7.45 – 7.28 (m, 12H), 4.01 (h, *J* = 5.3 Hz, 1H), 3.82 – 3.45 (m, 8H), 2.53 – 2.33 (m, 2H), 1.16 (dd, *J* = 6.8, 2.6 Hz, 6H), 1.08 (d, *J* = 6.8 Hz, 6H), 0.64 (s, 3H), 0.57 (d, *J* = 4.7 Hz, 3H). ^{13}C NMR (126 MHz, $CDCl_3$) δ 135.81, 134.53, 134.49, 134.42, 129.82, 129.75, 129.72, 127.84, 127.76, 117.67, 117.62, 77.30, 77.05, 76.79, 73.60, 73.54, 73.48, 73.41, 64.84, 64.74, 64.58, 64.45, 64.18, 64.06, 58.61, 58.46, 58.41, 58.26, 43.11, 43.08, 43.01, 42.98, 24.66, 24.59, 20.28, 20.23, -

2.22, -2.32, -3.18. ^{31}P NMR (202 MHz, $CDCl_3$) δ 148.38, 148.08. QTOF-HRMS (ESI) for $C_{35}H_{49}N_2O_4PSi_2$ [M+Na$^+$]: found 685.3048, calcd 685.3041.

Gram Scale Synthesis of 2,3-bis((methyldiphenylsilyl)oxy)propyl(2-cyanoethyl)diisopropylphosphoramidite (22). Reactions of **22** on the gram scale were carried out by using three 5 mL gas tight syringes attached to two Hamilton PHD Ultra syringe pumps. The phosphoramidite and Et_3N solutions were placed in one pump (P1), and the syringe containing the alcohol solution was placed in the other pump (P2). All reagent solutions were made with 5% DCM in dry MeCN. It should be noted that the alcohol solution was slightly turbid. P1 operated at a flowrate of 0.25 mL/min, and P2 operated at 0.5 mL/min so that the total flowrate was 1.5 mL/min. PFA tubing was used for these flow experiments (1/16" OD x 0.03" ID). The phosphoramidite and Et_3N was mixed in a standard T-mixer followed by mixing with the alcohol in a static T-mixer (Figure 3.15). Once all three reagents were mixed, they entered the home-made reactor consisting of tubing coiled around a 15 mL Falcon Tube and held in place with aluminum tape. The total volume of the reactor was 1.5 mL. Residence times were calculated using eq. 1. This assembly was subsequently placed in a temperature controlled oil bath where the temperature was set to 30 °C for the duration of the reaction. At the end of the tubing was a Luer lock assembly, where a needle was attached so that the crude reaction mixture emptied into a 20 mL scintillation vial that was placed under a septum sealed Ar atmosphere. A 100 psi back pressure regulator was placed at the end of the reaction line. The reaction mixture was then diluted with DCM and washed with saturated $NaHCO_3$ (3 x 30 mL). The washed organic layer was dried with anhydrous Na_2SO_4 and concentrated under reduced pressure. The crude product was then purified on a Biotage instrument flash purification system (hexane:EtOAc) (Refer to Table 3.7 for gradient). The product was isolated as a clear oil in 75% yield; R_f=0.27 (DCM:MeOH, 98:2); ^{1}H NMR (500 MHz, $CDCl_3$)

δ 7.66 – 7.47 (m, 8H), 7.45 – 7.28 (m, 12H), 4.01 (h, *J* = 5.3 Hz, 1H), 3.82 – 3.45 (m, 8H), 2.53 – 2.33 (m, 2H), 1.16 (dd, *J* = 6.8, 2.6 Hz, 6H), 1.08 (d, *J* = 6.8 Hz, 6H), 0.64 (s, 3H), 0.57 (d, *J* = 4.7 Hz, 3H). ^{13}C NMR (126 MHz, $CDCl_3$) δ 135.81, 134.53, 134.49, 134.42, 129.82, 129.75, 129.72, 127.84, 127.76, 117.67, 117.62, 77.30, 77.05, 76.79, 73.60, 73.54, 73.48, 73.41, 64.84, 64.74, 64.58, 64.45, 64.18, 64.06, 58.61, 58.46, 58.41, 58.26, 43.11, 43.08, 43.01, 42.98, 24.66, 24.59, 20.28, 20.23, -2.22, -2.32, -3.18. ^{31}P NMR (202 MHz, $CDCl_3$) δ 148.38, 148.08. QTOF-HRMS (ESI) for $C_{35}H_{49}N_2O_4PSi_2$ [M+Na$^+$]: found 685.3048, calcd 685.3041.

Synthesis of (2,2-dimethyl-1,3-dioxolan-4-yl)methyl 2-phenylacetate (18). In an oven dried 250 mL multi-neck round bottom flask equipped with a magnetic stir bar was placed solketal (9.3 mL, 75 mmol). The flask was dried via Schlenk techniques, and an Ar balloon was attached. Dry DCM (55 mL) and Et_3N (12 mL, 86 mmol) was added to the flask, and the mixture was allowed to cool to 0 °C in an ice bath. Phenylacetyl chloride (11 mL, 83 mmol) was then added dropwise and allowed to stir for 20 min at 0 °C and warmed up to 24 °C where it continued to react for another 1.5 h. The crude product was then poured over 60 mL DI H_2O in a 250 mL separatory funnel. The organic layer was extracted, and the aqueous layer was washed with DCM (3 x 30 mL). The combined organic extracts were dried with anhydrous Na_2SO_4 and concentrated under reduced pressure. The crude product was purified on a silica gel column (gradient of 9:1 to 8:2 Hexane:EtOAc) to yield the product as a clear yellow oil in 88% yield; R_f=0.42 (Hexane:EtOAc, 8:2); ^{1}H NMR (500 MHz, $CDCl_3$) δ 7.38 – 7.23 (m, 5H), 4.30 (qd, *J* = 6.1, 4.7 Hz, 1H), 4.15 (qd, *J* = 11.5, 5.3 Hz, 2H), 4.03 (dd, *J* = 8.5, 6.5 Hz, 1H), 3.69 (dd, *J* = 8.5, 6.2 Hz, 1H), 3.67 (s, 2H), 1.41 (s, 3H), 1.36 (s, 3H). ^{13}C NMR (126 MHz, $CDCl_3$) δ 171.36, 133.76, 129.29, 128.96, 128.62, 127.38, 127.21, 109.82, 77.36, 77.11, 76.85, 73.54, 66.26, 64.96, 41.14, 26.66, 25.43. QTOF-HRMS (ESI) for $C_{14}H_{18}O_4$ [M+Na$^+$]: found 273.1099, calcd 273.1097.

Synthesis of 2,3-dihydroxypropyl 2-phenylacetate (19). In a 250 mL round bottom equipped with a magnetic stir bar was placed **7** (3.0 g, 12 mmol) dissolved in THF (33 mL). A 1M HCl solution (33 mL) was then added to the flask and the reaction was allowed to stir for 3 h at 24 °C. A saturated solution of $NaHCO_3$ was then slowly added until all the CO_2 evolution ceased. The reaction mixture was then washed with EtOAc (3 x 150 mL) and dried with anhydrous Na_2SO_4 before being concentrated under reduced pressure. The crude product was then purified on a silica gel column (gradient of 98:2 to 96:4 DCM:MeOH) to yield the product as a white solid in 94% yield; R_f=0.92 ($CHCl_3$:MeOH:H_2O, 65:25:4); ^{1}H NMR (500 MHz, $CDCl_3$) δ 7.35 – 7.22 (m, 5H), 4.12 (dd, *J* = 5.5, 1.2 Hz, 2H), 3.85 (qd, *J* = 5.7, 3.7 Hz, 1H), 3.64 (s, 2H), 3.58 (dd, *J* = 11.6, 3.7 Hz, 1H), 3.48 (dd, *J* = 11.6, 6.1 Hz, 1H), 3.34 (s, 2H). ^{13}C NMR (126 MHz, $CDCl_3$) δ 172.14, 172.05, 133.77, 133.68, 129.28, 129.25, 128.82, 128.69, 127.30, 77.40, 77.14, 76.89, 70.07, 65.58, 63.33, 61.59, 41.25, 41.15. QTOF-HRMS (ESI) for $C_{11}H_{14}O_4$ [M+Na$^+$]: found 233.0786, calcd 233.0784.

Synthesis of 2,3-bis((methyldiphenylsilyl)oxy)propyl 2-phenylacetate (20). In a 50 mL oven dried multi-neck round bottom flask equipped with a magnetic stir bar was placed **8** (1.0 g, 4 mmol) and imidazole (0.95 g, 14 mmol). The flask was cycled 3 times with vacuum/Ar, and an Ar balloon was attached to the round bottom flask. DMF (10 mL) was added and the mixture was stirred until everything was dissolved. The reaction was subsequently cooled to 0 °C in an ice bath where DPMSCl (2.9 mL, 14 mmol) followed by Et_3N (1.3 mL, 10 mmol) was added. The reaction was stirred in the ice bath for 1.5 h until it was moved to a 50 °C oil bath and allowed to react for another 2.5 h. The reaction was then quenched with 40 mL of DI H_2O and extracted with EtOAc (3 x 40 mL). The combined organic layers were then washed with H_2O, then brine. The organic layer was dried with anhydrous Na_2SO_4 and concentrated under reduced pressure. The crude

product was then purified on a silica gel column (hexane:EtOAc) to yield the product as a turbid colorless oil in 89% yield (Refer to Table 3.5 for gradient); R_f=0.55 (Hexane:EtOAc, 8:2); ^{1}H NMR (500 MHz, $CDCl_3$) δ 7.59 – 7.12 (m, 27H), 4.28 (dd, *J* = 11.3, 3.6 Hz, 1H), 4.12 (dd, *J* = 11.2, 6.3 Hz, 1H), 4.06 (qd, *J* = 6.0, 3.5 Hz, 1H), 3.69 – 3.62 (m, 2H), 3.45 (s, 2H), 0.58 (d, *J* = 23.9 Hz, 7H); ^{13}C NMR (126 MHz, $CDCl_3$) δ 171.41, 136.17, 136.09, 135.54, 135.51, 134.44, 134.40, 134.37, 133.91, 129.93, 129.85, 129.30, 128.54, 127.91, 127.84, 127.05, 77.30, 77.04, 76.79, 71.54, 66.14, 64.41, 41.08, 31.62, 22.69, 14.16, -2.50, -3.21, -3.29. QTOF-HRMS (ESI) for $C_{37}H_{38}O_4Si_2$ [M+Na$^+$]: found 625.2203, calcd 625.2200.

Synthesis of 2,3-Bis((methyldiphenylsilyl)oxy)propan-1-ol (21). In an oven dried multi-neck round bottom flask equipped with a magnetic stir bar was placed **9** (0.85 g, 1.5 mmol). The flask was dried out via Schlenk techniques and placed under an Ar atmosphere via an Ar balloon attached to the flask. Dry toluene (10 mL) was then added to the flask and the solution was subsequently cooled to -78 °C with a dry ice/acetone bath. After 10 min of cooling, DIBAL-H (1M in hexane, 3.1 mL, 3.1 mmol) was added dropwise to the flask. The reaction was allowed to proceed at -78 °C for 1.5 h. A saturated solution of ammonium chloride (5 mL) was then added to the flask, and the reaction was warmed slowly to 23 °C. The solution was then diluted with 20 mL of EtOAc and 20 mL of DI H_2O. The heterogeneous solution was then filtered through a celite bed over a coarse glass frit to remove the alumina produced from the work-up. The organic layer was then collected, and the aqueous layer was then washed with EtOAc (3 x 20 mL). The combined organic extracts were then dried with anhydrous Na_2SO_4 and concentrated in vacuo. The crude product was then purified on a silica gel column and the product was isolated as a clear oil in 79% yield (Refer to Table 3.6 for gradient); R_f=0.44 (Hexane:EtOAc, 8:2); ^{1}H NMR (500 MHz, $CDCl_3$) δ 7.61 – 7.50 (m, 8H), 7.42 (tdt, *J* = 5.9, 3.0, 1.4 Hz, 4H), 7.39 – 7.31 (m, 8H), 4.14 (q, *J* = 7.2 Hz,

1H), 3.96 (qd, J = 5.9, 2.8 Hz, 1H), 3.76 – 3.62 (m, 4H), 2.06 (s, 1H), 1.28 (t, J = 7.1 Hz, 1H), 0.64 (d, J = 1.2 Hz, 3H), 0.58 (d, J = 1.2 Hz, 3H). ^{13}C NMR (126 MHz, $CDCl_3$) δ 135.99, 135.96, 135.52, 134.36, 133.99, 130.03, 129.96, 128.00, 127.93, 77.32, 77.07, 76.81, 73.53, 64.59, 64.50, 60.44, 21.09, 14.24, -2.55, -3.30. QTOF-HRMS (ESI) for $C_{29}H_{32}O_3Si_2$ [M+Na$^+$]: found 507.1781, calcd 507.1782.

3.5.5 Gradient Tables Used for Column Chromatography and NMR of All Compounds

This section describes the gradients used for automated flash chromatography as well as for the synthesis of **1** and **2**. NMR of all compounds are also reported here.

Table 3.4. Gradient table for the oxidation and acetonide deprotection of **11**.

Set of 72 mL collected	Mobile Phase
1	98:2 $CHCl_3$:MeOH
2	95:5 $CHCl_3$:MeOH
3	90:10 $CHCl_3$:MeOH
4	85:15 $CHCl_3$:MeOH
5	65:25:4 $CHCl_3$:MeOH:H_2O

Table 3.5. Purification of **20**.

Flow Rate	**Apolar:Polar** Solvent	Gradient Steps (in % EtOAc)		
		Start (%)	End (%)	Length (mL)
		0	0	72
		0	1	72
		1	1	72
		1	2	72
		2	2	72
		2	3	72
17 mL/min	Hex:EtOAc	3	3	72
		3	4	72
		4	4	72
		4	5	72
		5	5	63
		5	10	9
		10	10	72

Table 3.6. Purification of **21**.

Flow Rate	**Apolar:Polar** Solvent	Gradient Steps (in % EtOAc)		
		Start (%)	End (%)	Length (mL)
		0	1	72
		1	1	72
		1	2	72
		2	2	144
		2	3	72
17 mL/min	Hexane:EtOAc	3	3	144
		3	4	72
		4	4	144
		4	5	72
		5	5	72
		5	6	72
		6	6	144

Table 3.7. Purification of **22**.

Flow Rate	**Apolar:Polar** Solvent	Gradient Steps (in % EtOAc)		
		Start (%)	End (%)	Length (mL)
17 mL/min	Hexane:EtOAc	5	5	90 (equilibration)
		5	5	27
		30	30	78

Table 3.8. Purification of **5**.

Flow Rate	Apolar:Polar Solvent	Gradient Steps (in % MeOH)		
		Start (%)	End (%)	Length (mL)
17 mL/min	DCM:MeOH	0	0	72
		0	1	72
		1	1	72
		1	8	72
		8	8	288

Table 3.9. Purification of **6**. This gradient is run a second time on the same product, in order to get full separation. The first 72 mL of this gradient step are initial waste.

Flow Rate	**Apolar:Polar** Solvent	Gradient Steps (in % EtOAc)		
		Start (%)	End (%)	Length (mL)
15 mL/min	Hexane:EtOAc	0	5	576
		5	5	72
		5	7	360
		7	20	9
		20	20	135

Table 3.10. Purification of **7**. Used CHROMAFIL Xtra CA-45/25 filters while loading sample.

Flow Rate	**Apolar:Polar** Solvent	Gradient Steps (in % EtOAc)		
		Start (%)	End (%)	Length (mL)
17 mL/min	Hexane:EtOAc	0	1	144
		1	2	144
		2	3	144
		3	4	144
		4	6	144
		6	8	144

Table 3.11. Purification of **8**.

Flow Rate	**Apolar:Polar** Solvent	Gradient Steps (in % EtOAc)		
		Start (%)	End (%)	Length (mL)
		0	0	72
		0	1	72
		1	2	72
15 mL/min	Hexane:EtOAc	2	3	72
		3	4	72
		4	5	72
		5	6	48

3.5.6 NMR Spectra of All Compounds

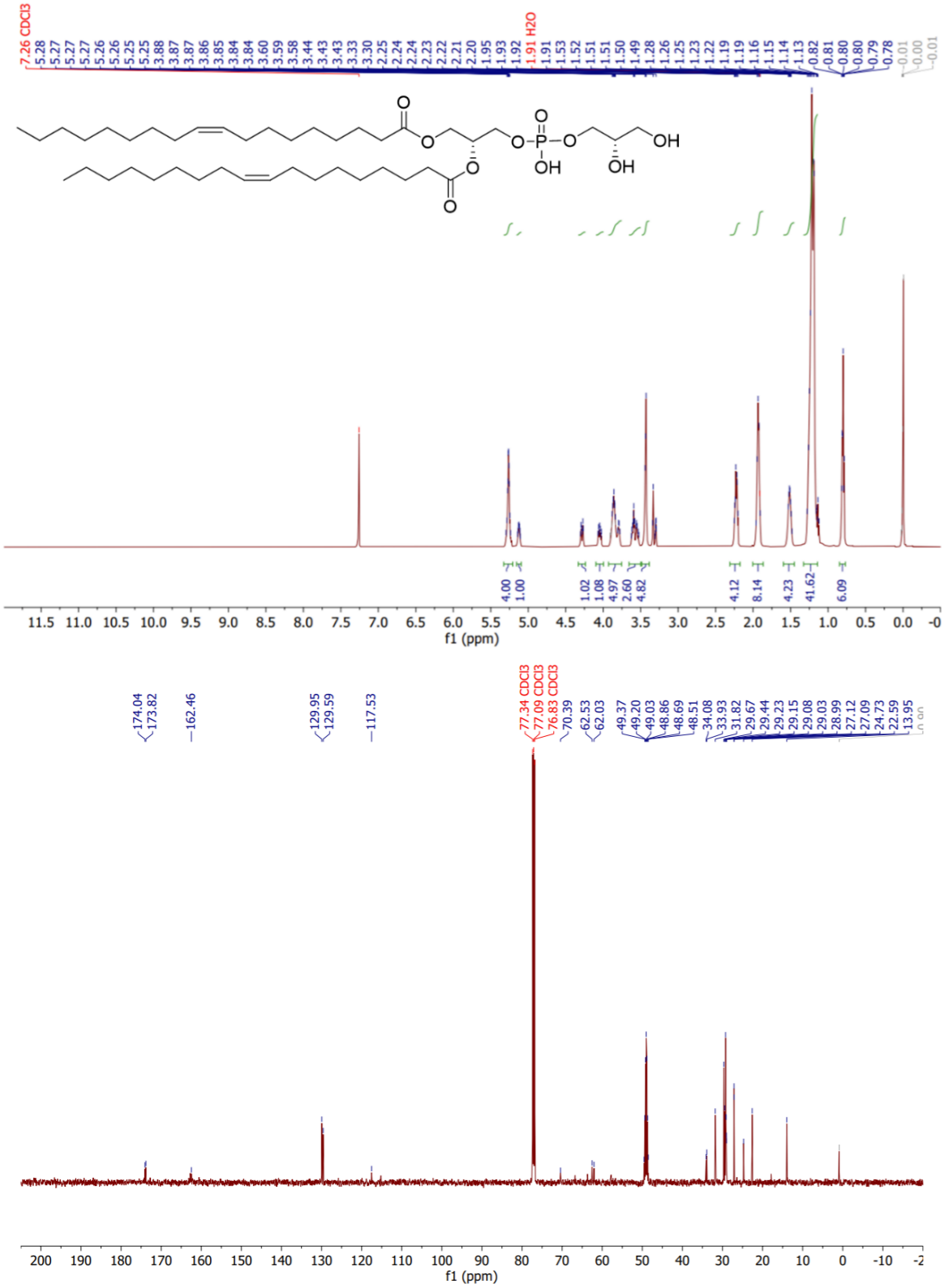

Figure 3.16. ^{1}H, ^{13}C, and ^{31}P NMR of **1**.

Figure 3.16 continued.

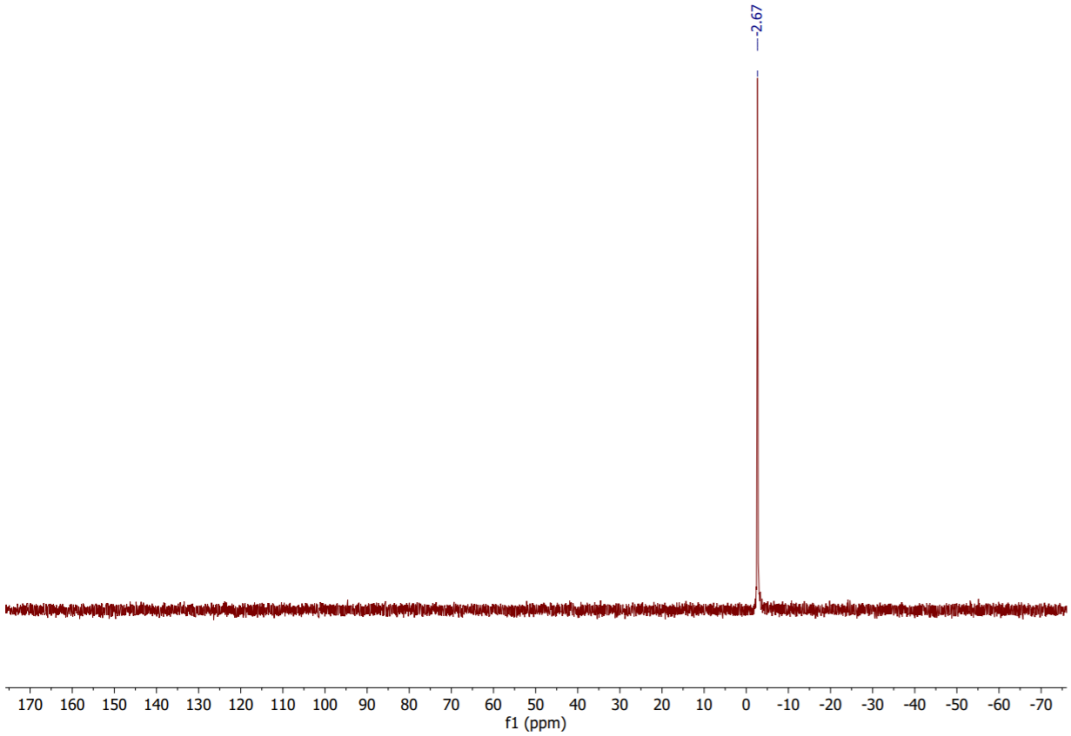

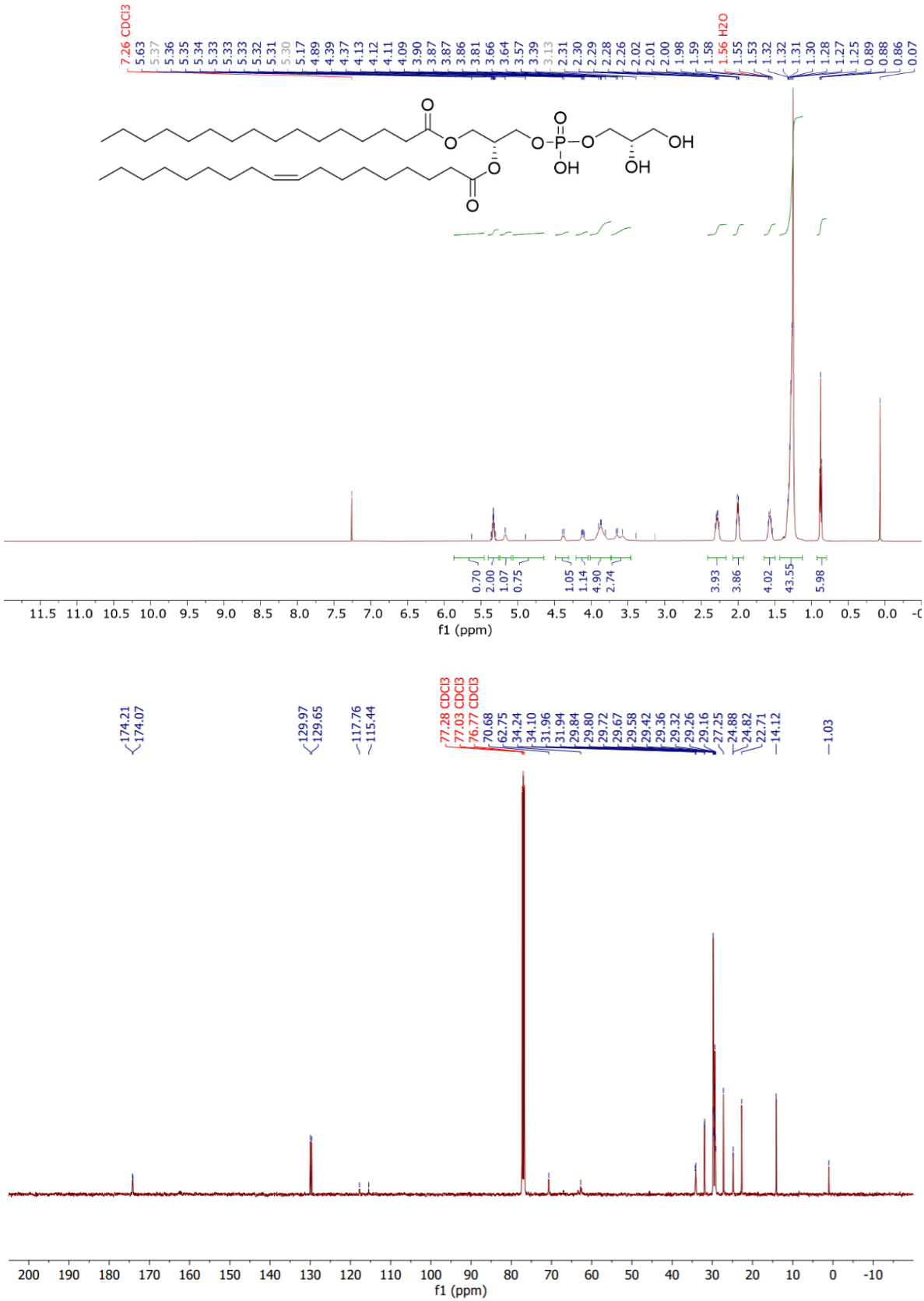

Figure 3.17. ^{1}H, ^{13}C, and ^{31}P NMR of **2**.

Figure 3.17 continued.

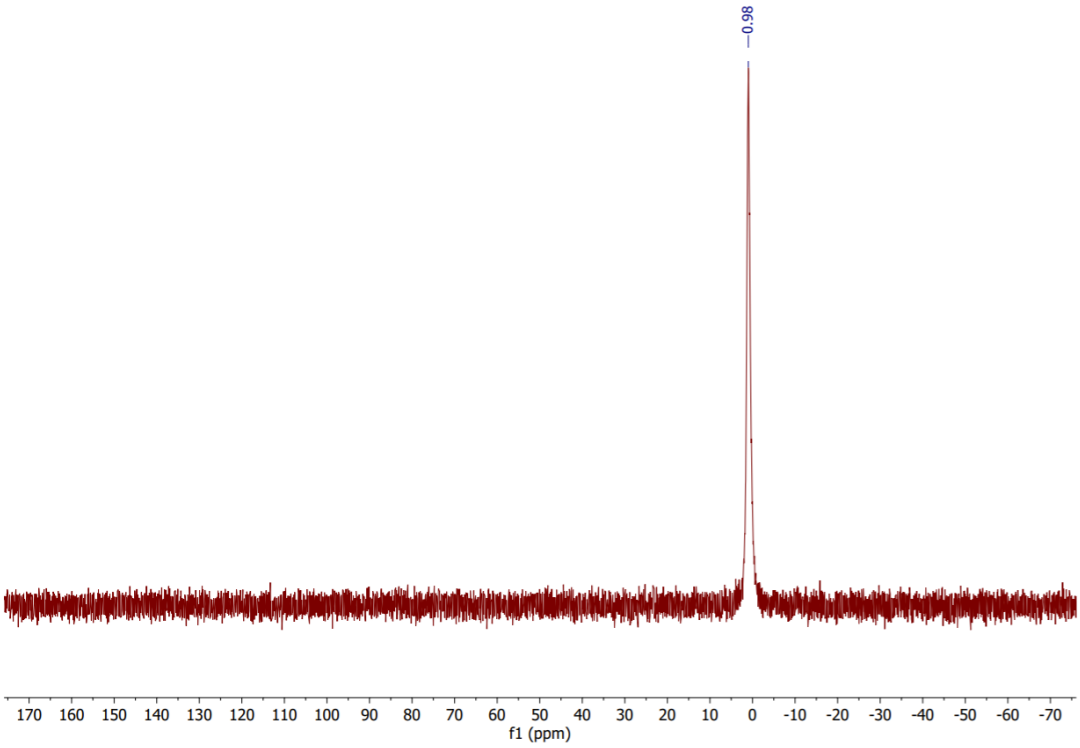

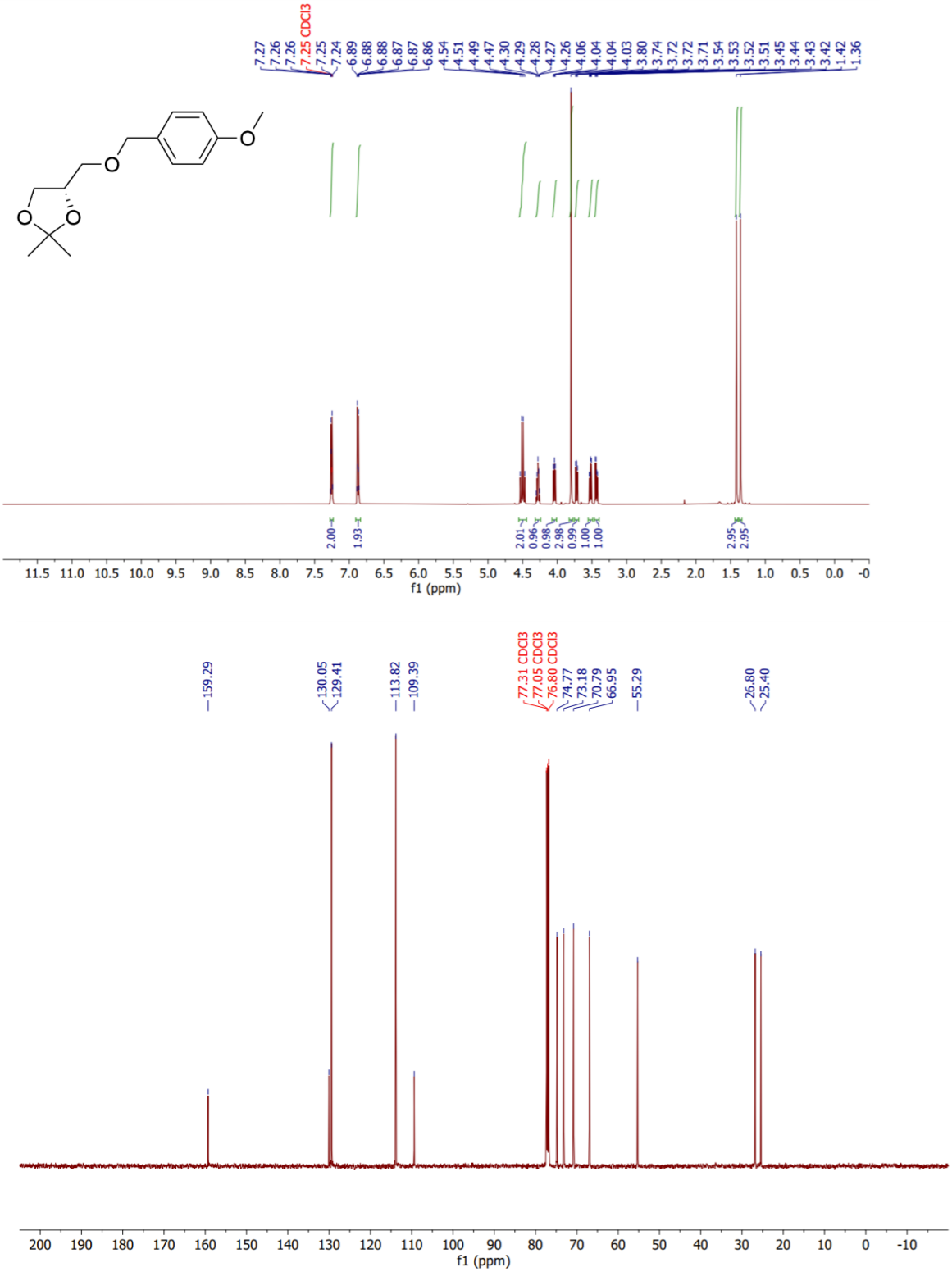

Figure 3.18. ^{1}H and ^{13}C NMR of **4**.

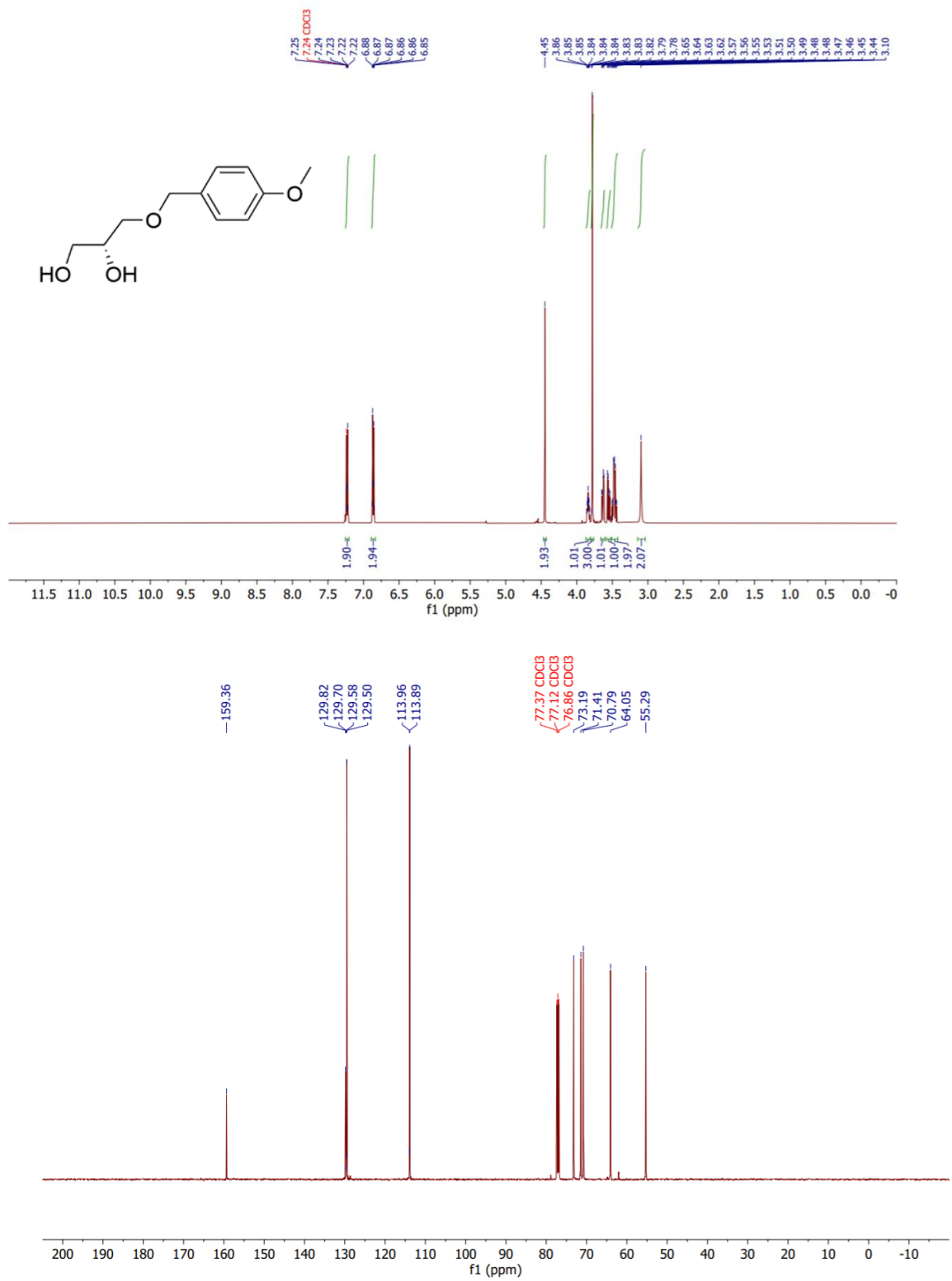

Figure 3.19. ^{1}H and ^{13}C NMR of **5**.

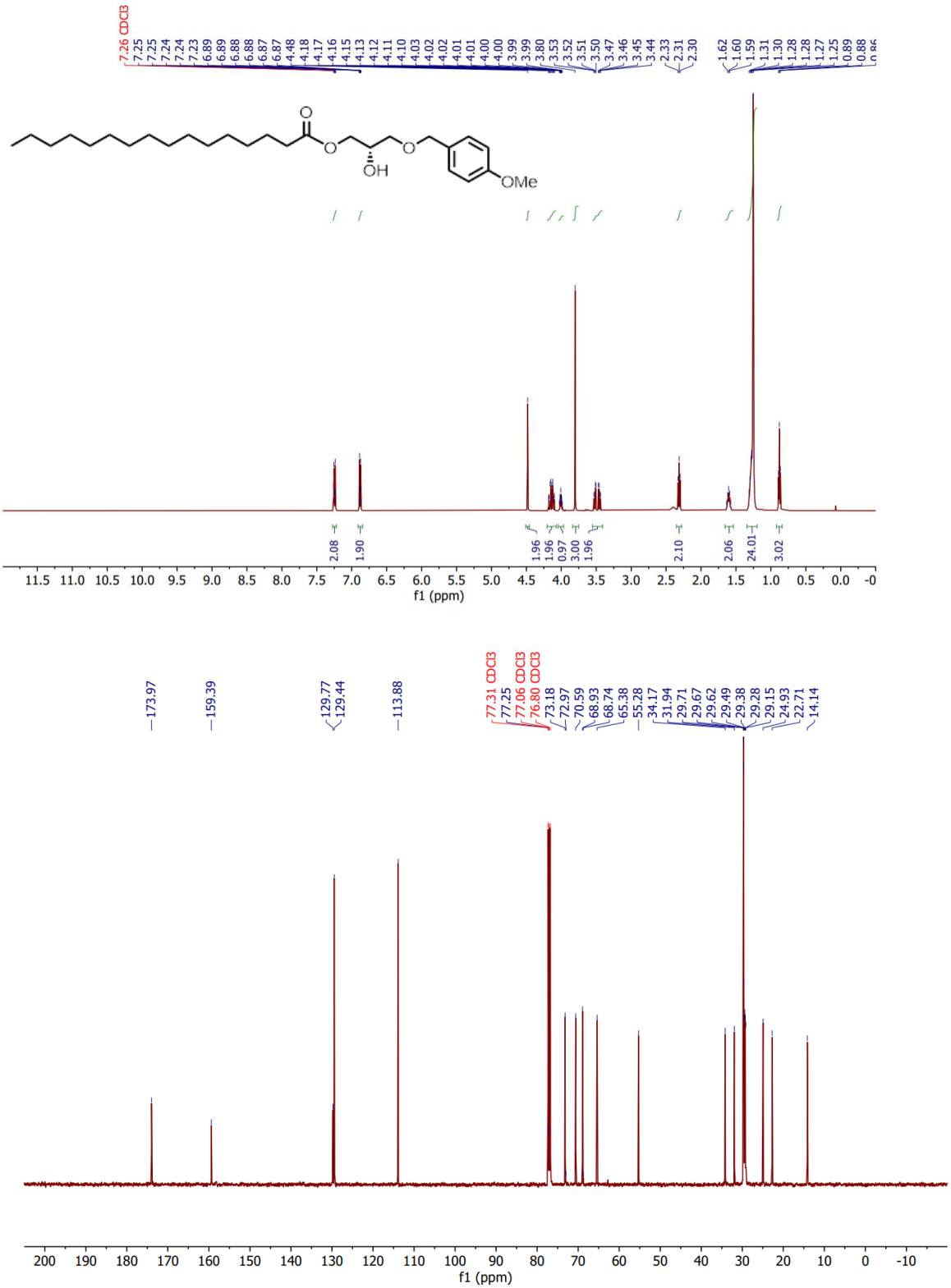

Figure 3.20. ^{1}H and ^{13}C NMR of **6a**.

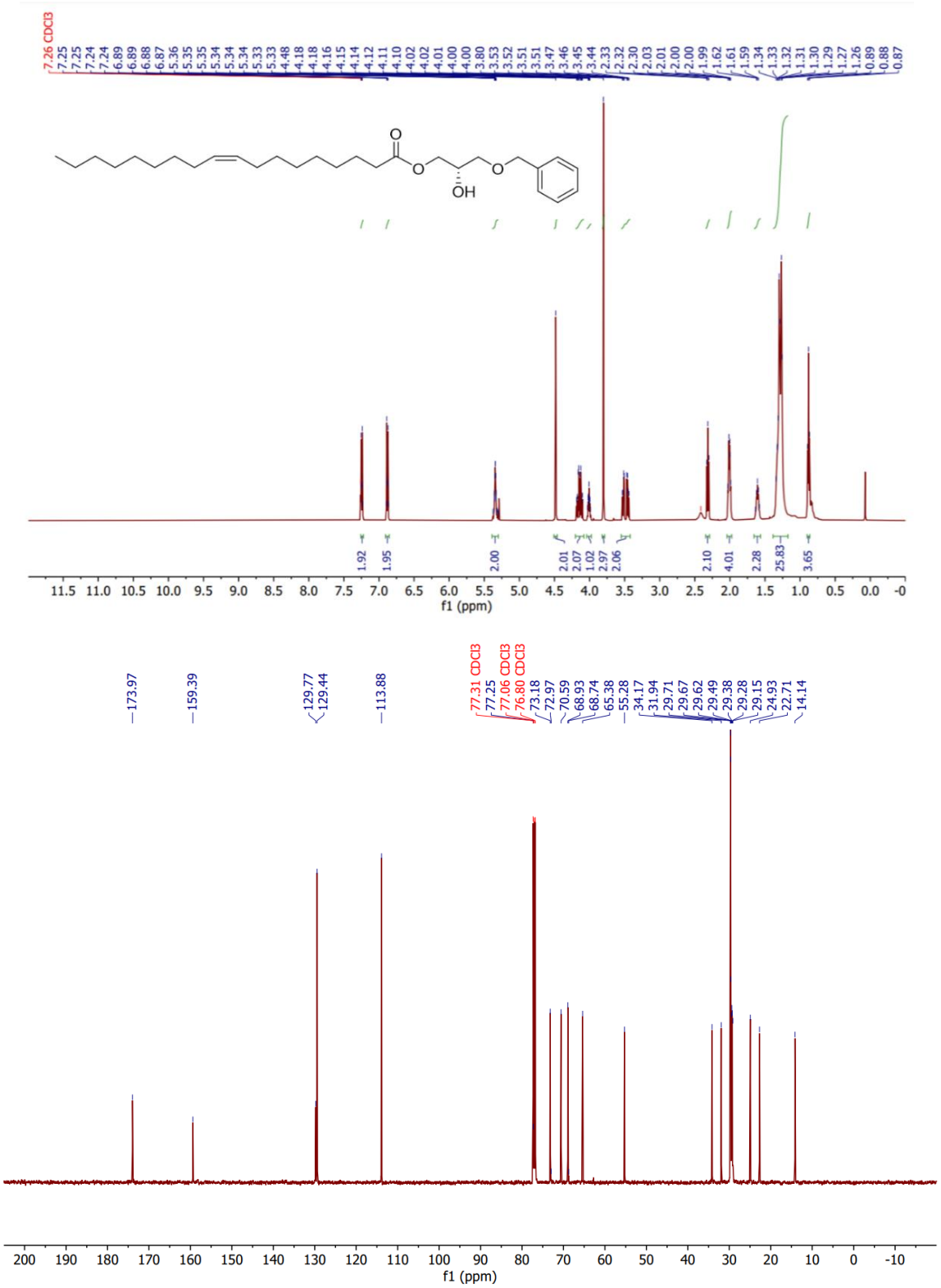

Figure 3.21. ^{1}H and ^{13}C NMR of **6b**.

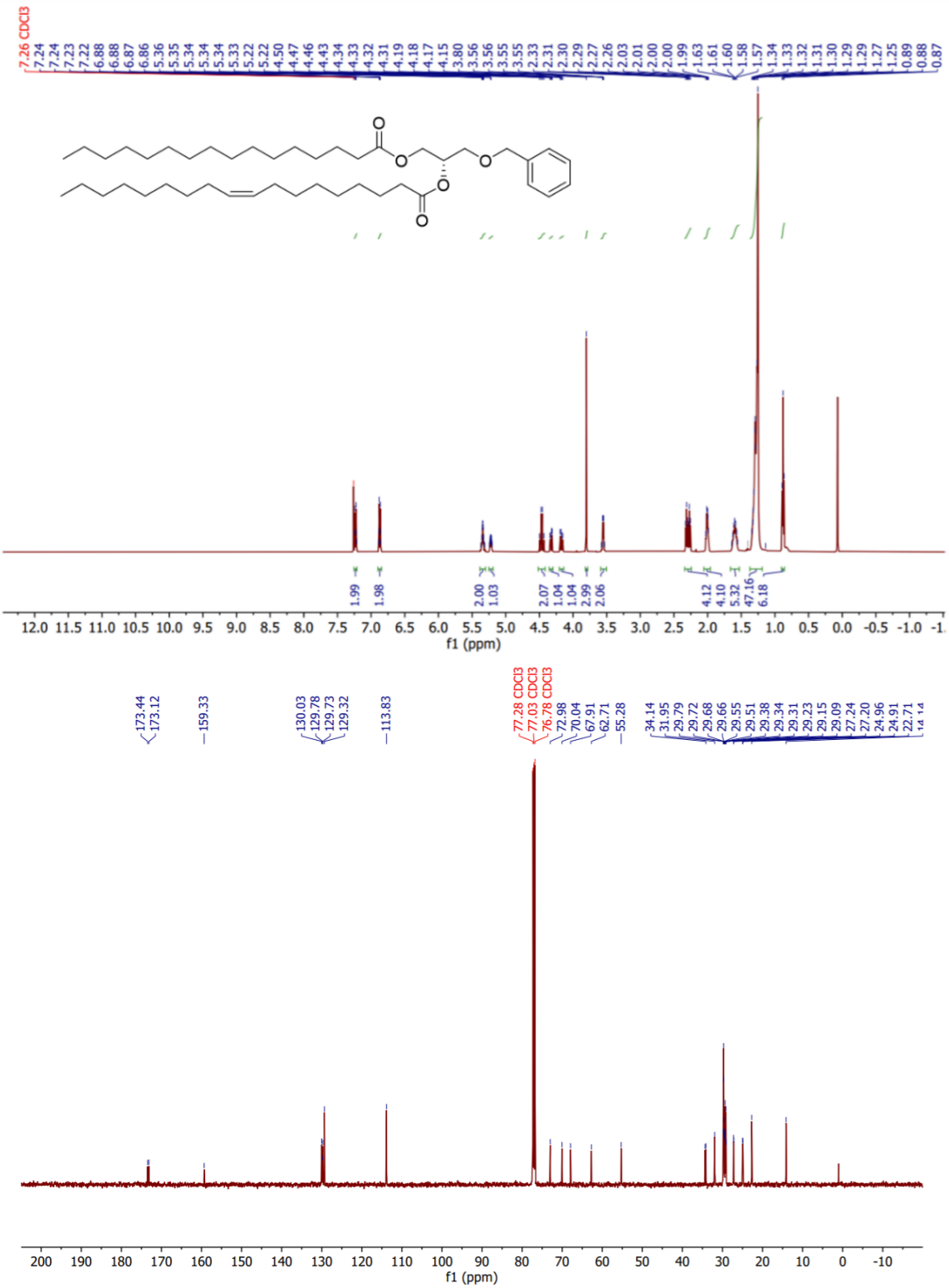

Figure 3.22. ^{1}H and ^{13}C NMR of **7a**.

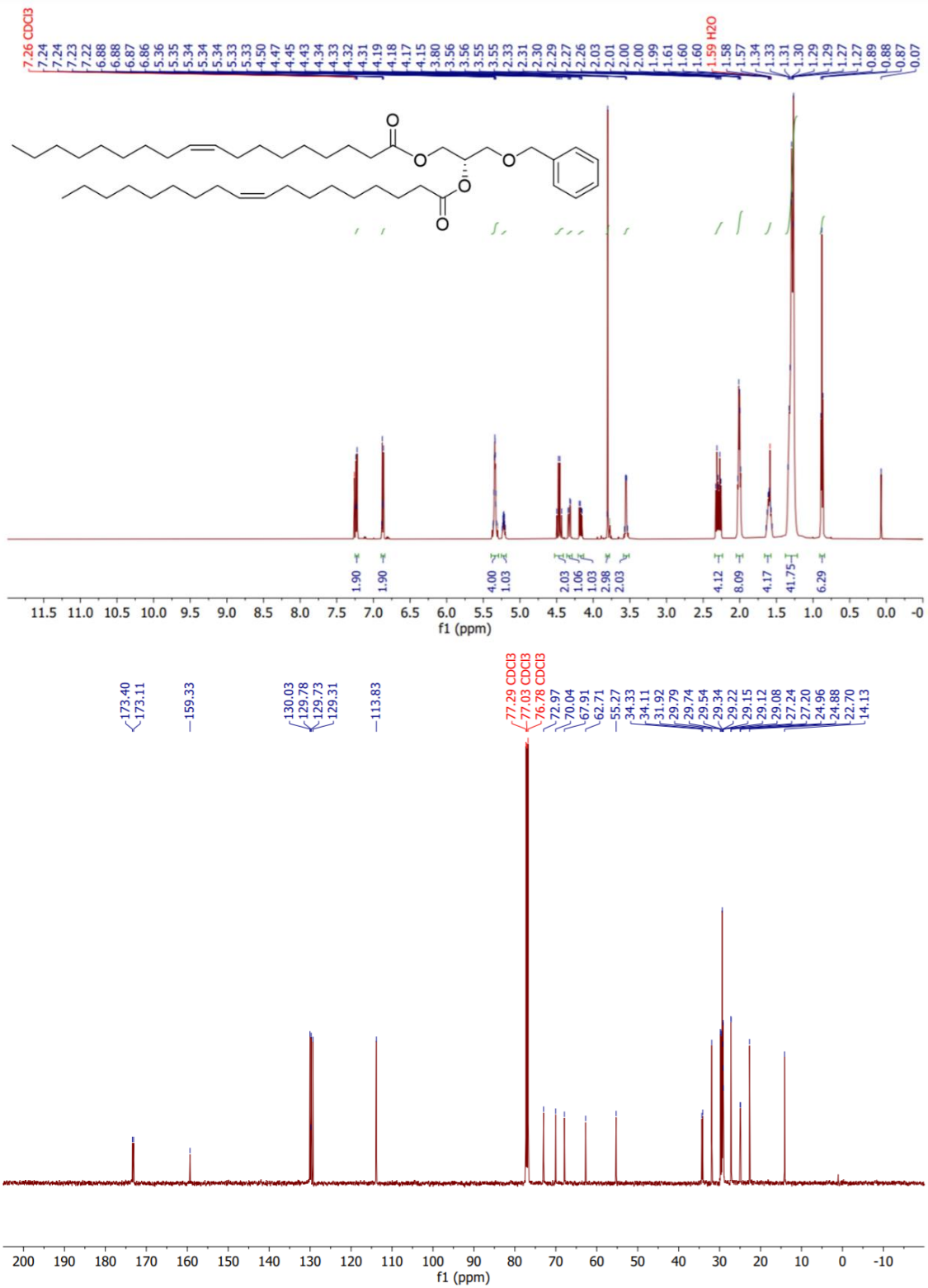

Figure 3.23. ^{1}H NMR and ^{13}C NMR of **7b**.

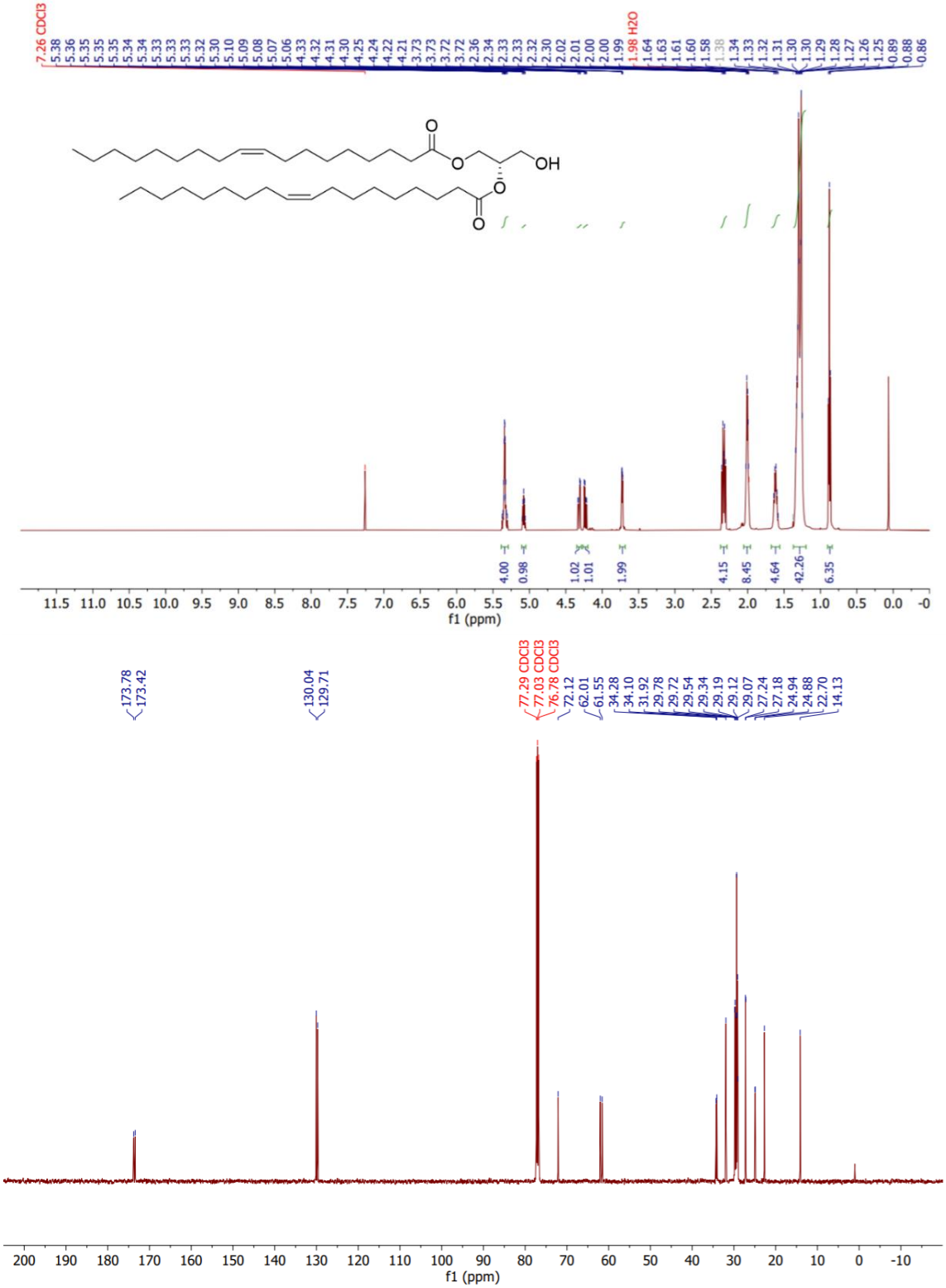

Figure 3.24. ^{1}H and ^{13}C NMR of **8b**.

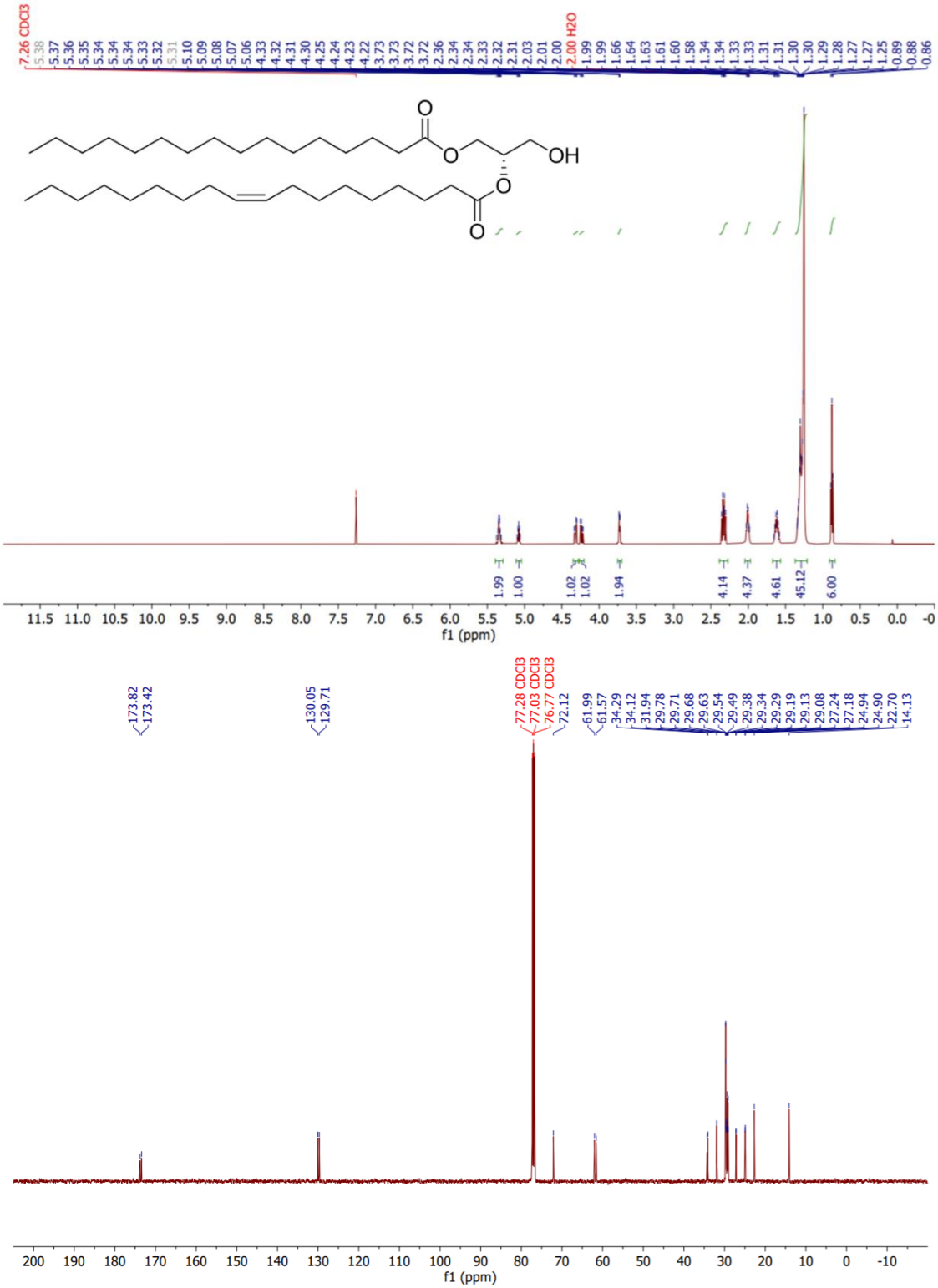

Figure 3.25. ^{1}H and ^{13}C NMR of **8a**.

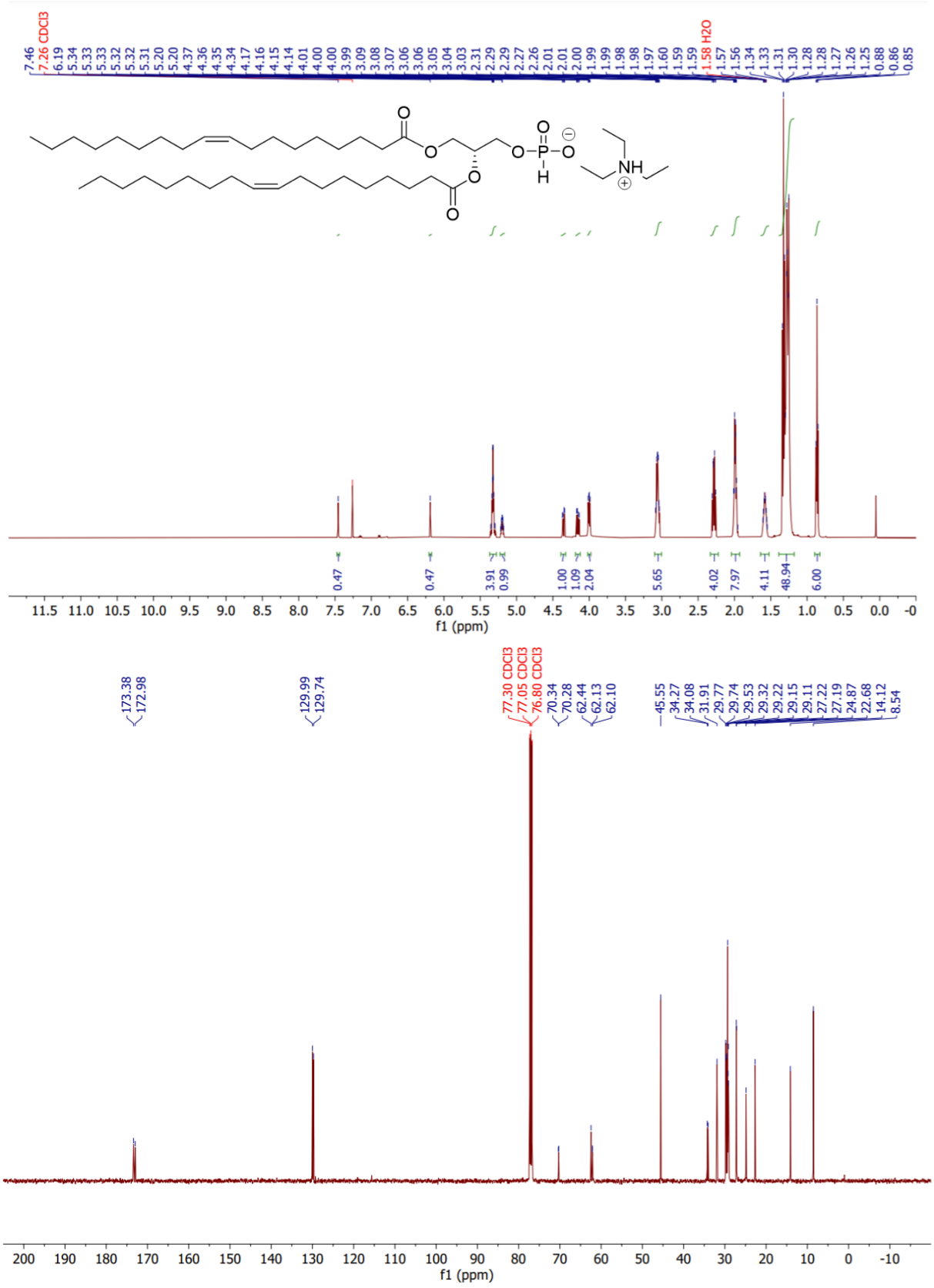

Figure 3.26. ^{1}H, ^{13}C, and ^{31}P NMR of **9b**.

Figure 3.26 continued.

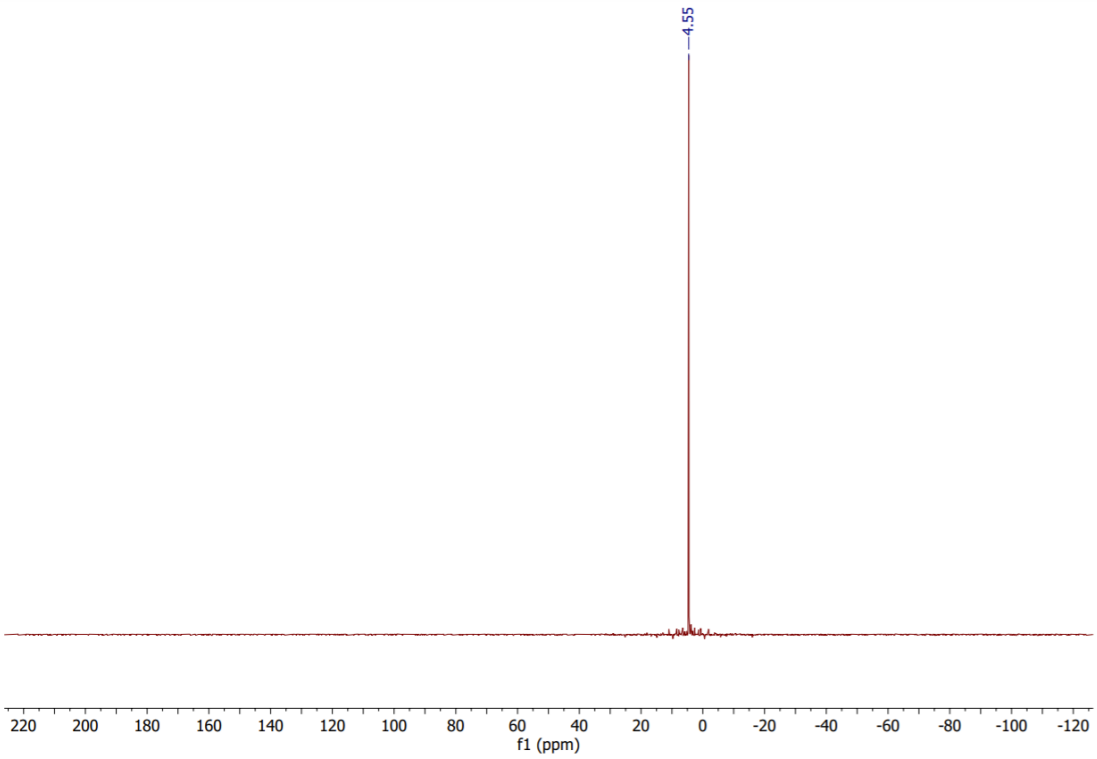

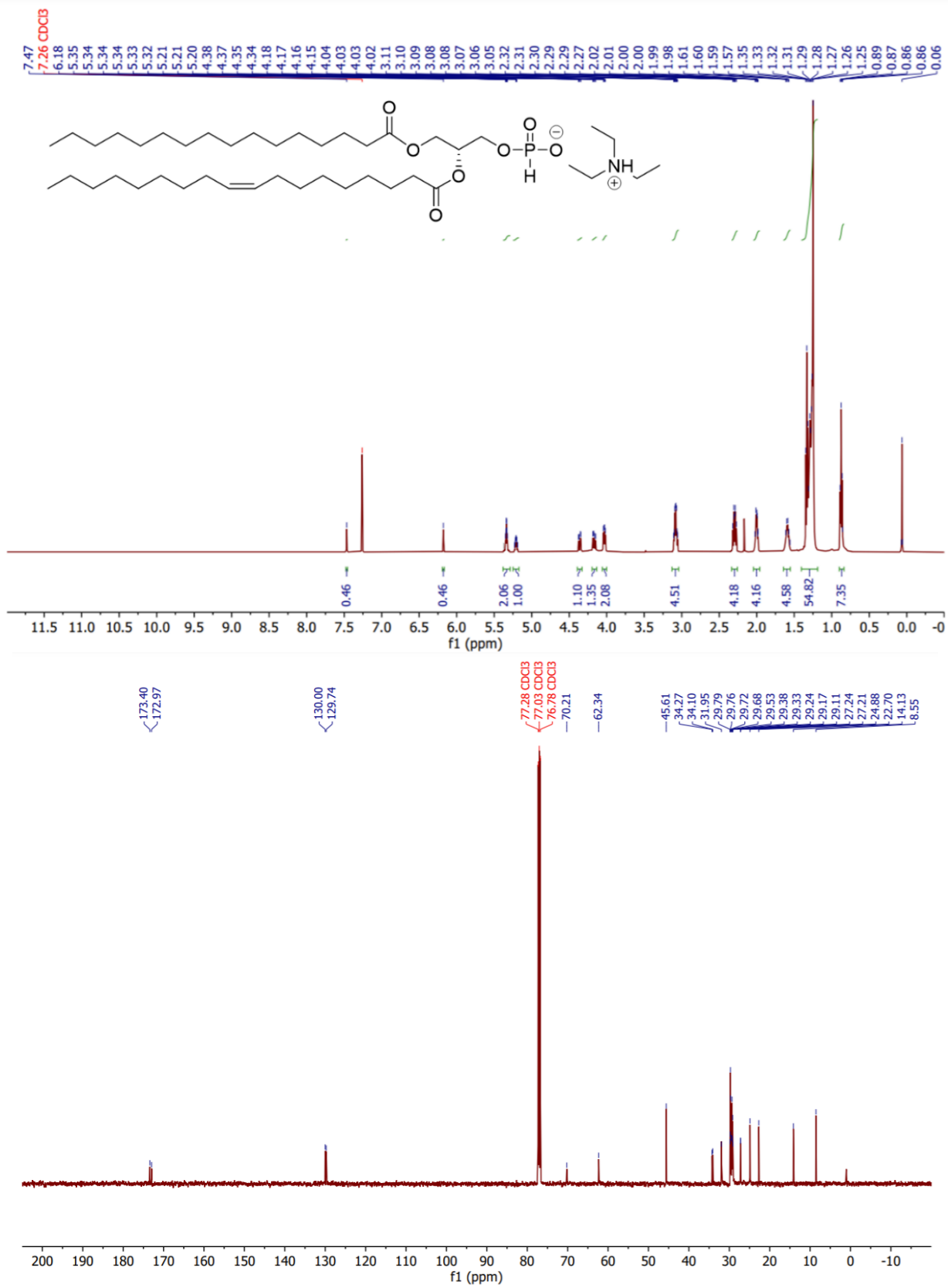

Figure 3.27. ^{1}H, ^{13}C, and ^{31}P NMR of **9a**.

Figure 3.27 continued.

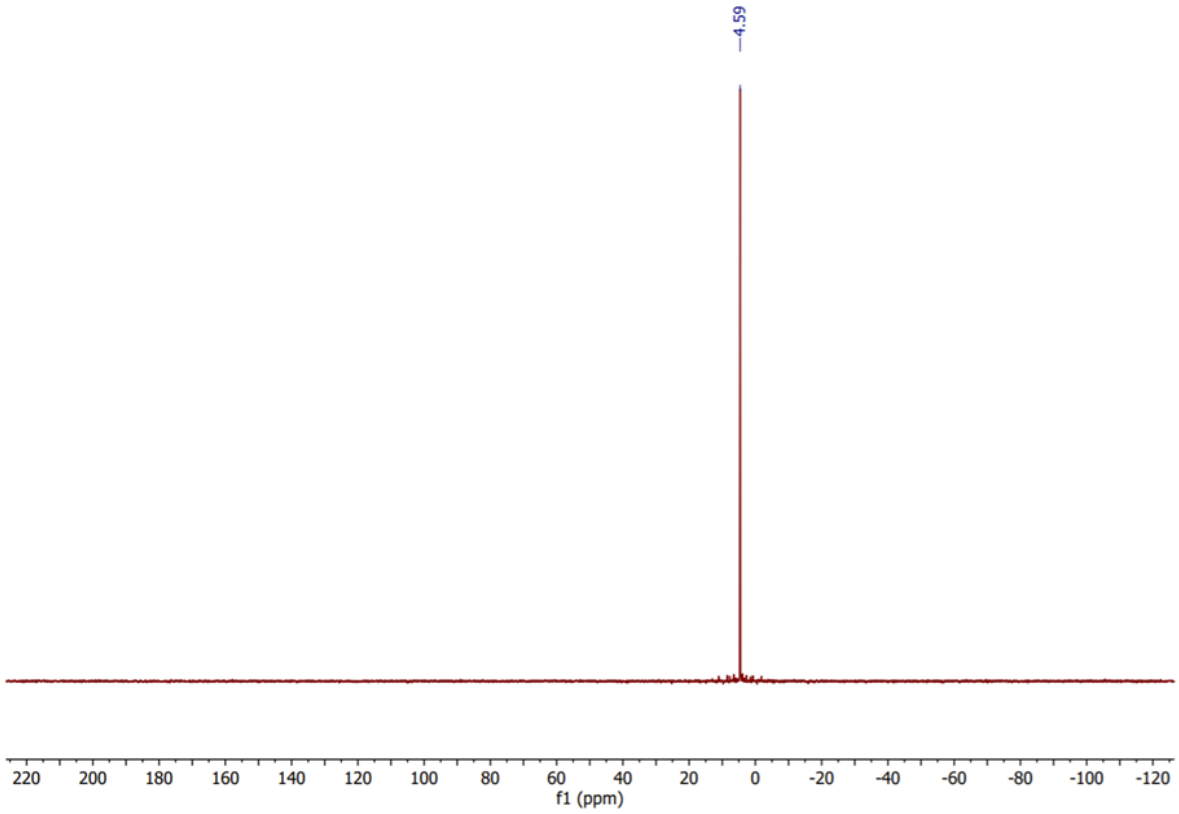

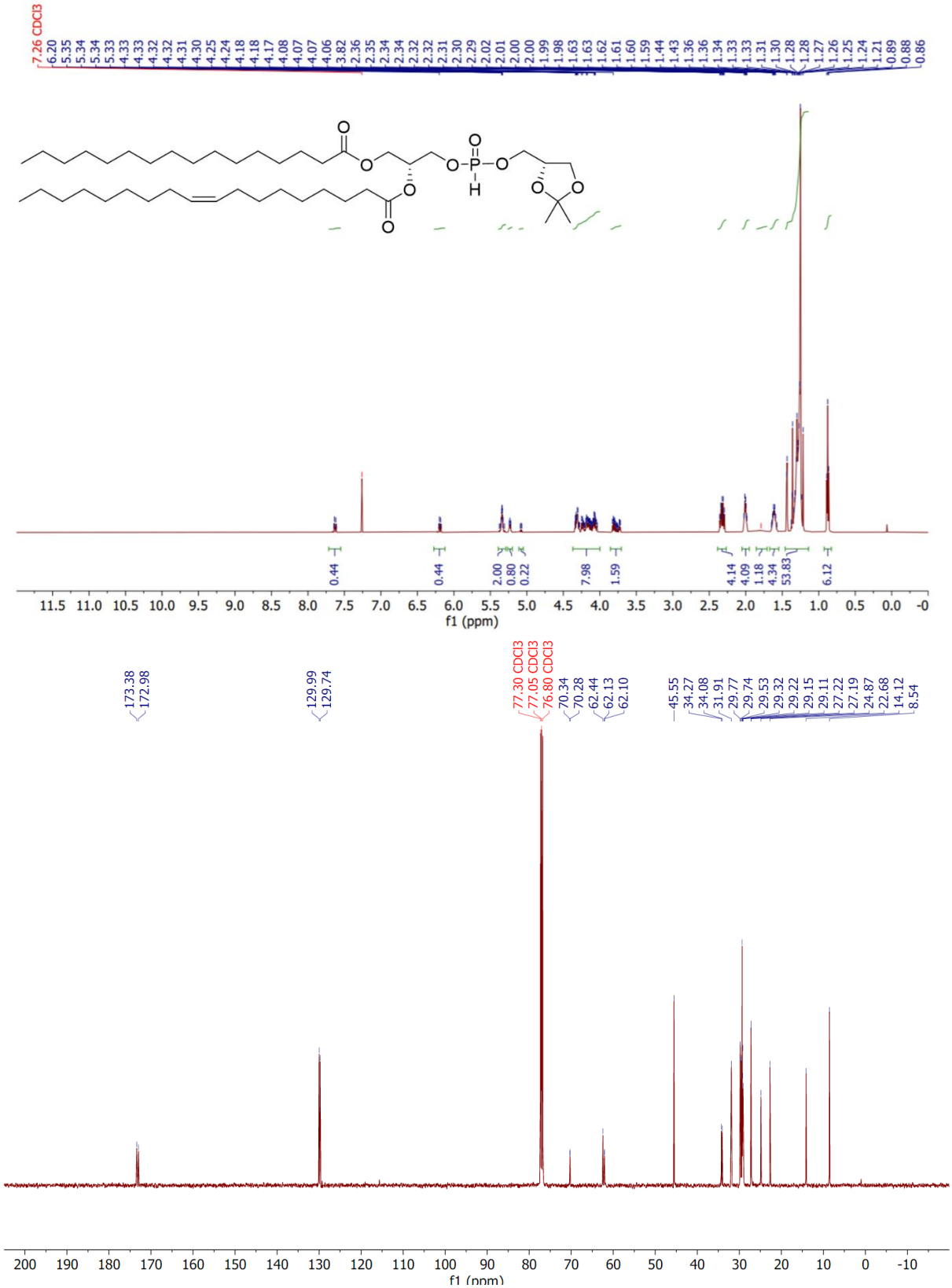

Figure 3.28. ^{1}H, ^{13}C, and ^{31}P NMR of **11a**.

Figure 3.28 continued.

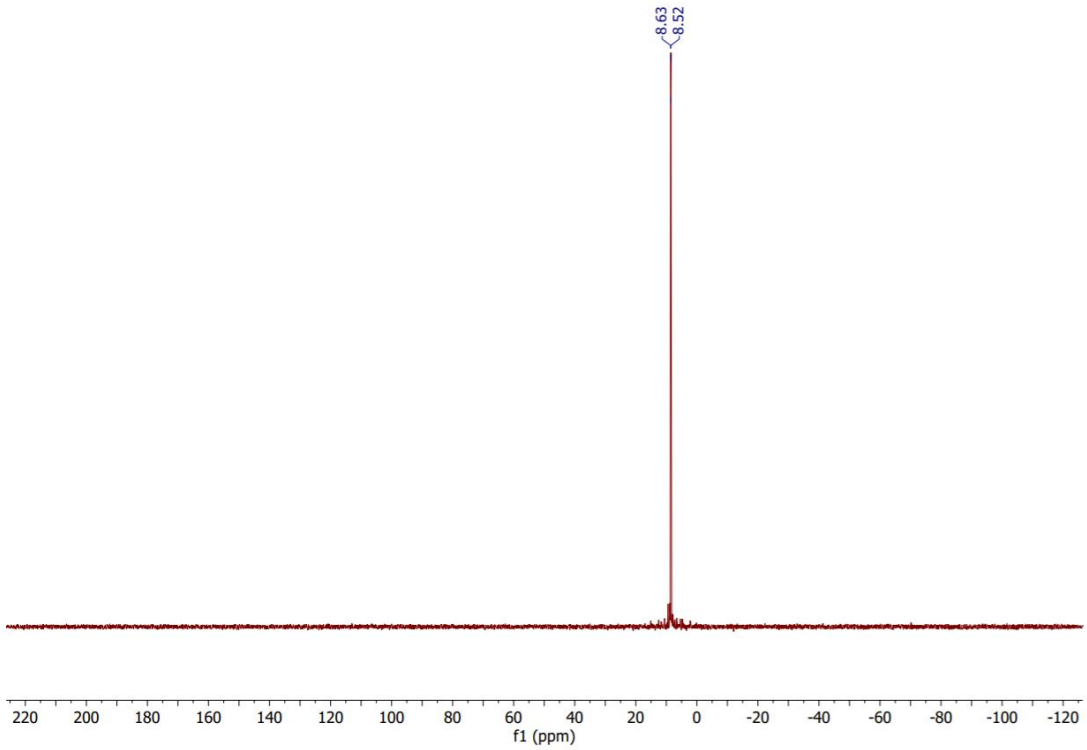

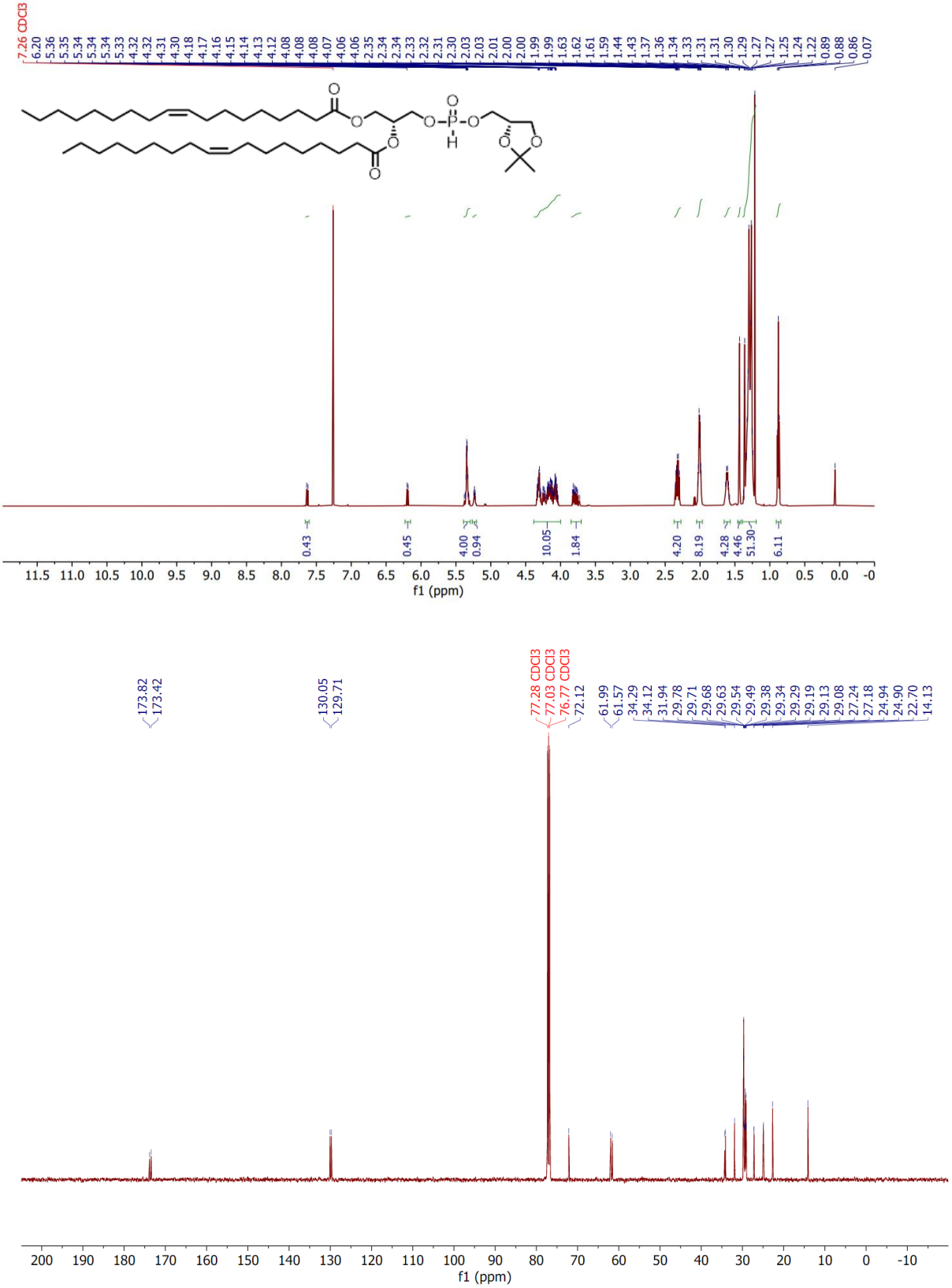

Figure 3.29. ^{1}H, ^{13}C, and ^{31}P NMR of **11b**.

Figure 3.29 continued.

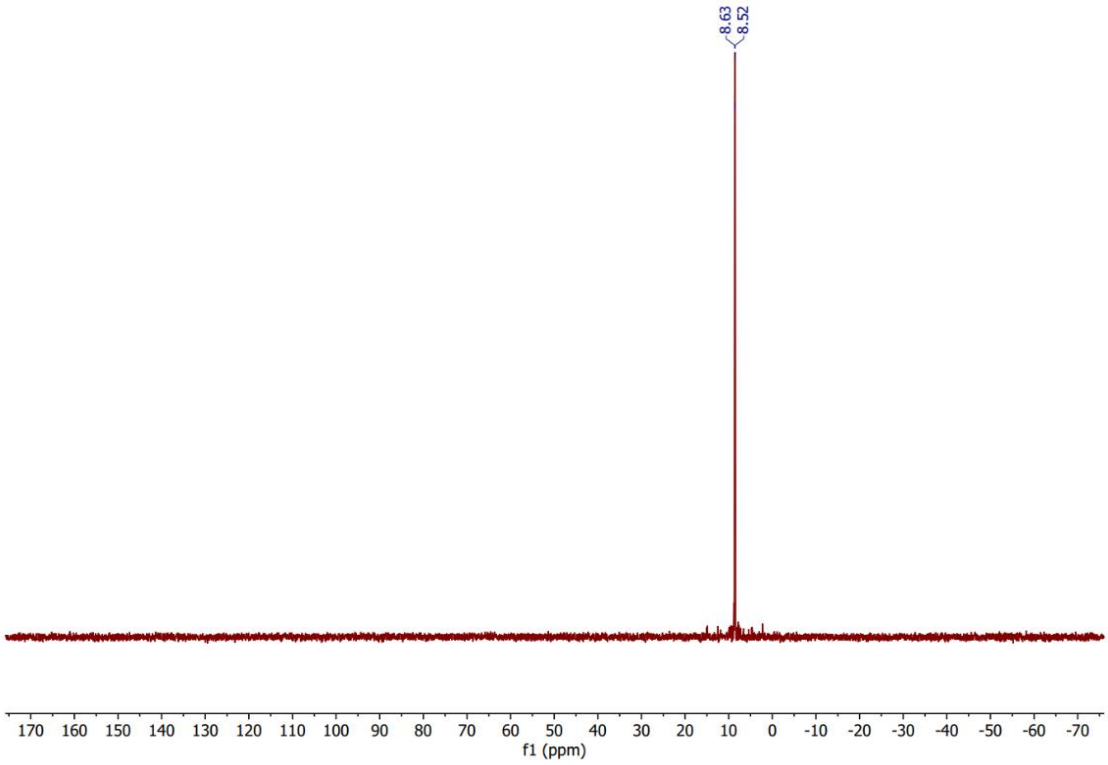

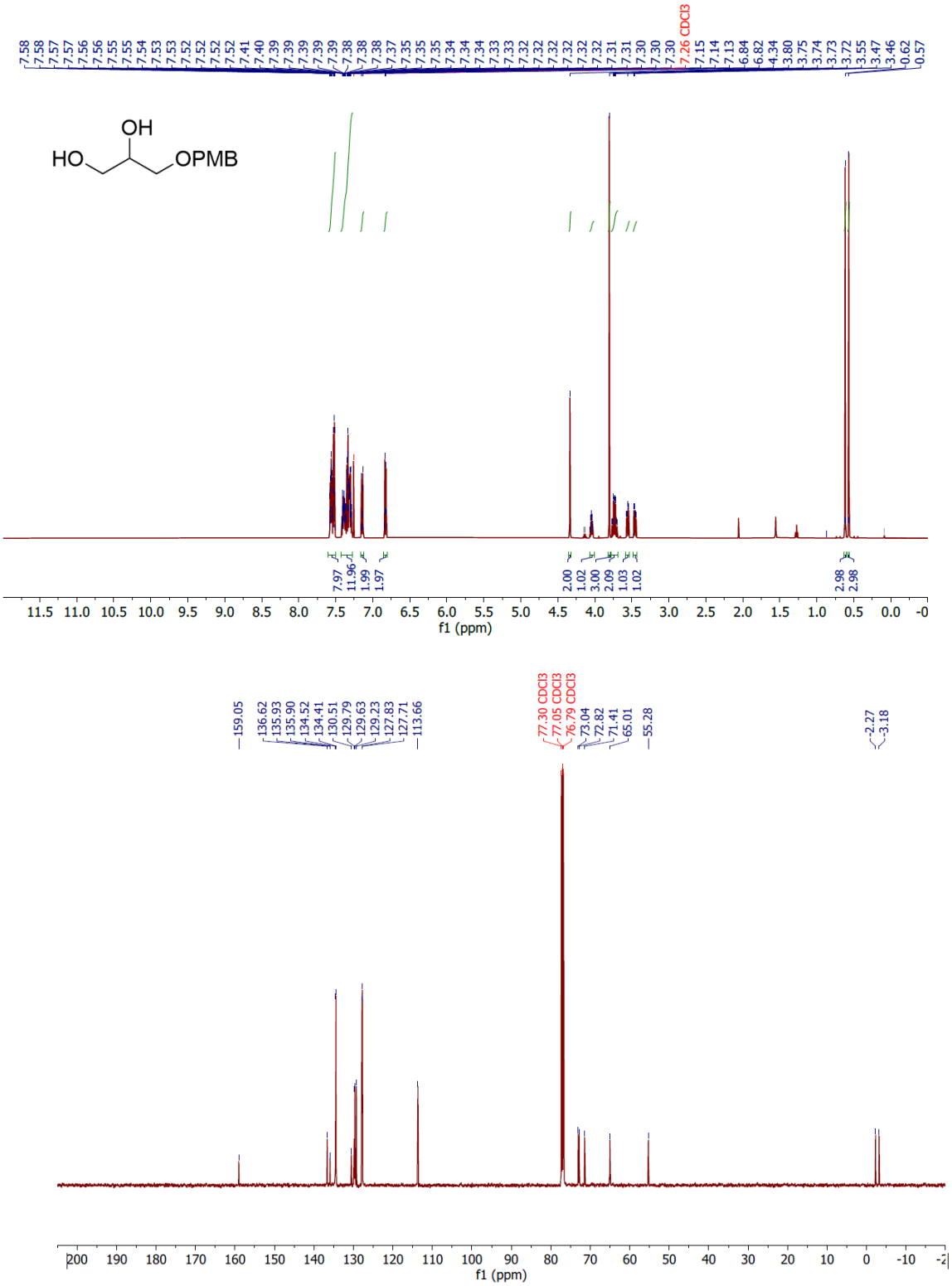

Figure 3.30. ^{1}H and ^{13}C NMR of **14**.

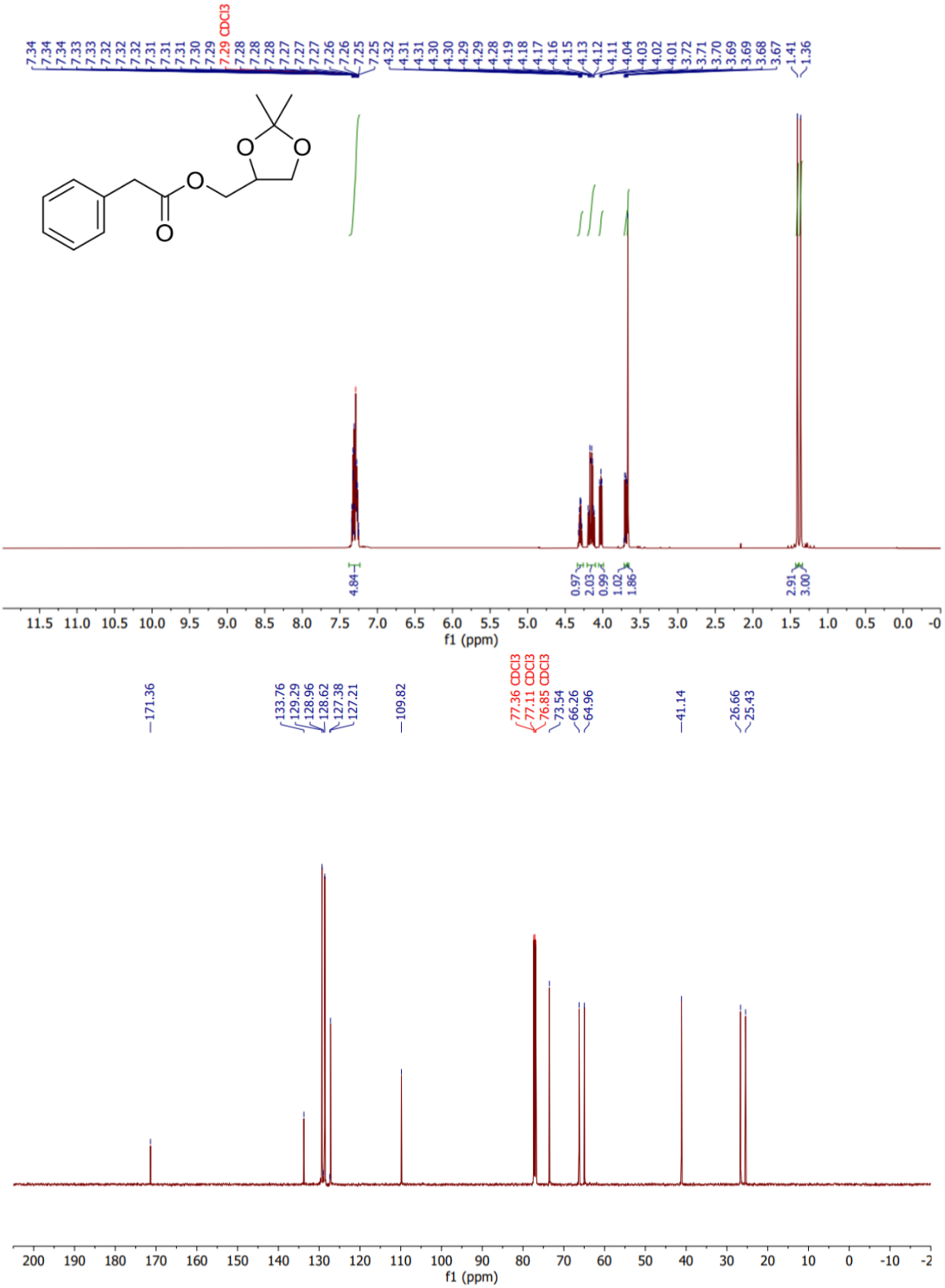

Figure 3.31. ^{1}H and ^{13}C NMR of **18**.

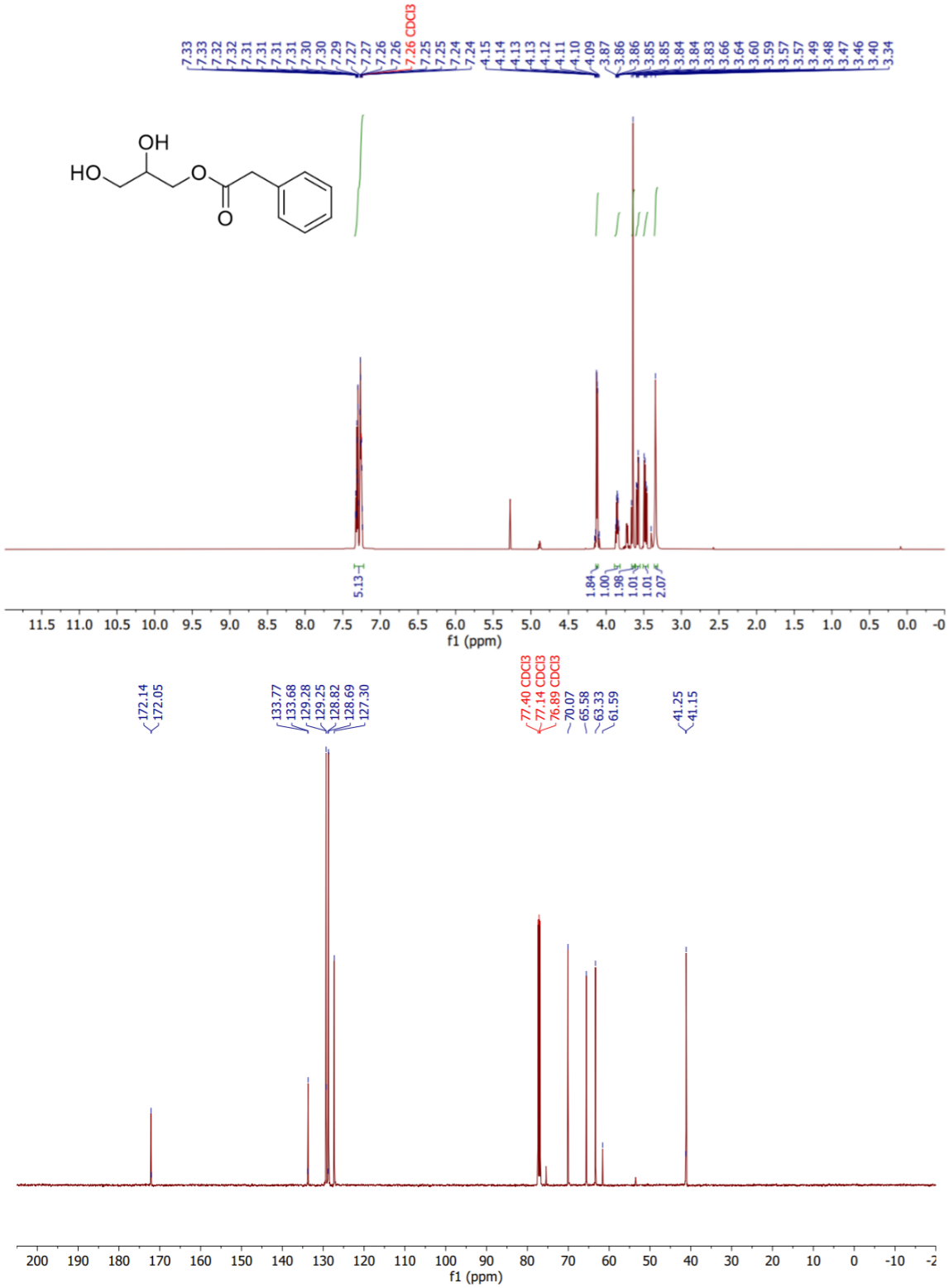

Figure 3.32. ^{1}H NMR and ^{13}C NMR of **19**.

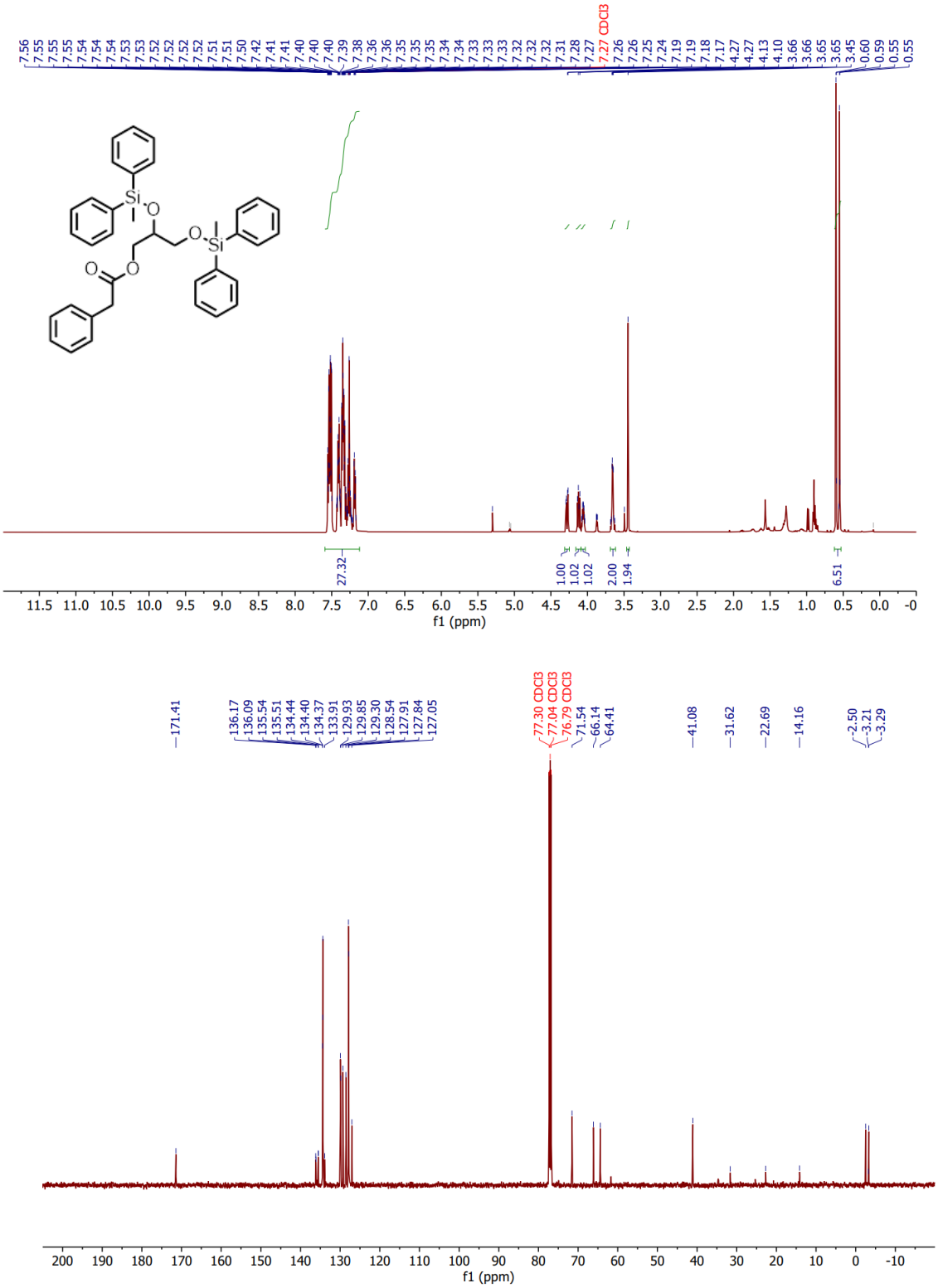

Figure 3.33. ^{1}H NMR and ^{13}C NMR of **20**.

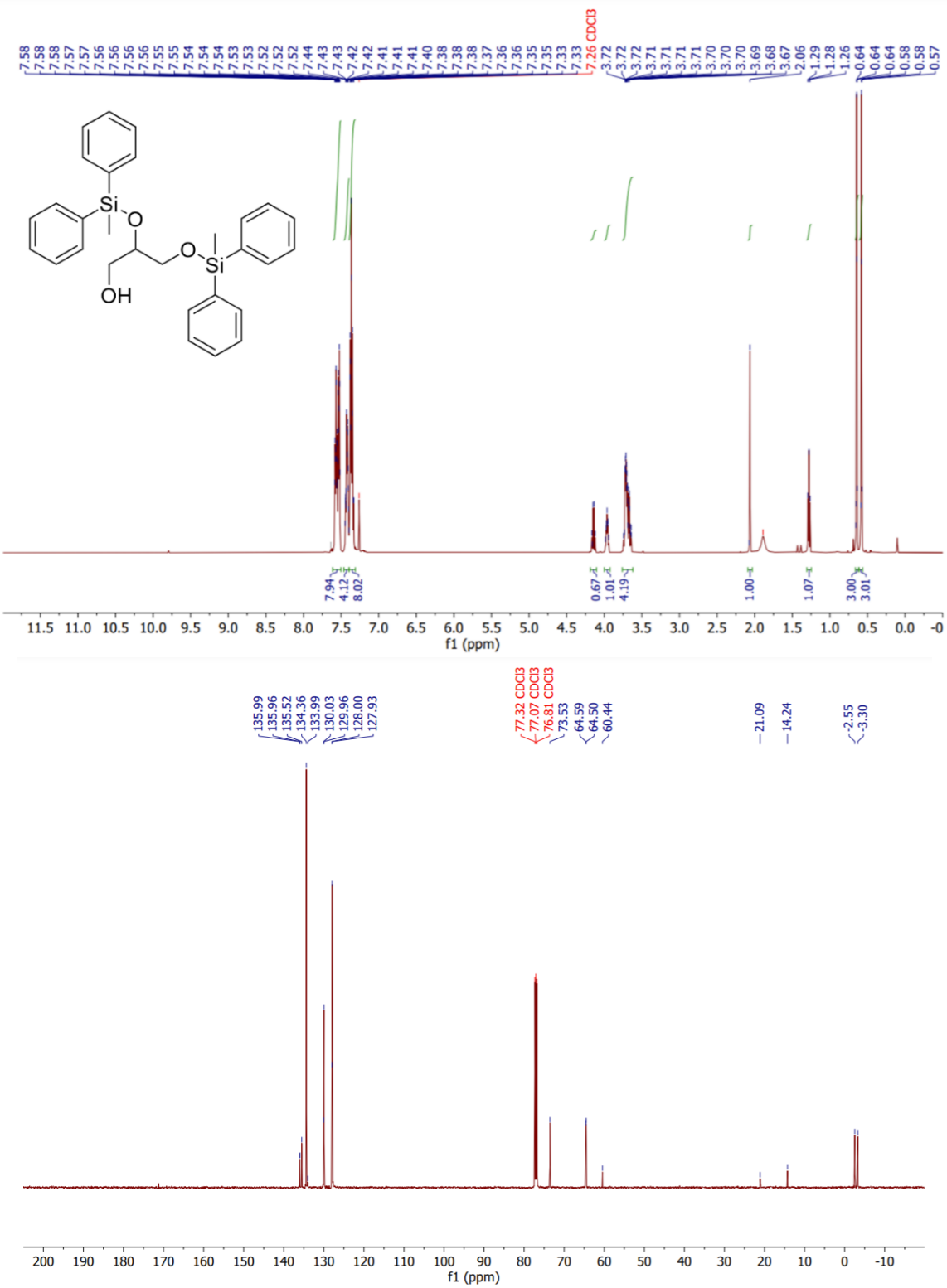

Figure 3.34. ^{1}H NMR and ^{13}C NMR of **21**.

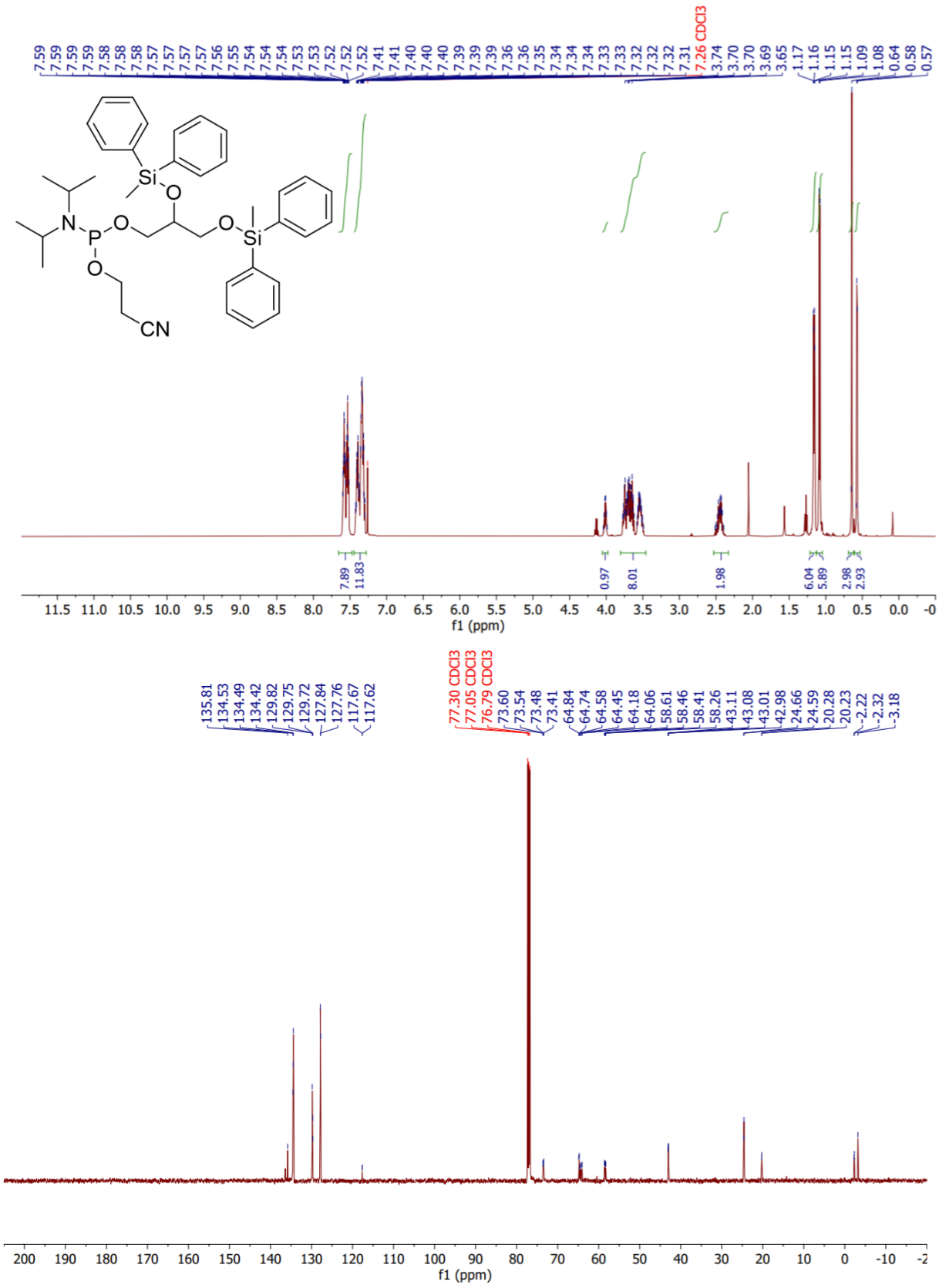

Figure 3.35. ^{1}H, ^{13}C, and ^{31}P NMR of **22**.

Figure 3.35 continued.

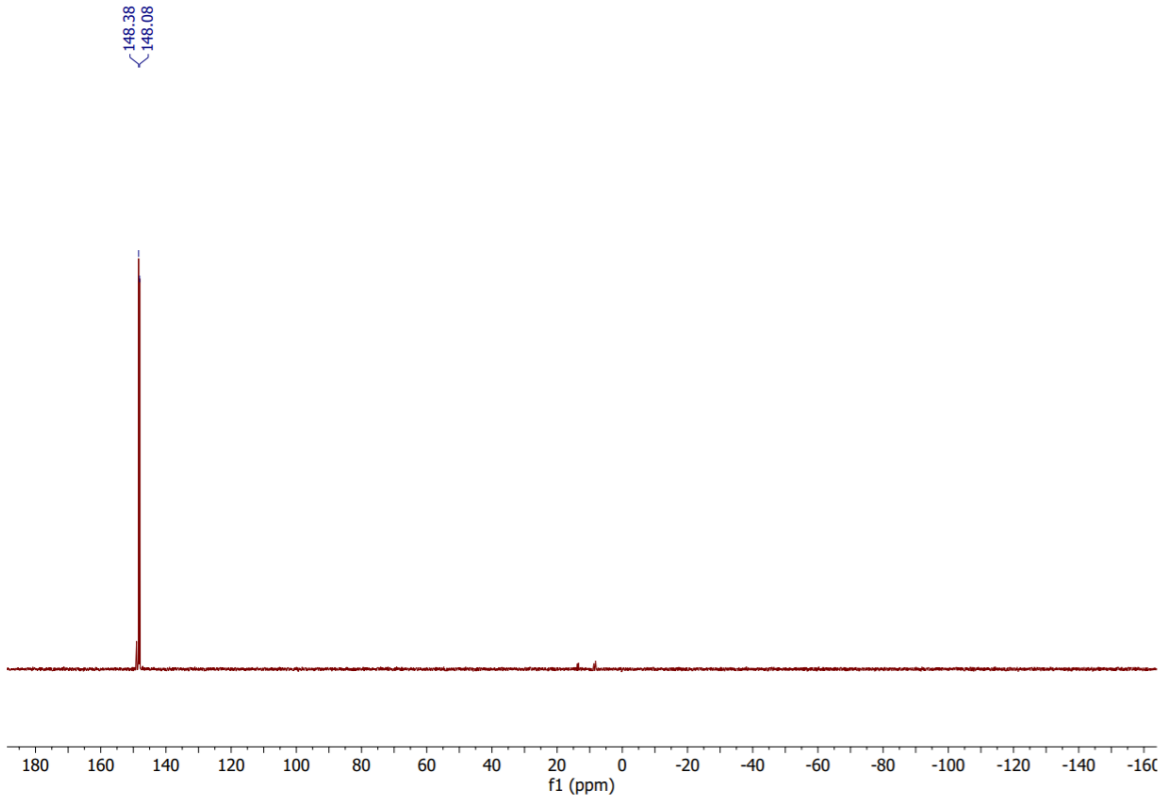

3.6 References

1. Tao, B. Y., Chapter 24 - Industrial Applications for Plant Oils and Lipids. In *Bioprocessing for Value-Added Products from Renewable Resources*, Yang, S.-T., Ed. Elsevier: Amsterdam, 2007; pp 611-627.

2. Kobayashi, T.; Stang, E.; Fang, K. S.; de Moerloose, P.; Parton, R. G.; Gruenberg, J., A lipid associated with the antiphospholipid syndrome regulates endosome structure and function. *Nature* **1998,** *392* (6672), 193-7.

3. Brotherus, J.; Renkonen, O., Subcellular distributions of lipids in cultured BHK cells: evidence for the enrichment of lysobisphosphatidic acid and neutral lipids in lysosomes. *Journal of lipid research* **1977,** *18* (2), 191-202.

4. Brotherus, J.; Renkonen, O.; Herrmann, J.; Fischer, W., Novel stereoconfiguration in lyso-bis-phosphatidic acid of cultured BHK-cells. *Chemistry and Physics of Lipids* **1974,** *13* (2), 178-182.

5. Somerharju, P.; Renkonen, O., Conversion of phosphatidylglycerol lipids to bis(monoacylglycero)phosphate in vivo. *Biochimica et Biophysica Acta (BBA) - Lipids and Lipid Metabolism* **1980,** *618* (3), 407-419.

6. Thornburg, T.; Miller, C.; Thuren, T.; King, L.; Waite, M., Glycerol reorientation during the conversion of phosphatidylglycerol to bis(monoacylglycerol)phosphate in macrophage-like RAW 264.7 cells. *Journal of Biological Chemistry* **1991,** *266* (11), 6834-6840.

7. Amidon, B.; Schmitt, J. D.; Thuren, T.; King, L.; Waite, M., Biosynthetic conversion of phosphatidylglycerol to sn-1:sn-1' bis(monoacylglycerol) phosphate in a macrophage-like cell Line. *Biochemistry* **1995,** *34* (16), 5554-5560.

8. Hullin-Matsuda, F.; Kawasaki, K.; Delton-Vandenbroucke, I.; Xu, Y.; Nishijima, M.; Lagarde, M.; Schlame, M.; Kobayashi, T., De novo biosynthesis of the late endosome lipid, bis(monoacylglycero)phosphates. *Journal of lipid research* **2007,** *48* (9), 1997-2008.

9. Struzik, Z. J.; Weerts, A. N.; Storch, J.; Thompson, D. H., Stereospecific synthesis of phosphatidylglycerol using a cyanoethyl phosphoramidite precursor. *Chemistry and Physics of Lipids* **2020,** *231*, 104933.

10. Beaucage, S. L.; Caruthers, M. H., Deoxynucleoside phosphoramidites—A new class of key intermediates for deoxypolynucleotide synthesis. *Tetrahedron Letters* **1981,** *22* (20), 1859-1862.

11. Burugupalli, S.; Richardson, M. B.; Williams, S. J., Total synthesis and mass spectrometric analysis of a Mycobacterium tuberculosis phosphatidylglycerol featuring a two-step synthesis of (R)-tuberculostearic acid. *Organic & Biomolecular Chemistry* **2017,** *15* (35), 7422-7429.

12. Murakami, K.; Molitor, E. J.; Liu, H.-w., An Efficient Synthesis of Unsymmetrical Optically Active Phosphatidyl Glycerol. *The Journal of Organic Chemistry* **1999,** *64* (2), 648-651.

13. Sato, R.; Itabashi, Y.; Fujishima, H.; Okuyama, H.; Kuksis, A., Simple synthesis of diastereomerically pure phosphatidylglycerols by phospholipase D-catalyzed transphosphatidylation. *Lipids* **2004,** *39* (10), 1025-1030.

14. Peterson, B. L.; Cummings, B. S., A review of chromatographic methods for the assessment of phospholipids in biological samples. *Biomedical chromatography : BMC* **2006,** *20* (3), 227-43.

15. Jiang, G.; Xu, Y.; Falguières, T.; Gruenberg, J.; Prestwich, G. D., Concise Synthesis of Ether Analogues of Lysobisphosphatidic Acid. *Organic Letters* **2005,** *7* (18), 3837-3840.

16. Jiang, G.; Xu, Y.; Prestwich, G. D., Practical Enantiospecific Syntheses of Lysobisphosphatidic Acid and Its Analogues. *The Journal of Organic Chemistry* **2006,** *71* (3), 934-939.

17. Vosse, C.; Wienken, C.; Cadenas, C.; Hayen, H., Separation and identification of phospholipids by hydrophilic interaction liquid chromatography coupled to tandem high resolution mass spectrometry with focus on isomeric phosphatidylglycerol and bis(monoacylglycero)phosphate. *Journal of Chromatography A* **2018,** *1565*, 105-113.

18. Jankowska, J.; Sobkowski, M.; Stawiński, J.; Kraszewski, A., Studies on aryl H-phosphonates. I. An efficient method for the preparation of deoxyribo- and ribonucleoside 3′-H-phosphonate monoesters by transesterification of diphenyl H-phosphonate. *Tetrahedron Letters* **1994,** *35* (20), 3355-3358.

19. Beaucage, S. L.; Caruthers, M. H., Synthetic strategies and parameters involved in the synthesis of oligodeoxyribonucleotides according to the phosphoramidite method. *Current protocols in nucleic acid chemistry* **2001,** *Chapter 3*, Unit 3.3.

20. Mallik, S.; Prasad, R.; Bhattacharya, A.; Sen, P., Synthesis of Phosphatidylserine and Its Stereoisomers: Their Role in Activation of Blood Coagulation. *ACS Medicinal Chemistry Letters* **2018,** *9* (5), 434-439.

21. Xiao, Q.; Sun, J.; Ju, Y.; Zhao, Y.-f.; Cui, Y.-x., Novel approach to the synthesis of AZT 5′-O-hydrogen phospholipids. *Tetrahedron Letters* **2002,** *43* (30), 5281-5283.

22. Wada, T.; Honda, F.; Sato, Y.; Sekine, M., First synthesis of H-phosphonate oligonucleotides bearing N-unmodified bases. *Tetrahedron Letters* **1999,** *40* (5), 915-918.

23. Pretula, J.; Kaluzynski, K.; Szymanski, R.; Penczek, S., Preparation of Poly(alkylene H-phosphonate)s and Their Derivatives by Polycondensation of Diphenyl H-Phosphonate with Diols and Subsequent Transformations. *Macromolecules* **1997,** *30* (26), 8172-8176.

24. Pérez, O.; Schipper, N.; Bollmark, M., Preparative Synthesis of an RP-Guanosine-3′,5′-Cyclic Phosphorothioate Analogue, a Drug Candidate for the Treatment of Retinal Degenerations. *Organic Process Research & Development* **2021,** *25* (11), 2453-2460.

25. Kobayashi, T.; Regens, C. S.; Denmark, S. E., Chapter 4 - Total Synthesis of Papulacandin D. In *Strategies and Tactics in Organic Synthesis*, Harmata, M., Ed. Academic Press: 2012; Vol. 8, pp 79-126.

26. Wang, Q.; Wang, Y.; Ding, J.; Wang, C.; Zhou, X.; Gao, W.; Huang, H.; Shao, F.; Liu, Z., A bioorthogonal system reveals antitumour immune function of pyroptosis. *Nature* **2020,** *579* (7799), 421-426.

27. Kremsky, J. N.; Sinha, N. D., Facile deprotection of silyl nucleosides with potassium fluoride/ 18-crown-6. *Bioorganic & Medicinal Chemistry Letters* **1994,** *4* (18), 2171-2174.

28. Akporji, N.; Lieberman, J.; Maser, M.; Yoshimura, M.; Boskovic, Z.; Lipshutz, B. H., Selective Deprotection of the Diphenylmethylsilyl (DPMS) Hydroxyl Protecting Group under Environmentally Responsible, Aqueous Conditions. *ChemCatChem* **2019,** *11* (23), 5743-5747.

29. Wleklinski, M.; Loren, B. P.; Ferreira, C. R.; Jaman, Z.; Avramova, L.; Sobreira, T. J. P.; Thompson, D. H.; Cooks, R. G., High throughput reaction screening using desorption electrospray ionization mass spectrometry. *Chemical Science* **2018,** *9* (6), 1647-1653.

30. Kele, Z.; Kupihar, Z.; Kovacs, L.; Janaky, T.; Szabo, P. T., Electrospray mass spectrometry of phosphoramidites, a group of acid-labile compounds. *Journal of mass spectrometry : JMS* **1999,** *34* (12), 1317-21.

31. Kern, N.; Dombray, T.; Blanc, A.; Weibel, J.-M.; Pale, P., Silver(I)-Catalyzed Deprotection of p-Methoxybenzyl Ethers: A Mild and Chemoselective Method. *The Journal of Organic Chemistry* **2012,** *77* (20), 9227-9235.

32. Oikawa, Y.; Yoshioka, T.; Yonemitsu, O., Specific removal of o-methoxybenzyl protection by DDQ oxidation. *Tetrahedron Letters* **1982,** *23* (8), 885-888.

33. Sandahl, A. F.; Nguyen, T. J. D.; Hansen, R. A.; Johansen, M. B.; Skrydstrup, T.; Gothelf, K. V., On-demand synthesis of phosphoramidites. *Nature Communications* **2021,** *12* (1), 2760.

34. Dreef, C. E.; Elie, C. J. J.; van der Marel, G. A.; van Boom, J. H., Synthesis of phosphonate analogues of myo-inositol phospholipids. *Tetrahedron Letters* **1991,** *32* (7), 955-958.

35. Vishwakarma, R. A.; Vehring, S.; Mehta, A.; Sinha, A.; Pomorski, T.; Herrmann, A.; Menon, A. K., New fluorescent probes reveal that flippase-mediated flip-flop of phosphatidylinositol across the endoplasmic reticulum membrane does not depend on the stereochemistry of the lipid. *Organic & Biomolecular Chemistry* **2005,** *3* (7), 1275-1283.

36. Liu, X.; Stocker, B. L.; Seeberger, P. H., Total Synthesis of Phosphatidylinositol Mannosides of Mycobacterium tuberculosis. *Journal of the American Chemical Society* **2006,** *128* (11), 3638-3648.

37. Baranova, E. O.; Dang, T. P. L.; Eremin, S. V.; Esipov, D. S.; Shastina, N. S.; Shvets, V. I., Synthesis of new derivatives of inositolcontaining phospholipid dimer analogs as potential inhibitors of virus adsorption. *Pharmaceutical Chemistry Journal* **2011,** *45* (6), 344-350.

38. Lindh, I.; Stawinski, J., A general method for the synthesis of glycerophospholipids and their analogs via H-phosphonate intermediates. *The Journal of Organic Chemistry* **1989,** *54* (6), 1338-1342.

39. Gan, C. H.; Wijaya, H.; Li, L.-H.; Wei, C.-F.; Peng, Y.-J.; Wu, S.-H.; Hua, K.-F.; Lam, Y., H-Phosphonate Synthesis and Biological Evaluation of an Immunomodulatory Phosphoglycolipid from Thermophilic Bacteria. *Organic Letters* **2020,** *22* (7), 2569-2573.

40. Kano, K.; Ishii, N.; Hirabayashi, Y.; Kamiguchi, H.; Greimel, P.; Matsuo, I., Stereocontrolled Synthesis of Lyso-phosphatidyl β-D-Glucoside. *ChemistrySelect* **2021,** *6* (26), 6811-6815.

41. Nguyen, J. M.; Townsend, S. D., Total Synthesis of the Photorhabdus temperata ssp. Cinereal 3240 Zwitterionic Trisaccharide Repeating Unit. *Organic Letters* **2021,** *23* (15), 5922-5926.

42. Tsybulskaya, I.; Kulak, T.; Kalinichenko, E.; Baranovsky, A.; Bogushevich, S.; Golubeva, M.; Kuzmitsky, B., Phospholipid derivatives of cladribine and fludarabine: Synthesis and biological properties. *Bioorganic & Medicinal Chemistry* **2015,** *23* (13), 3287-3296.

43. Kers, A.; Kers, I.; Stawiski, J.; Sobkowski, M.; Kraszewski, A., Studies on Aryl H-Phosphonates; Part 2: A General Method for the Preparation of Alkyl H-Phosphonate Monoesters. *Synthesis* **1995,** *1995* (04), 427-430.

44. Kers, A.; Kers, I.; Stawiński, J.; Sobkowski, M.; Kraszewski, A., Studies on aryl H-phosphonates. 3. Mechanistic investigations related to the disproportionation of diphenyl H-phosphonate under anhydrous basic conditions. *Tetrahedron* **1996,** *52* (29), 9931-9944.

45. Cieślak, J.; Sobkowski, M.; Kraszewski, A.; Stawiński, J., Aryl H-phosphonates. Part IV. A new method for internucleotide bond formation based on transesterification of aryl nucleoside H-phosphonate diesters. *Tetrahedron Letters* **1996,** *37* (26), 4561-4564.

46. Sobkowski, M.; Kraszewski, A.; Stawinski, J., Recent Advances in H-Phosphonate Chemistry. Part 1. H-Phosphonate Esters: Synthesis and Basic Reactions. In *Phosphorus Chemistry II: Synthetic Methods*, Montchamp, J.-L., Ed. Springer International Publishing: Cham, 2015; pp 137-177.

47. Kraszewski, A.; Stawinski, J., H-Phosphonates: Versatile synthetic precursors to biologically active phosphorus compounds. *Pure and Applied Chemistry* **2007,** *79* (12), 2217-2227.

48. Westheimer, F. H.; Huang, S.; Covitz, F., Rates and mechanisms of hydrolysis of esters of phosphorous acid. *Journal of the American Chemical Society* **1988,** *110* (1), 181-185.

CHAPTER 4. SYNTHESIS AND EVALUATION OF LABALED PHOSPHATIDYLGLYCEROL PROBES

4.1 Abstract

Niemann-Pick Type C disease (NPC) is a rare autosomal recessive lysosomal storage disorder that commonly results in death before the age of 20, and arises due to the accumulation of unesterified cholesterol within the late/endosome lysosomes (LE/LY) of cells. Impairment of cholesterol trafficking in the LE/LY is due to mutations in either the transmembrane NPC1 or lumen soluble NPC2 proteins. Evidence has suggested that a lysosomal specific phospholipid known as bis(monoacylglycero)phosphate (BMP) plays a large role in cholesterol trafficking potentially via protein-lipid interactions between BMP and NPC2 that may result in therapeutic opportunities for NPC patients. The mechanism of BMP biogenesis, however, is still largely under debate, especially regarding the enzymes involved. Phosphatidylglycerol (PG) has previously been shown to act as the biological precursor to BMP, and may provide mechanistic insights into BMP formation and degradation. Herein, we report the synthesis and evaluation of PG probes containing ^{13}C-labeled acyl chains via liquid chromatography coupled to tandem mass spectrometry (LC-MS/MS).

4.2 Introduction

Niemann-Pick Type C disease (NPC) is a rare autosomal recessive lysosomal storage disorder (LSD) that is found in about 1/89,000 – 1/120,000 live births.[1] NPC arises due to the aberrant accumulation of unesterified cholesterol within the late endosome/lysosome (LE/LY) membranes of cells that results in organomegaly, vertical supranuclear gaze palsy, progressive motor skill deficiencies, cognitive decline, and ultimately death often before adulthood.[2] Mutations

in either the NPC1 (95% of patients) or NPC2 (5% of patients) proteins, both are responsible for cholesterol trafficking in the LE/LY, leads to impaired cholesterol trafficking resulting in cell death. NPC1 is encoded by chromosome 18q11 and is a 1278-amino acid protein located in the limiting membrane of the LE/LY.[3-5] NPC1 is composed of 13 transmembrane (TM) spanning regions, where TM 3 – 7 comprise a sterol sensing domain, and 3 intraluminal domains including an N-terminal domain that accepts cholesterol.[6-7] NPC2, encoded by chromosome 14q42.3, is a small luminal protein of 132 amino acids (14.5 kDa).[8] NPC2 binds cholesterol via its isooctyl side chain in a 1:1 stoichiometry with submicromolar affinity (K_d = 30-50 nM) at both neutral and acidic pH values.[9-11]

Cholesterol trafficking in the LE/LY begins by entrance of cholesterol ester particles via low density lipoprotein receptor-mediated endocytosis.[12] From there, acid lipase operates in tandem with NPC2 to hydrolyze the cholesterol ester to yield an equivalent of a fatty acid and an unesterified cholesterol molecule with the hydroxyl group exposed to the lumen of the lysosome.[13] NPC2 then delivers cholesterol to the NTD of NPC1 by binding to domain C of NPC1 at low pH values[6, 14-16] where cholesterol is repackaged as cholesterol esters and sent to the plasma membrane or other organelles via trafficking proteins.[17-18] While significant strides have been made to elucidate mechanisms behind cholesterol trafficking in the LE/LY via NPC1 and NPC2, several questions remain unanswered, specifically regarding the mechanisms of cholesterol transport via NPC2. It is important to note that the LE/LY is a multivesicular body in which the majority of endocytosed cholesterol is concentrated within the intraluminal membranes (ILMs).[19-21] This suggests that NPC2 is capable of extracting cholesterol from the ILMs via contact of NPC2 with these membranes before delivering it to NPC1. While it was expected that mutations inside the binding pocket of NPC2 would result in impaired cholesterol efflux from *npc2-/-* cells, it was

surprising to observe a similar result from surface mutations of NPC2.[9, 22] Indeed, protein-lipid interactions between NPC2 and the ILMs are a major determinant of cholesterol trafficking in the LE/LY.

First isolated from pig and rabbit lung in 1967 by Body and Gray[23], bis(mono)acylglycerophosphate (BMP), formerly known as lysobisphosphatidic acid (LBPA), is a negatively charged glycerophospholipid located in the ILMs of the LE/LY. BMP comprises ~15% of the lysosomal lipid population and less that 1% of the global cellular lipid population making it an important lipid for the LE/LY.[24] BMP contains an unusual *sn*-1:*sn*-1' stereochemistry as opposed to the *sn*-3:*sn*-1' stereochemistry normally observed in most other glycerophospholipids with acyl chains located on the *sn*-2 and *sn*-2' positions rather than the more thermodynamically stable *sn*-1 and *sn*-1' positions (Figure 4.1).[25-29]

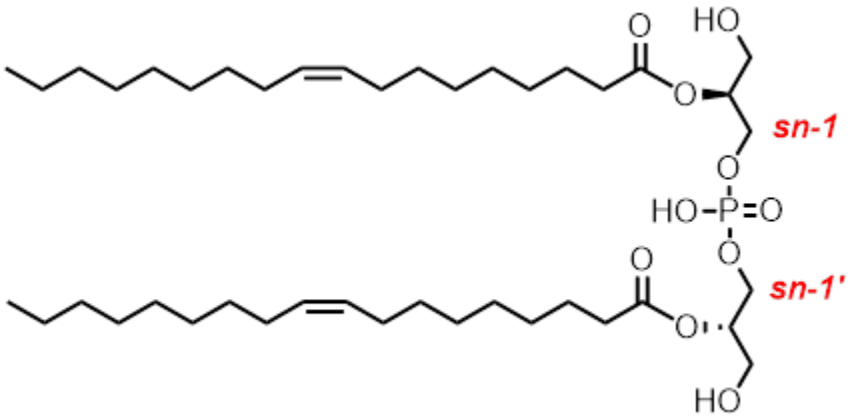

Figure 4.1. Structure of naturally occurring BMP containing di-18:1 acyl chains.

It is believed that this unique stereochemical configuration is made to remain inert to lysosomal enzymes that affect fatty acid hydrolysis such as phospholipase A2 (PLA2) that require an *sn*-3 phosphoglycerol backbone.[30-33] Additionally, membranes containing *sn*-1:*sn*-1' BMP may promote vesicle fusion with other membranes more easily than *sn*-3:*sn*-1' BMP as indicated by

the higher phase transition temperature and higher membrane areas observed in the naturally occurring *sn*-1:*sn*-1' BMP.[34] Acyl chain composition of BMP is dominated by dioleyl (di-18:1), however the acyl chains composition and BMP levels vary depending on the lysosomal storage disorder of the patient.[35-40] Interestingly, while di-18:1 BMP was the most prevalent species observed in NPC patients, di-22:6 species have been observed to be 50-fold higher compared to controls.[41]

Acyl chain composition can also affect cholesterol transfer rates, with BMP analogs containing di-18:1 species producing ~6-fold higher relative binding of cholesterol compared to the di-14:0 BMP species.[42] With regard to stereochemistry, naturally occurring *sn*-1:*sn*-1' BMP has been shown to not only engage with NPC2 to support its cholesterol binding function, but also with other endosomal proteins such as acid sphingomyelinase, making it an essential lipid for normal lysosomal operation.[43-46] Achieving an in-depth understanding of BMP biogenesis and catabolism could provide new clues for therapeutic interventions for NPC and other lysosomal storage disorders.

There is an apparent strong synergistic relationship between NPC2 and BMP. Cheruku *et al.* demonstrated that collisional cholesterol transfer rates between NPC2 and membranes of small unilamellar vesicles (SUVs) comprised of negatively charged phospholipids are higher than SUVs composed of neutrally charged phospholipids, indicating an electrostatic influence.[47] Additionally, similar cholesterol transfer rates were observed between negatively charged SUVs of different negatively charged lipid type, except for those that contained BMP. SUVs containing BMP displayed 30-fold greater cholesterol transfer relative to controls suggesting that there is a structural dependence on this phospholipid that augments the electrostatic interaction. McCauliff *et al.* modified the surface of NPC2 and established that the so-called "hydrophobic knob" of NPC2

was essential for interactions with BMP rich membranes.[48-49] Specifically, mutations outside the hydrophobic knob produced negligible differences in cholesterol transport rates, while point mutations on the hydrophobic knob resulted in decreased cholesterol transfer rates that were only 15% of the wild-type sequence. Kobayashi *et al*. demonstrated that the anti-LBPA antibody C64 results in disorganization of ILMs and marked cholesterol accumulation within the LE/LY that resembled an NPC phenotype.[24] It was also demonstrated that increasing BMP concentrations in *npc2-/-* cells, but not *npc1-/-* cells, resulted in increased cholesterol trafficking, further supporting the hypothesis that specific interactions occur between BMP and NPC2. These results may ultimately have therapeutic opportunities for NPC patients. As an example, Moreau *et al.* have recently demonstrated that drug induced increases in BMP resulted in decreased cholesterol overload by up to 25% in NPC cells, although behavioral improvement was not observed unless used in combination with miglustat. Similarly, phosphatidylglycerol (PG), the proposed biological precursor and isomer of BMP, has also demonstrated decreased cholesterol accumulation compared to the disease wildtype.[50] Furthermore, PG also stimulated autophagy in Purkinjie cells, likely due to the 50% increased production of BMP from PG.[51]

There is a direct correlation between the concentrations of PG and BMP within cells. Hullin-Matsuda *et al.* showed that cells deficient in phosphatidylglycerolphosphate (PGP) synthase, a key enzyme involved in the metabolic pathway of PG, decreased BMP synthesis by 2 fold compared to the wild-type, while overexpression of PGP synthase resulted in a 2-5 fold increased production of BMP.[52] Surprisingly, direct evidence for the metabolism of PG to BMP does not exist, nor are the enzymes involved definitively established. Waite and co-workers have proposed a biosynthetic pathway of PG to BMP by a lysophosphatidylglycerol (lyso-PG) intermediate that was established using radiolabeled PG (Figure 4.2).[53-55] This route would most

likely involve PG hydrolysis by phospholipase A2 at the *sn*-2 ester position. A transacylase identified in a macrophage-like cell line is then proposed wherein lyso-PG would act as both an acyl donor and acceptor for reacylation of the *sn*-2' position in the second step of the mechanism. The inversion of stereochemistry is proposed to occur by an unidentified enzyme; however intermolecular transfer of glycerol moieties is thought to be unlikely. While this route is well supported in the beginning steps, it does not provide insight into the stereochemical conversion from the *sn*-3 phosphate to the *sn*-1 phosphate. Additionally, this route does not consider other possible intermediates in the pathway, such as the production of acyl phosphatidylglycerol (acyl-PG), also known as hemi-BMP.

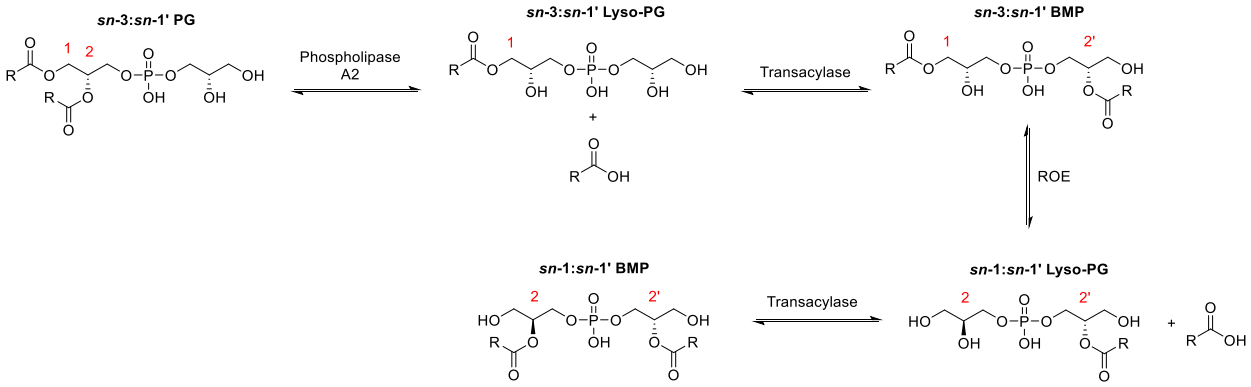

Figure 4.2. Proposed biological mechanism of PG to BMP by Waite and co-workers. ROE = Reorientation enzyme.

In order to gain further insight into the metabolic pathways of BMP biosynthesis and degradation, direct evidence of BMP formation from PG must be observed. This requires the use of synthetic lipid probes to monitor the metabolic products of PG. Additionally, identification of potential intermediates might provide insight into enzymes that might be involved in the pathway. To explore these questions, PG probes with ^{13}C-labeled acyl chains were synthesized where both the *sn*-1 and *sn*-2 acyl chains were labeled, and then just the *sn*-2 acyl chain was labeled. The

synthesized probes are also in the diastereochemically correct form of PG, something that has not been previously examined as the studies conducted by Waite and co-workers contained a racemic PG headgroup. We then produced unilamellar vesicles from labeled PG vesicles and then incubated them with HeLa cells before a Bligh and Dyer extraction of the lipid fraction for analysis (Figure 4.3). Using hydrophilic interaction liquid chromatography coupled to tandem mass spectrometry (HILIC-MS/MS) the products of PG metabolism were identified via lipidomic analysis. This effort required the use of expensive ^{13}C-labeled acyl chains ($4000/g), requiring a robust PG synthesis route. We previously reported the synthesis of PG incorporating unsymmetric acyl chains using H-phosphonate methodology that resulted in less variable yields and was more amendable towards our acyl chain composition containing unsaturation compared to previously reported methods.[56] Incorporating this approach towards the synthesis of our desired PG probes, we now report multiple metabolic products of PG and definitively establish the production of BMP from PG.

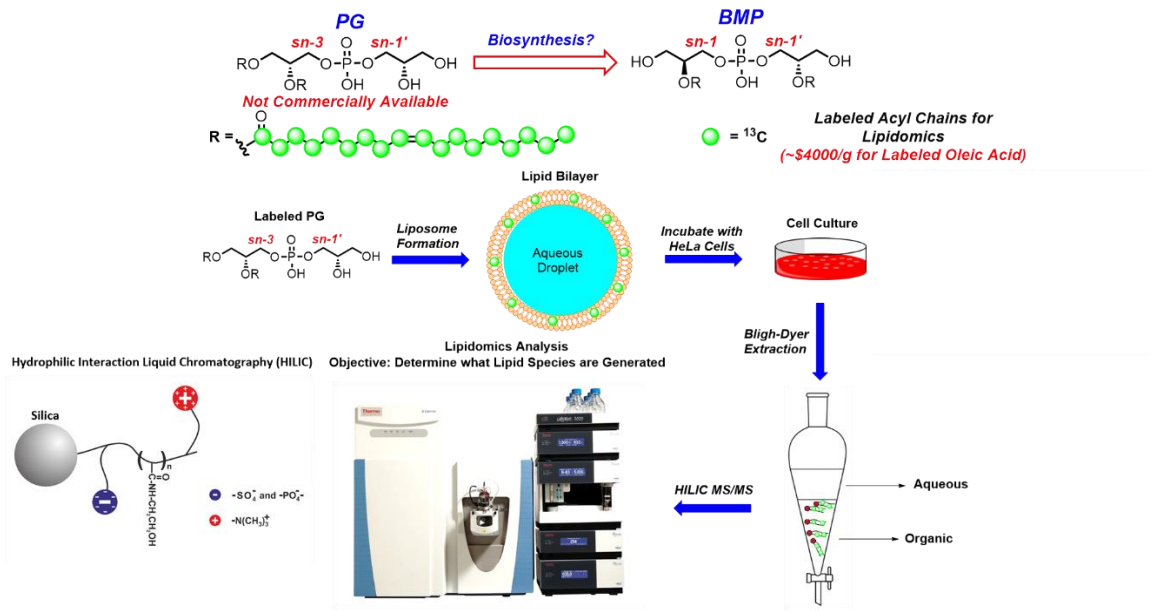

Figure 4.3. Experimental workflow of synthesized ^{13}C labeled PG probes. After synthesis of isotopically labeled PG, they were formulated into liposomes and incubated with HeLa cells. Lipids were extracted and analyzed via HILIC-MS/MS where lipid products made from PG may were determined.

Our goal was to synthesize two different PG probes where ^{13}C-labeled oleyl acyl chains were installed on the *sn*-2 and *sn*-1 positions, or only the *sn*-2 position. This would allow us to track the movement of acyl chains from one lipid species to another. We decided to synthesize di-18:1 PG because the most common BMP species in both NPC cells and healthy cells contain oleyl acyl chains. Although a di-22:6 BMP species would also be of interest, carrying these easily oxidizable polyunsaturated acyl chains through an entire synthesis of PG is significantly more challenging. The acyl chains chosen contained ^{13}C-labels on every carbon of the 18:1 chain to ensure the largest mass separation between native lipid species and synthetic lipid species. Given that the natural abundance of ^{13}C is ~1.1%, labeling each carbon on the chain also gives us confidence that there will be negligible signal overlap between the labeled compound and cellular PG species that might contain greater than or equal to one ^{13}C.

We previously reported the synthesis of PG using phosphoramidite[57] and H-phosphonate approaches.[56] Using the phosphoramidite method, we overcame challenges associated with the previous syntheses of PG, including the installation of unsaturated acyl chains and opportunities for post-head group modifications. However, the global deprotection step to simultaneously remove the tert-butyl silyl groups of the phosphoglycerol headgroup as well as the cyanoethyl group protecting the phosphate in this route proved to be arduous because of the need for rigorous chromatographic conditions required to remove the tetrabutylammonium ion including two silica columns, one ion exchange column, and one prep-HPLC method.[57] Additionally, yields were unacceptably variable for a route targeting ^{13}C-labeled PG. To circumvent this issue, we synthesized PG using an H-phosphonate methodology instead (Figure 4.4). The isolation of a bench and air-stable triethyl ammonium H-phosphonate salt intermediate proved to be readily purified by column chromatography. We were also able to phosphorylate the solketal starting material directly, eliminating the need for subsequent protection/deprotection transformations, ultimately reducing the number of synthetic steps from 11 to 8. Finally, we were also able to successfully install unsymmetric acyl chains onto the *sn*-1 and *sn*-2 positions, allowing us to selectively esterify different fatty acids onto the phosphoglycerol backbone in moderate yields.

Applying this strategy towards the synthesis of our desired PG probes, we began with the protection of (*S*)-solketal with *p*-methoxybenzylchloride under standard conditions to give **2** in 97% yield. Subsequent isopropylidene deprotection was carried out under acidic conditions to afford **3** in 90% yield. For the synthesis of the di-18:1 probe, we carried out a Steglich esterification with a slight excess of labeled oleic acid for complete coverage of both alcohols that provided **5b** in 81% yield. For the unsymmetric version of **5**, stoichiometric control was employed to successfully install ^{12}C oleic acid selectively on the *sn*-1 position to give **4** in 76% yield. For the esterification

of the *sn*-2 position, ^{13}C oleic acid was used in slight excess to give **5a** in 79% yield. Standard deprotection conditions of **5** with DDQ gave **6** in 57% yield. Acyl chain migration from the *sn*-2 position to the *sn*-3 position was prevented using kinetic control that was previously described.[57] Phosphorylation of **6** was conducted using inexpensive and readily available diphenyl phosphite that was subsequently treated with a H_2O/Et_3N solution to give **7** in 95% yield. Phosphorylation of (*R*)-solketal occurred after activation of **7** by pivalic acid to give **8** in 85% yield, taking precautions described previously. Finally, the oxidation from P^{III} to P^{V} was carried out under normal I_2 conditions in H_2O/Pyr. followed by treatment with TFA to yield **9** in 68% yield with an overall yield of 16%.

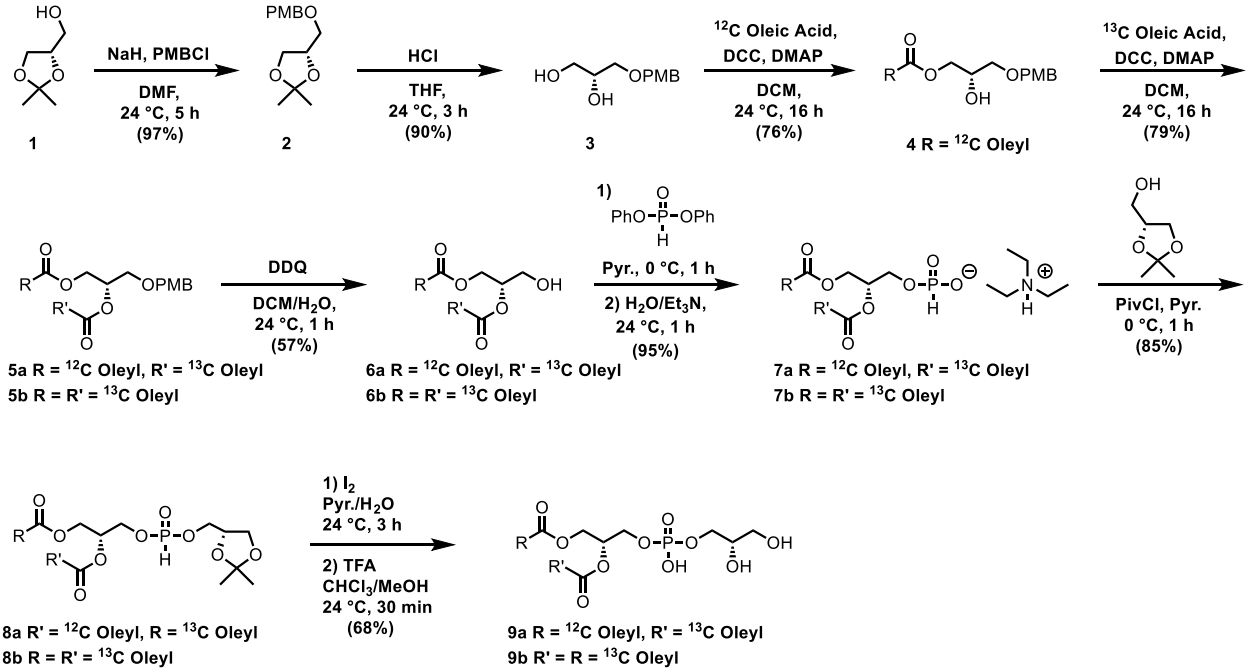

Figure 4.4. Synthesis of PG probes containing symmetric and unsymmetric acyl chains using H-phosphonate methodology.

We utilized HILIC-MS/MS to study the metabolic products of PG using a protocol reported by Vosse *et al*. that successfully separates of PG from BMP based on retention time.[58] HILIC combines the advantages of ion exchange, normal phase, and reverse phase chromatography, making it an attractive approach for the analytical separation of phospholipids that possess properties of all three of these interaction types.[59] HILIC stationary phases are typically silica functionalized with short-chain alkyl amides, amines, sulfates, and phosphates. While HILIC provides separation of phospholipids of cellular lipid extracts after treatment with labeled PG based on polarity, MS/MS was used to provide multiple reaction monitoring (MRM) information to identify selected lipid products (Figure 4.5). To investigate the presence of selected intermediates with our labeled PG probes, we conducted a HILIC-MS/MS experiment after incubation of PG at various concentrations with HeLa cells. MRM allowed us to identify our specified lipid species after analytical separation by HILIC. An additional benefit of using MRM was that selected phospholipids could still be observed independently of other species having similar retention times, so long as the masses are different. Both the retention time and fragmentation patterns were determined using analytical standards of BMP, PG, and selected intermediates. For all of our analyses, we decided to examine the ionized intact phospholipid as the precursor ion, and then the ^{12}C or ^{13}C fatty acid as the secondary fragment, because that would ensure the species being observed belongs to a lipid containing at least one ^{13}C-labeled acyl chain derived from our PG probe.

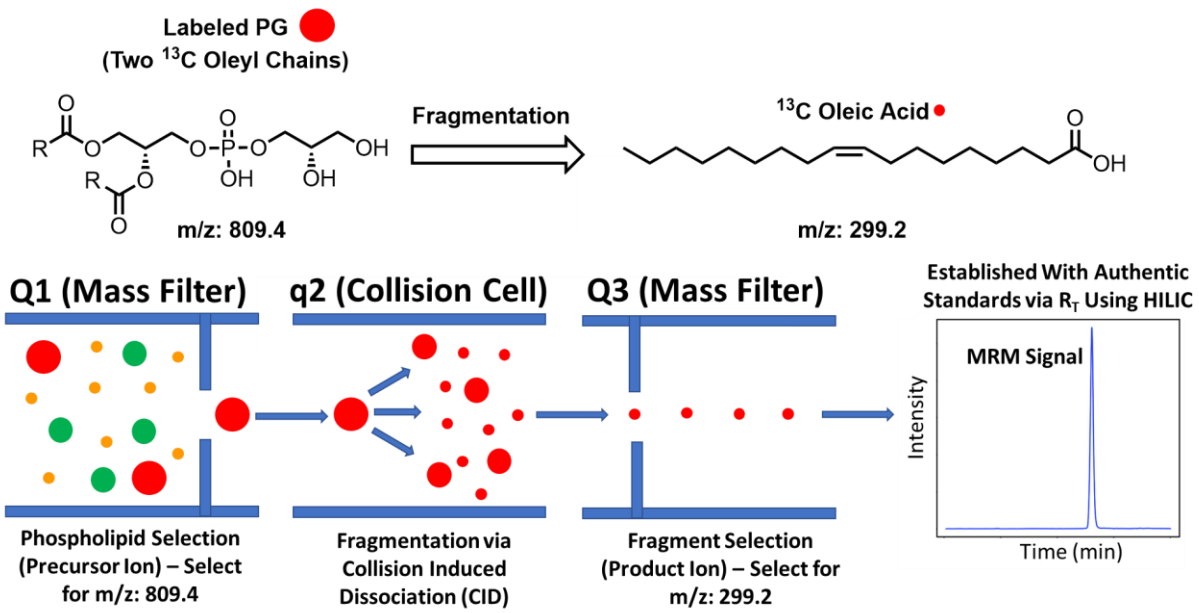

Figure 4.5. Demonstration of MRM using PG containing ^{13}C di-18:1 acyl chains as an example. A triple quadrupole mass spectrometer where each quadrupole is represented by Q1, q2, or Q3. In Q1, the desired phospholipid species to be fragmented (m/z: 809.4) is filtered. After entering q2, the selected phospholipid is then fragmented further. In Q3, the desired secondary fragment (m/z: 299.2) is filtered and detected as a measure of product ion count. The mass information is then corroborated to provide an intensity vs. time plot for the analyte of interest. HILIC is performed before this process to enable correlation of the mass data with the retention times of lipid standards.

Although Waite and co-workers proposed a mechanism of PG to BMP,[53-55] the enzymes responsible for the proposed intermediates were not definitively established. Attaining an in-depth understanding of these mechanisms will highlight enzymes that can potentially be targeted to enhance lysosomal BMP populations in an effort to increase cholesterol egress in NPC patients. Increased cholesterol efflux from NPC cells has been demonstrated upon treatment with both BMP and PG, therefore, both of these lipids are potential therapeutic targets. A lyso-PG intermediate was observed upon treatment of cells with radiolabeled PG most likely arising from the hydrolysis by PLA2 of the *sn*-2 position. The *sn*-1:*sn*-1' BMP species was the dominant isomer. Some *sn*-3:*sn*-1' BMP was observed, but it was determined that this was most likely an intermediate to *sn*-1:*sn*-1' BMP. Consistent with previously reported results, we observed a direct correlation

between increased labeled PG concentrations and labeled lyso-PG concentrations as indicated by increases in product ion counts at ~14.75 min and ~15.20 min, respectively, upon incubation with labeled PG (Figure 4.6). There appears to be two different isomers that are present in the HILIC-MS/MS traces. After comparison with standards and discussions with Avanti Polar Lipids, we concluded that the earlier eluting species belongs to *sn*-2 lyso-PG and the later eluting species belongs to the *sn*-1 labeled species. Interestingly, there appears to be a larger amount of *sn*-2 lyso-PG produced than the *sn*-1 lyso-PG. Given that the *sn*-1 position is more stable, it is surprising to see the cellular preference for the *sn*-2 position. Additionally, it is unclear whether or not the *sn*-1 lyso-PG observed arose due to acyl chain migration during the extraction and/or analysis, or whether cells preferentially produced *sn*-1 lyso-PG.

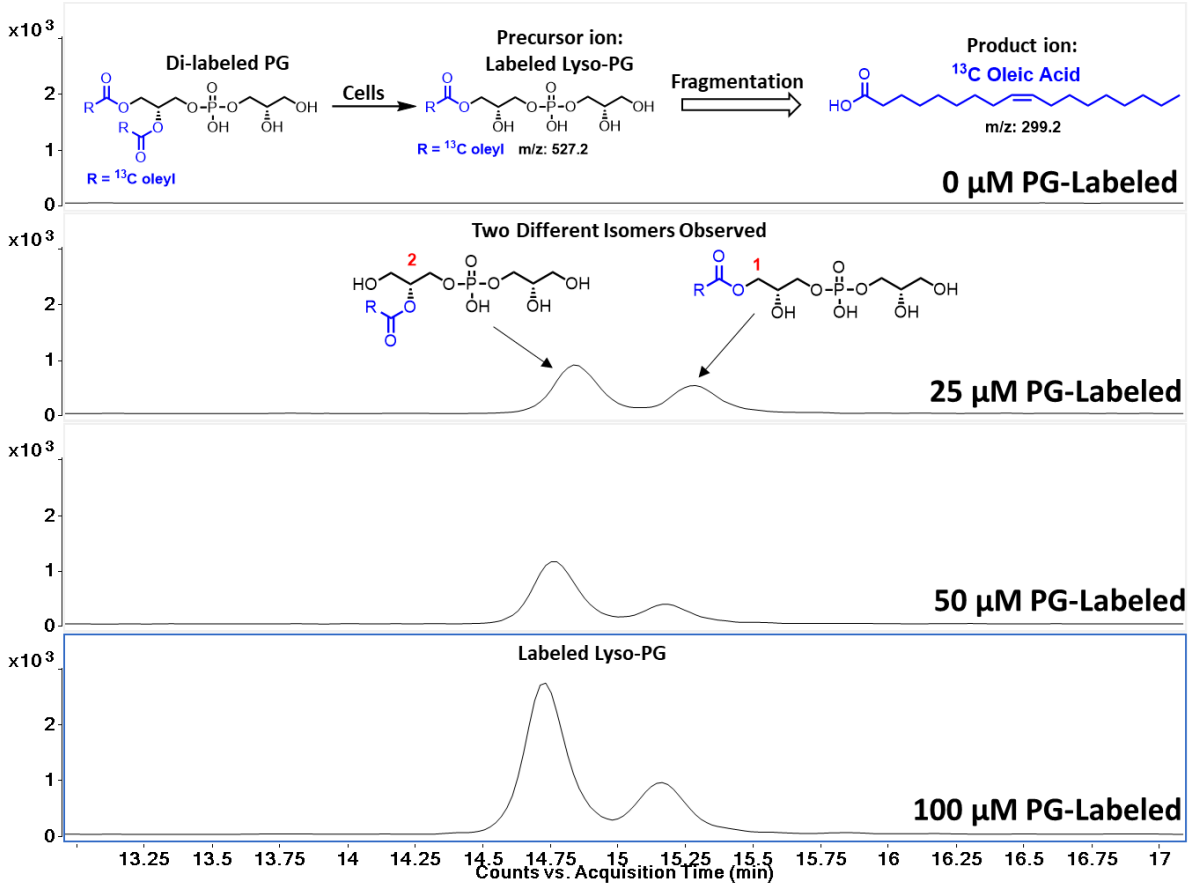

Figure 4.6. MRM of ^{13}C lyso-PG formation as a function of ^{13}C di-18:1 PG concentration. The precursor ion was ^{13}C labeled lyso-PG (m/z: 527.2) and the product ion was ^{13}C oleic acid (m/z: 299.2). Two isomers of lyso-PG appeared: one in the *sn*-2 form (retention time = 14.75 min), and one in the *sn*-1 form (retention time = 15.2 min).

It was also surprising to us to observe BMP (~11.25 min) containing two ^{13}C-labeled acyl chains (~11.25 min) increase as a function of increasing PG concentration (~12.5 min) (Figure 4.7). This observation opens several different pathways towards de novo BMP synthesis. Waite and co-workers proposed that two lyso-PG units act as both an acyl donor and an acyl acceptor to install the acyl chain in the second step of the proposed route.[53-55] This transformation would result in an observed glycerol-sn-glycerophosphate species.[55] However, our data suggests that BMP formation can occur via an intramolecular transformation where only one phospholipid species is involved rather than the transacylation route previously proposed. While it is possible that two

labeled lyso-PG species are produced and participate in a donor-acceptor transacylation reaction, the ^{13}C lyso-PG population in the cell is expected to be modest such that a bimolecular process involving two labeled lyso-PG units would be unlikely. Consequently, our results suggest an alternative intramolecular or concerted route that requires further investigation.

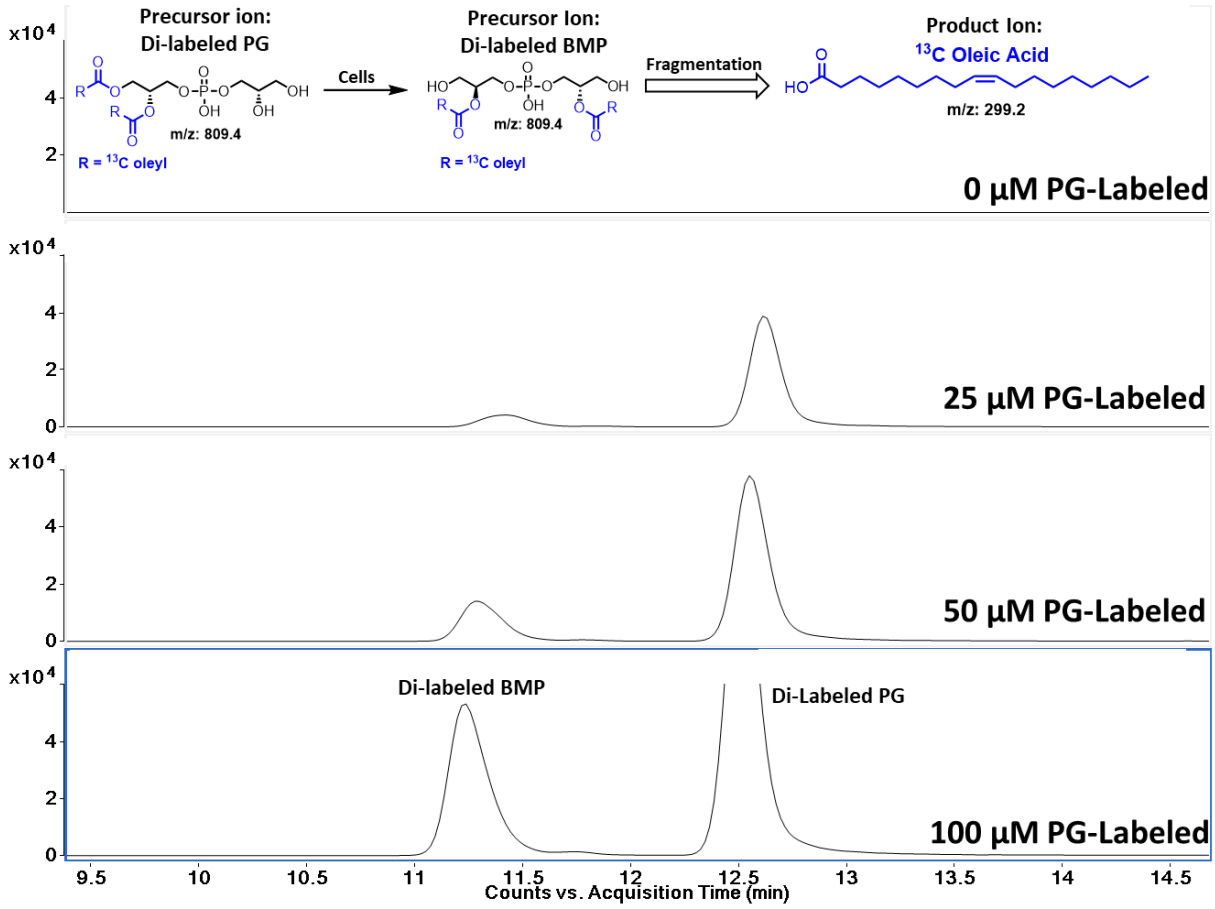

Figure 4.7. MRM of ^{13}C di-18:1 labeled PG and BMP. The precursor ions selected were BMP and PG (m/z: 809.4), and the product ion selected was ^{13}C oleic acid.

Next, we decided to monitor labeled cellular acyl-PG as a function of the cellular labeled PG concentration. Acyl-PG has been postulated to also be an intermediate during de novo synthesis of BMP, although this is not a proposed intermediate in the mechanism by Waite and co-workers. Thornburg *et al*. observed accumulation of acyl-PG in a macrophage-like cell-line leading to the

hypothesis that acyl-PG might be involved in BMP synthesis.[53] Our observations are consistent with previously reported data showing that increased PG concentrations in cells leads to increased acyl-PG levels. A single peak was observed for acyl-PG at ~10.30 min (Figure 4.8). The precursor ion was intact acyl PG containing two unlabeled acyl chains produced by the cell and one labeled ^{13}C acyl chain. The secondary fragment was an unlabeled ^{12}C oleyl chain. The position of the acyl chains, however, cannot conclusively be determined. On one hand, unsaturated acyl chains are usually located on the *sn*-2 and *sn*-2' positions of the glycerol moiety, making acylation of the *sn*-2' position possible. On the other hand, the *sn*-1 and *sn*-3' positions are more stable than the *sn*-2 and *sn*-2' positions, therefore, acylation of the *sn*-1 position is also possible. Standards of both the *sn*-2' and *sn*-3' acyl-PG isomers would be required to validate this hypothesis. Unfortunately, the control contained an unidentified species at ~10.1 min with the same mass and fragmentation pattern as acyl-PG, leading to a slight overlap in signals. However, the positive correlation between PG concentration and acyl-PG concentration can still be observed.

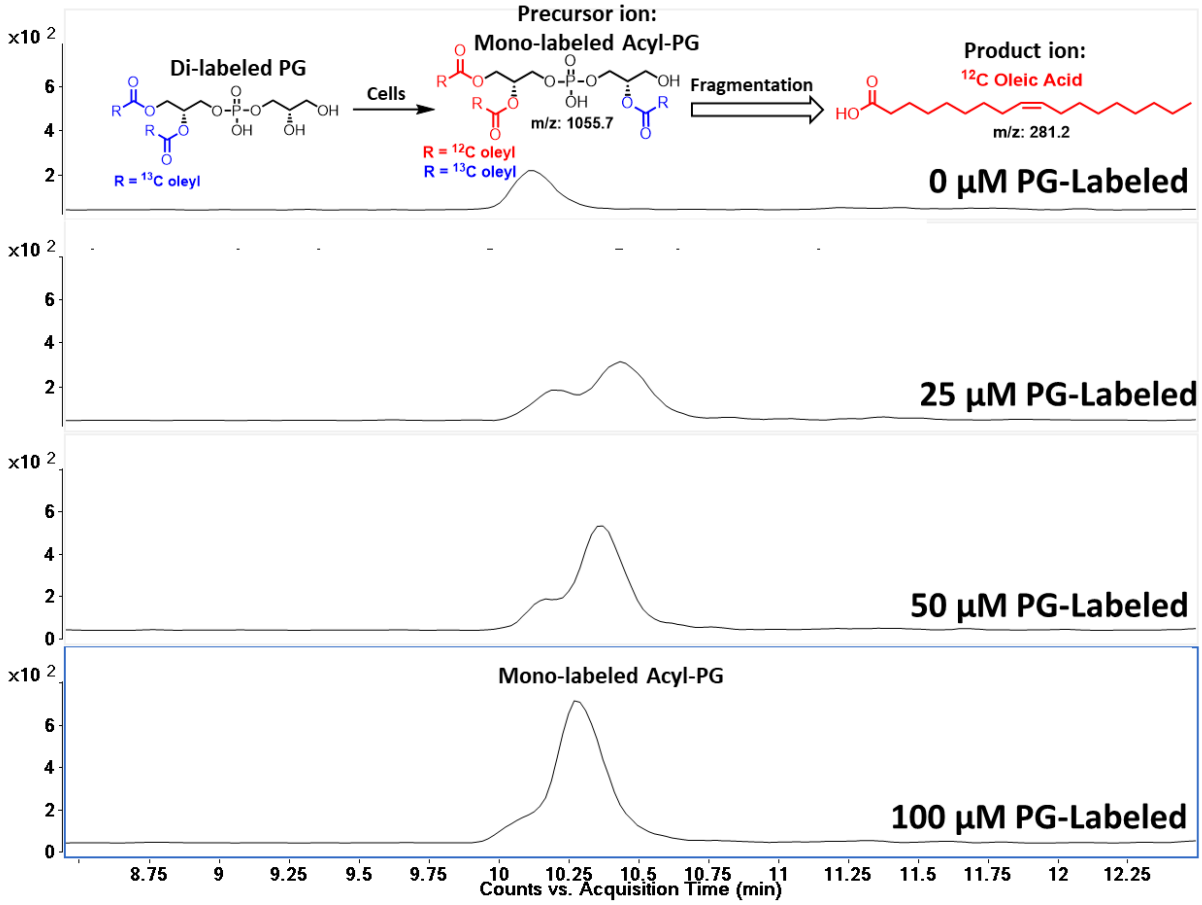

Figure 4.8. MRM of acyl-PG containing one ^{13}C oleyl chain and two ^{12}C oleyl chains. It should be noted that the positions of the labeled and unlabeled acyl chains cannot be determined in this experiment. The precursor ion identified was acyl-PG (m/z: 1055.7), and the secondary fragment identified was ^{12}C oleic acid (m/z: 281.2).

Experiments that monitored the movement of labeled acyl chains from one lipid species to another to investigate BMP biogenesis from PG have not been conducted before and, therefore, gave us the opportunity to report unique observations. Interestingly, we observed both PG and BMP species that contained both labeled and unlabeled oleyl chains (Figure 4.9). The precursor ions were the in tact phospholipid species PG and BMP at ~12.5 min and ~11.25 min, respectively, while the product ion was labeled oleic acid. These observations might arise from fatty acids that were cleaved from PG and/or BMP and transferred to a pool of fatty acids used for enzymatic lipid

remodeling via surface interactions with lipid droplets (LD) such as those seen between lysophosphatidylcholine acyl transferases and LDs composed of phosphatidylcholine in processes like the Land's cycle.[60-61]

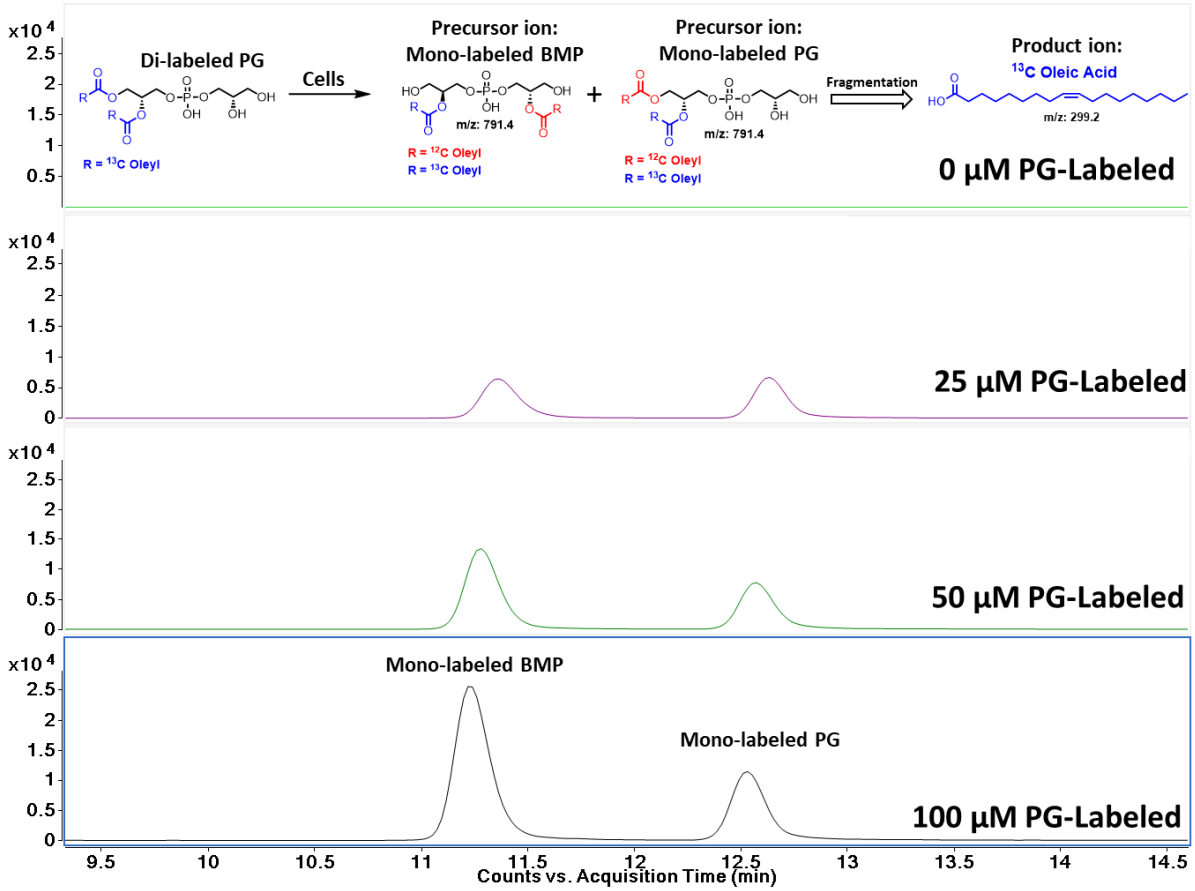

Figure 4.9. MRM of PG and BMP containing mixed acyl chain compositions where one chain is labeled with ^{13}C and one chain is ^{12}C. The precursor ions observed were PG and BMP (m/z: 791.4). The secondary fragment observed was ^{13}C oleic acid (m/z: 299.2).

Our lipidomic data idenitifies increases in labeled intermediates such as lyso-PG and acyl-PG that suggests multiple avenues for BMP biogenesis (Figure 4.10). Waite and co-workers provided one potential route towards BMP, however, there may be multiple pathways for the synthesis of BMP to maintain lipid homeostasis and proper LE/LY function. The first possible route involves a direct intramolecular transacylation to produce BMP from PG. This would involve

a transfer of the oleyl acyl chain from the *sn*-1 to the *sn*-2' acyl chain either in a single reaction or possibly by a phospholipase A1 hydrolysis and an acylation of the *sn*-2' position of the same acyl chain with an interconversion of stereochemistry from *sn*-3 to *sn*-1 via a coordinated complex of enzymes. This route provides two scenarios for the biosynthesis of BMP. The second route involves synthesis of BMP via an acyl PG intermediate. This route would begin by acylation, possibly by an acyl transferase, immediately onto the *sn*-2' position of the headgroup. While the *sn*-3' position is more thermodynamically stable, the cell normally locates unsaturated acyl chains on the secondary position. Two different routes might proceed from this intermediate. The first route involves hydrolysis of the *sn*-1 chain possibly by phospholipase A1, followed by an interconversion of stereochemistry to yield BMP. The second process would involve hydrolysis of the *sn*-2 chain, possibly by PLA2, and subsequent transacylation of the *sn*-1 acyl chain to the *sn*-2 position followed by an inversion of stereochemistry to give BMP. The third route we propose is most similar to Waite and co-workers involving a lyso-PG intermediate. In this route, PLA2 would hydrolyze the *sn*-2 chain to yield lyso-PG. We propose an alternate sequence of intermediate steps involving an acylation of the *sn*-2' position by an acyltransferase instead of another lyso-PG donor. Finally, an interconversion of stereochemistry from *sn*-3 to *sn*-1 followed by a transacylase of the *sn*-2 position would give BMP. Lipidomic experiments involving the unsymmetrically labeled PG containing one ^{13}C oleyl chain and one ^{12}C oleyl chain are underway and should shed more light on these possibilities.

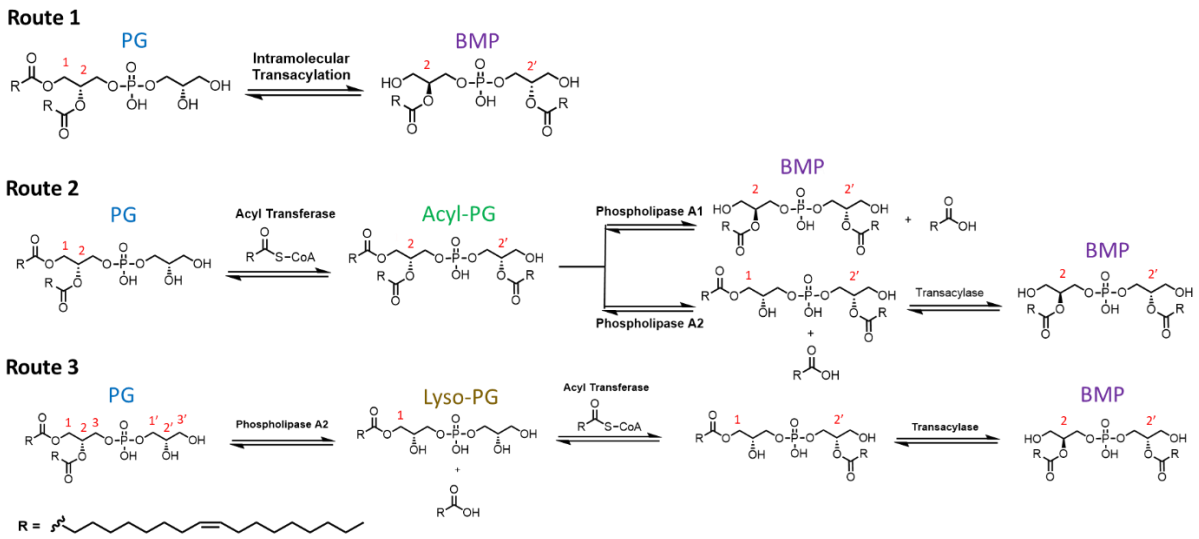

Figure 4.10. Current hypotheses for the biosynthesis of BMP from PG. Route 1 provides a route for intramolecular transacylation, either enzyme mediated or spontaneous. Route 2 provides a potential pathway to BMP from an acyl PG intermediate. Either an ester hydrolase (e.g. Phospholipase A1) would provide BMP or PLA2 would give BMP upon a transacylase reaction. Finally, Route 3 gives BMP via a lyso-PG intermediate. This may occur by a transacylase donor-acceptor reaction proposed by Waite and co-workers, or possibly by an acyltransferase. It should be noted that none of these routes provide a mechanism for stereochemical inversion as the unknown enzymes responsible for this are unknown.

4.3 Future Work: Synthesis of Photoaffinity Probes

To gain further insights into BMP biogenesis of PG, we are currently investigating the synthesis of PG containing photoaffinity probes (PAP) to definitively establish protein binding partners of PG and related intermediates. PAPs are photocrosslinking tools that react with ligand binding sites upon exposure to UV radiation. They are composed of a photo-crosslinker unit and a bioactive unit that binds the target protein. Upon irradiation with UV light, the photoactive species degrades into reactive intermediates that interact with the nearest C-H neighbor of the interacting biomolecule (Figure 4.11). After cross-linking with proteins, proteomic analysis can be used to identify PG bound enzymes.[62-63] The first PAP was implemented by Westheimer and

co-workers who used a *p*-nitrophenyl diazoacetate to crosslink a carbene species, generated by the spontaneous release of N_2 gas from the probe with chymotrypsin.[64]

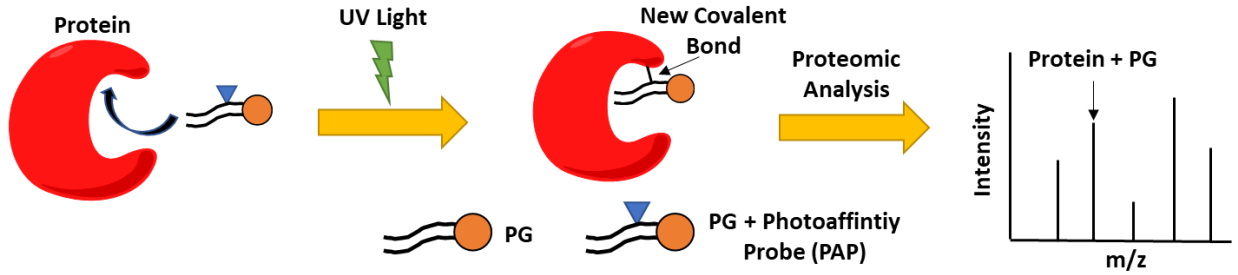

Figure 4.11. Workflow of PAPs. PG (orange circle and black tails) containing a photoactive unit (blue triangle) interact with their natural protein binding partners. Upon irradiation with UV light, the protein cross-links with the PAP and after purification are analyzed via proteomic analysis to determine the protein target and binding site.

The design of PAPs has expanded to predominately encompass benzophenones, aryl azides, and diazirines (Figure 4.12). The reactive species are diradicals, nitrenes, and carbenes, respectively.[65] Of the three classes of PAPs listed, diazirines appear the most attractive as they do not suffer the drawbacks of benzophenones and nitrenes.[66] Both benzophenones and nitrenes contain large aromatic groups and, in the case of benzophenones, a polar carbonyl group that can perturb the native biological membrane environment. Since we aim to corroborate the results from the proteomic work with the lipidomic experiments, we would like to install the photo-labile species onto the hydrophobic alkyl chain. The expected enzymes will not bind acyl chains containing large aromatic groups or electronegative atoms as favorably and, therefore, these variants might result in misleading data. On the other hand, diazirines are small hydrophobic three-membered rings that will minimally affect the environment. Additionally, carbenes generated from diazirines have shorter lifetimes (low- to mid-picosecond)[67-68] than nitrenes from aryl azides (mid-picosecond to nanosecond)[69-70] and diradicals from benzophenones (mid-nanosecond to

microsecond),[71-72] giving diazirines more selectivity for the binding site of the protein target. While shorter reactive lifetimes mean diazirines have lower cross-linking efficiencies (~10%) than the more widely used benzophenones (50% or greater), this is less of a concern today than it was decades ago because of the advancements of highly sensitive mass spectrometry techniques. Compared to aryl azides that generally require lower wavelength light for activation (250 nm – 400 nm), diazirines require longer wavelengths of light that result in less cell damage.[66] Therefore, we set out to synthesize PG probes in which the acyl chains were labeled with diazirines.

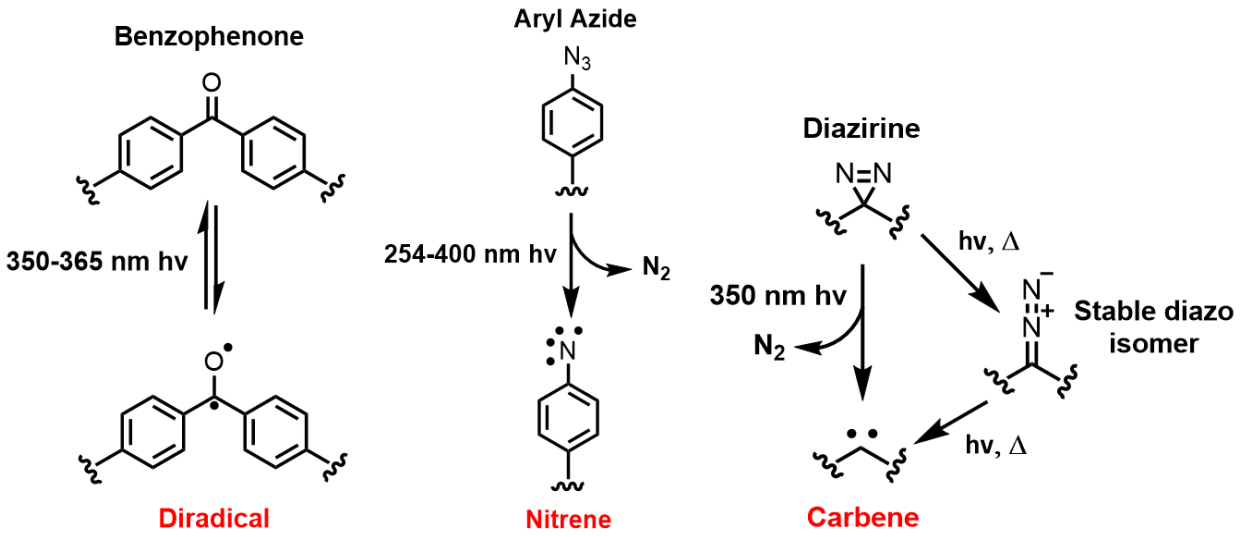

Figure 4.12. Activation and reactive intermediates of benzophenones, aryl azides, and diazirines. This figure was adapted from Murale *et al*.[65]

Another factor that needs to be considered when designing PAPs, specifically phospholipid PAPs, is the location of the photo-labile species on the acyl chain.[73] Precautions should be taken to ensure that recognition of the headgroup by whichever protein is interacting with the phospholipid is minimally disrupted. For the enzymes that are non-specific towards any single headgroup species, such as phospholipase A2,[74] labeling the headgroup would not be ideal since strong interactions are not present in that region of the molecule, potentially leading to a lower

likelihood of cross-linking in this region. Additionally, although diazirines are more hydrophobic relative to the aforementioned PAPs, they still contain two nitrogen atoms that can potentially participate in hydrogen bonding. Therefore, we want to install the diazirine on the β-carbon of the alkyl chain to group the electronegative species as close to each other as possible. It is synthetically convenient to place the label on the terminal end of the acyl chain. However, this is arguably the worst position for the label since it will disrupt the normal behavior of the lipid chain in the membrane. For example, 2D NMR experiments have revealed the terminal methyl groups of acyl chains in phospholipids not only interact deep within the hydrophobic lipid bilayer, but they also sample the lipid surface.[75] Placing a polar group at the end of the acyl chain might disrupt this behavior. Additionally Lindner *et al*. synthesized azide modified phosphatidylcholine (PC) probes where the azide was located either in the middle of the acyl chain, or on the terminal methyl group. PC probes that contains azides present on the terminal methyl group revealed unusual and unstable liposome formation while the other PC probes gave stable and extrudable liposomes further supporting the hypothesis that the location of the probe can affect the lipid's properties.[76]

4.4 Supporting Information

4.4.1 General Information

Commercial reagents for labeled PG synthesis were used as purchased from TCI Chemicals and MilliporeSigma. Organic solvents used were reagent grade purchased from Fisher Scientific. Dry solvents were purified using a Glass Contour Solvent System from Pure Process Technology, LLC, with Fisher HPLC grade DCM, Aldrich anhydrous DMF, and Fisher HPLC/ACS grade THF. Reactions were monitored by thin-layer chromatography using silica gel 60 F254 plates (Merck). UV light (254 nm) and staining with aqueous $KMnO_4$ was used to visualize the developed

chromatograms. Flash chromatography was performed using a Biotage SP4 A2A0 with RediSep Rf silica flash columns (12 g, 60 mg-1.2 g sample size) and collected in 9 mL fraction volumes or performed via manual silica column chromatography using silica gel 60 (MilliporeSigma, 0.040−0.063 MM). Compounds purified via automatic flash chromatography are accompanied with a gradient table in the Supplementary Material. All ^{1}H, ^{13}C and ^{31}P NMR spectra were recorded on a Bruker-AV-III-500-HD instrument. Chemical shifts (δ) are reported in parts per million relative to $CDCl_3$ (^{1}H NMR residual peak at δ =7.26 ppm, ^{13}C NMR residual peak at δ = 77.0 ppm) and coupling constants (*J*) are given in Hz. As a general note for NMR characterization, protons in ^{1}H NMR were coupled to ^{13}C resulting in a doubling of peaks corresponding to the ^{13}C oleyl chain. A ^{1}H and ^{13}C NMR of ^{13}C oleic acid is provided as a reference. High resolution mass measurements were acquired on an Agilent 6550 iFunnel LC/Q-TOF mass spectrometer (Agilent Technologies). Compounds 1-4 were synthesized according to previously reported methods in Chapter 3. Gradient tables for flash purification on a Biotage instrument are also referenced to Chapter 3.

4.4.2 Cell and Liposome Preparation

HeLa (ATTC #CCL-2) were cultured in DMEM (Gibco) supplemented with 10% (v/v) inactivated fetal bovine serum (Atlanta Biologicals), and 1% penicillin-streptomycin solution (Gibco). The liposomes were prepared by transferring the ^{13}C di-labeled 18:1/18:1 PG in chloroform to a sterile glass vessel and evaporating the solvent using a stream of nitrogen gas for 40 min. The lipid film was then dispersed in sterile PBS to obtain a 5 mM concentration. After hydrating the lipid film for 1 h on ice and following vortexing for 5 min, the multivesicular liposomes were then sonicated for 40 min at 4°C under nitrogen gas to make small unilamellar liposomes using a Branson sonifier set at duty cycle 70 and output control 3. They were then

centrifuged at 16,000 x g for 30 min to remove titanium particles and multilamellar liposomes. Cells were treated with liposomes when they reached 70-80% confluency. Prior to treatment, medium was replaced with fresh medium. Cells were incubated for 24 h at 37 °C with increasing concentrations (25, 50, or 100 uM) of di-18:1(^{13}C) PG. Following incubation, cells were washed with sterile PBS, harvested using Trypsin-EDTA, and twice resuspended in PBS and spun at 2000 rpm for 5 minutes at RT. Cell pellets were snap frozen on dry ice/acetone and stored at -80 °C.

4.4.3 HILIC/MS-MS Analysis

Sample preparation followed the procedure described by Vosse, *et al.* In summary, cell pellets were suspended in 0.2 mL water containing 0.1% NH_4Ac. Transfer to a 15 mL Falcon tube. 1.5 mL of methanol and 5 mL MTBE was added and shaken for 1 hour at room temperature. An additional 1.5 mL water was then added and shaken for 10 more minutes. The mixture was centrifuged at 1,430 x g for 5 minutes. The lipids were located in the upper phase. The lipid phase was transfered to a new 15 mL Falcon tube where it was Speedvac dried at room temperature. The dried lipids were reconstituted in 1 mL MTBE (750 µL): MeOH (250 µL) and diluted in a 1:20 (50 µL sample: 950 µL buffer) ration in 97% ACN:3% NH_4Ac (35 mM) and pH adjusted to 5.75. Samples were then submitted for HPLC-MS analysis. Samples were quantitated for acyl-PG, BMP, PG, and lyso-PG by HPLC/MS-MS. Separations were performed on an Agilent Rapid Res 1200 HPLC system using an iHILIC-Fusion (2.1 x 150 mm, 3.5 µm) column (Nest Group P/N 110.152.0310). Mobile phase A was water NH_4Ac 35 mM, pH 5.75 and mobile phase B was acetonitrile. Initial conditions were 3:97 A:B, held for 0.5 min, followed by a linear gradient to 25:75 at 26.5 minutes, followed by a linear gradient to 40:60 at 27 minutes, followed by a hold to 33 min. Column re-equilibration was performed by returning to 3:97 A:B at 35 minutes and held until 45 minutes. Column flow rate was 0.3 mL/min. Analytes were quantified by MS/MS utilizing

an Agilent 6460 triple quadrupole mass spectrometer with negative electrospray ionization (ESI). Quantitation was based on Multiple Reaction Monitoring (MRM) (Table 4.1).

Table 4.1. Precursor and product ions measured for each lipid species upon HILIC/MS-MS analysis. The isotopes of carbon listed are for each carbon on the respective chain. For example, the BMP/PG mono-labeled compound contains one fully labeled ^{13}C and one ^{12}C oleyl chain.

Compound Group	Precursor Ion	Product Ion	Polarity
Acyl-PG Unlabeled ($^{12}C/^{12}C/^{12}C$, 18:1/18:1/18:1)	1037.7	281.2	Negative
Acyl-PG Labeled ($^{13}C/^{12}C/^{12}C$, 18:1/18:1/18:1)	1055.7	281.2	Negative
BMP/PG unlabeled (Standards) ($^{12}C/^{12}C$, 18:1/18:1)	773.4	281.2	Negative
BMP/PG di-labeled ($^{13}C/^{13}C$, 18:1/18:1)	809.4	299.2	Negative
BMP/PG mono-labeled ($^{13}C/^{12}C$, 18:1/18:1)	791.4	299.2	Negative
Lyso-PG (Standard) (^{12}C, 18:1)	509.2	281.2	Negative
Lyso-PG labeled (^{13}C, 18:1)	527.2	299.2	Negative

4.4.4 Synthesis of (S)-3-((4-methoxybenzyl)oxy)propane-1,2-diyl dioleate (5a).

In an oven dried 100 mL three-neck round bottom flask was placed **4** (0.79 g, 1.7 mmol) and oleic acid (0.500 g, 1.7 mmol). The contents of the flask were treated with three cycles of vacuum/Ar and the flask was equipped with an Ar balloon and dry DCM (15 mL) was added. A solution of DCC (0.52 g, 2.5 mmol) and DMAP (0.31 g, 2.5 mmol) in dry DCM (15 mL) was prepared in a separate 100 mL round bottom flask equipped with an Ar balloon. This solution was transferred to the three-neck reaction flask via a cannula and stirred at 20 °C for 16 h. The formed salt was removed by vacuum filtration through a coarse glass frit containing Celite and the resulting filtrate was collected and concentrated under reduced pressure. To the crude product was added a minimal amount of hexane and the mixture was sonicated to dissolve the solid. The resulting solution was purified on a 4 cm diameter, 32 cm long manual silica gel column (hexane:EtOAc) to yield the desired product as a clear colorless oil in 79 % yield. The use of a

shorter column resulted in co-elution of oleic acid. A Biotage method was also developed for this procedure (hexane:EtOAc) (Refer to Table 3.10 for gradient); Rf=0.63 (hexane:EtOAc, 8:2); ^{1}H NMR (500 MHz, $CDCl_3$) δ 7.25 – 7.20 (m, 2H), 6.91 – 6.83 (m, 2H), 5.57 – 5.42 (m, 1H), 5.39 – 5.29 (m, 2H), 5.26 – 5.15 (m, 2H), 4.52 – 4.41 (m, 2H), 4.32 (dd, *J* = 11.9, 3.8 Hz, 1H), 4.17 (dd, *J* = 11.9, 6.5 Hz, 1H), 3.80 (s, 3H), 3.55 (dd, *J* = 5.2, 1.9 Hz, 2H), 2.44 (tt, *J* = 7.5, 4.0 Hz, 1H), 2.27 (dd, *J* = 8.0, 7.2 Hz, 2H), 2.22 – 2.09 (m, 3H), 2.06 – 1.96 (m, 4H), 1.88 (s, 2H), 1.57 (s, 4H), 1.53 – 1.35 (m, 11H), 1.35 – 1.23 (m, 21H), 1.23 – 1.06 (m, 10H), 1.06 – 0.93 (m, 2H), 0.88 (t, *J* = 6.9 Hz, 3H), 0.75 (tdd, *J* = 7.4, 5.5, 4.5 Hz, 2H). ^{13}C NMR (126 MHz, $CDCl_3$) δ 173.6, 173.4, 173.2, 172.9, 159.3, 130.6, 130.6, 130.3, 130.1, 130.0, 129.8, 129.7, 129.6, 129.4, 129.3, 129.1, 129.1, 113.8, 77.3, 77.0, 76.8, 73.0, 70.0, 67.9, 62.7, 55.3, 34.7, 34.4, 34.2, 34.1, 33.9, 32.2, 32.0, 32.0, 31.9, 31.8, 31.7, 31.7, 31.6, 31.5, 30.1, 30.0, 29.9, 29.8, 29.7, 29.7, 29.6, 29.5, 29.5, 29.4, 29.4, 29.3, 29.2, 29.2, 29.1, 29.0, 28.9, 28.9, 28.7, 27.5, 27.3, 27.2, 27.1, 27.0, 26.9, 25.3, 25.2, 25.1, 25.0, 24.9, 24.8, 24.7, 24.7, 24.6, 24.5, 23.0, 22.7, 22.4, 14.3, 14.1, 14.0.

4.4.5 Synthesis of (S)-1-((4-Methoxybenzyl)oxy)-3-(palmitoyloxy)propan-2-yl oleate (5b).

In an oven dried 100 mL three-neck round bottom flask was placed **3** (0.34 g, 1.6 mmol) and oleic acid (1.0 g, 3.3 mmol). The contents of the flask were treated with three cycles of vacuum/Ar and the flask was equipped with an Ar balloon and dry DCM (15 mL) was added. A solution of DCC (0.76 g, 3.7 mmol) and DMAP (0.45 g, 3.7 mmol) in dry DCM (15 mL) was prepared in a separate 100 mL round bottom flask equipped with an Ar balloon. This solution was transferred to the three-neck reaction flask via a cannula and stirred at 20 °C for 16 h. The formed salt was removed by vacuum filtration through a coarse glass frit containing Celite and the resulting filtrate was collected and concentrated under reduced pressure. To the crude product was added a minimal amount of hexane and the mixture was sonicated to dissolve the solid. The resulting solution was

purified on a 4 cm diameter, 32 cm long manual silica gel column (hexane:EtOAc) to yield the desired product as a clear colorless oil in 87 % yield. The use of a shorter column resulted in co-elution of oleic acid. A Biotage method was also developed for this procedure (hexane:EtOAc) (Refer to Table 3.10 for gradient); Rf=0.63 (hexane:EtOAc, 8:2); ^{1}H NMR (500 MHz, $CDCl_3$) δ 7.25 – 7.21 (m, 2H), 6.89 – 6.85 (m, 2H), 5.56 – 5.40 (m, 2H), 5.28 – 5.14 (m, 3H), 4.52 – 4.40 (m, 2H), 4.33 (ddd, *J* = 11.9, 3.8, 2.7 Hz, 1H), 4.17 (ddd, *J* = 11.9, 6.4, 3.2 Hz, 1H), 3.80 (s, 3H), 3.55 (dd, *J* = 5.2, 1.9 Hz, 2H), 2.41 (dtq, *J* = 18.8, 7.5, 3.8 Hz, 2H), 2.15 (ddt, *J* = 19.9, 8.3, 4.4 Hz, 6H), 1.96 – 1.81 (m, 4H), 1.80 – 1.65 (m, 2H), 1.54 – 1.29 (m, 23H), 1.29 – 1.05 (m, 21H), 1.00 (tdd, *J* = 7.4, 5.5, 4.4 Hz, 3H), 0.75 (tdd, *J* = 7.4, 5.5, 4.5 Hz, 3H). ^{13}C NMR (126 MHz, $CDCl_3$) δ 173.6, 173.3, 173.2, 172.9, 159.3, 130.6, 130.6, 130.3, 130.1, 130.0, 129.8, 129.7, 129.6, 129.4, 129.3, 129.1, 129.1, 113.8, 77.3, 77.0, 76.8, 73.0, 70.0, 67.9, 65.7, 65.6, 65.4, 62.7, 55.3, 34.7, 34.5, 34.4, 34.2, 34.0, 33.9, 33.7, 32.2, 32.1, 32.0, 32.0, 31.9, 31.8, 31.7, 31.7, 31.6, 31.5, 30.1, 30.0, 29.9, 29.9, 29.8, 29.7, 29.7, 29.6, 29.5, 29.5, 29.4, 29.3, 29.2, 29.2, 29.1, 29.0, 28.9, 28.8, 28.7, 27.7, 27.5, 27.3, 27.2, 27.1, 27.0, 27.0, 26.9, 26.9, 26.7, 26.4, 26.3, 25.3, 25.2, 25.1, 25.0, 24.9, 24.8, 24.7, 24.7, 24.6, 24.6, 24.5, 23.0, 22.7, 22.4, 14.3, 14.0.

4.4.6 Synthesis of (S)-3-Hydroxypropane-1,2-diyl dioleate (6a).

In a 100 mL round bottom flask was placed **5a** (0.9 mmol, 0.664 g) and DCM/H_2O (15 mL, 5% H_2O). Following the addition of DDQ (0.30 g, 1.3 mmol), the reaction flask was completely wrapped in aluminum foil and stirred at 20 °C for 1 h. The reaction mixture turned from dark green to a dark shade of red. The mixture was diluted with DCM and vacuum filtered through a coarse glass frit with Celite. The collected filtrate was washed with saturated $NaHCO_3$ solution (40 mL), swirling gently to mix. The organic layer was washed again with $NaHCO_3$ (80 mL) and swirled vigorously to mix. Again, the organic layer was washed with $NaHCO_3$ (2 × 100 mL), this

time shaken to combine. The resulting organic solution was dried with anhydrous Na_2SO_4 before concentration under reduced pressure. The crude product was purified on a Biotage flash purification system (hexane:EtOAc) to yield the desired product as a clear colorless oil in a 55% yield (Refer to Table 3.11 for gradient); R_f=0.36 (hexane:EtOAc, 8:2); ^{1}H NMR (500 MHz, $CDCl_3$) δ 5.55 – 5.42 (m, 1H), 5.39 – 5.31 (m, 2H), 5.26 – 5.14 (m, 1H), 5.11 – 5.03 (m, 1H), 4.36 – 4.20 (m, 2H), 3.72 (q, *J* = 3.6 Hz, 2H), 2.46 (tq, *J* = 7.5, 3.7 Hz, 1H), 2.32 (t, *J* = 7.6 Hz, 2H), 2.21 (tq, *J* = 7.5, 3.7 Hz, 1H), 2.14 (d, *J* = 11.2 Hz, 2H), 2.06 – 1.96 (m, 5H), 1.94 – 1.83 (m, 2H), 1.76 (dt, *J* = 8.3, 4.1 Hz, 1H), 1.67 – 1.56 (m, 2H), 1.55 – 1.35 (m, 10H), 1.35 – 1.23 (m, 20H), 1.23 – 1.06 (m, 9H), 1.05 – 0.95 (m, 2H), 0.88 (t, *J* = 6.9 Hz, 3H), 0.75 (tdd, *J* = 7.4, 5.5, 4.5 Hz, 1H). ^{13}C NMR (126 MHz, $CDCl_3$) δ 174.1, 174.0, 173.8, 173.6, 173.2, 130.6, 130.6, 130.3, 130.1, 130.0, 129.8, 129.7, 129.6, 129.4, 129.1, 77.3, 77.0, 76.8, 72.1, 62.0, 61.6, 34.6, 34.5, 34.4, 34.2, 34.1, 33.9, 33.7, 32.2, 32.1, 32.0, 32.0, 31.9, 31.8, 31.8, 31.7, 31.6, 31.5, 30.1, 30.0, 30.0, 29.9, 29.9, 29.8, 29.7, 29.7, 29.6, 29.5, 29.5, 29.4, 29.4, 29.3, 29.2, 29.1, 29.0, 29.0, 28.9, 28.8, 28.7, 28.6, 27.5, 27.5, 27.3, 27.2, 27.2, 27.1, 27.0, 26.9, 26.9, 26.8, 26.6, 25.3, 25.2, 25.1, 25.0, 24.9, 24.9, 24.7, 24.7, 24.6, 24.5, 23.0, 22.7, 22.4, 14.3, 14.1, 14.0.

(S)-1-Hydroxy-3-(palmitoyloxy)propan-2-yl oleate (6b). Clear oil in 57% yield; R_f=0.36 (Hexane:EtOAc, 8:2); ^{1}H NMR (500 MHz, $CDCl_3$) δ 5.58 – 5.43 (m, 2H), 5.27 – 5.15 (m, 2H), 5.12 – 5.02 (m, 1H), 4.36 – 4.17 (m, 2H), 3.73 (dd, *J* = 5.0, 1.8 Hz, 2H), 2.46 (ddp, *J* = 11.4, 7.5, 3.8 Hz, 2H), 2.20 (dtt, *J* = 10.3, 6.5, 3.3 Hz, 2H), 2.13 (s, 4H), 1.75 (s, 4H), 1.57 – 1.30 (m, 23H), 1.30 – 1.06 (m, 21H), 1.00 (tdd, *J* = 7.4, 5.5, 4.5 Hz, 3H), 0.75 (tdd, *J* = 7.4, 5.6, 4.5 Hz, 3H). ^{13}C NMR (126 MHz, $CDCl_3$) δ 174.0, 173.6, 173.5, 173.2, 130.6, 130.6, 130.3, 130.1, 130.0, 129.8, 129.7, 129.6, 129.4, 129.1, 129.1, 77.3, 77.0, 76.8, 72.1, 65.7, 65.6, 65.5, 65.4, 62.0, 61.6, 34.6, 34.5, 34.4, 34.2, 34.0, 33.9, 33.7, 32.2, 32.1, 32.0, 32.0, 31.9, 31.8, 31.7, 31.7, 31.6, 31.5, 30.1,

30.0, 29.9, 29.9, 29.8, 29.7, 29.7, 29.6, 29.5, 29.5, 29.4, 29.3, 29.3, 29.2, 29.1, 29.0, 29.0, 28.9, 28.8, 28.6, 27.5, 27.4, 27.3, 27.2, 27.2, 27.1, 27.0, 26.9, 26.9, 26.8, 26.7, 26.6, 26.4, 25.2, 25.2, 25.0, 24.9, 24.8, 24.7, 24.7, 24.6, 24.6, 24.4, 23.0, 22.7, 22.4, 14.3, 14.0.

4.4.7 Synthesis of (R)-2,3-Bis(oleoyloxy)propyl phosphonate (7a).

In an oven dried 10 mL, 2-neck round bottom flask equipped with a stir bar was placed alcohol **6b** (0.23 mmol, 0.15 g). The flask was then dried using Schlenk techniques followed by the attachment of an Ar balloon. The starting material was then dissolved in dry pyridine (4 mL) and the solution was cooled to 0 °C in an ice bath. Diphenyl phosphite (0.27 mL, 1.4 mmol) was added dropwise and the solution was stirred for 1 h. The solution was then allowed to warm to room temperature where a 1:1 H_2O:Et_3N solution (5 mL) was added to the round bottom flask where it was stirred for an additional 1 h. The pyridine was removed from the solution under reduced pressure by azeotropically drying 3 times with toluene. The crude oil was then dissolved with DCM (30 mL) and washed with saturated $NaHCO_3$ (3 x 15 mL) where it was dried with anhydrous Na_2SO_4 and concentrated under reduced pressure. The product was purified using a silica gel column to yield a white semi-solid in 95% yield (gradient from 10:0 to 9.5:0.5 $CHCl_3$:MeOH containing 0.5% Et_3N); R_f=0.23 (Hexane:EtOAc, 8:2); ^{1}H NMR (500 MHz, $CDCl_3$) δ 5.48 (s, 1H), 5.39 – 5.28 (m, 2H), 5.21 (q, *J* = 5.0 Hz, 2H), 4.35 (dd, *J* = 11.9, 4.0 Hz, 1H), 4.17 (dd, *J* = 11.9, 6.2 Hz, 1H), 4.09 (dt, *J* = 8.6, 4.8 Hz, 2H), 3.10 (qd, *J* = 7.3, 4.8 Hz, 7H), 2.51 – 2.38 (m, 1H), 2.29 (dd, *J* = 8.0, 7.2 Hz, 2H), 2.23 – 2.16 (m, 1H), 2.13 (s, 2H), 2.05 – 1.96 (m, 3H), 1.88 (s, 2H), 1.65 – 1.54 (m, 2H), 1.38 (t, *J* = 7.3 Hz, 21H), 1.35 – 1.22 (m, 19H), 1.16 (d, *J* = 17.1 Hz, 9H), 1.04 – 0.95 (m, 2H), 0.92 – 0.83 (m, 3H), 0.75 (tdd, *J* = 7.4, 5.6, 4.5 Hz, 1H). ^{13}C NMR (126 MHz, $CDCl_3$) δ 173.6, 173.2, 172.7, 130.6, 130.3, 130.0, 130.0, 129.8, 129.7, 129.6, 129.1, 120.2, 115.4, 77.3, 77.0, 76.8, 65.8, 65.5, 45.8, 34.6, 34.4, 34.3, 34.1, 34.0, 33.8, 32.2, 32.0, 32.0, 31.9, 31.8, 31.7, 31.7, 31.6,

30.1, 30.0, 29.9, 29.8, 29.8, 29.5, 29.5, 29.4, 29.2, 29.2, 29.1, 29.0, 27.5, 27.3, 27.2, 27.1, 27.0, 27.0, 26.9, 26.9, 25.1, 25.0, 24.9, 24.9, 24.8, 24.6, 24.6, 24.5, 23.0, 22.7, 22.4, 14.3, 14.1, 14.0, 8.6, 1.0. ^{31}P NMR (203 MHz, $CDCl_3$) δ 5.80.

(R)-2-(Oleoyloxy)-3-(palmitoyloxy)propyl phosphonate (7b). White semi-solid in 92% yield; R_f=0.23 (Hexane:EtOAc, 8:2); ^{1}H NMR (500 MHz, $CDCl_3$) δ 5.49 (d, *J* = 7.7 Hz, 2H), 5.31 – 5.03 (m, 3H), 4.36 (ddd, *J* = 11.9, 3.8, 2.7 Hz, 1H), 4.16 (ddd, *J* = 11.9, 6.3, 3.2 Hz, 1H), 4.06 – 3.99 (m, 2H), 3.07 (qd, *J* = 7.4, 4.6 Hz, 7H), 2.47 – 2.37 (m, 2H), 2.21 – 2.07 (m, 6H), 1.77 – 1.67 (m, 2H), 1.50 – 1.36 (m, 21H), 1.35 (t, *J* = 7.3 Hz, 15H), 1.24 – 1.08 (m, 20H), 1.00 (tdd, *J* = 7.4, 5.5, 4.4 Hz, 3H), 0.75 (tdd, *J* = 7.3, 5.5, 4.5 Hz, 3H). ^{13}C NMR (126 MHz, $CDCl_3$) δ 173.6, 173.2, 173.1, 172.7, 130.6, 130.5, 130.3, 130.0, 130.0, 129.8, 129.7, 129.6, 129.4, 129.3, 129.1, 129.1, 77.3, 77.0, 76.8, 65.8, 65.5, 65.5, 62.4, 45.7, 34.6, 34.4, 34.3, 34.1, 34.0, 33.9, 33.7, 32.2, 32.1, 32.0, 32.0, 31.9, 31.8, 31.7, 31.7, 31.6, 31.5, 30.1, 30.0, 29.9, 29.8, 29.8, 29.7, 29.7, 29.6, 29.5, 29.5, 29.4, 29.2, 29.2, 29.1, 29.0, 29.0, 28.9, 28.7, 27.5, 27.3, 27.2, 27.1, 27.0, 27.0, 26.9, 26.9, 26.7, 26.4, 25.1, 25.0, 24.9, 24.9, 24.8, 24.7, 24.6, 24.5, 24.4, 23.0, 22.7, 22.4, 14.3, 14.0, 8.6. ^{31}P NMR (203 MHz, $CDCl_3$) δ 4.48.

4.4.8 Synthesis of (2R)-3-(((S)-2,2-dimethyl-1,3-dioxolan-4-yl)methoxy)propane-1,2-dioleyl phosphonate (8a).

To an oven dried 10 mL 2-neck round bottom flask equipped with a stir bar was placed **8a** (0.175 g, 0.22 mmol). The flask was cycled 3 times with vacuum/Ar, and an was balloon attached. Dry pyridine (5 mL) followed by solketal (0.035 mL, 0.27 mmol) was then added. The reaction temperature was lowered to 0 °C via an ice bath and pivaloyl chloride (0.13 mL, 1.1 mmol) was subsequently added dropwise to the reaction. The solution changed from transparent to a colorful violet. The reaction was stirred for 1 h and then warmed slowly to room temperature. Pyridine was

then stripped from the solution azeotropically with toluene under reduced pressure. The crude oil was then redissolved in DCM (30 mL) and the solution was washed with saturated $NaHCO_3$ (2 x 10 mL). The organic layer was then dried with anhydrous Na_2SO_4 and concentrated under reduced pressure. The crude product was then purified on a silica gel column to yield a colorless oil in 85% yield (gradient of 100:0 to 98:2 DCM

:MeOH); R_f=0.34 (Hexane:EtOAc, 8:2); ^{1}H NMR (500 MHz, $CDCl_3$) δ 5.49 (s, 1H), 5.41 – 5.29 (m, 2H), 5.24 (d, *J* = 4.7 Hz, 1H), 4.40 – 3.97 (m, 6H), 3.86 – 3.64 (m, 2H), 2.41 – 2.26 (m, 5H), 2.21 (s, 1H), 2.13 (s, 2H), 2.01 (q, *J* = 6.4 Hz, 4H), 1.88 (s, 2H), 1.62 (d, *J* = 9.3 Hz, 2H), 1.52 – 1.35 (m, 14H), 1.35 – 1.23 (m, 21H), 1.23 – 1.07 (m, 11H), 1.04 – 0.97 (m, 2H), 0.88 (t, *J* = 6.9 Hz, 3H), 0.79 – 0.72 (m, 1H). ^{13}C NMR (126 MHz, $CDCl_3$) δ 174.1, 173.7, 173.2, 173.0, 172.8, 172.5, 130.6, 130.1, 130.0, 129.8, 129.7, 129.6, 129.4, 129.1, 77.3, 77.0, 76.8, 65.7, 65.4, 34.7, 34.5, 34.5, 34.4, 34.2, 34.2, 34.0, 33.9, 33.7, 32.2, 32.0, 31.9, 31.7, 31.7, 31.6, 30.1, 29.8, 29.7, 29.5, 29.5, 29.4, 29.3, 29.3, 29.2, 29.1, 29.0, 29.0, 27.5, 27.2, 27.2, 27.0, 26.9, 25.2, 24.8, 24.6, 23.0, 22.7, 22.4, 14.3, 14.1, 14.0. ^{13}C NMR (126 MHz, $CDCl_3$) δ 174.1, 173.7, 173.2, 173.0, 172.8, 172.5, 130.6, 130.1, 130.0, 129.8, 129.7, 129.6, 129.4, 129.1, 77.3, 77.0, 76.8, 65.7, 65.4, 34.7, 34.5, 34.5, 34.4, 34.2, 34.2, 34.0, 33.9, 33.7, 32.2, 32.0, 31.9, 31.7, 31.7, 31.6, 30.1, 29.8, 29.7, 29.5, 29.5, 29.4, 29.3, 29.3, 29.2, 29.1, 29.0, 29.0, 27.5, 27.2, 27.2, 27.0, 26.9, 25.2, 24.8, 24.6, 23.0, 22.7, 22.4, 14.3, 14.1, 14.0. ^{31}P NMR (203 MHz, $CDCl_3$) δ 8.62, 8.51.

(2R)-1-(((S)-2,2-Dimethyl-1,3-dioxolan-4-yl)methoxy)(hydroxy)-3-(palmitoyloxy)propan-2-oleyl phosphonate (8b). Clear oil in 72% yield; R_f=0.35 (Hexane:EtOAc, 8:2); ^{1}H NMR (500 MHz, $CDCl_3$) δ 5.49 (d, *J* = 4.1 Hz, 2H), 5.31 – 5.03 (m, 3H), 4.43 – 3.94 (m, 9H), 3.90 – 3.62 (m, 2H), 2.45 (s, 2H), 2.19 (d, *J* = 14.1 Hz, 2H), 2.13 (s, 4H), 1.88 (s, 4H), 1.53 – 1.33 (m, 29H), 1.23 – 1.08 (m, 23H), 1.05 – 0.95 (m, 3H), 0.75 (tdd, *J* = 7.4, 5.6, 4.5 Hz, 3H). ^{13}C NMR (126 MHz,

$CDCl_3$) δ 174.0, 173.6, 173.5, 173.4, 173.2, 173.0, 173.0, 172.6, 172.5, 130.6, 130.6, 130.3, 130.1, 130.0, 129.8, 129.7, 129.6, 129.4, 129.1, 129.1, 77.3, 77.0, 76.8, 65.8, 64.1, 34.6, 34.5, 34.4, 34.4, 34.2, 34.2, 34.1, 34.0, 33.9, 33.8, 33.7, 33.6, 32.2, 32.1, 32.0, 32.0, 31.9, 31.8, 31.7, 31.7, 31.6, 31.5, 30.1, 30.0, 29.9, 29.8, 29.7, 29.7, 29.6, 29.5, 29.5, 29.4, 29.4, 29.3, 29.2, 29.2, 29.1, 29.0, 28.9, 28.8, 28.7, 27.5, 27.3, 27.2, 27.1, 27.0, 26.9, 26.7, 25.2, 25.1, 24.9, 24.8, 24.6, 24.6, 24.5, 23.0, 22.7, 22.4, 14.3, 14.0. ^{31}P NMR (203 MHz, $CDCl_3$) δ 8.63, 8.52.

Synthesis of (2R)-3-((((S)-2,3-dihydroxypropoxy)(hydroxy)phosphoryl)oxy)propane-1,2-diyl dioleate (9a).

To a 10 mL round bottom flask was added H-phosphonate **8a** (0.150 g, 0.18 mmol). A 9:1 v/v of H_2O/Pyr. (5 mL) was added to flask and the temperature was lowered to 0 °C. I_2 (0.14 g, 0.55 mmol) was then added, and the reaction warmed to 24 °C with stirring for 3 h. The pyridine was then removed from the solution by azeotropically drying three times with toluene. The resulting oil was then diluted with 45 mL of DCM and washed with a solution of saturated Na_2SO_3 (2 x 10 mL) and once with brine (10 mL). The organic layer was then dried with anhydrous Na_2SO_4 and concentrated under reduced pressure. The crude product was then purified on a manual silica gel column (gradient of 98:2 $CHCl_3$:MeOH to 65:25:4 $CHCl_3$:MeOH:H_2O as parts, not percentages) (Refer to Table 3.4 for gradient). Fractions were collected in 13 x 100 mm cell culture tubes in 72 mL intervals between each change in mobile phase composition (9 mL/fraction). Product appeared from fractions 25 – 32. The isolated product was concentrated under reduced pressure in a 20 mL scintillation vial and then $CHCl_3$ (5 mL) was added to dissolve the oil. After cooling the solution to 0 °C in an ice bath, MeOH (0.1 mL) and TFA (0.5 mL dropwise) were added to the reaction mixture. The reaction was allowed to stir for 30 min at room temperature. Saturated $NaHCO_3$ was then added, and the solution was diluted with $CHCl_3$ (30 mL). The mixture was transferred to a

separatory funnel where MeOH (20 mL) and then H_2O (10 mL) was added followed by shaking. The organic layer was collected, dried with anhydrous Na_2SO_4, and concentrated under reduced pressure. The crude product was then purified using a gradient of 98:2 $CHCl_3$:MeOH to 65:25:4 $CHCl_3$:MeOH:H_2O to yield a white semi-solid in 68% yield; R_f=0.46 ($CHCl_3$:MeOH:H_2O, 65:25:4 as parts, not percentages); ^{1}H NMR (500 MHz, $CDCl_3$) δ 5.48 (s, 1H), 5.39 – 5.27 (m, 2H), 5.20 (d, *J* = 18.9 Hz, 2H), 4.37 (d, *J* = 11.4 Hz, 1H), 4.14 (dd, *J* = 11.5, 6.7 Hz, 1H), 3.92 (d, *J* = 25.3 Hz, 4H), 3.76 – 3.57 (m, 2H), 2.43 (s, 1H), 2.28 (t, *J* = 7.6 Hz, 2H), 2.18 (s, 1H), 2.13 (s, 2H), 2.00 (q, *J* = 6.7 Hz, 3H), 1.88 (s, 2H), 1.57 (q, *J* = 7.2 Hz, 2H), 1.51 – 1.35 (m, 9H), 1.35 – 1.22 (m, 19H), 1.22 – 1.06 (m, 9H), 1.03 – 0.96 (m, 2H), 0.88 (t, *J* = 6.8 Hz, 3H), 0.75 (tt, *J* = 7.4, 3.6 Hz, 1H). ^{13}C NMR (126 MHz, $CDCl_3$) δ 173.9, 173.4, 130.6, 130.2, 130.0, 129.9, 129.8, 129.7, 129.6, 129.4, 129.1, 129.0, 77.3, 77.0, 76.8, 34.6, 34.3, 34.2, 33.9, 33.7, 32.2, 32.1, 32.0, 32.0, 31.9, 31.8, 31.8, 31.7, 31.6, 31.5, 30.1, 30.0, 29.9, 29.8, 29.7, 29.6, 29.5, 29.4, 29.4, 29.3, 29.2, 29.1, 29.1, 29.0, 28.9, 28.8, 28.7, 27.5, 27.4, 27.3, 27.2, 27.0, 26.9, 25.2, 25.0, 24.9, 24.8, 24.7, 24.6, 24.5, 23.0, 22.7, 22.4, 14.3, 14.1, 14.0. ^{31}P NMR (203 MHz, $CDCl_3$) δ -0.64.

(2R)-1-((((S)-2,3-Dihydroxypropoxy)(hydroxy)phosphoryl)oxy)-3-(palmitoyloxy)propan-2-yl oleate (9b). A white semi-solid in 70% yield; R_f = 0.46 ($CHCl_3$:MeOH:H_2O, 65:25:4 as parts, not percentages). ^{1}H NMR (500 MHz, $CDCl_3$) δ 5.45 (dt, *J* = 9.8, 4.6 Hz, 2H), 5.16 (dtt, *J* = 11.7, 8.8, 4.0 Hz, 3H), 4.32 (dt, *J* = 12.2, 2.8 Hz, 1H), 4.15 – 4.03 (m, 1H), 3.92 (dq, *J* = 20.0, 7.6 Hz, 5H), 3.75 – 3.55 (m, 2H), 2.50 (s, 4H), 2.39 (p, *J* = 5.7 Hz, 2H), 2.12 (ddd, *J* = 16.0, 8.0, 4.3 Hz, 6H), 1.67 (s, 2H), 1.54 – 1.26 (m, 22H), 1.26 – 1.02 (m, 21H), 0.96 (ddd, *J* = 9.9, 8.2, 6.1 Hz, 3H), 0.76 – 0.65 (m, 3H). ^{13}C NMR (126 MHz, $CDCl_3$) δ 174.3, 174.1, 173.8, 173.7, 130.6, 130.5, 130.3, 130.2, 130.0, 129.9, 129.9, 129.8, 129.7, 129.6, 129.6, 129.3, 129.2, 129.0, 129.0, 77.3, 77.1, 76.8, 70.4, 63.8, 62.6, 49.8, 49.6, 49.4, 49.3, 49.1, 36.8, 34.5, 34.3, 34.2, 34.0, 33.9, 33.7,

33.6, 32.2, 32.0, 32.0, 31.9, 31.9, 31.7, 31.7, 31.6, 31.6, 31.5, 30.0, 30.0, 29.9, 29.8, 29.7, 29.6, 29.5, 29.4, 29.4, 29.2, 29.2, 29.1, 29.0, 28.8, 28.6, 27.4, 27.3, 27.2, 27.1, 27.0, 26.8, 26.3, 25.0, 24.9, 24.8, 24.7, 24.5, 24.4, 24.3, 22.9, 22.6, 22.3, 14.2, 14.0, 13.9. ^{31}P NMR (203 MHz, $CDCl_3$) δ -3.19.

4.4.9 NMR of All Compounds. Red Indicates ^{13}C label.

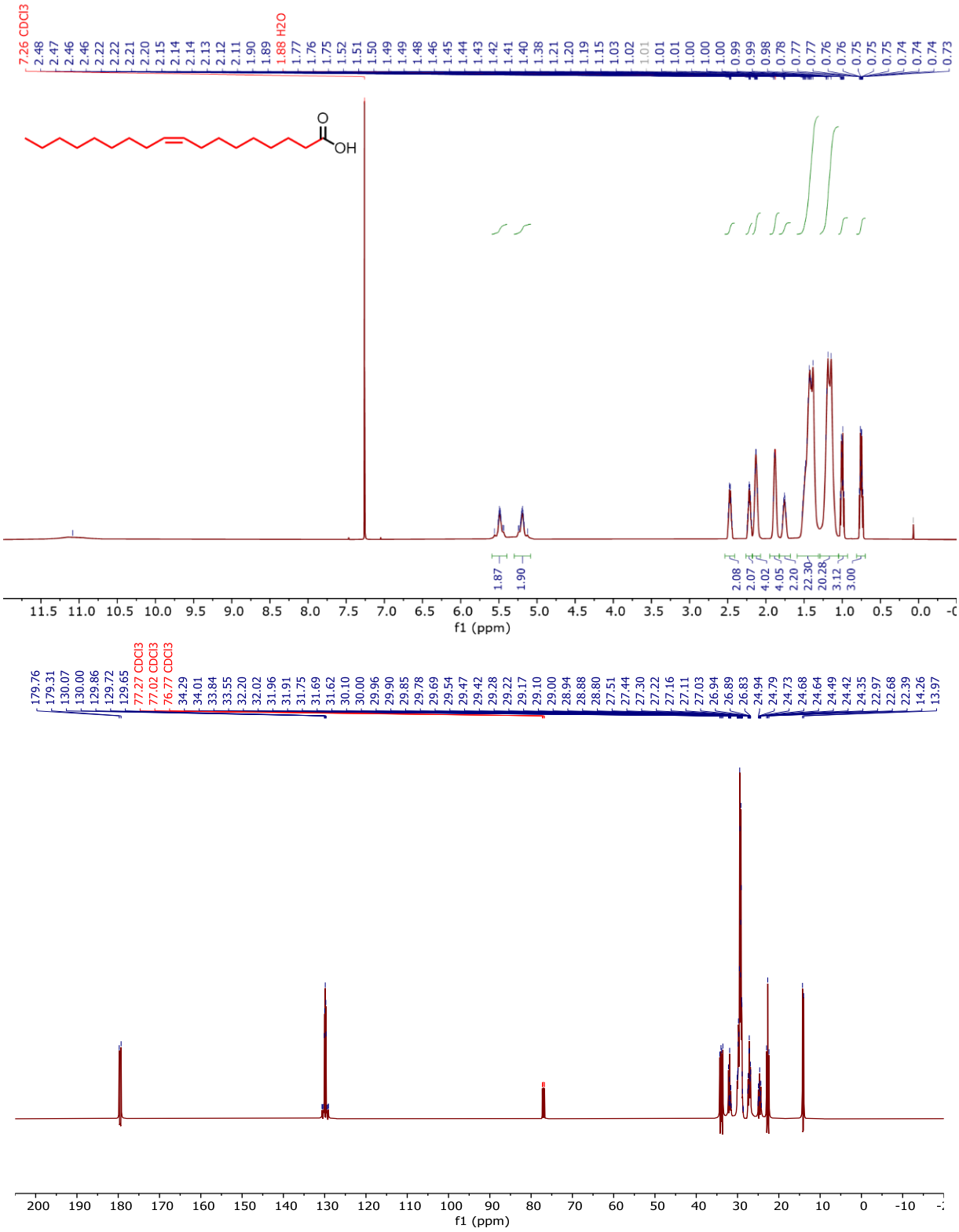

Figure 4.13. ^{1}H and ^{13}C NMR of ^{13}C Oleic Acid.

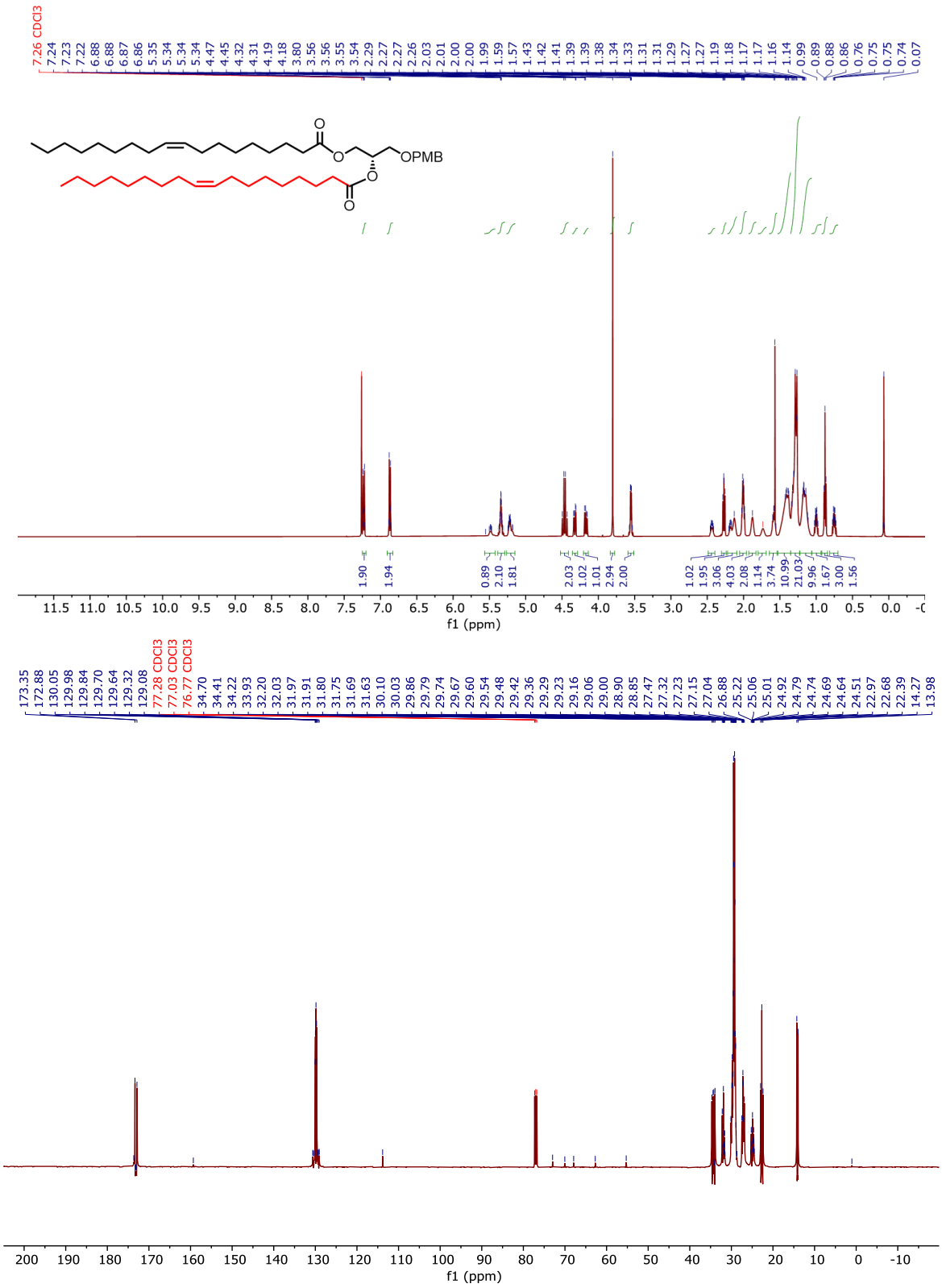

Figure 4.14. ^{1}H and ^{13}C NMR of **5a**.

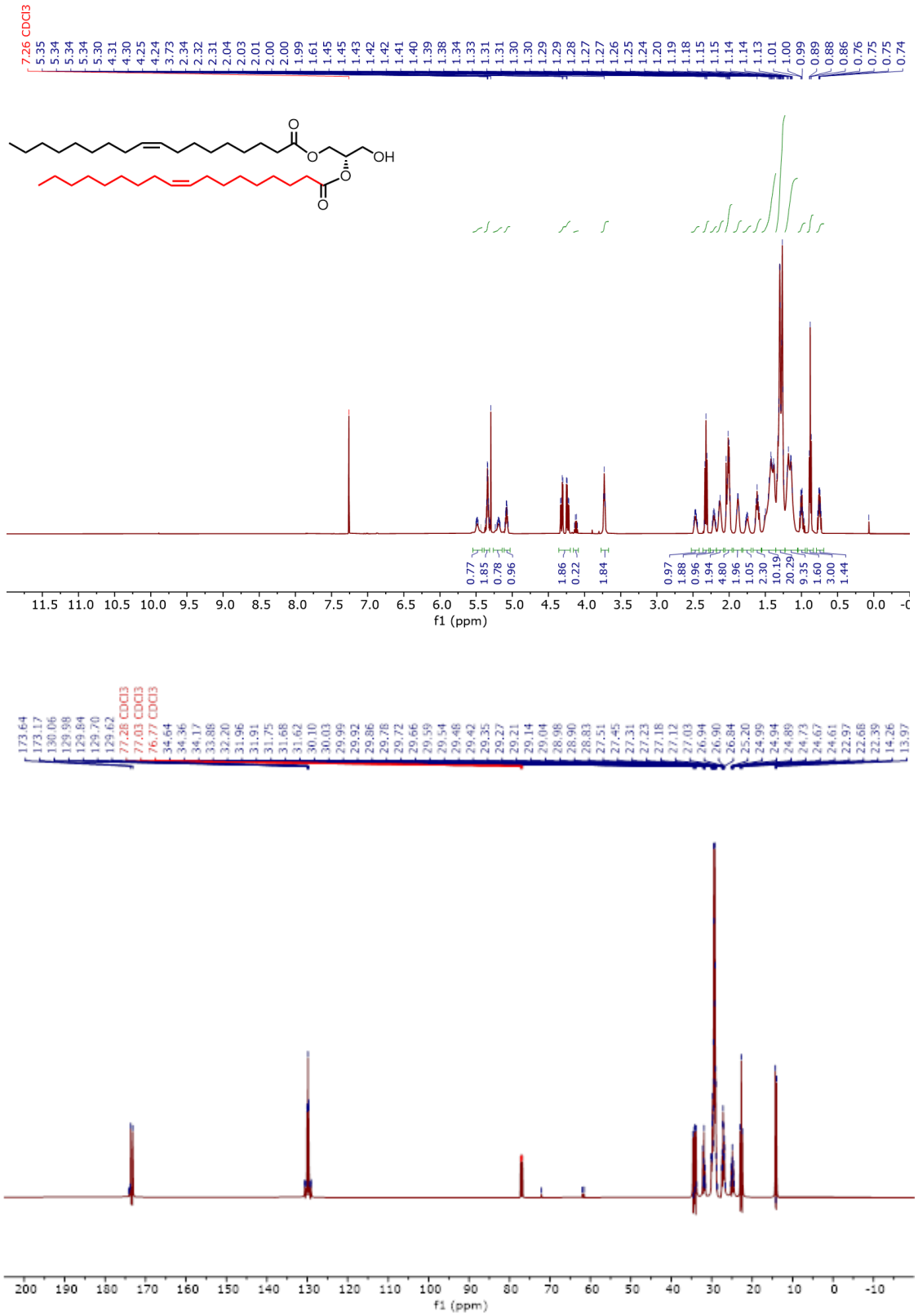

Figure 4.15. ^{1}H and ^{13}C NMR of **6a**.

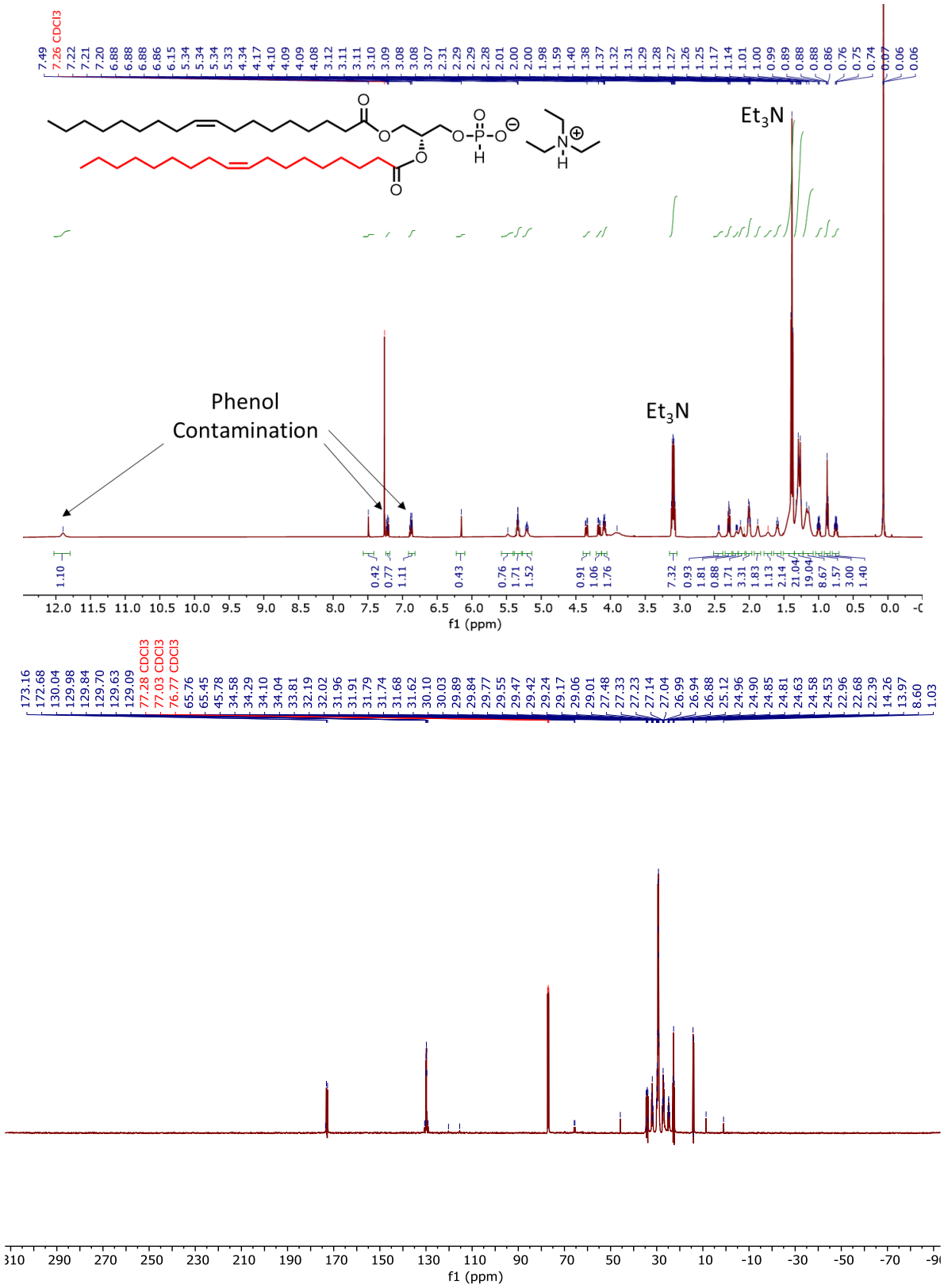

Figure 4.16. ^{1}H, ^{13}C, and ^{31}P NMR of ^{13}C **7a**.

Figure 4.16 continued.

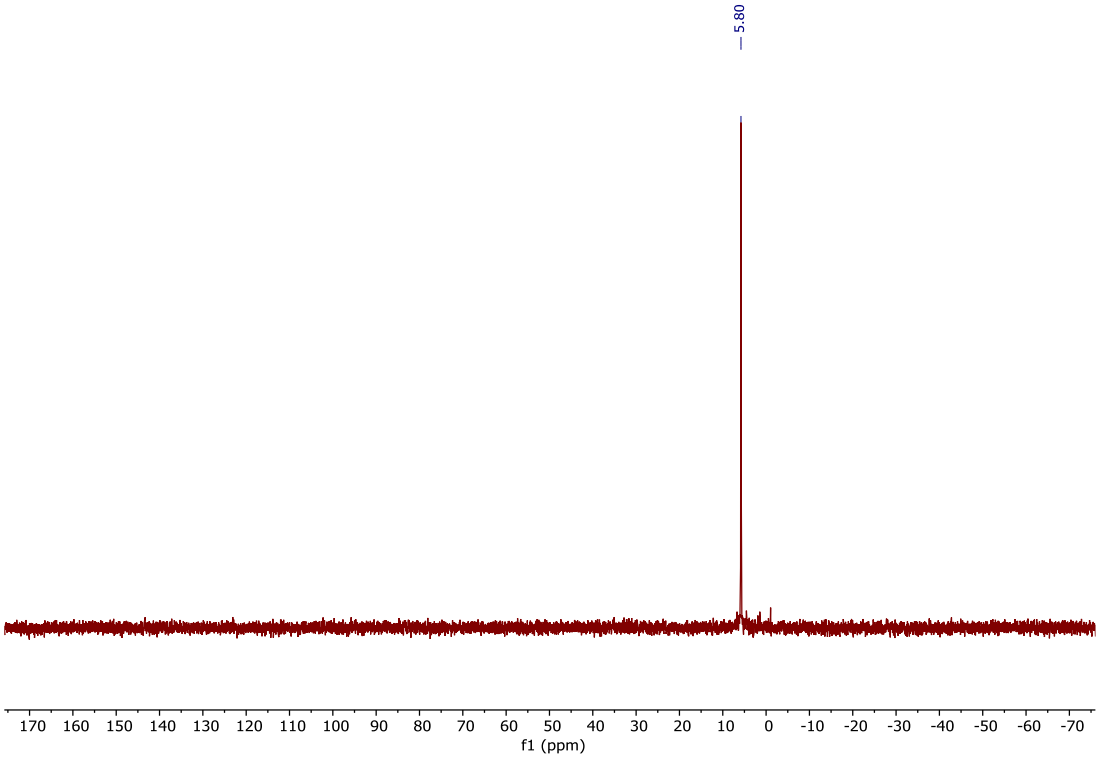

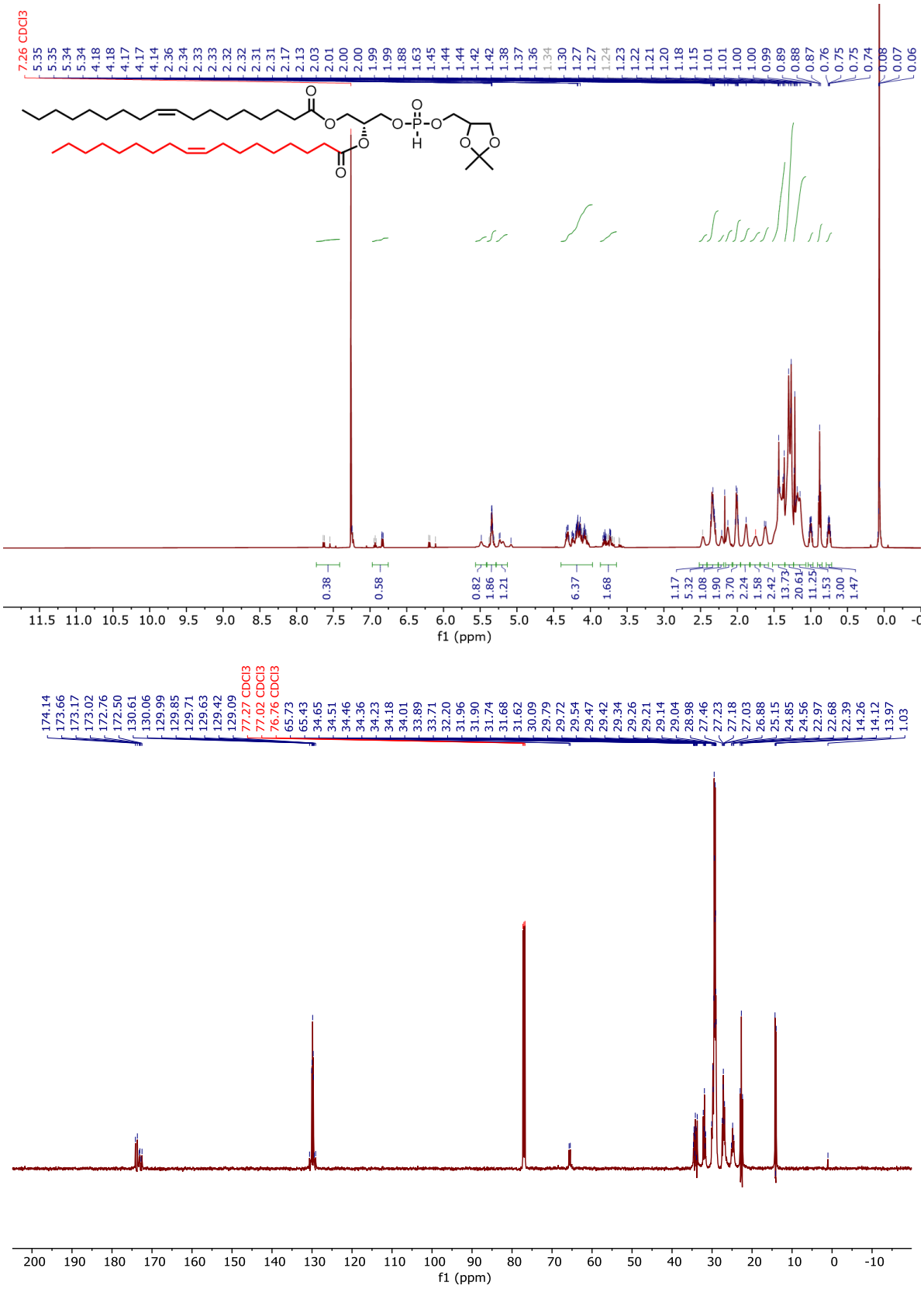

Figure 4.17. ^{1}H, ^{13}C, and ^{31}P NMR of ^{13}C **8a**.

Figure 4.17 continued.

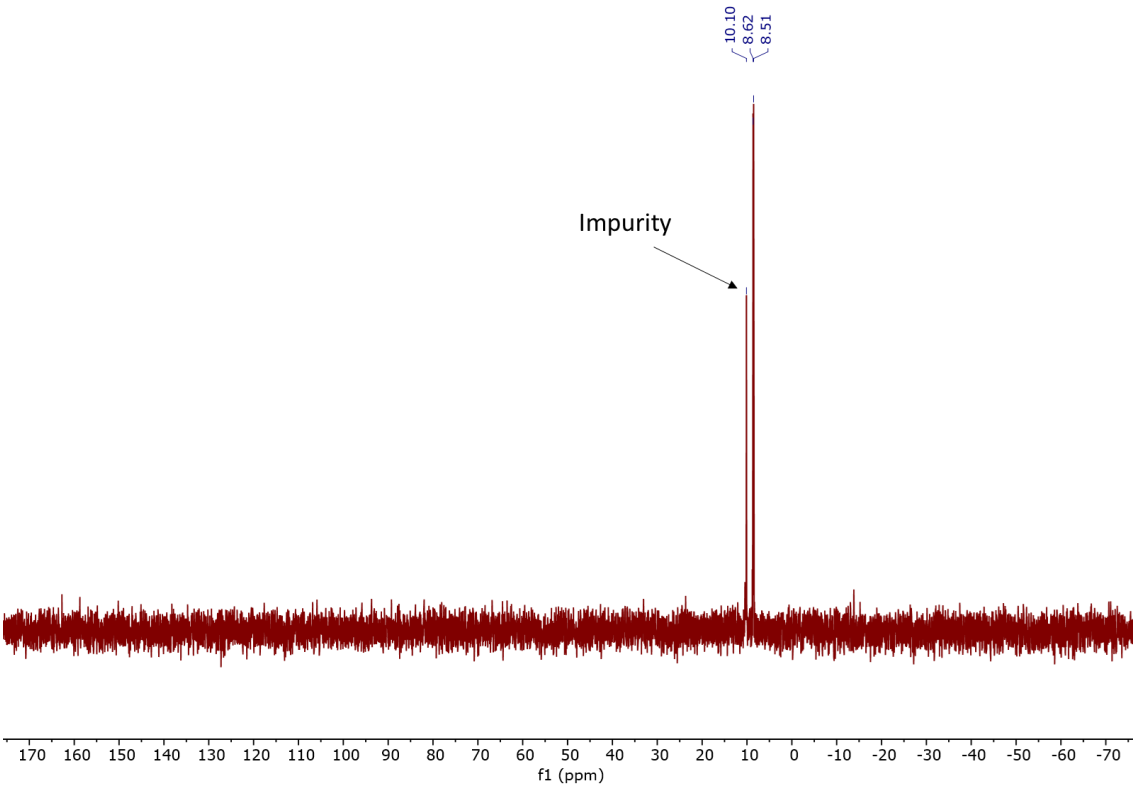

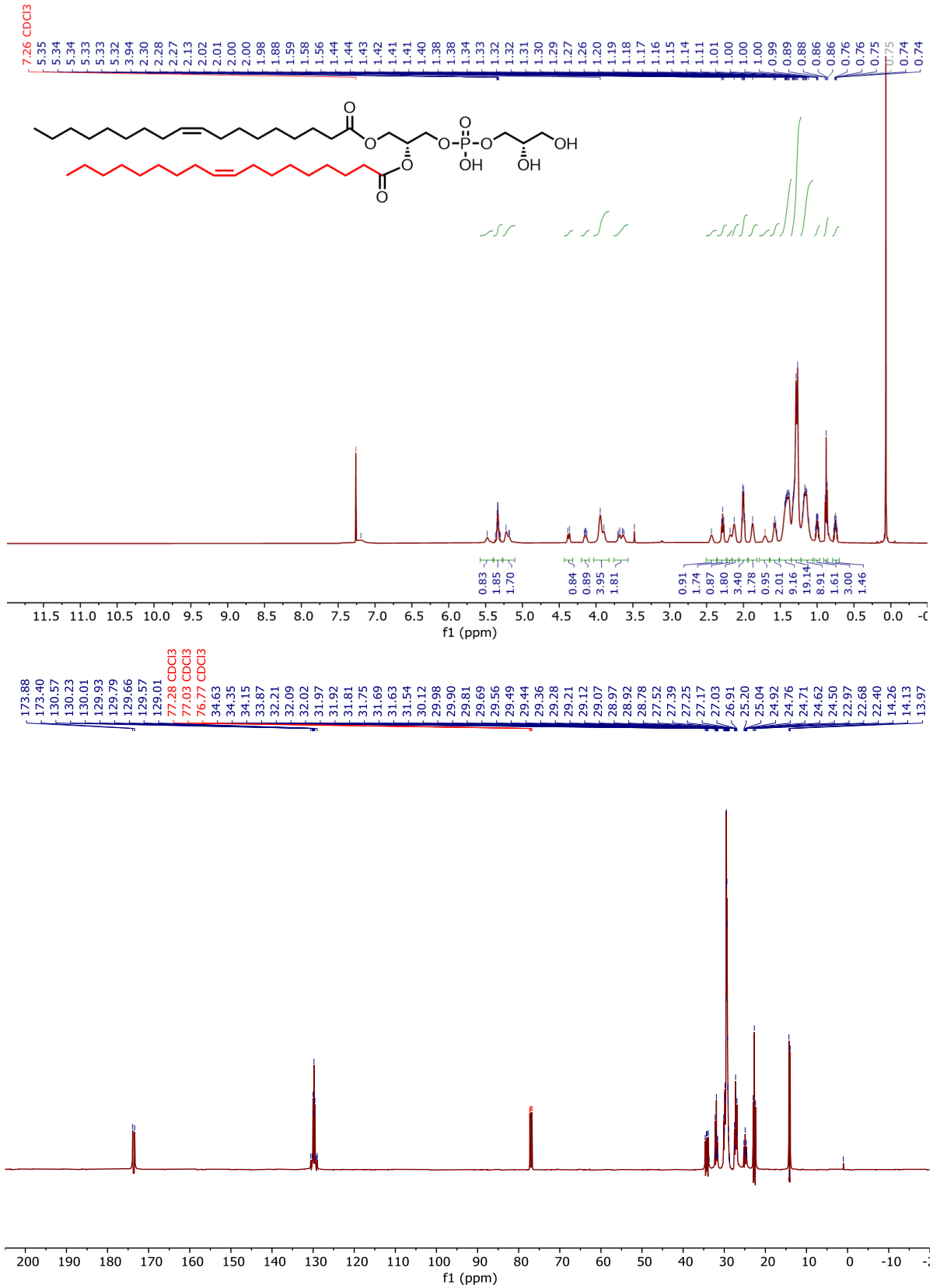

Figure 4.18. ^{1}H, ^{13}C, and ^{31}P NMR of ^{13}C **9a**.

Figure 4.18 continued.

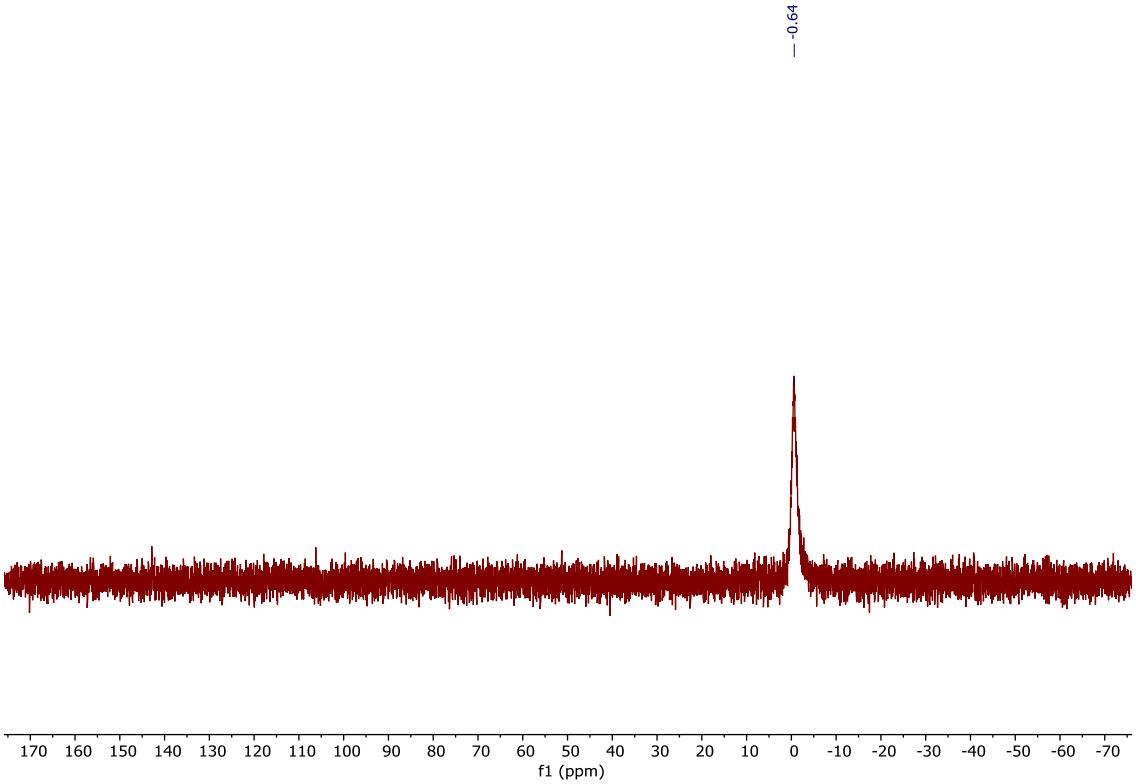

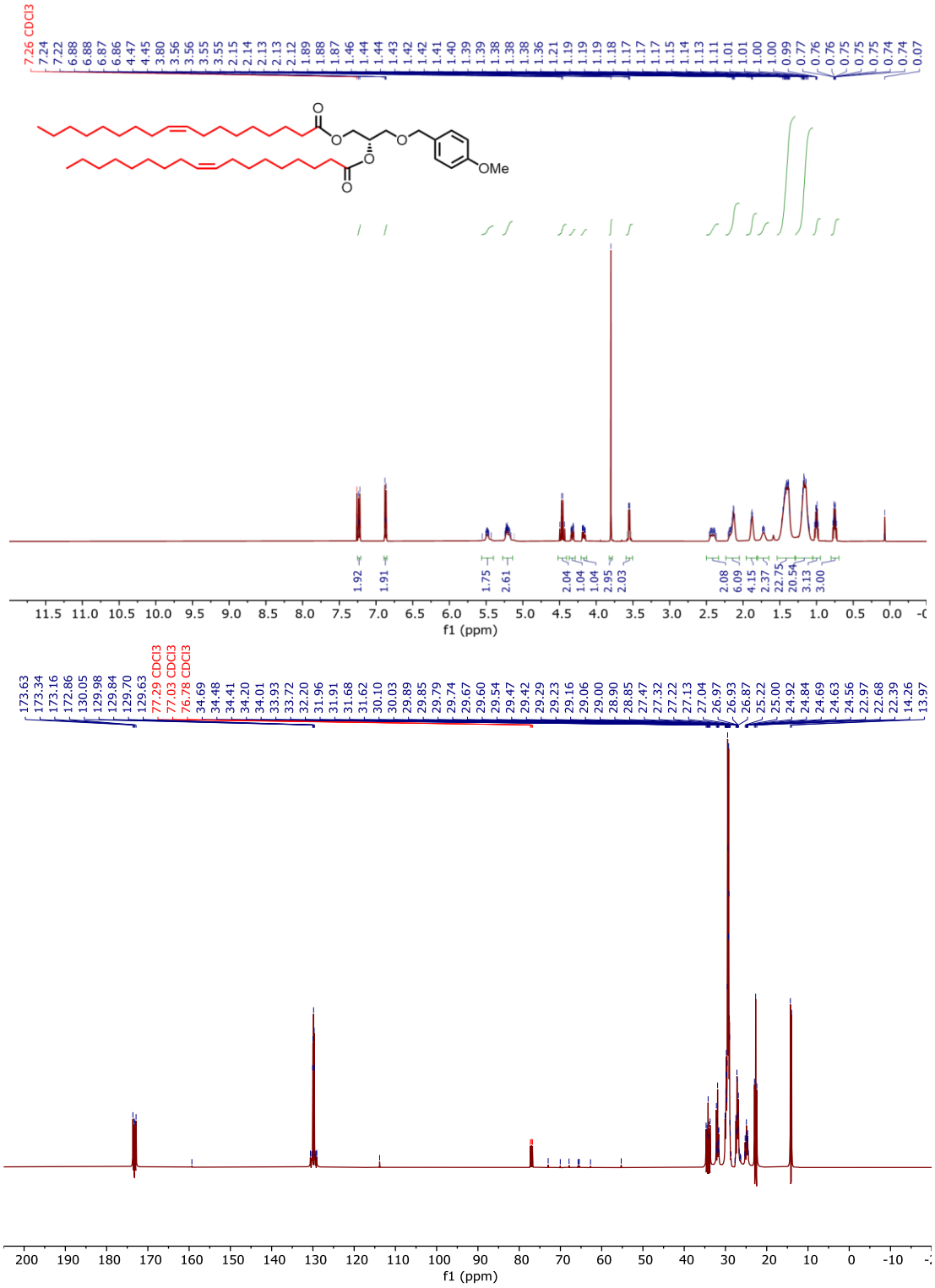

Figure 4.19. ^{1}H and ^{13}C NMR of **5b**.

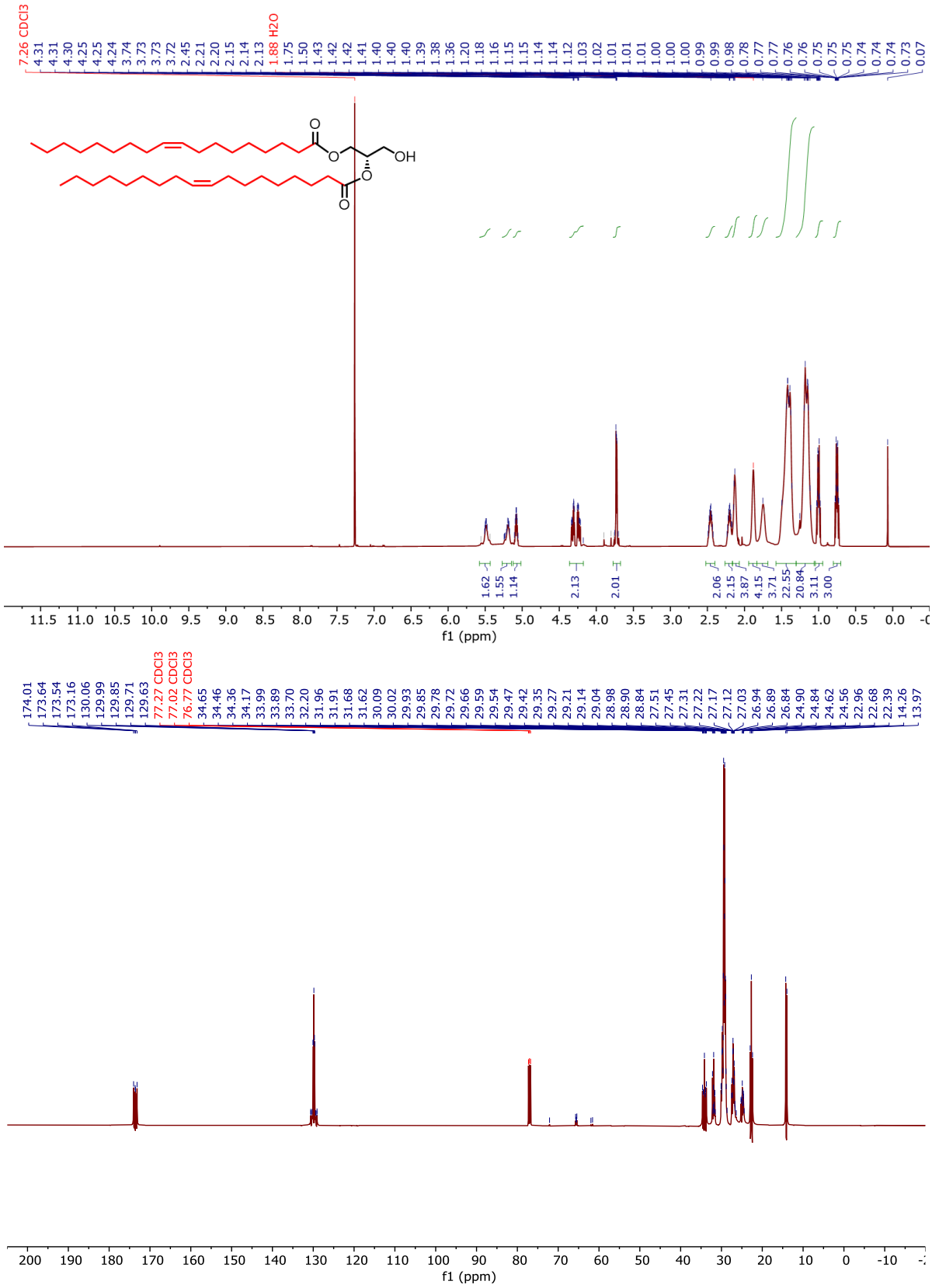

Figure 4.20. ^{1}H and ^{13}C NMR of **6b**.

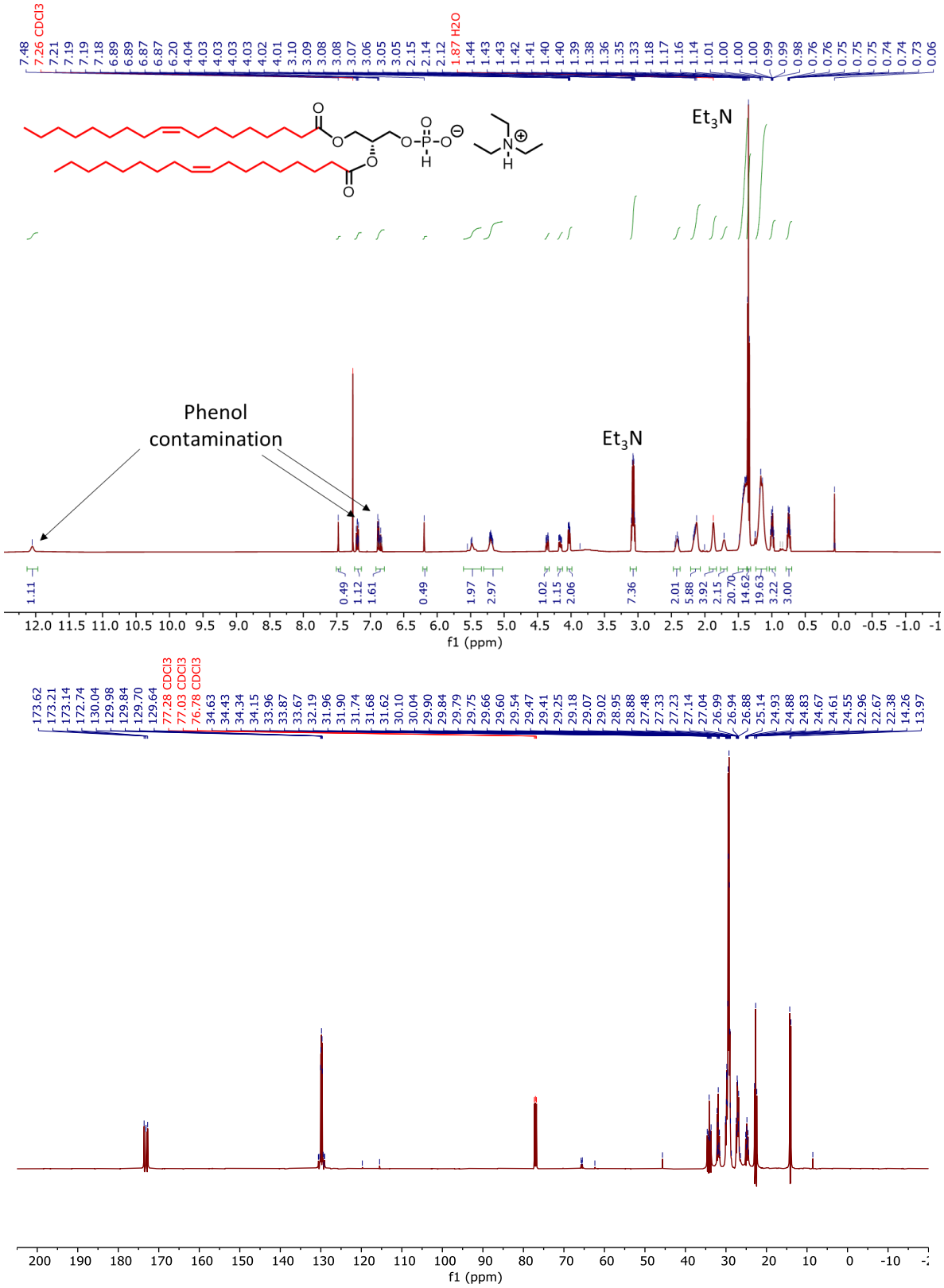

Figure 4.21. ^{1}H,^{13}C, and ^{31}P NMR of **7b**.

Figure 4.21 continued.

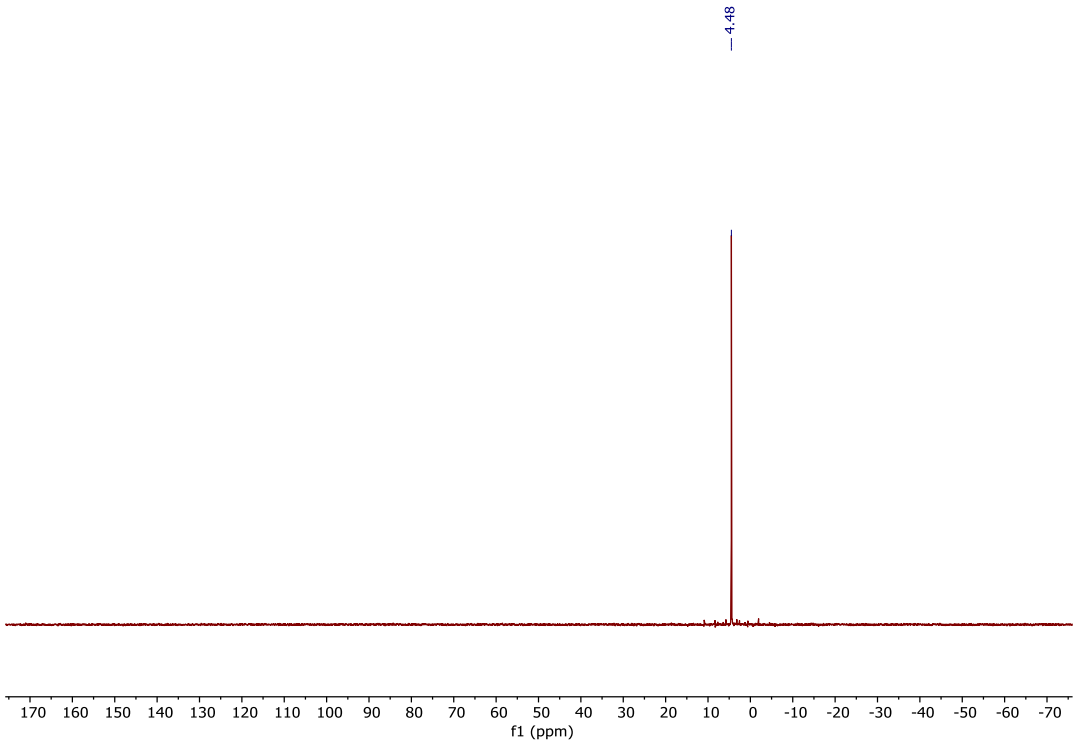

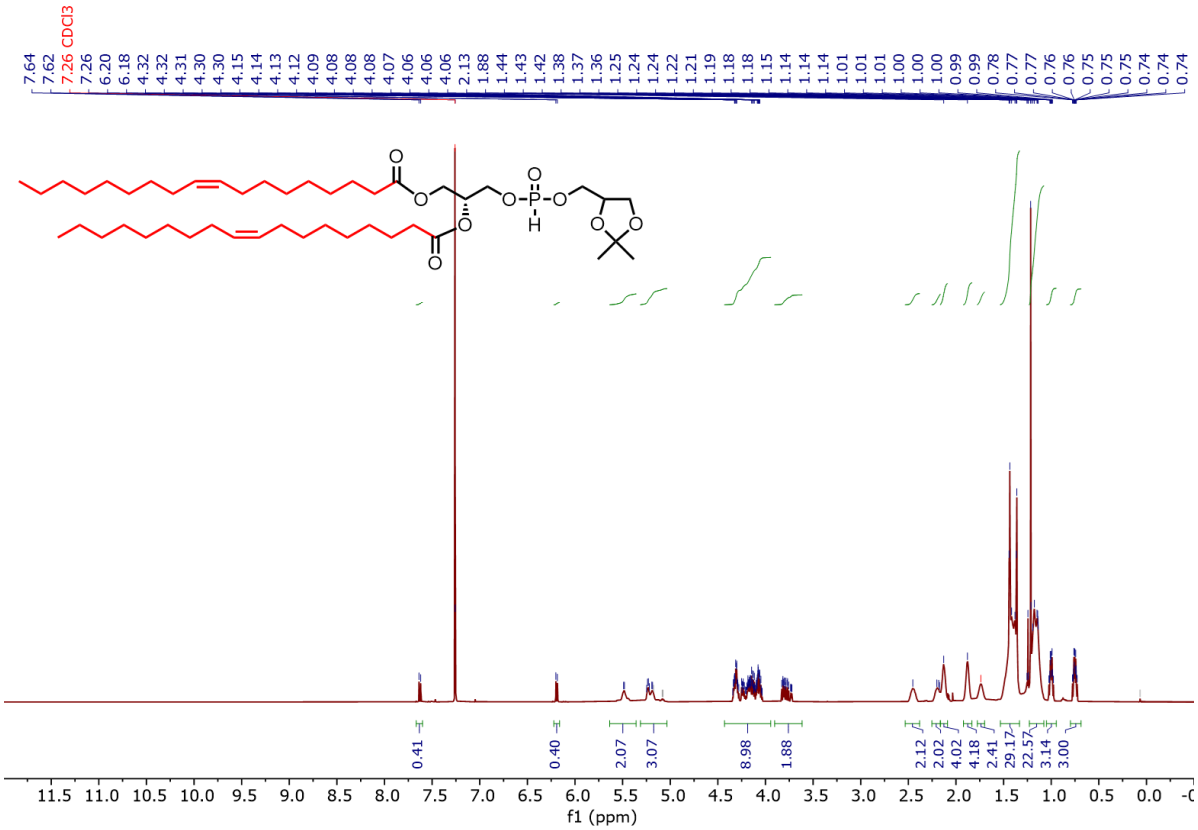

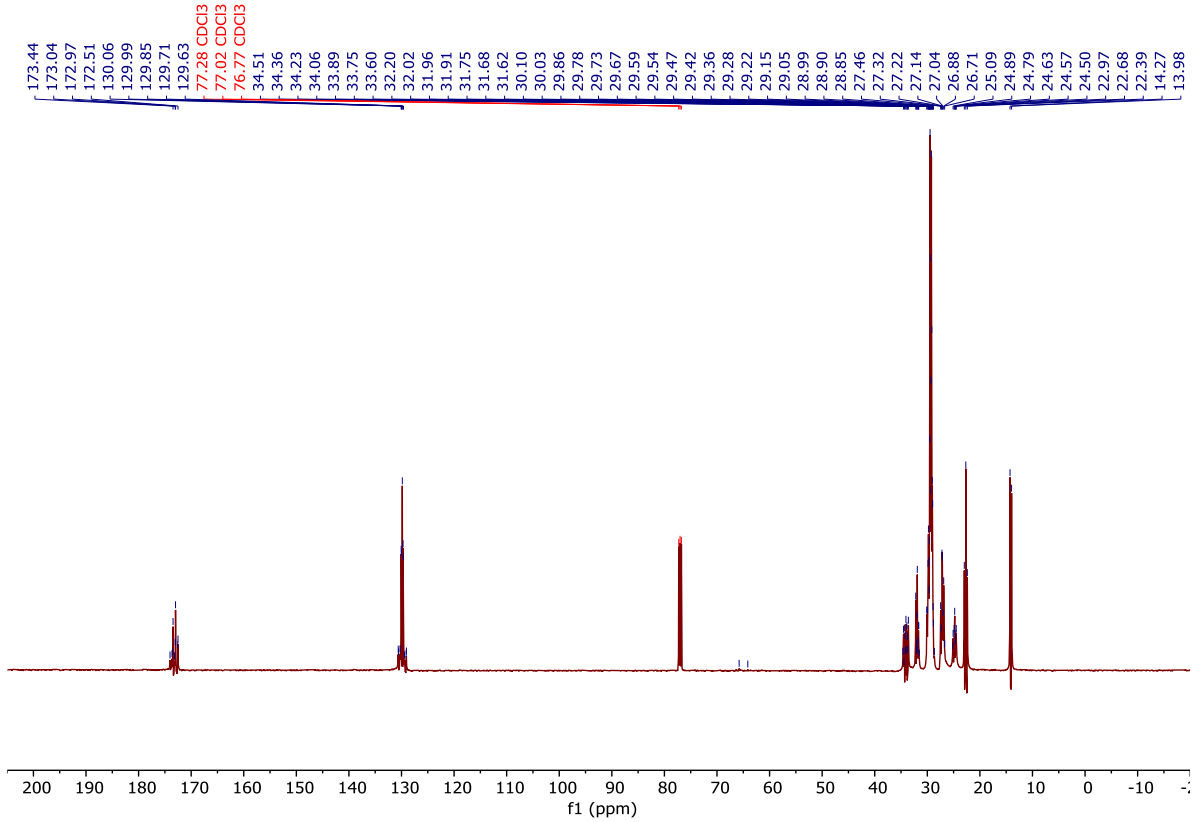

Figure 4.22. ^{1}H,^{13}C, ^{31}P NMR of **8b**.

Figure 4.22 continued.

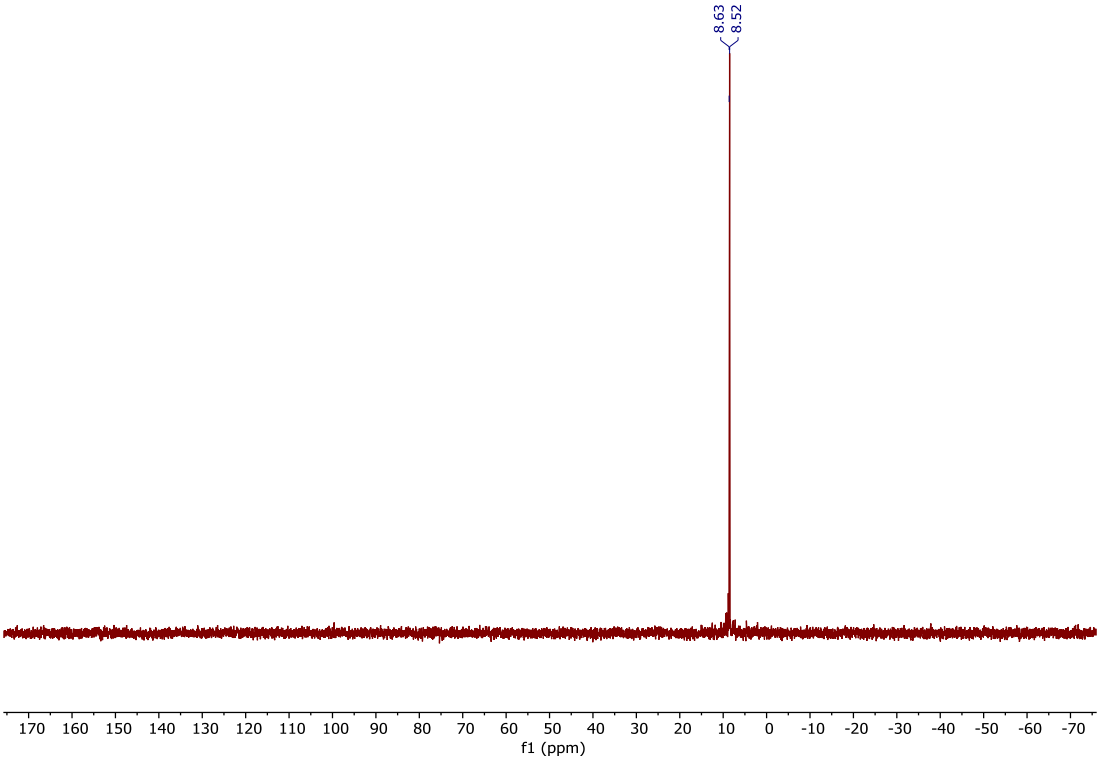

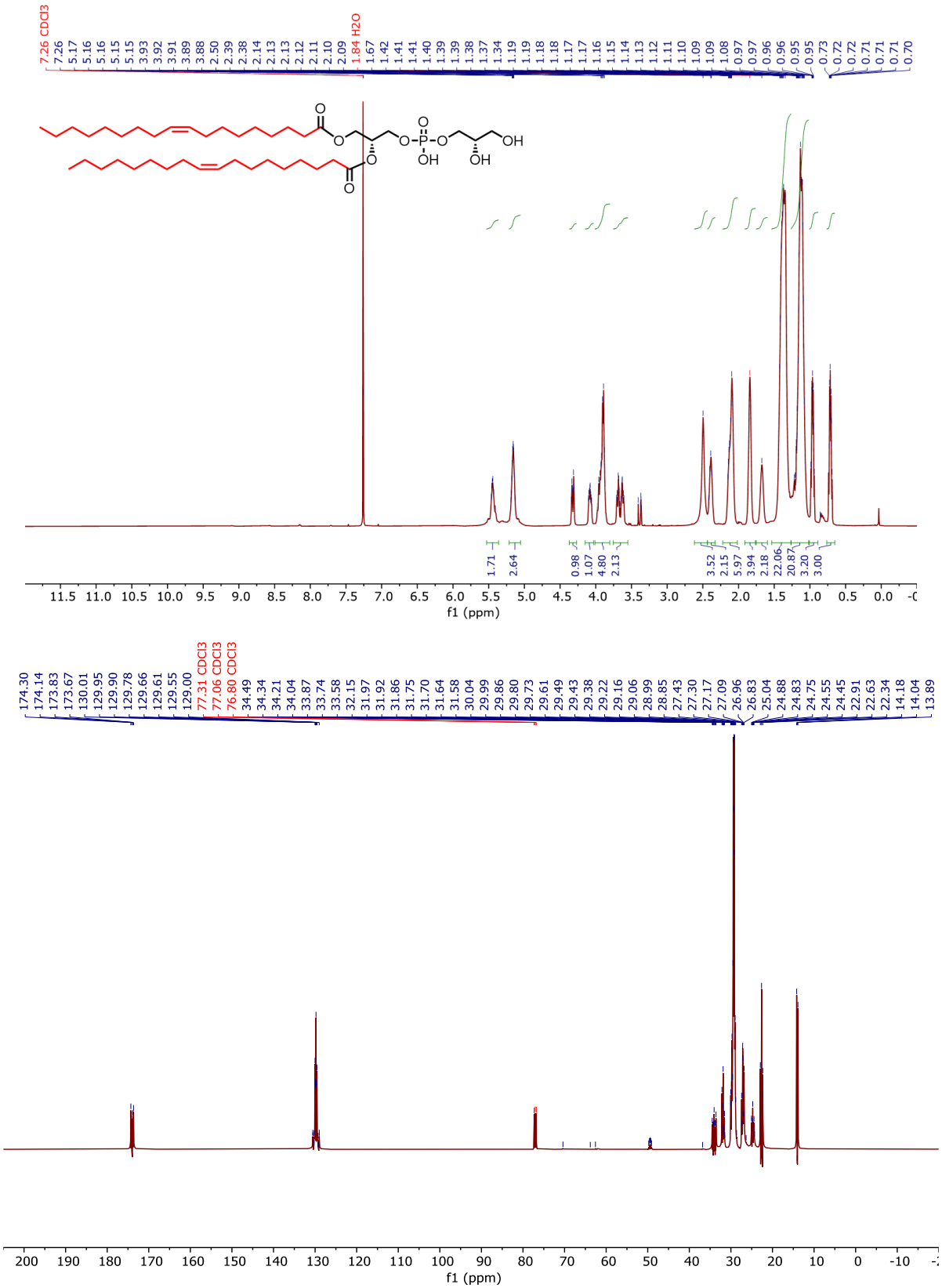

Figure 4.23. ^{1}H,^{13}C, ^{31}P NMR of **9b**.

Figure 4.23 continued.

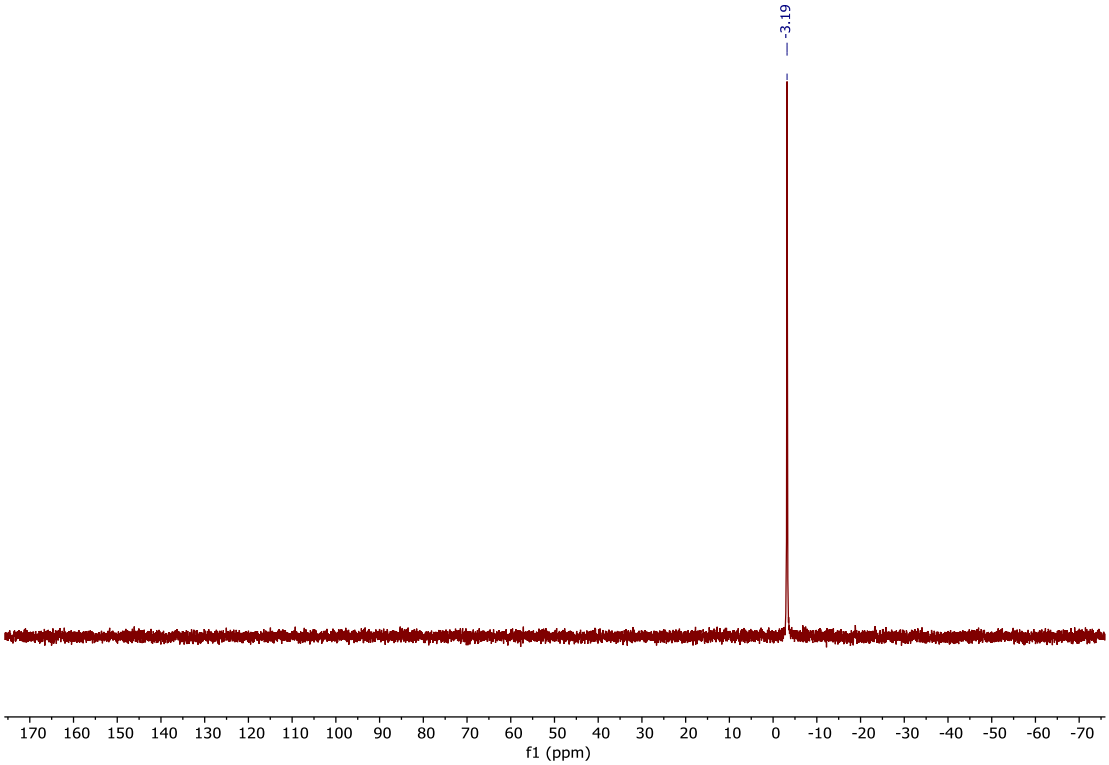

4.5 References

1. Burton, B. K.; Ellis, A. G.; Orr, B.; Chatlani, S.; Yoon, K.; Shoaff, J. R.; Gallo, D., Estimating the prevalence of Niemann-Pick disease type C (NPC) in the United States. *Molecular Genetics and Metabolism* **2021,** *134* (1), 182-187.

2. Vanier, M. T., Niemann-Pick disease type C. *Orphanet Journal of Rare Diseases* **2010,** *5* (1), 16.

3. Morris, J. A.; Zhang, D.; Coleman, K. G.; Nagle, J.; Pentchev, P. G.; Carstea, E. D., The genomic organization and polymorphism analysis of the human Niemann-Pick C1 gene. *Biochemical and biophysical research communications* **1999,** *261* (2), 493-8.

4. Carstea, E. D.; Morris, J. A.; Coleman, K. G.; Loftus, S. K.; Zhang, D.; Cummings, C.; Gu, J.; Rosenfeld, M. A.; Pavan, W. J.; Krizman, D. B.; Nagle, J.; Polymeropoulos, M. H.; Sturley, S. L.; Ioannou, Y. A.; Higgins, M. E.; Comly, M.; Cooney, A.; Brown, A.; Kaneski, C. R.; Blanchette-Mackie, E. J.; Dwyer, N. K.; Neufeld, E. B.; Chang, T. Y.; Liscum, L.; Strauss, J. F., 3rd; Ohno, K.; Zeigler, M.; Carmi, R.; Sokol, J.; Markie, D.; O'Neill, R. R.; van Diggelen, O. P.; Elleder, M.; Patterson, M. C.; Brady, R. O.; Vanier, M. T.; Pentchev, P. G.; Tagle, D. A., Niemann-Pick C1 disease gene: homology to mediators of cholesterol homeostasis. *Science (New York, N.Y.)* **1997,** *277* (5323), 228-31.

5. Davies, J. P.; Ioannou, Y. A., Topological Analysis of Niemann-Pick C1 Protein Reveals That the Membrane Orientation of the Putative Sterol-sensing Domain Is Identical to Those of 3-Hydroxy-3-methylglutaryl-CoA Reductase and Sterol Regulatory Element Binding Protein Cleavage-activating Protein*. *Journal of Biological Chemistry* **2000,** *275* (32), 24367-24374.

6. Kwon, H. J.; Abi-Mosleh, L.; Wang, M. L.; Deisenhofer, J.; Goldstein, J. L.; Brown, M. S.; Infante, R. E., Structure of N-terminal domain of NPC1 reveals distinct subdomains for binding and transfer of cholesterol. *Cell* **2009,** *137* (7), 1213-1224.

7. Gong, X.; Qian, H.; Zhou, X.; Wu, J.; Wan, T.; Cao, P.; Huang, W.; Zhao, X.; Wang, X.; Wang, P.; Shi, Y.; Gao, G. F.; Zhou, Q.; Yan, N., Structural Insights into the Niemann-Pick C1 (NPC1)-Mediated Cholesterol Transfer and Ebola Infection. *Cell* **2016,** *165* (6), 1467-1478.

8. Naureckiene, S.; Sleat, D. E.; Lackland, H.; Fensom, A.; Vanier, M. T.; Wattiaux, R.; Jadot, M.; Lobel, P., Identification of HE1 as the Second Gene of Niemann-Pick C Disease. *Science (New York, N.Y.)* **2000,** *290* (5500), 2298-2301.

9. Friedland, N.; Liou, H.-L.; Lobel, P.; Stock, A. M., Structure of a cholesterol-binding protein deficient in Niemann–Pick type C2 disease. *Proceedings of the National Academy of Sciences* **2003,** *100* (5), 2512.

10. Xu, S.; Benoff, B.; Liou, H.-L.; Lobel, P.; Stock, A. M., Structural Basis of Sterol Binding by NPC2, a Lysosomal Protein Deficient in Niemann-Pick Type C2 Disease*. *Journal of Biological Chemistry* **2007,** *282* (32), 23525-23531.

11. Okamura, N.; Kiuchi, S.; Tamba, M.; Kashima, T.; Hiramoto, S.; Baba, T.; Dacheux, F.; Dacheux, J. L.; Sugita, Y.; Jin, Y. Z., A porcine homolog of the major secretory protein of human epididymis, HE1, specifically binds cholesterol. *Biochimica et biophysica acta* **1999,** *1438* (3), 377-87.

12. Brown Michael, S.; Goldstein Joseph, L., A Receptor-Mediated Pathway for Cholesterol Homeostasis. *Science (New York, N.Y.)* **1986,** *232* (4746), 34-47.

13. Li, F.; Zhang, H., Lysosomal Acid Lipase in Lipid Metabolism and Beyond. *Arteriosclerosis, Thrombosis, and Vascular Biology* **2019,** *39* (5), 850-856.

14. Baker, S. M.; Petukh, M., Effect of pH on the Ability of N-Terminal Domain of Human NPC1 to Recognize, Bind, and Transfer Cholesterol. *ACS Omega* **2020,** *5* (45), 29222-29230.

15. Qian, H.; Wu, X.; Du, X.; Yao, X.; Zhao, X.; Lee, J.; Yang, H.; Yan, N., Structural Basis of Low-pH-Dependent Lysosomal Cholesterol Egress by NPC1 and NPC2. *Cell* **2020,** *182* (1), 98-111.e18.

16. Dubey, V.; Bozorg, B.; Wüstner, D.; Khandelia, H., Cholesterol binding to the sterol-sensing region of Niemann Pick C1 protein confines dynamics of its N-terminal domain. *PLoS Comput Biol* **2020,** *16* (10), e1007554-e1007554.

17. Goldstein, J. L.; Brown, M. S., The low-density lipoprotein pathway and its relation to atherosclerosis. *Annual review of biochemistry* **1977,** *46*, 897-930.

18. Chang, T. Y.; Chang, C. C. Y.; Cheng, D., ACYL-COENZYME A:CHOLESTEROL ACYLTRANSFERASE. *Annual review of biochemistry* **1997,** *66* (1), 613-638.

19. Möbius, W.; van Donselaar, E.; Ohno-Iwashita, Y.; Shimada, Y.; Heijnen, H. F.; Slot, J. W.; Geuze, H. J., Recycling compartments and the internal vesicles of multivesicular bodies harbor most of the cholesterol found in the endocytic pathway. *Traffic* **2003,** *4* (4), 222-31.

20. Tarling, E. J.; Edwards, P. A., ATP binding cassette transporter G1 (ABCG1) is an intracellular sterol transporter. *Proceedings of the National Academy of Sciences of the United States of America* **2011,** *108* (49), 19719-24.

21. Pfrieger, F. W.; Vitale, N., Cholesterol and the journey of extracellular vesicles. *Journal of lipid research* **2018,** *59* (12), 2255-2261.

22. Ko, D. C.; Binkley, J.; Sidow, A.; Scott, M. P., The integrity of a cholesterol-binding pocket in Niemann–Pick C2 protein is necessary to control lysosome cholesterol levels. *Proceedings of the National Academy of Sciences* **2003,** *100* (5), 2518.

23. Body, D. R.; Gray, G. M., The isolation and characterisation of phosphatidylglycerol and a structural isomer from pig lung. *Chemistry and Physics of Lipids* **1967,** *1* (3), 254-263.

24. Kobayashi, T.; Stang, E.; Fang, K. S.; de Moerloose, P.; Parton, R. G.; Gruenberg, J., A lipid associated with the antiphospholipid syndrome regulates endosome structure and function. *Nature* **1998,** *392* (6672), 193-7.

25. Brotherus, J.; Renkonen, O., Subcellular distributions of lipids in cultured BHK cells: evidence for the enrichment of lysobisphosphatidic acid and neutral lipids in lysosomes. *Journal of lipid research* **1977,** *18* (2), 191-202.

26. Joutti, A., The stereoconfiguration of newly formed molecules of BIS(monoacylglycero)phosphate in BHK cells. *Biochimica et Biophysica Acta (BBA) - Lipids and Lipid Metabolism* **1979,** *575* (1), 10-15.

27. Joutti, A.; Brotherus, J.; Renkonen, O.; Laine, R.; Fischer, W., The stereochemical configuration of lysobisphosphatidic acid from rat liver, rabbit lung and pig lung. *Biochimica et Biophysica Acta (BBA) - Lipids and Lipid Metabolism* **1976,** *450* (2), 206-209.

28. Tan, H.-H.; Makino, A.; Sudesh, K.; Greimel, P.; Kobayashi, T., Spectroscopic Evidence for the Unusual Stereochemical Configuration of an Endosome-Specific Lipid. *Angewandte Chemie International Edition* **2012,** *51* (2), 533-535.

29. Goursot, A.; Mineva, T.; Bissig, C.; Gruenberg, J.; Salahub, D. R., Structure, Dynamics, and Energetics of Lysobisphosphatidic Acid (LBPA) Isomers. *The Journal of Physical Chemistry B* **2010,** *114* (47), 15712-15720.

30. Kuipers, O. P.; Dijkman, R.; Pals, C. E. G. M.; Verheij, H. M.; Haas, G. H. d., Evidence for the involvement of tyrosine-69 in the control of stereospecificity of porcine pancreatic phospholipase A2. *Protein Engineering, Design and Selection* **1989,** *2* (6), 467-471.

31. Linderoth, L.; Andresen, T. L.; Jørgensen, K.; Madsen, R.; Peters, G. H., Molecular Basis of Phospholipase A2 Activity toward Phospholipids with sn-1 Substitutions. *Biophysical Journal* **2008,** *94* (1), 14-26.

32. Abe, A.; Shayman, J. A., The role of negatively charged lipids in lysosomal phospholipase A2 function. *Journal of lipid research* **2009,** *50* (10), 2027-2035.

33. Matsuzawa, Y.; Hostetler, K. Y., Degradation of bis(monoacylglycero)phosphate by an acid phosphodiesterase in rat liver lysosomes. *Journal of Biological Chemistry* **1979,** *254* (13), 5997-6001.

34. Hayakawa, T.; Hirano, Y.; Makino, A.; Michaud, S.; Lagarde, M.; Pageaux, J.-F.; Doutheau, A.; Ito, K.; Fujisawa, T.; Takahashi, H.; Kobayashi, T., Differential Membrane Packing of Stereoisomers of Bis(monoacylglycero)phosphate. *Biochemistry* **2006,** *45* (30), 9198-9209.

35. Kobayashi, T.; Beuchat, M.-H.; Chevallier, J.; Makino, A.; Mayran, N.; Escola, J.-M.; Lebrand, C.; Cosson, P.; Kobayashi, T.; Gruenberg, J., Separation and Characterization of Late Endosomal Membrane Domains *. *Journal of Biological Chemistry* **2002,** *277* (35), 32157-32164.

36. Showalter, M. R.; Berg, A. L.; Nagourney, A.; Heil, H.; Carraway, K. L.; Fiehn, O., The Emerging and Diverse Roles of Bis(monoacylglycero) Phosphate Lipids in Cellular Physiology and Disease. *International Journal of Molecular Sciences* **2020,** *21* (21), 8067.

37. Liu, N.; Tengstrand, E. A.; Chourb, L.; Hsieh, F. Y., Di-22:6-bis(monoacylglycerol)phosphate: A clinical biomarker of drug-induced phospholipidosis for drug development and safety assessment. *Toxicology and Applied Pharmacology* **2014,** *279* (3), 467-476.

38. Anderson, D. M. G.; Ablonczy, Z.; Koutalos, Y.; Hanneken, A. M.; Spraggins, J. M.; Calcutt, M. W.; Crouch, R. K.; Caprioli, R. M.; Schey, K. L., Bis(monoacylglycero)phosphate lipids in the retinal pigment epithelium implicate lysosomal/endosomal dysfunction in a model of Stargardt disease and human retinas. *Sci Rep* **2017,** *7* (1), 17352.

39. Akgoc, Z.; Sena-Esteves, M.; Martin, D. R.; Han, X.; d'Azzo, A.; Seyfried, T. N., Bis(monoacylglycero)phosphate: a secondary storage lipid in the gangliosidoses. *Journal of lipid research* **2015,** *56* (5), 1006-13.

40. Hein, L. K.; Duplock, S.; Fuller, M., Selective reduction of bis(monoacylglycero)phosphate ameliorates the storage burden in a THP-1 macrophage model of Gaucher disease. *Journal of lipid research* **2013,** *54* (6), 1691-1697.

41. Meikle, Peter J.; Duplock, S.; Blacklock, D.; Whitfield, Phillip D.; Macintosh, G.; Hopwood, John J.; Fuller, M., Effect of lysosomal storage on bis(monoacylglycero)phosphate. *Biochemical Journal* **2008,** *411* (1), 71-78.

42. Xu, Z.; Farver, W.; Kodukula, S.; Storch, J., Regulation of Sterol Transport between Membranes and NPC2. *Biochemistry* **2008,** *47* (42), 11134-11143.

43. Perrotta, C.; Cervia, D.; De Palma, C.; Assi, E.; Pellegrino, P.; Bassi, M. T.; Clementi, E., The emerging role of acid sphingomyelinase in autophagy. *Apoptosis : an international journal on programmed cell death* **2015,** *20* (5), 635-44.

44. Reagan, J. W.; Hubbert, M. L.; Shelness, G. S., Posttranslational Regulation of Acid Sphingomyelinase in Niemann-Pick Type C1 Fibroblasts and Free Cholesterol-enriched Chinese Hamster Ovary Cells*. *Journal of Biological Chemistry* **2000,** *275* (48), 38104-38110.

45. Devlin, C.; Pipalia, N. H.; Liao, X.; Schuchman, E. H.; Maxfield, F. R.; Tabas, I., Improvement in Lipid and Protein Trafficking in Niemann-Pick C1 Cells by Correction of a Secondary Enzyme Defect. *Traffic* **2010,** *11* (5), 601-615.

46. Taniguchi, M.; Kitatani, K.; Kondo, T.; Hashimoto-Nishimura, M.; Asano, S.; Hayashi, A.; Mitsutake, S.; Igarashi, Y.; Umehara, H.; Takeya, H.; Kigawa, J.; Okazaki, T., Regulation of autophagy and its associated cell death by "sphingolipid rheostat": reciprocal role of ceramide and sphingosine 1-phosphate in the mammalian target of rapamycin pathway. *The Journal of biological chemistry* **2012,** *287* (47), 39898-39910.

47. Cheruku, S. R.; Xu, Z.; Dutia, R.; Lobel, P.; Storch, J., Mechanism of cholesterol transfer from the Niemann-Pick type C2 protein to model membranes supports a role in lysosomal cholesterol transport. *The Journal of biological chemistry* **2006,** *281* (42), 31594-604.

48. McCauliff, L. A.; Xu, Z.; Li, R.; Kodukula, S.; Ko, D. C.; Scott, M. P.; Kahn, P. C.; Storch, J., Multiple Surface Regions on the Niemann-Pick C2 Protein Facilitate Intracellular Cholesterol Transport. *The Journal of biological chemistry* **2015,** *290* (45), 27321-27331.

49. McCauliff, L. A.; Langan, A.; Li, R.; Ilnytska, O.; Bose, D.; Waghalter, M.; Lai, K.; Kahn, P. C.; Storch, J., Intracellular cholesterol trafficking is dependent upon NPC2 interaction with lysobisphosphatidic acid. *eLife* **2019,** *8*.

50. Moreau, D.; Vacca, F.; Vossio, S.; Scott, C.; Colaco, A.; Paz Montoya, J.; Ferguson, C.; Damme, M.; Moniatte, M.; Parton, R. G.; Platt, F. M.; Gruenberg, J., Drug-induced increase in lysobisphosphatidic acid reduces the cholesterol overload in Niemann-Pick type C cells and mice. *EMBO reports* **2019,** *20* (7), e47055.

51. Ilnytska, O.; Lai, K.; Gorshkov, K.; Schultz, M. L.; Tran, B. N.; Jeziorek, M.; Kunkel, T. J.; Azaria, R. D.; McLoughlin, H. S.; Waghalter, M.; Xu, Y.; Schlame, M.; Altan-Bonnet, N.; Zheng, W.; Lieberman, A. P.; Dobrowolski, R.; Storch, J., Enrichment of NPC1-deficient cells with the lipid LBPA stimulates autophagy, improves lysosomal function, and reduces cholesterol storage. *The Journal of biological chemistry* **2021,** *297* (1), 100813.

52. Hullin-Matsuda, F.; Kawasaki, K.; Delton-Vandenbroucke, I.; Xu, Y.; Nishijima, M.; Lagarde, M.; Schlame, M.; Kobayashi, T., De novo biosynthesis of the late endosome lipid, bis(monoacylglycero)phosphate. *Journal of lipid research* **2007,** *48* (9), 1997-2008.

53. Thornburg, T.; Miller, C.; Thuren, T.; King, L.; Waite, M., Glycerol reorientation during the conversion of phosphatidylglycerol to bis(monoacylglycerol)phosphate in macrophage-like RAW 264.7 cells. *Journal of Biological Chemistry* **1991,** *266* (11), 6834-6840.

54. Amidon, B.; Schmitt, J. D.; Thuren, T.; King, L.; Waite, M., Biosynthetic conversion of phosphatidylglycerol to sn-1:sn-1' bis(monoacylglycerol) phosphate in a macrophage-like cell Line. *Biochemistry* **1995,** *34* (16), 5554-5560.

55. Heravi, J.; Waite, M., Transacylase formation of bis(monoacylglycerol)phosphate. *Biochimica et Biophysica Acta (BBA) - Molecular and Cell Biology of Lipids* **1999,** *1437* (3), 277-286.

56. Struzik, Z. J.; Biyani, S.; Grotzer, T.; Storch, J.; Thompson, D. H., Synthesis of Phosphatidyl Glycerol Containing Unsymmetric Acyl Chains Using H-Phosphonate Methodology. *Molecules* **2022,** *27* (7), 2199.

57. Struzik, Z. J.; Weerts, A. N.; Storch, J.; Thompson, D. H., Stereospecific synthesis of phosphatidylglycerol using a cyanoethyl phosphoramidite precursor. *Chemistry and Physics of Lipids* **2020,** *231*, 104933.

58. Vosse, C.; Wienken, C.; Cadenas, C.; Hayen, H., Separation and identification of phospholipids by hydrophilic interaction liquid chromatography coupled to tandem high resolution mass spectrometry with focus on isomeric phosphatidylglycerol and bis(monoacylglycero)phosphate. *Journal of Chromatography A* **2018,** *1565*, 105-113.

59. Buszewski, B.; Noga, S., Hydrophilic interaction liquid chromatography (HILIC)--a powerful separation technique. *Analytical and bioanalytical chemistry* **2012,** *402* (1), 231-247.

60. Wang, B.; Tontonoz, P., Phospholipid Remodeling in Physiology and Disease. *Annual review of physiology* **2019,** *81*, 165-188.

61. Swinnen, J. V.; Dehairs, J.; Talebi, A., Membrane Lipid Remodeling Takes Center Stage in Growth Factor Receptor-Driven Cancer Development. *Cell metabolism* **2019,** *30* (3), 407-408.

62. Lee, W.; Huang, Z.; am Ende, C. W.; Seneviratne, U., Protocol for clickable photoaffinity labeling and quantitative chemical proteomics. *STAR Protocols* **2021,** *2* (2), 100593.

63. Robinette, D.; Neamati, N.; Tomer, K. B.; Borchers, C. H., Photoaffinity labeling combined with mass spectrometric approaches as a tool for structural proteomics. *Expert Rev Proteomics* **2006,** *3* (4), 399-408.

64. Singh, A.; Thornton, E. R.; Westheimer, F. H., The Photolysis of Diazoacetylchymotrypsin. *Journal of Biological Chemistry* **1962,** *237* (9), PC3006-PC3008.

65. Murale, D. P.; Hong, S. C.; Haque, M. M.; Lee, J.-S., Photo-affinity labeling (PAL) in chemical proteomics: a handy tool to investigate protein-protein interactions (PPIs). *Proteome Science* **2017,** *15* (1), 14.

66. Hill, J. R.; Robertson, A. A. B., Fishing for Drug Targets: A Focus on Diazirine Photoaffinity Probe Synthesis. *Journal of Medicinal Chemistry* **2018,** *61* (16), 6945-6963.

67. Hassan, M. M.; Olaoye, O. O., Recent Advances in Chemical Biology Using Benzophenones and Diazirines as Radical Precursors. *Molecules* **2020,** *25* (10), 2285.

68. Zhang, Y.; Burdzinski, G.; Kubicki, J.; Platz, M. S., Direct Observation of Carbene and Diazo Formation from Aryldiazirines by Ultrafast Infrared Spectroscopy. *Journal of the American Chemical Society* **2008,** *130* (48), 16134-16135.

69. Marcinek, A.; Platz, M. S.; Chan, S. Y.; Floresca, R.; Rajagopalan, K.; Golinski, M.; Watt, D., Unusually long lifetimes of the singlet nitrenes derived from 4-azido-2,3,5,6-tetrafluorobenzamides. *The Journal of Physical Chemistry* **1994,** *98* (2), 412-419.

70. Xue, J.; Luk, H. L.; Eswaran, S. V.; Hadad, C. M.; Platz, M. S., Ultrafast infrared and UV-vis studies of the photochemistry of methoxycarbonylphenyl azides in solution. *J Phys Chem A* **2012,** *116* (22), 5325-5336.

71. Clark, W. D. K.; Litt, A. D.; Steel, C., Lifetimes and rate constants of triplet aromatic ketones in organic solvents. *Journal of the Chemical Society D: Chemical Communications* **1969,** (19), 1087-1089.

72. Okamoto, M.; Teranishi, H., Effect of pressure on the primary process of benzophenone photoreduction. *Journal of the American Chemical Society* **1986,** *108* (20), 6378-6380.

73. Xia, Y.; Peng, L., Photoactivatable Lipid Probes for Studying Biomembranes by Photoaffinity Labeling. *Chemical Reviews* **2013,** *113* (10), 7880-7929.

74. Shayman, J. A.; Kelly, R.; Kollmeyer, J.; He, Y.; Abe, A., Group XV phospholipase A_2, a lysosomal phospholipase A_2. *Prog Lipid Res* **2011,** *50* (1), 1-13.

75. Ellena, J. F.; Hutton, W. C.; Cafiso, D. S., Elucidation of cross-relaxation pathways in phospholipid vesicles utilizing two-dimensional proton NMR spectroscopy. *Journal of the American Chemical Society* **1985,** *107* (6), 1530-1537.

76. Lindner, S.; Gruhle, K.; Schmidt, R.; Garamus, V. M.; Ramsbeck, D.; Hause, G.; Meister, A.; Sinz, A.; Drescher, S., Azide-Modified Membrane Lipids: Synthesis, Properties, and Reactivity. *Langmuir* **2017,** *33* (20), 4960-4973.